FLORIDA STATE UNIVERSITY

COLLEGE OF ARTS AND SCIENCES

SEARCH FOR HEAVY STABLE CHARGED PARTICLES AT $\sqrt{S} = 13$ TEV UTILIZING A MULTIVARIATE APPROACH

By

ANDREW KENJIRO ACKERT

A Dissertation submitted to the
Department of Physics
in partial fulfillment of the
requirements for the degree of
Doctor of Philosophy

2017

Andrew Kenjiro Ackert defended this dissertation on March 31, 2017.
The members of the supervisory committee were:

Todd Adams
Professor Directing Dissertation

Jerry Magnan
University Representative

Harrison Prosper
Committee Member

Joseph Owens
Committee Member

Jorge Piekarewicz
Committee Member

The Graduate School has verified and approved the above-named committee members, and certifies that the dissertation has been approved in accordance with university requirements.

ACKNOWLEDGMENTS

I wish to thank my advisor Dr. Todd Adams. He showed great support and patience through the duration of my graduate career. His availability to always help and explain concepts greatly improved my understanding, and his diligent work in helping me to prepare this document was invaluable.

I would also like to take this time to express my gratitude to the other members of the FSU High Energy Physics faculty. Dr. Harrison Prosper and Dr. Andrew Askew were very patient at times with my plethora of questions. I would like to thank Dr. Joseph Owens III, Dr. Jorge Piekarewicz, and Dr. Jerry Magnan for being on my defense committee and showing great patience as I completed the results presented in this document.

I will also take this time to thank Florida State University for being my home away from home for the past 9 years. I can honestly say that I will miss being one of its students. The faculty and staff at FSU have always been friendly and hospitable. The professors that I have had through my tenure here have always managed to do exceedingly well in their instruction. I would like to acknowledge the Florida State University Women in Mathematics, Science, and Engineering program that helped provide funds to sponsor my research assistantship.

This research would not have been possible without the HSCP group within the CMS collaboration, especially Loic Quertenmont and Joze Zobec. Additionally without the CMS collaboration and experiment, none of this research would have existed.

I want to thank my family. My father, John Ackert, has always been a guiding hand in my life and will forever be. My mother, Akemi Ackert, has and will always be my moral compass, as I have never before met a person as kind and caring as she. Without either of them, I would not be here and I owe them everything. Finally I would like to thank my fiance, Kirst LaVoy. The last few months of my dissertation have been a very stressful time, and I could not have asked for a more understanding person to steadfastly traverse the wave of emotions on a daily basis.

TABLE OF CONTENTS

LIST OF TABLES

LIST OF FIGURES

ABSTRACT

Heavy stable charged particles (HSCPs) have been searched for at the Large Hadron Collider since its initial data taking in 2010. The search for heavy stable charged particles provide a means of directly probing the new physics realm, as they produce a detector signature unlike any particle discovered to date. The goal of this research is to investigate an idea that was introduced in the later stages of 2010-2012 data taking period. Rather than utilizing the current tight selection on the calculated particle mass the hypothesis is that by incorporating a multivariate approach, specifically an artificial neural network, the remaining selection criteria could be loosened allowing for a greater signal acceptance while maintaining acceptable background rejection via the multivariate discriminator from the artificial neural network. The increase in signal acceptance and retention or increase in background rejection increases the discovery potential for HSCPs and as a secondary objective calculates improved limits on the HSCP signal models.

The multivariate approach was developed and tested using 2.5 fb^{-1} of 2015 data at $\sqrt{s} = 13$ TeV based on both the past tracker-only and Tracker+TOF HSCP analyses. The multivariate analyses were able to produce improved upper cross section limits on both expected and observed cross sections compared to the past 2015 results. The lower mass limits produced by the multivariate analyses are also improved, but the improvement was found to be less than 5% higher compared to the past 2015 HSCP search results.

A final comparison of the multivariate approach to past HSCP searches was conducted on 12.9 fb^{-1} of 2016 data at $\sqrt{s} = 13$ TeV. No statistically significant excess of data over background prediction is observed. Therefore no evidence of HSCPs is claimed. The tracker-only (Tracker+TOF) multivariate analysis produced lower mass limits of 1870 (1820) GeV for gluinos with 10% R-hadrons produced neutral, 1260 (1210) GeV for stops, 680 (670) GeV for decay-product staus, 340 (370) GeV for directly pair-produced staus, 720 (750) GeV for modified Drell-Yan $|Q| = 1e$, and 700 (900) GeV for modified Drell-Yan $|Q| = 2e$. Overall, the multivariate approach produced improved lower mass limits compared to the results from the past 2016 HSCP search.

The overall improvements in cross section and mass limits using the multivariate approach produced the best limits on HSCPs to date. Furthermore the multivariate approach is shown as a viable method of searching for HSCPs. With the HSCP search covering a broad range of beyond

the Standard Model physics, the lack of evidence and subsequent limits produced place important restrictions on the theoretical models that predict HSCPs.

CHAPTER 1

INTRODUCTION

The Standard Model of particle physics (SM) is the current working theory that describes all observed fundamental particles and their interactions. In its current form, the SM has been used to great success in describing phenomena observed at particle collider experiments and has withstood numerous tests over the past several. However, there are several phenomena that cannot be explained within the context of current the SM. Examples include phenomena such as dark matter [1], dark energy [2], the matter anti-matter asymmetry, and even such a fundamental phenomena as gravity. A realm of theoretical particle physics known as beyond the Standard Model (BSM) physics seeks to answer these open questions by expanding or altogether replacing the SM with new theories.

One of the primary goals of the Large Hadron Collider (LHC) is to search for evidence of new physics (new with respect to the SM) in order to shed light on which, if any, of the current BSM theories could be true. A properly favored BSM theory is called supersymmetry [3]. In its simplest form, supersymmetry postulates that for every SM particle there exists a supersymmetric partner whose spin quantum differs by 1/2. By making certain assumptions about parameters of supersymmetry, such as mass scales for some of the supersymmetric particles or the energy scale and/or the mechanism by which the supersymmetry is broken, supersymmetry models with fewer free parameters have emerged (e.g. the minimal supersymmetric model [4]). This has the advantage of predicting new physics phenomena that can be produced at the energy scale available at the LHC. Many new physics searches have been carried out at the LHC [5, 6] with no evidence discovered. One way to directly probe the new physics realm is searching for new particles. A type of new particles are known as heavy stable charged particles.

In the most basic description, a heavy stable charged particle (HSCP) is any particle that is heavy (mass $>$ 100 GeV), is long-lived with regards to the size of modern collider experiments, and has a non-zero electrical charge. HSCPs can be detected by searching for a larger energy deposition per unit length (dE/dx) and larger time-of-flight (TOF) compared to standard model

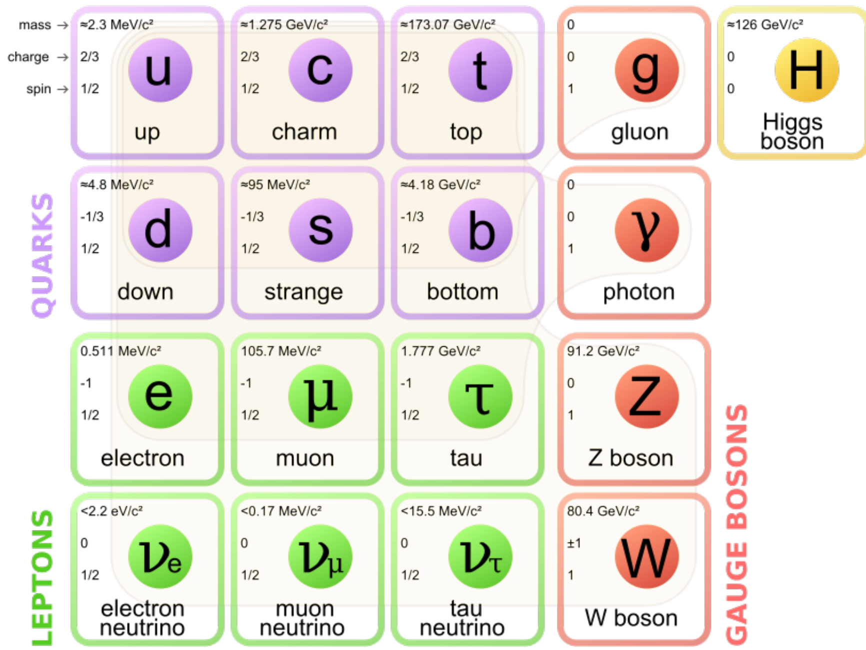

Figure 1.1: The fundamental standard model particles along with their basic properties of mass, charge, and spin. The different categories of fundamental particles (quarks, leptons, gauge bosons, higgs boson) are grouped together and have matching color [19].

particles. The search for such a signature is a means of directly probing the new physics realm without being constrained by a specific theoretical model. HSCPs are found in several beyond the Standard Model theories (e.g. supersymmetry [3], B-L standard model extension [7], vectorlike confinement [8], hidden valley models [9]). Therefore HSCP searches are also able to restrict or eliminate such theories based on the search results. To date, several searches have been carried out by high energy collider collaborations including D0 [10] and CDF [11] at the Tevatron, and by ATLAS [12–14] and CMS [15–18] at the Large Hadron Collider.

1.1 HSCP Benchmark Theories

HSCPs may exist in two general categories: lepton-like or hadron-like. The lepton-like HSCPs interact predominantly via the electromagnetic force. The Gauge Mediate Supersymmetry Breaking model [20] has been chosen as a benchmark lepton-like model for this analysis. In addition, a modified Drell-Yan (DY) production is also studied. In total, two types of lepton-like HSCP particles were chosen as signal types to search for: staus and modified DY fermions.

The staus are the supersymmetric partner to the tau and in this research are modeled via the minimal Gauge Mediated Supersymmetry Breaking model [21]. In the minimal Gauge Mediated Supersymmetry Breaking model the staus are the next-to-lightest supersymmetric particle with the gravitino being the lightest supersymmetric particle. In the primary model, staus are produced through the decays of other supersymmetric particles. These additional supersymmetric particles (mostly supersymmetric quarks and gluons) are predominantly produced through strong interactions. In an alternative production mode, the staus are directly produced from the proton-proton collisions, primarily through electroweak interactions. In the case where squarks and gluinos have masses too large to be produced at the LHC, the direct production mode becomes relevant. This research is sensitive to either model and will use GMSB stau to indicate staus produced via decay, and PP stau to indicate the directly produced staus. The modified DY model [22] takes the existing SM DY process and modifies the theory by the inclusion of new massive spin 1/2 particles. These particles are allowed to have arbitrary electric charge and are considered neutral under $SU(3)_C$ and $SU(2)_L$ which causes them to only couple to the photon and Z boson.

Two types of hadron-like particles were chosen as benchmark signals: gluinos and stops. Gluinos are the supersymmetric partner to the SM gluon. This research focuses on gluinos produced via the Split SUSY model [23]. In the Split SUSY model used for gluinos, the base assumption is that the top squark mass is large (order 10 TeV), and thus the gluino becomes a "long-lived" particle with a lifetime up to approximately one hundred seconds as well as being the lightest supersymmetric particle. In Split SUSY, the gluinos carry quantum color charge and due to their long lifetimes are allowed to form hadrons with SM quarks and/or gluons. The bound state is called an R-hadron for the unit of R-partiy that the hadron possesses.

Top squarks or "stops" are the supersymmetric partner to the top quark. With respect to this analysis, the stops are modeled in similar fashion as the gluinos by using the Split SUSY model, this time without the squark mass assumption that was used for the gluino modeling. As with gluinos, they form R-hadrons that are simulated traveling through the detector.

The interactions of R-hadrons from both gluinos and stops are modeled in this analysis two ways: the cloud interaction model [24, 25] and the charge suppressed (CS) model [26]. In the cloud interaction model, the R-hadron is pictured as having a SUSY particle as a nucleus, with SM partons surrounding it forming a "cloud" of SM particles around the SUSY particle. Due to hadronic interactions with the layers of material in a particle detector, the R-hadron can "swap" SM particles and therefore the overall charge of the R-hadron can change. The R-hadron can go from charged to neutral or vice versa, a process called charge exchange. In the CS model, the hadronic interactions result in nearly all of the R-hadrons becoming neutral prior to reaching the outer layers of a detector.

The theoretical cross sections for the gluino and stop models were computed to Next-to-Leading Order (NLO) combined with Next-to-Leading Logarithmic order (NL0+NLL)[27–30]. The staus and modified DY models were computed to NLO. All signal types used PROSPINO [31] with parton distribution function (PDFs) computed with CTEQ6.6M [32].

In the following chapters, the Compact Muon Solenoid (CMS) will be described (Chapter 2) followed by a discussion of the standard HSCP analysis (Chapter 3). The results from studies involving the multivariate technique used and comparisons to the standard HSCP analysis will be presented (Chapter 4) followed by a summary (Chapter 5).

CHAPTER 2

EXPERIMENTAL APPARATUS

The data presented in this document were collected using the Large Hadron Collider (LHC) to provide the proton beams and the Compact Muon Solenoid (CMS) experiment to record the collision data. Both are located at the European Organization for Nuclear Research (CERN) in Switzerland.

2.1 The Large Hadron Collider

The Large Hadron Collider is the collective name of the largest particle accelerator that provides the high energy protons used in collisions at CERN. Situated across the French and Swiss border near Geneva, Switzerland, the LHC is a 27 kilometer ring that sits in a tunnel 50-175 meters below the surface. Beginning in 2015, the LHC has accelerated protons to an energy of 6.5 TeV per beam, producing $\sqrt{s} = 13$ TeV. The LHC accelerator ring is the final stage of acceleration. The protons begin as a bottle of hydrogen gas, and are striped of their electrons via an electric field. The first accelerator is the Linac 2, a linear accelerator, which accelerates the protons to an energy of 50 MeV. The protons are then injected into the Proton Synchrotron Booster and accelerated up to 1.4 GeV. Next the protons are accelerated in the Proton Synchrotron up to 25 GeV. Then the protons are injected into the Super Proton Synchrotron which accelerates the protons to 450 GeV. The final step is injecting the protons into the LHC ring which accelerates the protons to the desired 6.5 TeV [33].

The protons circulating within the main ring are concentrated in "bunches," with a beam of bunches circulating in one direction, and the other beam circulating in the opposite. The beginning of Run 2 in 2015 had a spacing of 50 ns between bunch crossings. The spacing was reduced then reduced to 25 ns between bunch crossings and remained at 25 ns for 2016.

During each bunch crossing, due to the number of protons per bunch (up to 1.15×10^{11} in 2015 and 2016), there is a probability for more than one collision to occur. Each proton-proton collision is referred to as a primary vertex, as opposed to a secondary or tertiary vertex due to a decay process. From the primary vertices, a single collision is labeled as the *selected* primary vertex of interest. The other primary vertices are labeled as "pile up" (PU) vertices, and their resulting products known as pile up. For the remainder of this research, the selected primary vertex will be referred to as *the* primary vertex.

2.2 The Compact Muon Solenoid Detector

The CMS detector is a large cylindrical device measuring 15 meters in diameter, 21.6 meters in length, and weighing approximately 14,000 tonnes. A highly detailed description of the CMS detector can be found in Ref. [34]. The CMS detector is comprised of several "subdetectors" in a layered configuration. From innermost to outermost the layers are: the tracker, the electromagnetic calorimeter (ECAL), the hadronic calorimeter (HCAL), the superconducting solenoid, the muon detector, and the hadronic forward calorimeter (HF) as shown in Fig. 2.1. These layers are also separated into a barrel region and endcap region. The entire apparatus was designed in five large "slices" that allow the machine to be separated for maintenance and upgrade purposes, while also allowing for the different sections to be lowered and raised from the cavern during initial installation and for future possible large scale upgrades.

CMS uses a coordinate system with the z-axis pointed along the counterclockwise beam line, the x-axis pointed inward toward the center of the LHC ring, and the y-axis pointed upward. From these cartesian coordinates, the typical physics spherical coordinates are taken to be ρ as the radial direction emanating from the center of the detector, θ as the angle of inclination from the z-axis, and ϕ as the aximuthal angle in the x-y plane. Rather than directly using θ, a quantity known as psudeorapidity, η, is used with $\eta = -\ln(\tan(\theta/2))$, which results in $\eta = 0$ along the x-y plane and $\eta \to \infty$ as one approaches the z-axis. Using η, the barrel region is defined as $0 \leq |\eta| \leq 1.44$ and the endcap region is $1.5 < |\eta| < 3.0$, with the in between being a region where the different subdetector components overlap.

The tracker is comprised of concentric layers of silicon. Charged particles deposit energy in the silicon allowing for an accurate measurement of position and momentum out to $|\eta| \leq 2.5$. The ECAL primarily measures the energy deposition of electrons and photons via the light emissions of lead tungstate crystals with coverage out to $|\eta| \leq 3$. The HCAL is a sampling calorimeter comprised of alternating layers of silicon and brass with principle function to measure the energy deposition from hadrons that pass through the ECAL. The HCAL has the same coverage as the

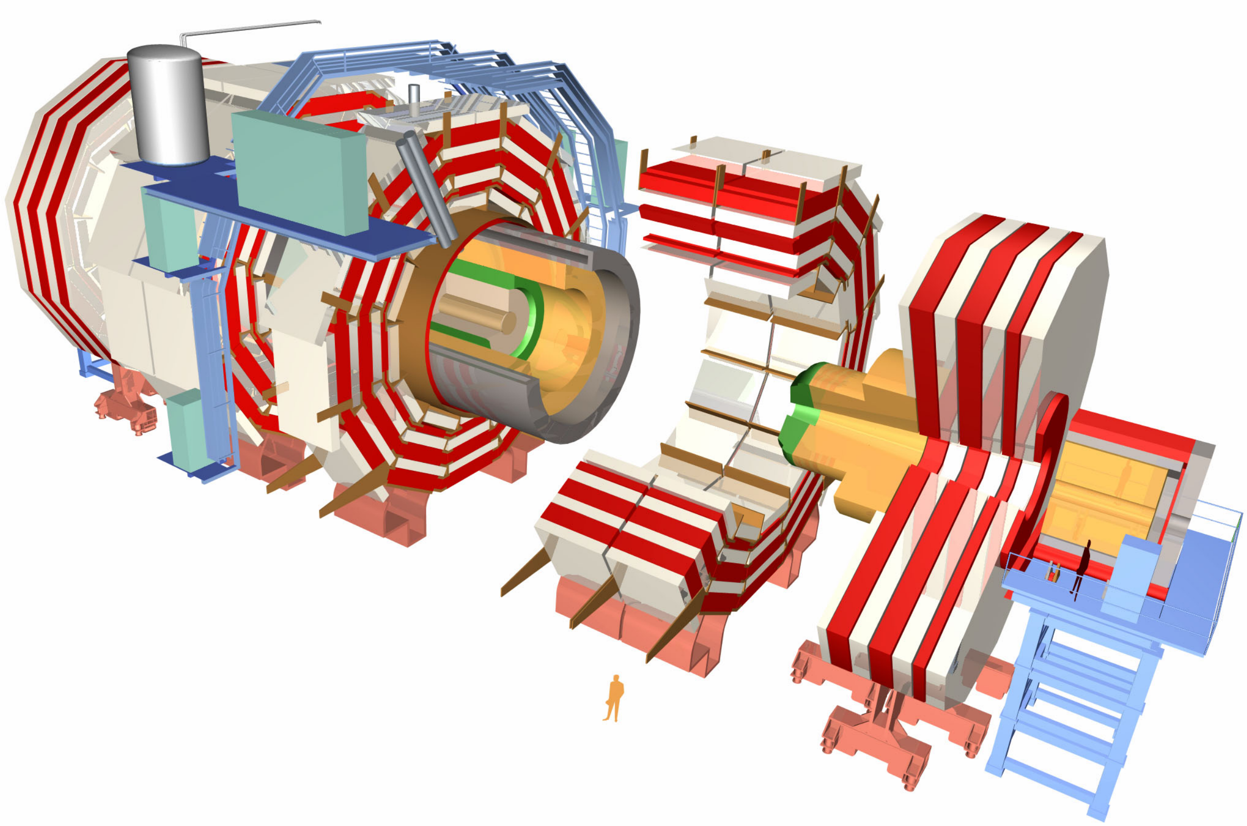

Figure 2.1: A 3-D rendering of the CMS detector with sections separated to show the interior. The various layers are color coded: pixel tracker (tan), strip tracker (light gray), ECAL (green), HCAL (orange), solenoid (dark gray), and muon system (white and red) [35].

ECAL. Outside of the HCAL is the 3.8 Tesla superconducting solenoid. The strong magnetic field from the solenoid causes the bending of charged particles needed to determine momentum from the tracker. Outside of the superconducting solenoid is the muon detector comprised of layers of steel and gas-ionizing devices. An oppositely oriented magnetic field throughout the muon system allows for precision position and momentum measurements of muons as they leave the detector. The muon system has coverage of $|\eta| \leq 2.4$. Finally, the HF is an addition to the HCAL in the endcap "forward" regions ($3 \leq |\eta| \leq 5$) and allows for detection and measuring of particles traveling closer to the beamline. For the HSCP analyses, the tracker and muon system are the primary components of the CMS detector used to gather measurements.

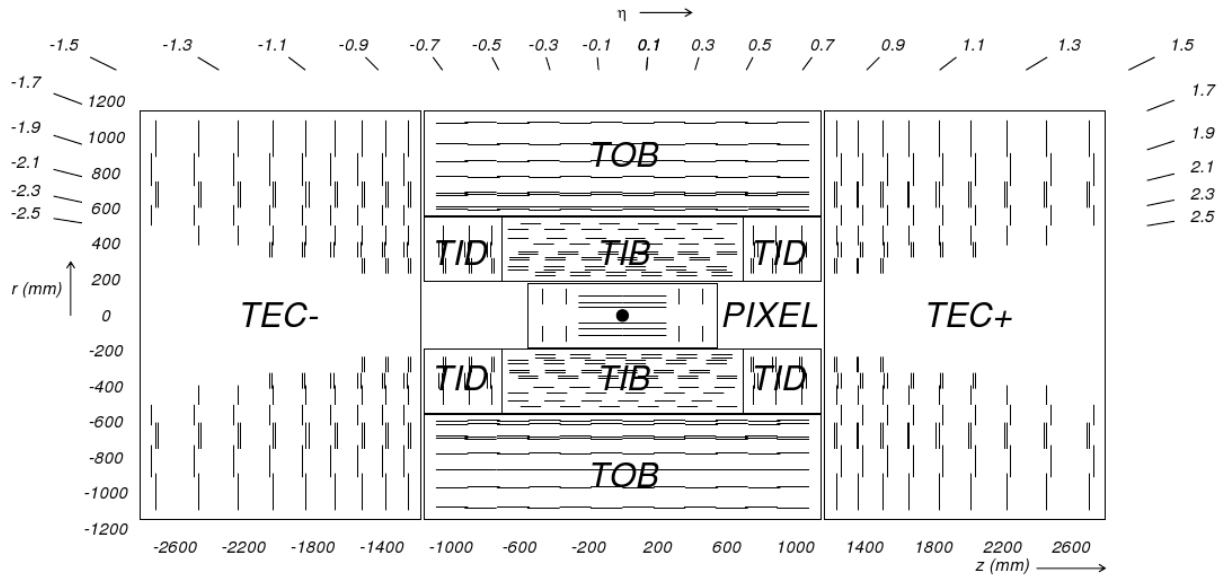

Figure 2.2: Cross sectional diagram of the tracker subdetector indicating the pixel detector and the various regions of the strip tracker. For reference, distances radially outward from the beam (r) and distances along the beam axis (z) are listed, as well as markings indicated the η at which the various components are located[36].

2.2.1 The Tracker Subdetector

The tracker subdetector is 5.8 m in length and 2.5 m in diameter. It can be further divided into two principle technologies: the silicon pixel and the silicon strip trackers. The pixel detector utilizes silicon pixels (measuring 100 x 150 μm^2) to provide three dimensional position measurements (r, ϕ, z). The strip tracker utilizes silicon strips of varying widths and lengths (to be discussed) with each strip providing two dimensional position measurements (r, ϕ in the barrel and ϕ, z in the endcap). An overall diagram of the tracker can be seen in Fig. 2.2.

The barrel pixel detector is contained in three cylindrical layers located at radii of 4.4, 7.3, and 10.2 cm from the beam line. The pixels are grouped together in the barrel region with readout chips, power supply cables, and readout cables along with a high density interconnect to form modules. Depending on the location within the barrel, the modules are configured in 8 or 16 readout chips, with each chip covering 52x80 pixels. In total the barrel region contains 800 modules with 672 full modules containing 16 readout chips and 128 half modules containing 8 readout chips. The modules for all three layers are housed in two half cylindrical housings. The half modules are located at the edges where the two cylindrical housings meet.

Within the endcap region, the pixel detector is composed of two disks on each end of the pixel barrel. The pixel sensors are bonded to different configurations of readout chips (the chips are the same type as those in the barrel) to form a plaquette. The plaquettes are formed in 1x2, 2x3, 2x4, 1x5, and 2x5 (rows x columns) of readout chips and pixels, and are arranged in trapezoidal shaped modules along with the high density interconnect of the module, power supply and readout cables. The modules are arranged into half disks, with two half disks comprising each endcap layer. The endcap layers are located along the z axis at ±34.5 cm and ±46.5 cm from the center of the CMS detector extending in radius from 6 cm out to 15 cm from the beam line. Overall the pixel tracker contains $\approx 6.6x10^7$ channels with a spatial resolution roughly 10 μm in x-y and 20-40 μm in z.

The strip detector is comprised of charge sensitive silicon strips divided into 4 regions: inner barrel (TIB), outer barrel (TOB), tracker inner disks (TID), and tracker endcap (TEC). TIB, TOB, TID, and TEC contain 4, 6, 3, and 9 layers respectively. The four layers in the TIB are located at 25.5, 33.9, 41.85, and 49.8 cm away from the beam line, with the two innermost layers containing double sided modules and the outer two layers containing single sided modules. In the TOB, a single cylindrical "wheel" structure supports four disks forming six detection layers. The layers are located at radii of 60.8 cm, 69.2 cm, 78 cm, 86.8 cm, 96.5 cm, and 108 cm, with an overall length of 218 cm for the wheel structure. The three disk layers of the TID span a radius of 20-50 cm from the beamline and between 80-90 cm in distance from the detector center along the beamline. The two innermost disks containing double sided modules, and the outermost disk containing single sided modules. Finally the nine disk layers in the TEC are located radially from 22 cm to 113.5 cm and from 124 cm to 280 cm from the center of the detector along the z axis. The different strip sensor geometries used throughout the strip detector are listed in Table 2.1. For all of the strip sensor geometries, the strips have a sensor pitch to width ratio of 0.25.

The silicon strips within the barrel region layers are oriented parallel to the beamline and oriented radially in the endcap regions. An additional set of sensor modules are located back to back with the sensor modules in the two inner most layers of the TIB, TOB, TID, TEC and the fifth layer of the TEC. These additional modules' strips are oriented orthogonal to the other strips in the layer, allowing orthogonal position measurements (z in the barrel and r in the endcap). In

Table 2.1: The different detector geometries within the silicon strip tracker. Listed are the pitch, the thickness, the length, and the naming scheme for each geometry. The TID rings and first 3 TEC rings use the same sensor layout, however are listed separately due to differences in module geometry.

Subsystem location	naming scheme	pitch (μm)	length (mm)	thickness (μm)
TIB layers 1-2	IB1	80	116.9	320
TIB layers 3-4	IB2	120	116.9	320
TOB layers 5-6	OB1	122	183.2	500
TOB layers 1-4	OB2	183	183.2	500
TID ring 1	W1A	81-112	85.2	320
TID ring 2	W2A	113-143	88.2	320
TID ring 3	W3A	123-139	110.7	320
TEC ring 1	W1B	81-112	85.2	320
TEC ring 2	W2B	113-143	88.2	320
TEC ring 3	W3B	123-158	110.7	320
TEC ring 4	W4B	113-139	115.2	320
TEC ring 5	W5B	126-156	144.4	500
TEC ring 6	W6B	163-205	181.0	500
TEC ring 7	W7B	140-172	201.8	500

total the strip detector contains 15148 modules housing 9.6 x 10^6 strips and contains a total of 14 sensor geometries (see Table 2.1).

When a charged particle passes through one of the tracking layers, the silicon medium becomes ionized and creates electron-hole pairs. The electric field induced in the medium due to the input voltage forces charge to accumulate on the pixel or strip sensor and then is read out by the readout chips in Analog-Digital Converter (ADC) counts. The readout is limited to 8 bits which allows for reading from 0-255 ADC counts. The final ADC count readouts (254, 255 counts) are used to indicate energy losses in the 254-1024 range and greater than 1024 ADC count range. A minimum ionizing particle at normal incidence results in $\approx$ 95 ADC counts for $\approx$ 300 μm thick silicon sensors. Saturation effects occur at $\approx$ 3 times MIP levels for the 320 μm thick strip sensors. Saturation effects occur at $\approx$ 2 times MIP levels for the 500 μm thick strip and the pixel sensors [37, 38]. The ADC counts are converted back to units of energy during data analysis.

2.2.2 The Muon Subdetector

As the outermost layer, the muon subdetector is the final piece of the CMS detector before a particle escapes. The muon subdetector is comprised of three different gas-ionizing technologies

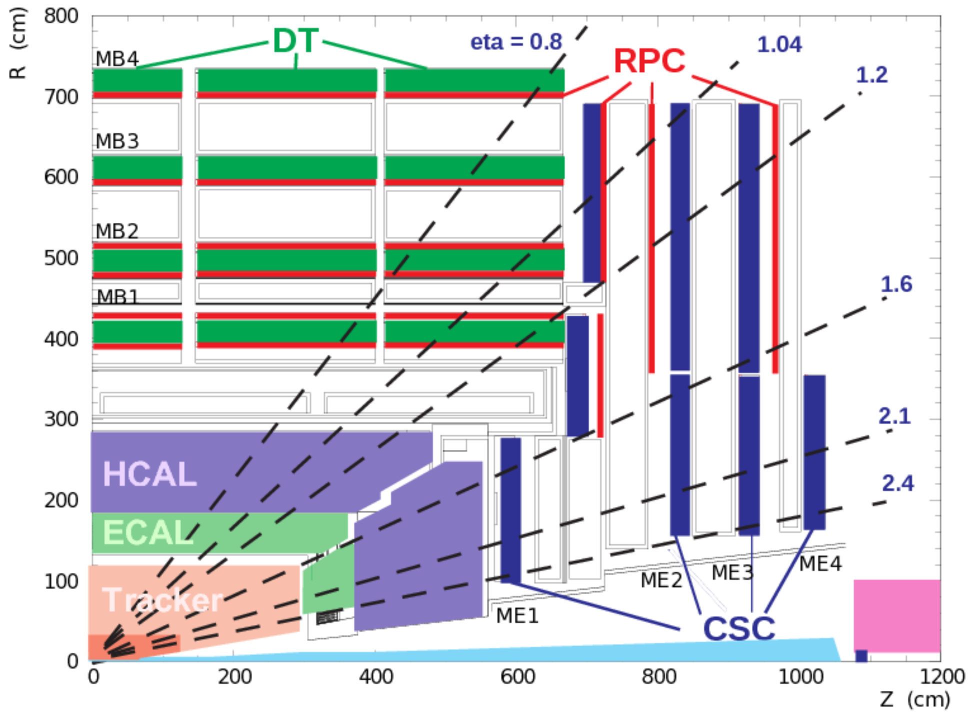

Figure 2.3: Cross section diagram of the different muon systems and their respective layouts. For reference, distances radially outward from the beam (r) and distances along the beam axis (z) are listed, as well as markings (dashed blue lines) indicated the η at which the various components sit. The drift tubes are in dark green, the resistive plate chambers are marked in red, and the cathode strip chambers are in dark blue.

within four active layers, with three steel return yoke layers, and a 2 Tesla magnetic field oriented in the opposite direction with respect to the inner solenoid. The muon subdetector provides measurements of position, momentum, and timing.

The barrel region of the muon detector is comprised of drift tubes and resistive plate chambers. The endcaps utilize cathode strip chambers and resistive plate chambers. The drift tubes within the outer layers have conducting wires parallel to the beam line while the inner layers wires run orthogonal allowing for position determination. The cathode strip chambers contain six planes of azimuthally oriented anode wires in between seven cathode strip panels. The resistive plate chamber modules consists of two gaps with a common set of readout strips in between [34]. Figure 2.3 shows a cross section diagram of the muon system and where the different technologies are located.

The signals used to track particle position throughout the muon system are obtained primarily by the drift tubes and cathode strip chambers due to their finer spatial resolution, while the resistive plate chambers' small timing resolution (< 3 ns) allows for accurate triggering (recording) of events. The resistive plate chambers also provide a coarser position measurement to supplement the drift tubes and cathode strip chambers. All three technologies work together to form a slight redundancy in measurements. Depending on the requirements of the particular analysis, the muon subdetector often works in conjunction with the tracker to identify muons and quantify their momentum and positions through the CMS detector.

2.2.3 Reconstruction

In order for physics analyses to be carried out, the information from the different subdetectors in a given bunch crossing (event) undergo a process known as event reconstruction. During reconstruction, the information recorded by the different subdetectors are used to recreate physical objects (e.g photons, electrons, etc.), assign them physical properties (e.g position, momentum, etc), and provide information about the event itself (e.g total energy, number of objects, etc). Reconstruction algorithms also produce objects known as jets, which represent the shower of particles produced during the hadronization of quarks or gluons.

The process of reconstruction differs depending on what object is being reconstructed, but in general the goal is to determine if the depositions of energy were created from the same object or were from different objects. In the case of this analysis, the focus is on tracks in the tracker and/or muon detectors.

2.2.4 Track Reconstruction

In the tracker, a track begins as a series of electric signals produced as a result of a charged particle interacting with the material of the tracker (rec hits). The rec hits that are above the minimal threshold (zero-suppression) are grouped together in clusters within each layer of the tracker. The cluster position is calculated from the clustering algorithm, and form the building blocks that make up a track.

Beginning with a "seed", a set of 2-3 inner clusters that can be aligned to form a helical curve, the tracking algorithm begins to extrapolate outward to determine which clusters in the subsequent tracking layers can be associated to which seed. It does this via the Combinatorial Tracking Finder

(CTF), which is a modified combinatorial Kalman Filter [39–42]. The CTF algorithm accepts or rejects clusters to add to the track by comparing a χ^2 value between the cluster and the path of the track. In the case of multiple hits near the fitted curve, the cluster with the smallest resulting χ^2 value is selected. After each cluster is added, the track is refit. The CTF algorithm also accounts for the particle energy loss through the tracking layers as it updates the track fit.

After the clusters are grouped into tracks, a final track fitting algorithm determines the best estimate of the parameters of the track. The tracks are then rejected based on loose quality control criteria (e.g number of hits, χ^2 of hits to fitted curve). The tracks passing the quality control are stored in a standalone collection, as well as being used as the building blocks for reconstructing other types of objects such as electrons [43]. Figure 2.4 shows the efficiency for reconstructing a track across a range of transverse momentum (see Sec. 3.1.3).

2.2.5 Muon Reconstruction

The muon detector reconstruction uses hits from the different layers of the muon chambers to reconstruct a track within the muon system, known as a "standalone" muon track. As a charged particle passes through a muon spectrometer, the gaseous medium is ionized and the corresponding signal amplitude and timing are recorded. In the case of a long lived particle, the calculated time of flight for the hit relies on the recorded time-of-flight to the spectrometer, the propagation time of the signal (e.g along the wire in a drift tube), and an off-time correction used in the case of slow moving particles (such as HSCPs).

The initial reconstruction uses the time-of-flight to the spectrometer and the propagation time to determine a trajectory between the various layers of the muon system. The off-time correction is then iterated over beginning at ≈ 0 for SM $\beta \approx 1$ particles and applied to the hits within the muon system. With the proper off-time corrections, the hits in the individual modules of the muon system align and produce a fit in agreement with a helical path. Without the off-time correction, a slow moving particle position within the muon system layers is reconstructed further away from the wire (drift tubes) or strips (cathode strip chambers) that produced the readout signal than the true position.

To further identify muons (or muon-like objects) the reconstruction combines tracks from the tracker and the standalone muon tracks into a single reconstructed object known as a global muon track. The combination can proceed two ways: the standalone track is matched with a tracker

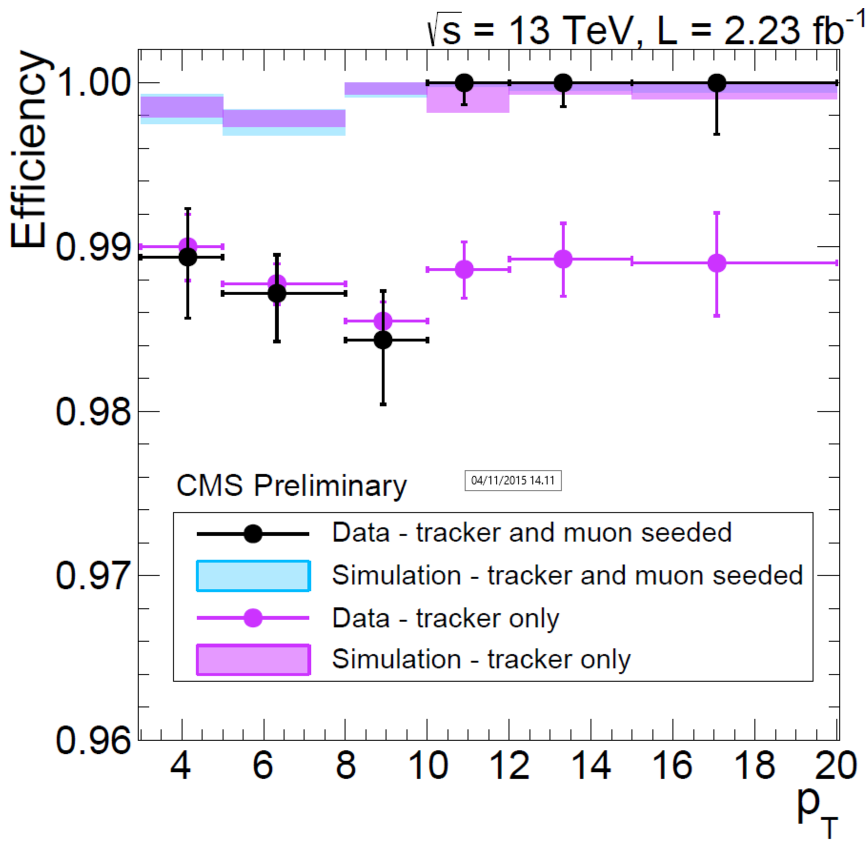

Figure 2.4: Track efficiency as a function of track p_T in GeV. Shown here are data (black and purple markers) as well as MC simulation (solid blue and purple). Differences in efficiency between tracker only tracks and tracks that also have a matched muon seed are also shown [44].

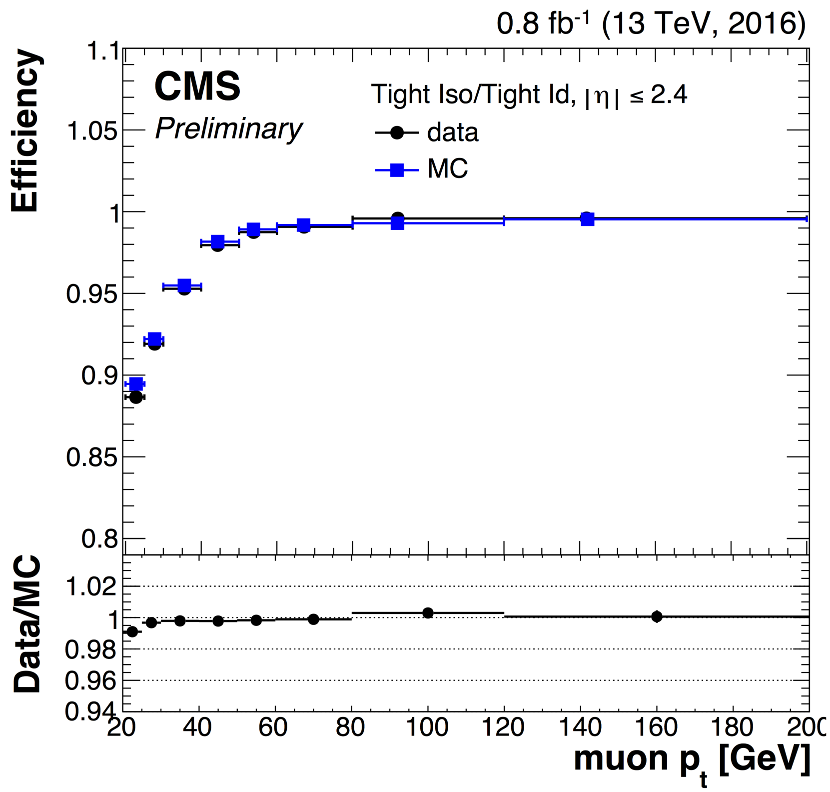

Figure 2.5: Muon reconstruction efficiency as a function of track p_T in 2016 data. The tracks are from well isolated reconstructed muons passing a tight quality control selection. Shown are efficiencies for both data (black) and a Z$\rightarrow \mu\mu$ MC sample (blue) [46].

track (outside-in) or a tracker track is matched with a standalone track (inside-out). The outside-in method is preferred since it takes into account all the hits coming from both of the input tracks to create a new global fit producing the global muon track, also known as a global muon. However the outside-in method has limitations especially in the lower p_T region, therefore the inside-out method is also used. In the inside-out method, a tracker track is extrapolated outward to the muon subdetector and if at least one hit in a muon chamber falls close enough to the extrapolated track, the hit (or hits) from the muon system are added to the tracker track to form a tracker muon. As seen in Fig. 2.5, the muon reconstruction algorithm is nearly fully efficient for both data and MC muons with p_T greater than approximately 50 GeV [45].

2.2.6 Missing Transverse Energy

For a given event, certain particles may be produced and leave the detector without causing a noticeable amount of energy deposition in the detectors. The predominant SM particle to do so is a neutrino. However, while such particles would remain directly unobserved, their presence can be inferred and indeed some information about them can be obtained. In an effort to do so, the experiment employs a variable known as Missing Transverse Energy (MET).

Within the CMS Experiment, MET ($\not{E}_{\mathrm{T}}$) is described as the magnitude of the imbalance in the transverse momentum of all visible particles within the detector (Eq. 2.1). For the purposes of this analysis, the concentration is on the quantity known as particle flow MET (PFMET) which utilizes all of the visible particles that are reconstructed using the PF algorithm, in contrast to the MET calculation using the energies found in the calorimeters.

$$\not{E}_{\mathrm{T}} = |\ \vec{\not{E}}_{\mathrm{T}}\ | = | - \sum_{i \in \mathrm{all}} \vec{p}_{\mathrm{T}i}| \tag{2.1}$$

where $\vec{p}_{\mathrm{T}i}$ are the transverse momentum vectors of all reconstructed particle flow objects (e.g electrons, jets, photons). Due to to systematics within various reconstruction algorithms that comprise the reconstructed particles, as well as the factors from the detector elements themselves (such as detector mis-alignments), corrections to the MET value are applied offline.

2.2.7 Triggering

With collisions happening at 25 nanosecond intervals, the LHC produces events at a rate of approximately 1 GHz. Due to the limitations in hardware and software required to reconstruct the information of an event, the current rate at which events can be recorded is roughly 400 Hz at the CMS detector. The selection of events to be recorded is accomplished through a combination of hardware and software based algorithms called triggers. The triggers select events containing physics deemed "interesting" to researchers, as opposed to the vast majority of events that contain physics that have historically been well and thoroughly studied (e.g. elastic collisions). The first stage of the triggering process is called level 1 (L1), followed by the high level trigger (HLT).

L1 triggers are algorithms utilizing hardware to make quick decisions about an event. At L1, the different subdetectors undergo a quick version of reconstruction without linking to one another. The L1 triggers bring produce an event passing rate of 100 kHz. From there, the HLTs utilize a streamlined version of the full offline event reconstruction to select which events to record. The HLTs bring down the event recording rate to the average 400 Hz currently used [47].

The specific triggers used in obtaining the data for this analysis are presented in the following chapter.

CHAPTER 3

STANDARD HSCP ANALYSES

The CMS collaboration has conducted HSCP searches during Run I at $\sqrt{s} = 7$ and 8 TeV and Run II at $\sqrt{s} = 13$ TeV. Each search looked for anomalous dE/dx and $1/\beta$ to select HSCP candidates from tracks with larger transverse momentum. Discovery and limit setting for different benchmark signals involved selecting on a mass calculated from the track dE/dx and momentum. The previous mass based HSCP analyses (the "standard" HSCP analyses) produced cross section and mass limits for the different benchmark signals.

3.1 Analyses Variables

The standard HSCP analyses rely heavily on how charged particles deposit energy as the particles pass through a substance, the rate per unit length of which is known as dE/dx. The Bethe formula provides an approximate description of dE/dx for the regions of $0.1 < \beta\gamma < 1000$ which for a muon corresponds to an approximate momentum range of 10 MeV to 100 GeV. For the regions outside of this range, other approximations are utilized as shown in Fig. 3.1. For the energies available at the LHC collisions, most SM particles are produced near the minimum ionizing level of $\beta\gamma \approx 5$ ($\beta = v/c, \gamma = 1/\sqrt{1-\beta^2}$), hence the focus for the standard HSCP analyses is the region covered by the Bethe formula,

$$\frac{dE}{dx} = Kz^2 \frac{Z}{A} \frac{1}{\beta^2} \left[\frac{1}{2} \ln \frac{2m_e c^2 \beta^2 \gamma^2 W_{max}}{I_{excitation}^2} - \beta^2 - \frac{\delta(\beta\gamma)}{2} \right], \tag{3.1}$$

where K = $4\pi N_A r_e^2 m_e c^2 = 0.307075$ MeV cm^2 / mol, Z and A are the atomic number and the molar mass of the material, z is the particle charge, m_e is the electron mass, $\delta(\beta\gamma)$ is a correction due to density effects, W_{max} is the max energy transfer in a collision between the particle and the electrons in the material, and $I_{excitation}$ is the mean excitation energy of the material.

Plotting the result of the Bethe formula as well as experimental data shows that as particle momentum drops below the point of minimum ionization, the energy loss increases quickly (Fig. 3.1).

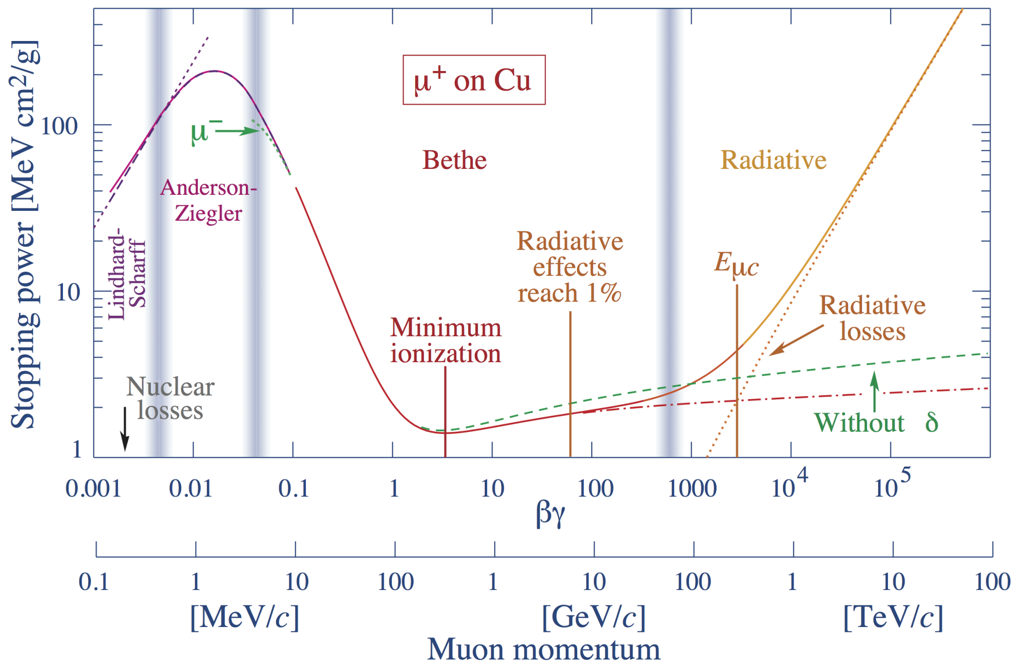

Figure 3.1: Stopping power versus momentum of a muon for copper. The solid lines represent experimental data, and the dotted lines represent the results of plotting the aforementioned approximations [48].

The HSCP analyses utilize this increased energy loss in identifying HSCP candidates by searching for tracks that create an anomalously large dE/dx when compared to SM particles.

3.1.1 dE/dx Estimate I_h

Though the HSCP analyses search for anomalous values of dE/dx compared to SM particles, the CMS detector does not directly record dE/dx for reconstructed tracks. It does however record the cluster level information about the hits that comprise the track. For each of the hit clusters (either pixel or strip), the total charge is converted from ADC counts to energy and is divided by the path length the particle traversed in the layer that housed the cluster. The path length is calculated from the fitted track and the known geometry of the various layers of the tracker.

The calculated energy loss per path length for each of the tracker clusters are used to estimate the dE/dx for each reconstructed particle (I_h with units of MeV/cm). The fluctuation of energy loss in the individual layers of the tracker follow a Landau distribution and due to the highly non-Gaussian nature of a Landau distribution, the mean value of the energy loss per path length in

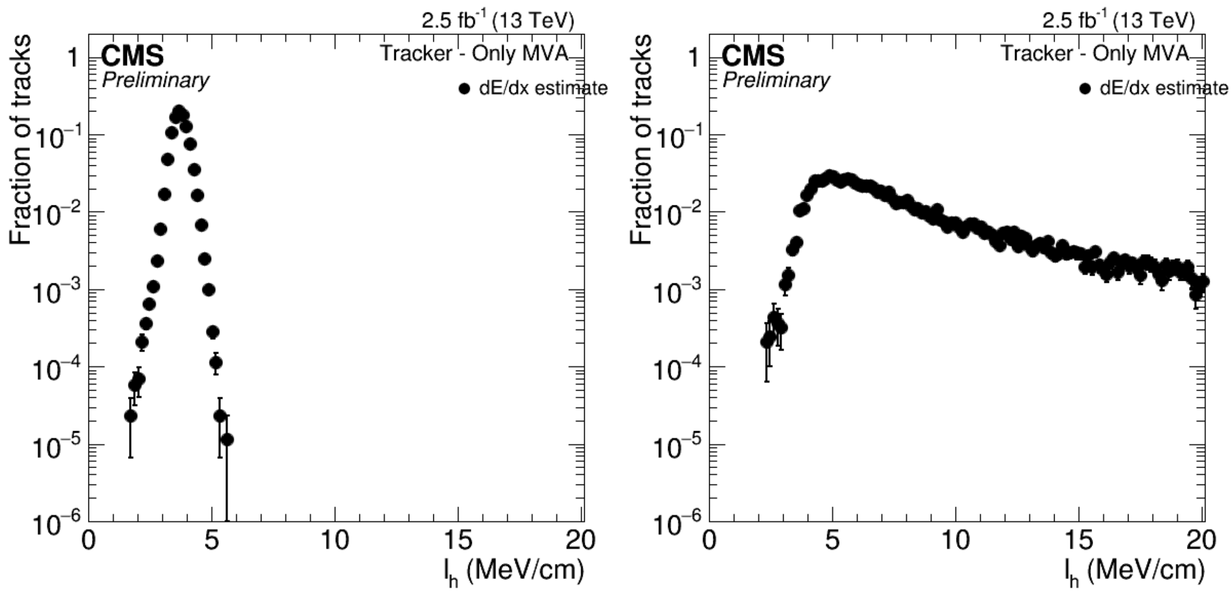

(a) SM Background MC

(b) Signal Sample MC

Figure 3.2: Distributions of the dE/dx estimation $\mathrm{I_h}$ for SM background (left) and a gluino mass = 1000 GeV MC sample (right).

the track clusters is not a suitable choice in estimating particle dE/dx. Instead, $\mathrm{I_h}$ is taken as the most probable value of dE/dx and is calculated by using the clusters along the track in the various layers of the tracker as inputs to a harmonic-2 estimator [49] of the form,

$$I_h = \left(\frac{1}{N_{85\%}} \sum_{i=1}^{N_{85\%}} c_i^{-2} \right)^{-1/2} . \tag{3.2}$$

Here the c_i is the i-th energy loss per unit path length and $\mathrm{N}_{85\%}$ denotes that the I_h estimation only uses the upper 85% of hits with respect to their charge values. The exclusion of the lower valued tracker hits in the estimation reduces the influence of instrumental bias within the tracker. A comparison of the $\mathrm{I_h}$ distribution for SM particles and a HSCP samples are shown for MC simulations in Fig. 3.2.

3.1.2 dE/dx Discriminant $\mathrm{I_{as}}$

In addition to using the dE/dx estimator ($\mathrm{I_h}$), the HSCP analysis relies on a discriminant variable $\mathrm{I_{as}}$. The value of $\mathrm{I_{as}}$ indicates how likely the energy deposition in each layer of the tracker is due to a MIP versus an HSCP. To calculate $\mathrm{I_{as}}$, the hits along the track are compared with those

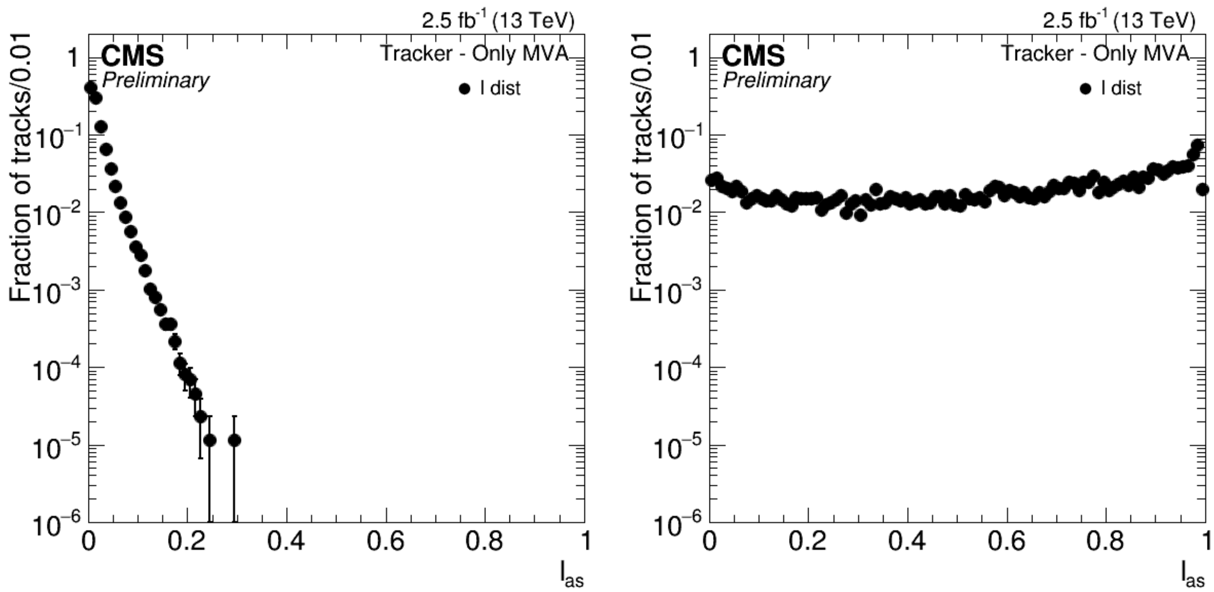

(a) SM Background MC

(b) Signal Sample MC

Figure 3.3: Distributions of $\mathrm{I_{as}}$ for SM background MC (left) and a gluino mass = 1000 GeV MC sample (right).

of MIPs and the track hits are assigned a value of the probability (P_i) that a MIP produces a charge equal to or less than the measured charge in that i-th layer. These probabilities are obtained by comparing the track hits in each layer against templates for the charge depositions amongst the tracker layers created by MIPs. The P_i is calculated for each measurement along the track path and summed according to:

$$I_{\mathrm{as}} = \frac{3}{N}\left(\frac{1}{12N} + \sum_{i=1}^{N}\left[P_i\left(P_i - \frac{2i-1}{2N}\right)^2\right]\right), \tag{3.3}$$

where N is the number of measurements comprising the track. By construction, the resulting discriminant $\mathrm{I_{as}}$ tends towards 0 for MIPs and toward higher values for HSCPs, as shown in Fig. 3.3 for SM and a signal MC sample. This leads to better discrimination between SM MIPs and HSCPs compared to $\mathrm{I_h}$.

3.1.3 Momentum and Transverse Momentum

The determination of a reconstructed particle momentum depends on the method by which the particle was reconstructed. For instance, the momentum measurement of a charged particle is

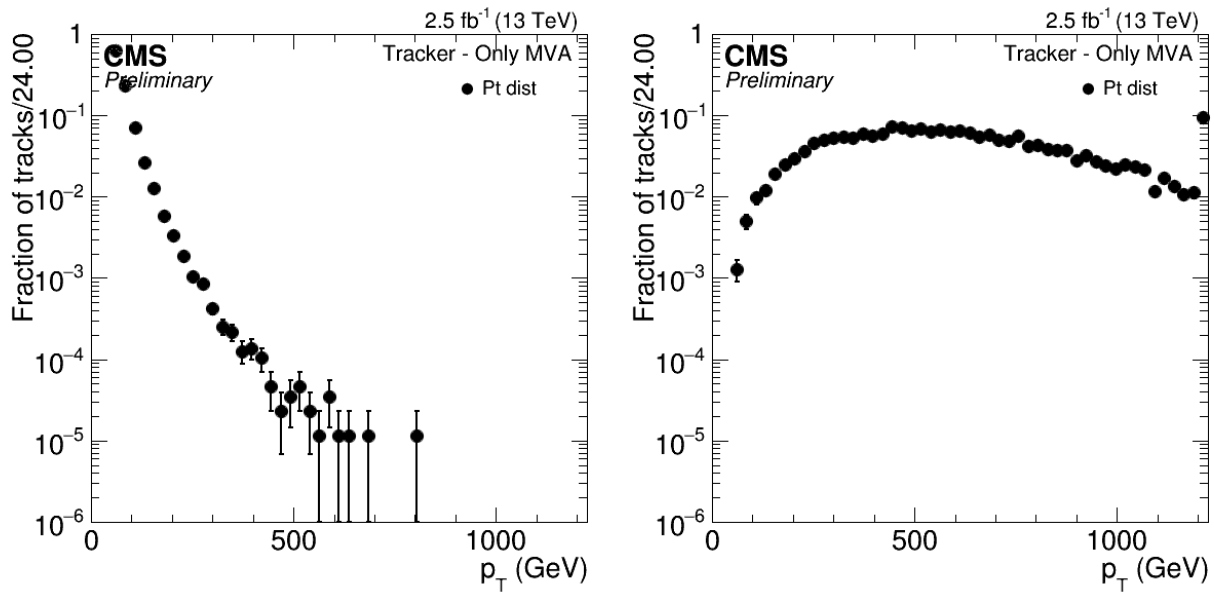

(a) SM Background MC

(b) Signal Sample MC

Figure 3.4: Distributions of p_T for SM background MC (left) and a gluino mass = 1000 GeV MC sample (right).

determined from the curvature of the track associated with the particle. For a neutral particle such as a photon, the momentum measurement is approximated by its energy, and thus the measurements from the calorimeters are used. In the case of an HSCP, the momentum is taken by measuring the curvature of the HSCP path. In this research, the reconstructed HSCP paths are either from the fits due to tracks in the tracker if a muon was not reconstructed or from the fit of global muon tracks if a muon was reconstructed. Once the final path has been fitted, the reconstruction algorithm determines the radius of curvature of the fitted path and, assuming a helical curve with charge equal to 1 electron charge ($|Q|$=1e), an estimation of the true momentum is obtained.

Potential HSCP candidates are selected from tracks with transverse momentum, p_T, greater than 55 GeV. Transverse momentum is the component the momentum in the x-y plane. The magnitudes of momentum and transverse momentum are related by $p = p_T \cosh \eta$. Figure 3.4 shows the p_T distributions of SM and signal MC samples.

3.1.4 Time-of-Flight

The Time-of-Flight (TOF) of a candidate is used in the Tracker+TOF analysis. Due to the large mass and lower overall momentum, HSCPs should arrive at the various subdetectors later than their SM counterparts. In order to eliminate the path length dependance within TOF values, the HSCP analyses utilize an estimate of reconstructed $1/\beta$. SM particles travel at nearly the speed of light, c, and have $\beta \approx 1$.

The β of a particle is related to the off-time correction (δ_t) of the signals within the DT and CSC chambers by

$$\frac{1}{\beta} = 1 + \frac{c\delta_t}{L} \tag{3.4}$$

with L being the distance travelled from the interaction point to the muon spectrometer. The final value of $1/\beta$ is calculated as a weighted average of the individual $1/\beta$ measurements along the reconstructed path.

In the CSCs of the muon system, the weights used in the $1/\beta$ calculation are determined in each measurement by:

$$w_i = \frac{d_i^2}{\sigma_i^2}. \tag{3.5}$$

where, d_i is the distance to the i-th measurement and σ_i is the time resolution for the CSC detectors which is 7.0 ns for the cathode strips and 8.6 ns for the anode wires.

For the DTs, the weight in each of the measurements is given by:

$$w_i = \frac{(n-2)d_i^2}{n\sigma_i^2}. \tag{3.6}$$

In Eq.3.6, the time resolution (σ_i) for the DT measurements is 3.0 ns, and n is the number of measurements used to determine δ_t. The (n-2)/n form accounts for the two parameter straight line calculation used to determine δ_t. Shown in Fig. 3.5, SM particles are reconstructed with a peak $1/\beta \approx 1$ and the $1/\beta$ distribution for HSCPs tails out to larger values.

3.1.5 Mass

The mass of an unknown particle can be determined through the relationship,

$$I_h = K\frac{m^2}{p^2} + C, \tag{3.7}$$

where K and C are empirically determined constants. The values of K and C are extracted from fits of Eq. 3.7 to low momentum tracks from data and simulation. The values for K and C for both 2015 and 2016 are listed in Table 3.1. As can be seen in Fig. 3.6, the resulting values of K and C create a mass distribution from I_h and p that contains excesses at the kaon, proton, and deuteron masses.

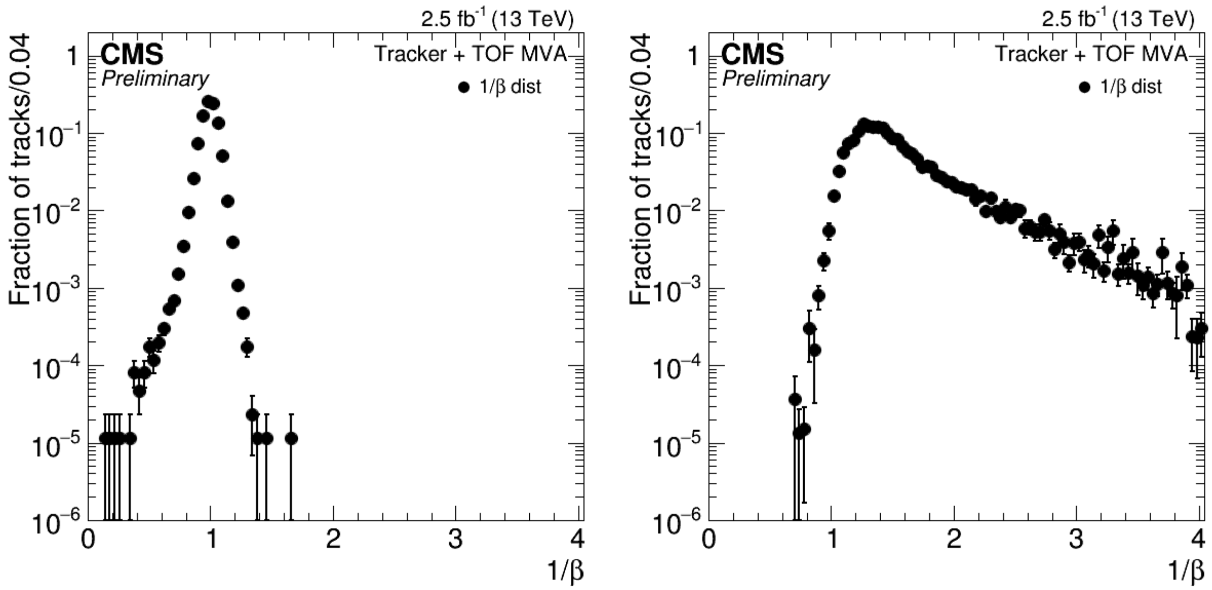

(a) SM Background MC

(b) Signal Sample MC

Figure 3.5: Distributions of $1/\beta$ for SM background MC (left) and a gluino mass = 1000 GeV MC sample (right).

Table 3.1: Values of K and C used in 3.7 for 2015 and 2016 data and MC samples. For each year, the K and C values were derived from mass line fits applied to low momentum tracks from data.

Year	K (MeV/cm)	C (MeV/cm)
Data 2015	2.68	3.38
Data 2016	2.68	3.92
MC 2015	2.54	3.34
MC 2016	2.94	3.20

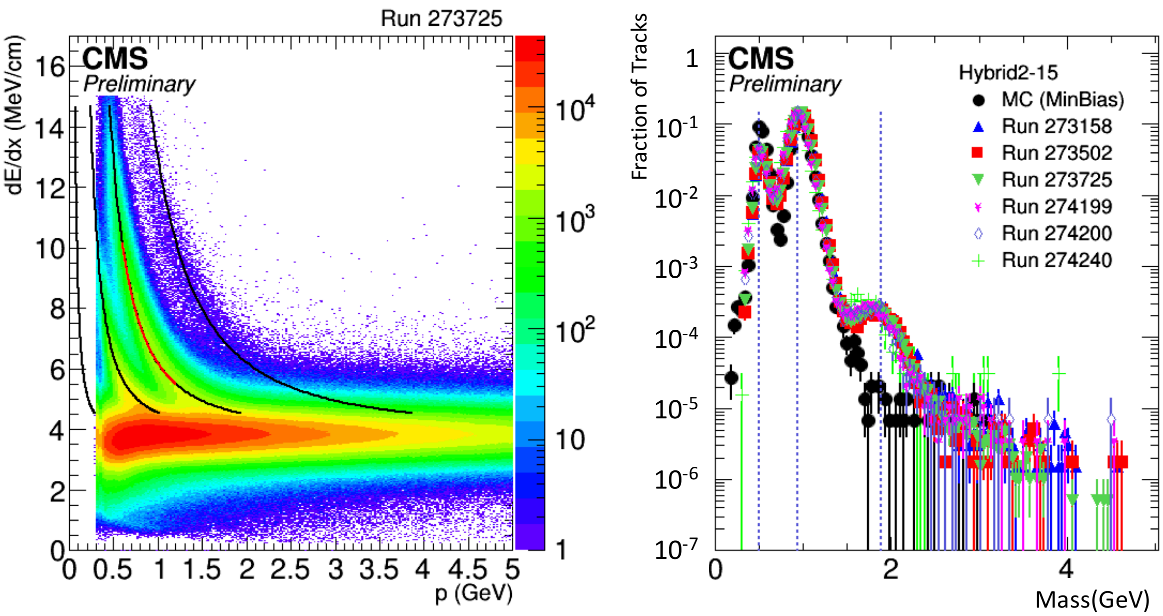

Figure 3.6: Left: Distribution of dE/dx versus momentum for low momentum tracks. The color scale represents the number of tracks present along the dE/dx and momentum ranges. The black lines represent different mass hypotheses for the pion, kaon, proton, and deuteron (left to right). Right: Distribution of mass calculated with Eq. 3.7 for several data runs and SM simulation of minimum bias collisions. For convenience, vertical lines have been drawn for the kaon, proton, and deuteron masses. The deuteron mass does not appear for the minimum bias MC sample as it was not included as part of the simulation.

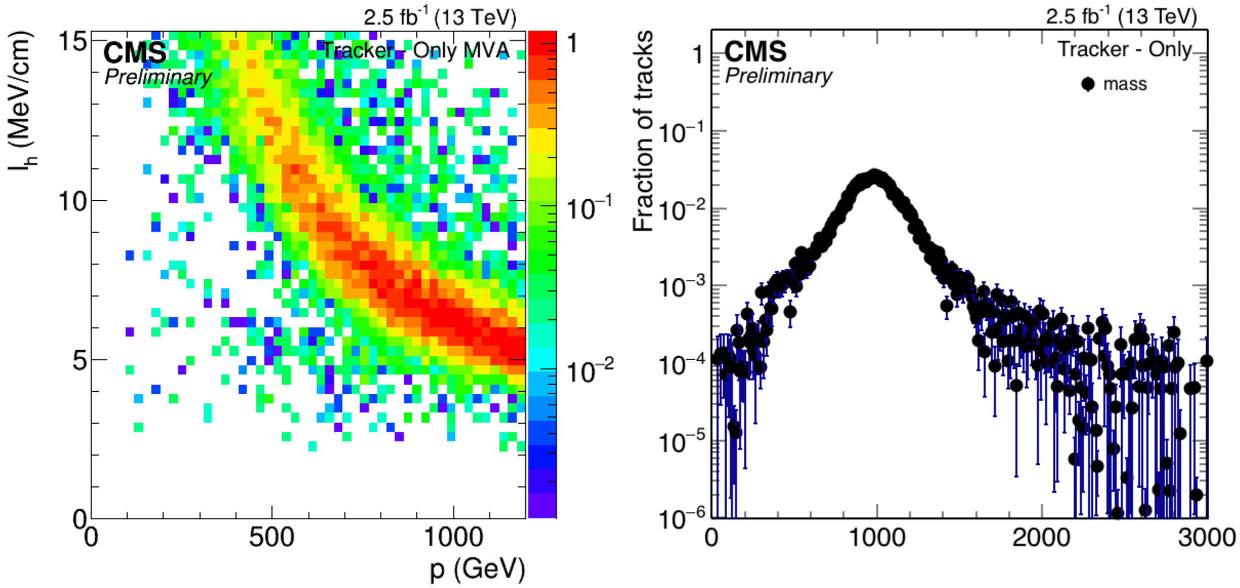

(a) I_h vs p (b) mass

Figure 3.7: Distributions of the dE/dx estimate (I_h) versus momentum for SM background MC (left) and the calculated mass distribution (right) for a gluino mass = 1000 GeV MC signal sample.

3.2 Simulation Samples

The properties of the BSM benchmark signals (gluinos, stops, staus, modified DY) and their signature in the CMS detector are investigated via Monte Carlo (MC) simulations. For all of the signal samples, the HSCPs are set as stable particles.

In the case of R-hadron production, PYTHIA 8.153 [50], with the underlying event tune CUETP8M1 [51] was used to produce MC samples of stops and gluinos with masses between 100-2600 GeV. Different fractions of gluinos hadronizing into a gluino-gluon state were modeled. The different fractions (10% and 50% denoted f10 and f50) will affect the fraction of neutral R-hadrons that are produced. Furthermore, an additional model for charge suppression (CS) was produced for both gluino and stop R-hadrons.

For the each of the stau production models (GMSB and PP), PYTHIA 6.4 [52] with the Z2* tune [53] was used. In the minimal Gauge Mediated Supersymmetry Breaking model, Snowmass Points and Slopes (SPS) 7 slope [54] was used to create the stau as the next-to-lightest supersymmetric particle, and ISASUGRA [55] v.7.69 was used to generate the mass spectrum and decay tables. The energy scale at which supersymmetry breaking occurs was varied between 31 to 510

TeV, with fixed $N_{mes} = 3$, $\tan\beta = 10$, $\mu > 0$, $C_{grav} = 10000$, and $M_{mes}/\Lambda = 2$ SUSY parameters. This resulted in a range of long lived staus with masses between 100-1600 GeV.

The Modified DY samples were also produced with PYTHIA 6.4 with the Z2* tune. Masses range from 100-2600 GeV, but with two charges, $|Q|$=1e and $|Q|$=2e. All of the signal MC signal samples were produced by the CMS MC central production group.

For the background, SM private simulations without pileup were generated by the HSCP group due to a bug that affected the simulated dE/dx for the centrally produced background samples. However, since the background samples are only used for control purposes in testing the data-driven background method (mentioned later in this chapter), the lack of pileup in the private simulations does not affect their usage. The SM background samples are comprised of DY $\rightarrow \mu\mu$ + jets and W $\rightarrow l\nu$ + jets.

3.3 Data

As mentioned in the introduction, the HSCP analyses within the CMS collaboration have been carried out using both the 2015 and 2016 $\sqrt{s} = 13$ TeV data. For both data collection years, the single muon, double muon, and MET datasets were used corresponding to data that had satisfied a single muon trigger, double muon, or MET trigger. Not all of the luminosity blocks (one luminosity block is roughly 2 minutes of data taking) are deemed to be of acceptable quality for use in physics analysis. The listing of which luminosity blocks have been examined and deemed acceptable are contained in the so-called Java Script Object Notation (JSON) files. The files used for 2015 and 2016 are listed in Table 3.2. The 2015 data correspond to 2.5 fb^{-1} of integrated luminosity and the 2016 data correspond to 12.9 fb^{-1}. The 2016 data used in this research covered Runs 273158 to 276811 and was not the complete 2016 dataset. These runs cover the same data as the most current 2016 CMS HSCP results as presented in Ref. [18].

3.3.1 Analysis Triggers

The specific events used from the 2015 and 2016 data within the HSCP analyses are required to have satisfied at least one of the following triggers: Mu45_eta2p1, Mu50, PFMET170_NoiseCleaned, or PFMET170_HBHECleaned (2016 data only). HSCPs should either manifest with the same signature as a muon or as MET within the detector. The specified triggers had the lowest threshold

Table 3.2: The JSON files used for running over the 2015 and 2016 datasets

Data Year	JSON filename
2015	Cert_246908-260627_13TeV_PromptReco_Collisions15_25ns_JSON_Silver_v2.txt
2016	Cert_246908-260627_13TeV_PromptReco_Collisions15_25ns_JSON_Silver_v2.txt

for their respective type of trigger without being prescaled to less than 1; prescaling being the ratio of events triggered to those recorded.

The Mu45_eta2p1 and Mu50 triggers require that the high level trigger reconstruction find at least one muon whose p_T is greater than 45 and 50 GeV respectively. In the case of the Mu45_eta2p1, the muon passing the p_T requirement must further be found in the $|\eta| \leq 2.1$ region of the muon system to limit the event recording rate. The Mu50 trigger accepts muons from the entire $|\eta| \leq 2.4$ coverage of the muon system.

The PFMET170 trigger requires an event to have MET $\geq$ 170 GeV during the high level trigger reconstruction. The "NoiseCleaned" aspect refers to the fact that the MET value is taken after two processes were applied: JetId cleaning and HBHE cleaning. The JetId cleaning involves the removal of low quality jets from the HLT MET calculation. The HBHE cleaning removes HCAL towers that had a larger than desired noise level from the HLT MET calculation. However, for the 2016 data collection, the PFMET170_NoiseCleaned trigger was deactivated and replaced with the PFMET170_HBHECleaned trigger which follows the same algorithm, but without the JetId cleaning applied.

Each type of benchmark HSCP particle (R-hadrons, or lepton-like) should fall into 3 categories: charged throughout, neutral, or particles that undergo charge exchange. The muon triggers are designed to be sensitive to the lepton-like HSCPs and R-hadrons that remain charged throughout the detector. The PFMET trigger assists in the search for HSCPs that do not properly reconstruct for the muon trigger such as R-hadrons that undergo charge exchange. R-hadrons that undergo charge exchange have two general scenarios. First, the R-hadron may be produced charged after hadronization, interact with the tracker layers causing hits to be registered, and then undergo charge exchange. If a charged R-hadron becomes neutral between the tracker and the muon system, a high

Table 3.3: 2016 Trigger Efficiencies for various benchmark signal samples.

Signal Model	Mu50	PFMET170	Total
Gluino M 1000 GeV	24.1%	23.7%	42.1%
Gluino M 1600 GeV	13.2%	33.4%	41.8%
GMSB Stau M 308 GeV	95.1%	0.7%	96.1%
GMSB Stau M 871 GeV	84.1%	5.3%	90.3%
PP Stau M 308 GeV	92.5%	1.2%	92.6%
PP Stau M 871 GeV	84.1%	7.8%	85.4%

p_T track would be reconstructed without a corresponding muon track nor corresponding energy in the calorimeters. The HLT reconstruction will record the track, but reject it for further use in the particle flow algorithm. The rejected track would not contribute to the MET calculation, thus increasing the value of the resultant MET. The R-hadron can be produced neutral and undergo charge flipping to produce a track in the muon system. Because the MET algorithm does not include stand-alone muons, the R-hadron will increase the calculated MET. A summary of the trigger efficiencies for various signal models is given in Table 3.3 for the dominant Mu50 and PFMET170 triggers. Also included is a total trigger efficiency that indicates the additional efficiency that the Mu45_eta2p1 trigger provides. As can be seen in Table 3.3, for the lepton-like HSCPs, the majority of the trigger efficiency is a result of the muon trigger. For the hadron-like HSCPs, the muon trigger and the MET trigger both add to the overall trigger efficiencies, with the MET trigger becoming the more efficient as the signal mass increases.

For the purposes of this research, the 2015 dataset was used for testing the MVA HSCP analysis. The larger 2016 dataset was used to produce final conclusions for this research.

3.4 Standard HSCP Analysis

The standard HSCP analyses that have been conducted by the CMS collaboration have been selection based analyses. Potential discovery of HSCPs was done by selecting on I_{as} and p_T for the tracker-only and I_{as}, p_T, and $1/\beta$ for the Tracker+TOF analysis. Additionally, mass selection is used for both analyses. The process by which the analyses obtain their final selection and place limits on benchmark HSCP signals can be seen as 4 key steps: HSCP candidate reconstruction and pre-selection, background estimation, final selection, and limit setting. The following is an overall summary of the standard HSCP analyses found in Refs. [17, 18] upon which the HSCP MVA analyses are based.

3.4.1 HSCP Candidate Reconstruction and Preselection

HSCP candidates are created from tracker tracks or global muons from events passing one of the analysis triggers. The creation of an HSCP candidate involves recording its track parameters, isolation values, and muon timing properties for the Tracker+TOF analysis.

Preselection applies a loose quality control on the HSCP candidates to ensure that the HSCP candidate tracks are of good quality. The preselection values are such that the effect on signal efficiency is minimal compared to the effect on SM particles, as can be seen in Figs. 3.8 and 3.9. The η and p_T selection are $|\eta| > 2.1$ and $p_T > 55$ GeV. The p_T requirement is higher than the minimum required to pass the muon trigger to ensure the trigger is fully efficient.

Track quality criteria are applied with the goal that reconstructed HSCP candidate tracks are of sufficient quality that their p_T value and the calculated dE/dx value are reliable. The transverse displacement (d_{xy}) and longitudinal displacement (d_z) of the track to the closest vertex ensure that the track is compatible with a good quality primary vertex. The track is required to have a relative uncertainty on its p_T measurement (σ_{p_T}/p_T) less than 10%. The track fit is required to be of sufficient quality by placing a requirement of chi squared per degree of freedom ($\chi^2/ndof$) less than five on the fit. Requiring that at least one pixel hit and more than seven strip hist are associated with the track ensures the track has sufficient points of measurement. In addition, at least 80% of the hits along the track must be valid. The tracks are required to be well isolated by requiring the sum of the p_T of all other tracks within a cone of a given radius of 0.3 in η and ϕ ($R(\eta, \phi) = \sqrt{\Delta\eta^2 + \Delta\phi^2}$) be less than 50 GeV. The sum of the energy of the calorimeters within the same $\Delta R\,(\eta, \phi) < 0.3$ cone is required to be less than 30% of the HSCP candidate momentum, $(E_{cal}/p) < 0.3$. The isolation requirements are to eliminate tracks that have been reconstructed in an area of high activity that may produce overlapping hits.

In order to ensure the quality of the calculated dE/dx value, the track clusters undergo a shape test and the track is required to contain at least five clusters that pass the shape test. The shape test filters clusters whose energy deposition is inconsistent with that of a single particle, for example

Table 3.4: The preselection criteria applied to the HSCP candidate tracks for the tracker-only and Tracker+TOF analyses. All of the criteria in the upper portion are applied to both analyses. The bottom portion are only applied to the Tracker+TOF analysis.

Variable	value
$\|\eta\|$	< 2.1
p_T	> 55 GeV
d_z	< 0.5 cm
d_{xy}	< 0.5 cm
$\sigma_{pT}/p_{\mathrm{T}}$	0.25
Track $\chi^2/ndof$	< 5
# Pixel Hits	> 1
# Strip Hits	> 7
Fraction of Valid Hits	> 0.8
$\sum p_T^{trk}\,(\Delta R < 0.3)$	< 50 GeV
$E_{cal}\,(\Delta R < 0.3)\,/p$	< 0.3
dE/dx Strip Shape Test	yes
# of dE/dx Measurements	> 5
Tracker+TOF only	
# of TOF Measurement	> 7
$\sigma_{1/\beta}/1/\beta$	< 0.15
$1/\beta$	> 1

clusters created by two or more particle passing through a layer in close proximity. In the case of multiple particles passing through a tracker layer in close proximity, the tracker rec hits from the different particles could be grouped into a single cluster and the result would have a dE/dx larger than that of an average minimum ionizing particle. The shape test checks if the cluster only has a single maximum and that the adjacent strips contain energies in the correct proportions consistent with a charged particle passing through one or two strips. The energy “leak” of a signal from the maximum strip into its neighbors comes as a result of capacitive coupling between the silicon strips and is called “cross-talk.” Only the clusters that pass the shape test are used in the final calculation of dE/dx for that track.

For the Tracker+TOF analysis, the preselection includes all of the aforementioned selection criteria with the addition of requiring the muon track have greater than seven measurements entering the $1/\beta$ calculation. The $1/\beta$ estimate itself is required to be greater than 1, and with a relative uncertainty $\sigma_{1/\beta}/1/\beta$ less than 0.15. The selection variables and their values are listed in Table 3.4.

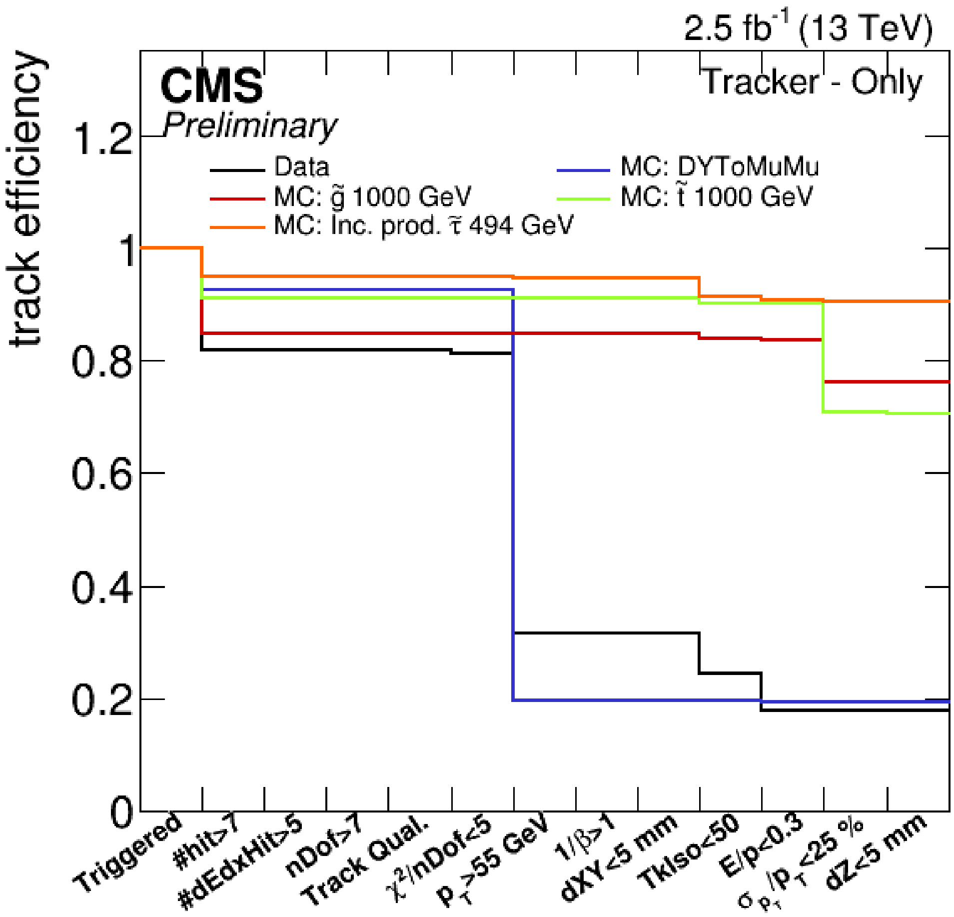

Figure 3.8: Efficiency of tracks passing the various preselection criteria for the tracker-only analysis for data (black), SM MC (blue), and gluino, stop, and GMSB stau signal MC.

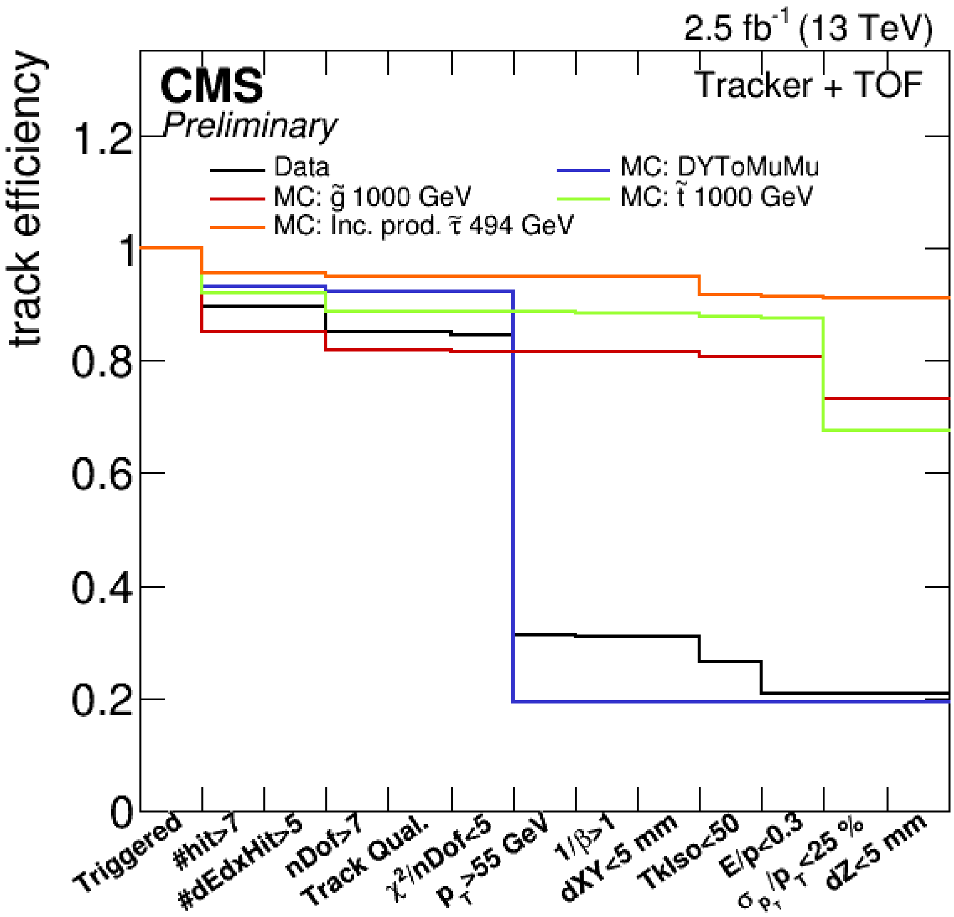

Figure 3.9: Efficiency of tracks passing the various preselection criteria for the Tracker+TOF analysis for data (black), SM MC (blue), and gluino, stop, and GMSB stau signal MC.

Table 3.5: The efficiencies for HSCP candidates that pass the trigger requirement to pass the remaining preselection criteria for a selection of signal models.

Model	mass(GeV)	Tracker only	Tracker+TOF
Gluino	1000	0.762	0.732
Gluino	1600	0.532	0.504
Gluino	2000	0.215	0.204
Stop	1000	0.707	0.676
Stop	1600	0.451	0.420
Stop	2000	0.196	0.142
GMSB Stau	494	0.955	0.910
GMSB Stau	871	0.920	0.920
GMSB Stau	1599	0.649	0.647
PP Stau	494	0.947	0.939
PP Stau	871	0.914	0.939
PP Stau	1599	0.636	0.654
DY $\vert Q\vert = 1e$	600	0.903	0.908
DY $\vert Q\vert = 1e$	1000	0.894	0.892
DY $\vert Q\vert = 1e$	1400	0.761	0.757
DY $\vert Q\vert = 2e$	600	0.840	0.841
DY $\vert Q\vert = 2e$	1000	0.697	0.687
DY $\vert Q\vert = 2e$	1400	0.496	0.476

The preselection efficiencies for the tracker-only and Tracker+TOF analyses for a selection of the benchmark signal samples are given in Table 3.5.

3.4.2 Background Estimation

In the case of the HSCP analysis, the main source of background is detector related mismeasurements of SM particles due to SM particles with anomalously large dE/dx. The background estimate for the HSCP analysis is a "data-driven" background estimate, (i.e. MC simulation is not used to produce it, only to validate). This is accomplished by the "ABCD" method [56], where the data is divided up into different regions based on selection criteria. In a two dimensional (x_1 and x_2) example, the phase space is divided up into four regions A, B, C, and D using two selection values v_1 on x_1 and v_2 on x_2. A contains entries that fail both selection, regions B and C contains entries that pass v_1 and v_2 respectively while failing the other, and region D contains entries that pass both selection. There are two key assumptions in this method: (1) the signal region (D) is

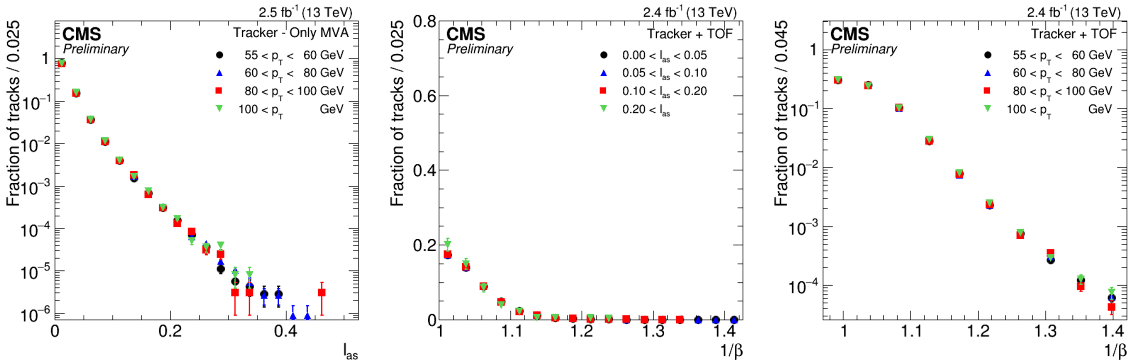

(a) p_T and I_{as} (b) TOF and I_{as} (c) TOF and p_T

Figure 3.10: a) The distribution of p_T in different regions of I_{as} for data that passed the preselection criteria. b) The distribution of TOF in different regions of I_{as} for data that passed the preselection criteria. c) The distribution of TOF in different regions of p_T for data the passed the preselection criteria. In all three cases, the agreement of the distributions between the different regions for each of the respective plots shows the non-correlation of the variables.

where the desired signal is located with negligible amounts of signal in the other regions, and (2) the input variables used in the selection criteria are independent of each other.

As seen in Fig. 3.10, the selection variables I_{as} and $\mathrm{p_T}$ and $1/\beta$ are shown to be non-correlated in the data by taking slices in one variable and comparing the distribution of the remaining variable(s). The data can be divided up into 4 (8) regions for the 2 (3) selection variables used in the tracker-only (Tracker+TOF) analysis. Table 3.6 shows the naming scheme used in the HSCP analyses for different regions.

By using data outside of the signal region (which should be the background by construction)

Table 3.6: The labeling scheme for the regions used in the data-driven background prediction. For the tracker-only analysis the $1/\beta$ selection is not used.

I_{as}	p_{T}	tracker-only	$1/\beta$	Tracker+TOF
fail	fail	A	pass	A
pass	fail	B	pass	B
fail	pass	C	pass	C
pass	pass	D	pass	D
fail	fail	–	fail	E
pass	fail	–	fail	F
fail	pass	–	fail	G
pass	pass	–	fail	H

and extrapolating into the region of interest, a background estimate can be made. The background estimate uses the ratio of the number of candidates within the background regions,

$$\begin{aligned} \frac{N_A}{N_B} &= \frac{N_C}{N_D} \\ N_{D_{estimate}} &= \frac{N_B N_C}{N_A} \end{aligned} \tag{3.8}$$

where N_A, N_B, and N_C, are the observed number of entries in regions A, B, and C, while $N_{D_{estimate}}$ is the resulting background estimation for region D. In the case of the Tracker+TOF analysis, $1/\beta$ is included as a third dimension. The additional regions allows multiple ratio combinations to compute a background estimate. Due to the lower statistical uncertainty, the D region estimate in the Tracker+TOF analysis is given by

$$N_{D_{estimate}} = \frac{N_A N_G N_F}{{N_E}^2}. \tag{3.9}$$

The background distributions are created using the regions adjacent to the signal region (e.g. B and C) to create a probability distribution of the values for each of the mass calculation input variables, p and I_h. From each distribution, all combinations of p and I_h are used to create a background prediction of the mass distribution (Eq. 3.7) for background events. The bin contents of the input variable distributions are varied 100 times according to a Poisson distribution peaked at the original bin content. Each of the varied input distributions are used to create a background mass distribution. The mass distributions are averaged and the resulting mean mass distribution is renormalized to the estimated number of background predicted by the ABCD method. The renormalized mean is used as the final data-driven background distribution. The mass distribution for the background prediction can be seen in Figs. 3.11 and 3.12 as the "Data-based SM prediction."

3.4.3 Final Selection

After the preselection, final selection criteria are applied to the HSCP candidates. The selection criteria determine the candidates entering the observed mass distribution as well as those used to create the estimated background mass distribution. The analysis searches for a statistically significant excess over the background estimate in the signal region. The final selection criteria on I_{as} and $1/\beta$ reduce the amount of background as much as possible while retaining signal efficiency

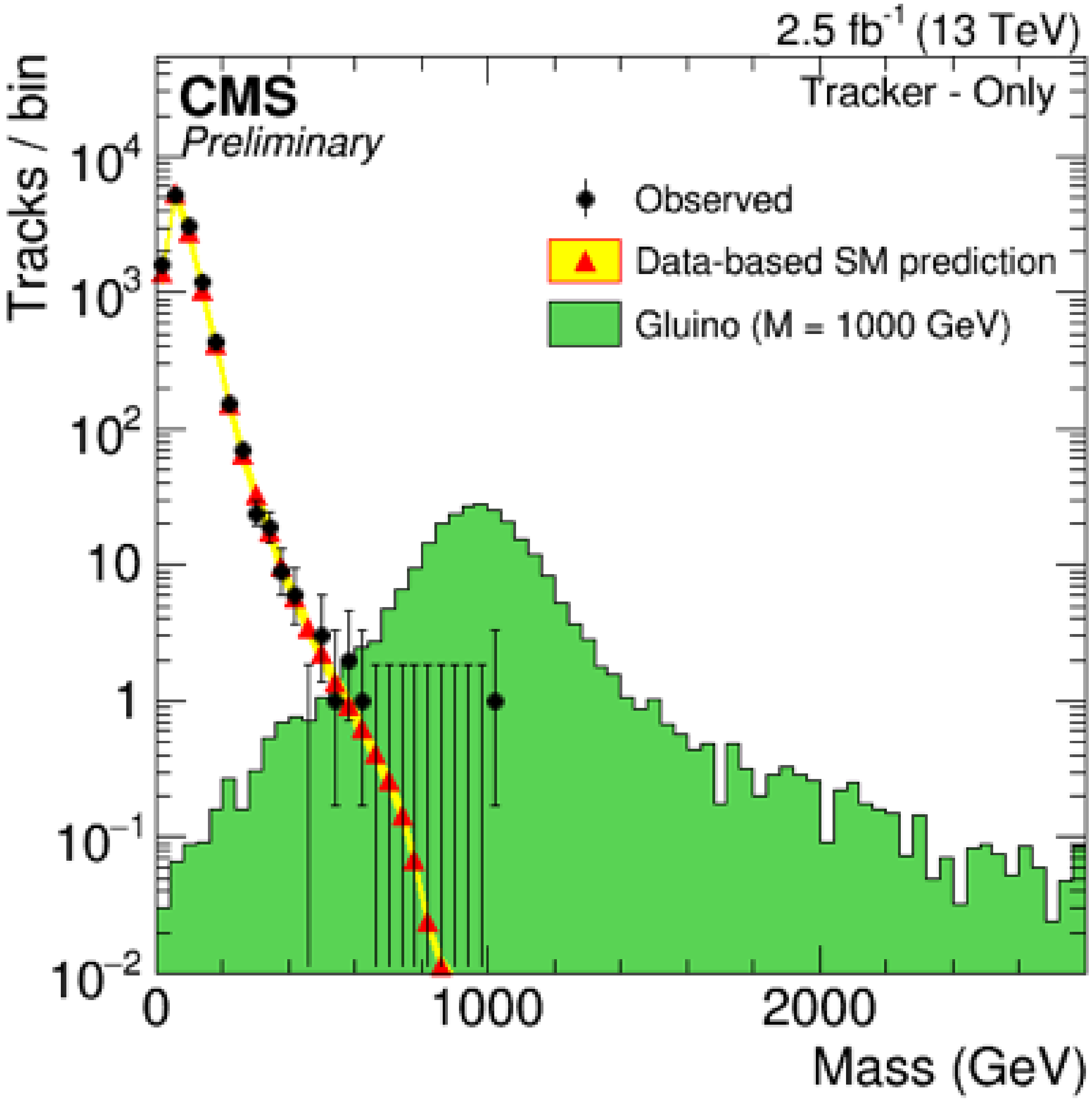

Figure 3.11: Mass distribution of HSCP candidates that pass the loose final selection criteria in the tracker-only analysis for 2015 data. Shown in green is the mass distribution for candidates from a simulated sample of gluino mass = 1000 GeV that pass the loose final selection. The yellow and red distribution shows the masses from background prediction with the yellow band representing the uncertainty on the background prediction. The black markers are the data that pass the loose final selection.

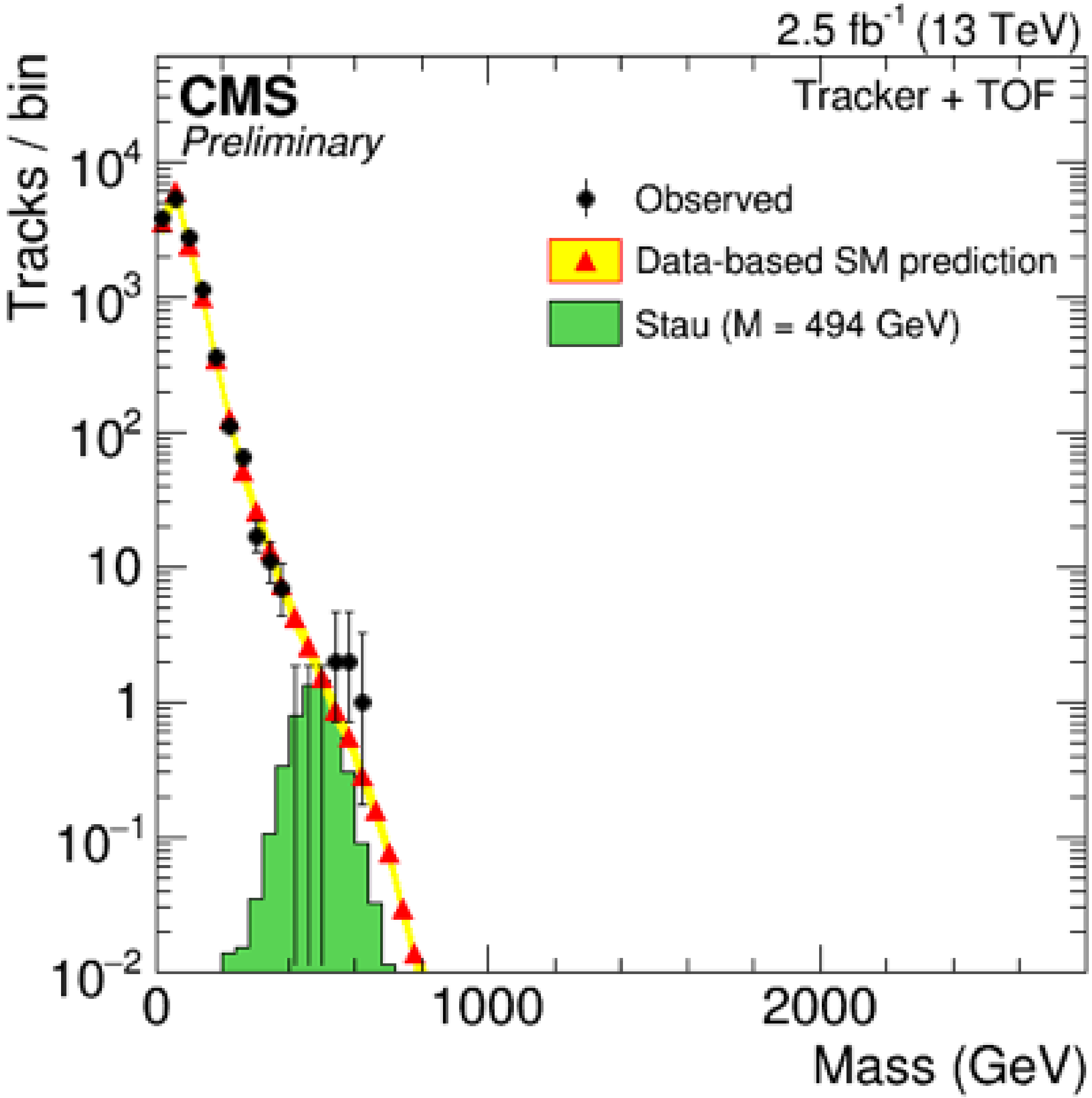

Figure 3.12: Mass distribution of HSCP candidates that pass the loose final selection criteria in the Tracker+TOF analysis for 2015 data. Shown in green is the mass distribution for candidates from a simulated sample of GMSB stau mass = 494 GeV that pass the loose selection. The yellow and red distribution shows the masses from background prediction with the yellow band representing the uncertainty on the background prediction. The black markers are the data that pass the loose selection.

Table 3.7: The loose and tight selection criteria used for both the 2015 and 2016 HSCP tracker-only and Tracker+TOF analyses.

tracker-only		
Selection Variables	loose value	tight value
I_{as}	0.1	0.3
p_T	60 GeV	65 GeV
mass	—	0 - 400 GeV
Tracker+TOF		
Selection Variables	loose value	tight value
I_{as}	0.05	0.175
p_T	60 GeV	65 GeV
$1/\beta$	1.05	1.25
mass	—	0 - 400 GeV

across the signal models and therefore selection was not optimized for one particular signal model. Two sets of selection value are used in the analysis: one loose and one tight. The loose selection criteria are used as a control to monitor the behavior of the data-based SM prediction. The tight criteria are used for final analysis. Additionally, a mass selection is included with the tight selection and is varied from 0 to 400 GeV in 100 GeV intervals to search for an observed excess (Table 3.7). The mass distributions resulting from applying loose and tight selection (without the mass selection) for the tracker-only and Tracker+TOF analyses are shown in Figs. 3.11 and 3.12. Table 3.8 lists the number of observed and predicted events for the final selection criteria in the tracker-only and Tracker+TOF analyses using the 2015 data. The 2016 data will be presented in Chapter 4. Summary tables listing the results using data from 2015 for the standard HSCP analyses are given in Tables 3.9 to 3.12. No statistically significant excess is found in the number of observed data versus the background prediction therefore no evidence of HSCPs is claimed. Restrictions on the benchmark theories are made by placing limits on the observed and expected production cross sections.

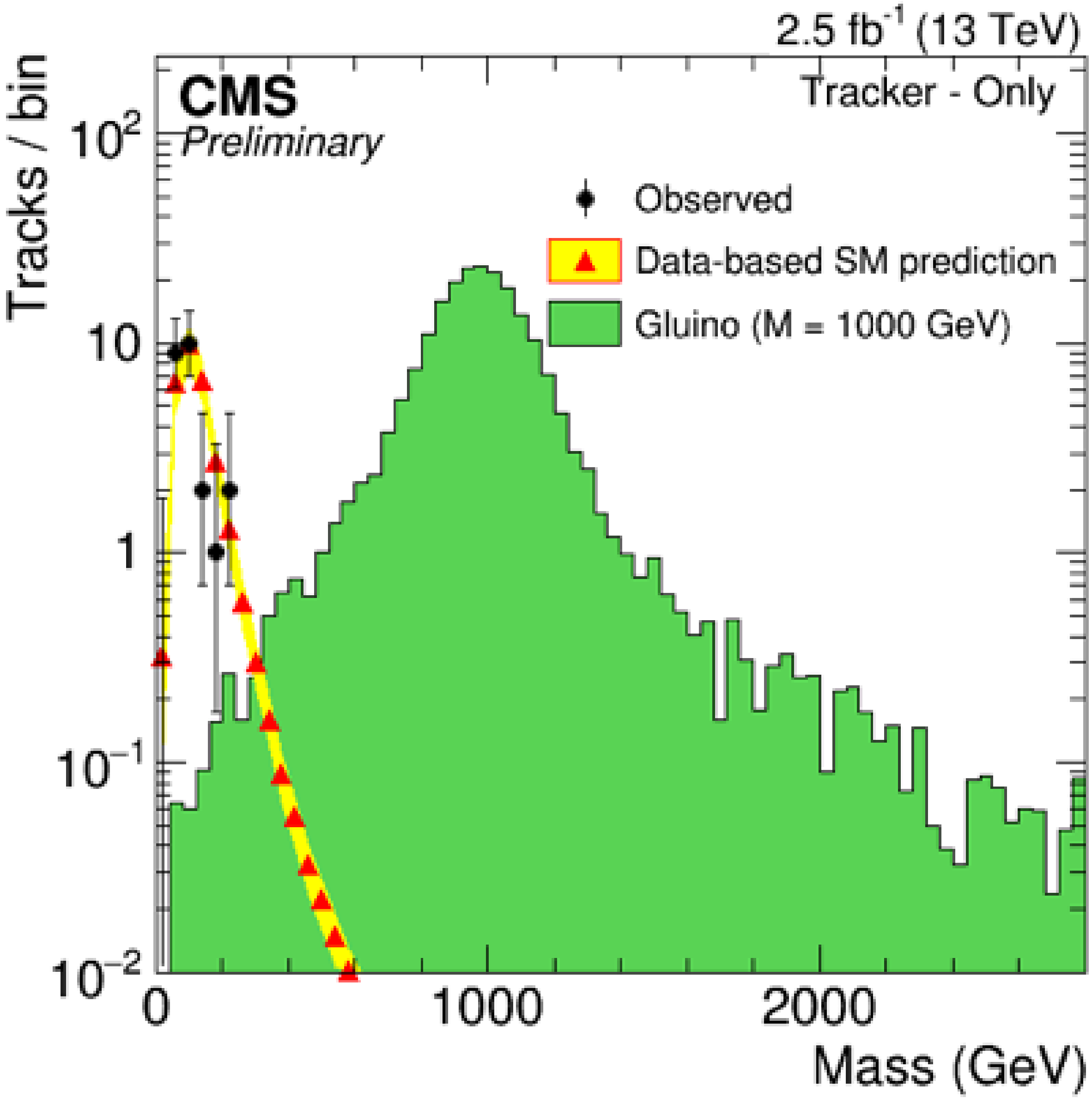

Figure 3.13: Mass distribution of HSCP candidates that pass the final tight selection criteria in the tracker-only analysis using 2015 data. Shown in green is the mass distribution for candidates from a simulated sample of gluino mass = 1000 GeV that pass the final tight selection. The yellow and red distribution shows the masses from background prediction with the yellow band representing the uncertainty on the background prediction. The black markers are the data that pass the final tight selection.

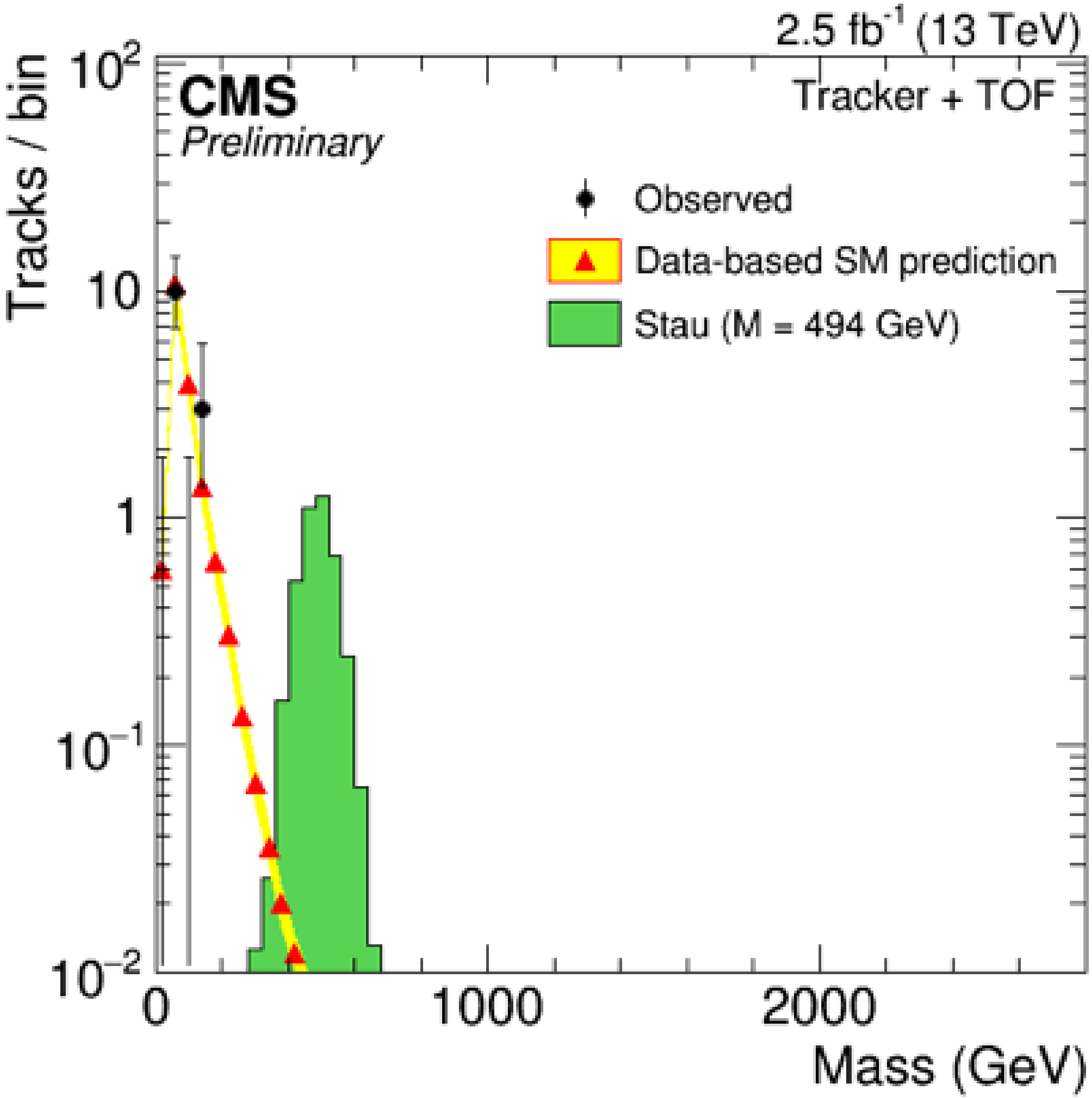

Figure 3.14: Mass distribution of HSCP candidates that pass the tight final tight selection criteria in the Tracker+TOF analysis for 2015 data. Shown in green is the mass distribution for candidates from a simulated sample of GMSB stau mass = 494 GeV that pass the final tight selection. The yellow and red distribution shows the masses from background prediction with the yellow band representing the uncertainty on the background prediction. The black markers are the data that pass the final tight selection.

Table 3.8: Selection criteria for the tracker-only and Tracker+TOF with the number of predicted and observed events in 2015 data.

Analysis	Selection				Number of events	
	p_T (GeV)	I_{as}	$1/\beta$	Mass (GeV)	Predicted	Observed
tracker-only	65	0.3	—	0	28.7± 6	24
	65	0.3	—	100	20.7± 4.4	15
	65	0.3	—	200	3.8± 0.8	2
	65	0.3	—	300	0.82± 0.18	0
	65	0.3	—	400	0.25± 0.05	0
Tracker+TOF	65	0.175	1.250	0	18.2± 3.7	14
	65	0.175	1.250	100	5.4± 1.1	4
	65	0.175	1.250	200	5.4± 0.19	0
	65	0.175	1.250	300	0.06± 0.04	0
	65	0.175	1.250	400	0.01± 0.00	0

Table 3.9: Summary of the theoretical cross section (ThXsec), expected cross section limit at 95% CL (ExpXsec), and observed cross section limits at 95% CL (ObsXsec) for a range of gluino signal mass points for the tracker-only analysis using 2015 data. The limits were produced using 2015 data and tight final selection. Included are the selection criteria (p_T, I_{as}, $1/\beta$, and Mass), as well as the signal efficiency (Seff), number of predicted background (Bckg. Pred), and observed data (obs) that pass the selection criteria. Shown are f = 10%,50% for gluino models including the the charged suppressed interaction models (denoted with an N).

Model	Mass (GeV)	$p_T >$ (GeV)	$I_{as} >$	$1/\beta >$	Mass> (GeV)	Bckg. Pred	Obs	Seff	ThXsec (pb)	ExpXsec (pb)	ObsXsec (pb)
Gluino f=0.1	800	65	0.3	—	350	0.435 ± 0.093	0	0.223	1.5	5.5E-3	5.5E-3
Gluino f=0.1	1200	65	0.3	—	590	0.046 ± 0.010	0	0.220	8.4E-2	5.6E-3	5.6E-3
Gluino f=0.1	1600	65	0.3	—	720	0.017 ± 0.004	0	0.166	8.0E-3	7.5E-3	7.5E-3
Gluino f=0.1	2000	65	0.3	—	770	0.012 ± 0.003	0	0.112	9.7E-4	1.1E-2	1.1E-2
Gluino f=0.5	800	65	0.3	—	340	0.491 ± 0.105	0	0.129	1.5	9.5E-3	9.5E-3
Gluino f=0.5	1200	65	0.3	—	580	0.050 ± 0.011	0	0.127	8.4E-2	.9.7E-3	9.7E-3
Gluino f=0.5	1600	65	0.3	—	710	0.018 ± 0.004	0	0.096	8.0E-3	1.3E-2	1.3E-2
Gluino f=0.5	2000	65	0.3	—	760	0.013 ± 0.003	0	0.063	9.7E-4	2.0E-2	2.0E-2
GluinoN f=0.1	600	65	0.3	—	250	1.690 ± 0.369	0	0.141	1.5	5.5E-3	5.5E-3
GluinoN f=0.1	1200	65	0.3	—	590	0.050 ± 0.011	0	0.183	8.4E-2	5.6E-3	5.6E-3
GluinoN f=0.1	1600	65	0.3	—	680	0.023 ± 0.005	0	0.142	8.0E-3	7.5E-3	7.5E-3
GluinoN f=0.1	2000	65	0.3	—	670	0.024 ± 0.005	0	0.099	9.7E-4	1.1E-2	1.1E-2

Table 3.10: Summary of the theoretical cross section (ThXsec), expected cross section limit at 95% CL (ExpXsec), and observed cross section limits at 95% CL (ObsXsec) for a range of stop signal mass points for the tracker-only analysis using 2015 data. The limits were produced using 2015 data and tight final selection. Included are the selection criteria (p_T, I_{as}, $1/\beta$, and Mass), as well as the signal efficiency (Seff), number of predicted background (Bckg. Pred), and observed data (obs) that pass the selection criteria. Shown are stop models including the charged suppressed interaction models (denoted with an N).

Model	Mass (GeV)	$p_T >$ (GeV)	$I_{as} >$	$1/\beta >$	Mass> (GeV)	Bckg. Pred	Obs	Seff	ThXsec (pb)	ExpXsec (pb)	ObsXsec (pb)
Stop	600	65	0.3	—	40	28.700 ± 6.030	24	0.266	1.7E-1	2.4E-2	1.8E-2
Stop	1000	65	0.3	—	320	0.632 ± 0.136	0	0.260	6.0E-3	4.7E-3	4.7E-3
Stop	1800	65	0.3	—	660	0.026 ± 0.06	0	0.163	4.6E-5	7.4E-3	7.4E-3
Stop N	600	65	0.3	—	90	22.500 ± 4.710	16	0.169	1.7E-1	3.1E-2	2.3E-2
Stop N	1000	65	0.3	—	320	0.632 ± 0.136	0	0.195	6.0E-3	7.4E-3	6.1E-3
Stop N	1800	65	0.3	—	550	0.063 ± 0.014	0	0.124	4.6E-5	9.9E-3	9.9E-3

Table 3.11: Summary of the theoretical cross section (ThXsec), expected cross section limit at 95% CL (ExpXsec), and observed cross section limits at 95% CL (ObsXsec) for a range of stau signal mass points for the Tracker+TOF analysis using 2015 data. The limits were produced using 2015 data and tight final selection. Included are the selection criteria (p_T, I_{as}, $1/\beta$, and Mass), as well as the signal efficiency (Seff), number of predicted background (Bckg. Pred), and observed data (obs) that pass the selection criteria. Shown are the GMSB and PP stau production modes.

Model	Mass (GeV)	$p_T >$ (GeV)	$I_{as} >$	$1/\beta >$	Mass> (GeV)	Bckg. Pred	Obs	Seff	ThXsec (pb)	ExpXsec (pb)	ObsXsec (pb)
GMSB Stau	308	65	0.175	1.25	130	0.081 ± 0.016	0	0.431	2.5E-2	2.9E-3	2.9E-3
GMSB Stau	494	65	0.175	1.25	260	0.008 ± 0.002	0	0.592	1.9E-3	2.1E-3	2.1E-3
GMSB Stau	651	65	0.175	1.25	380	0.002 ± 0.000	0	0.662	4.1E-4	1.9E-3	1.9E-3
PP Stau	200	65	0.175	1.25	40	0.924 ± 0.187	0	0.242	8.0E-3	7.1E-3	4.9E-3
PP Stau	308	65	0.175	1.25	110	0.130 ± 0.026	0	0.315	1.5E-3	3.9E-3	3.9E-3
PP Stau	494	65	0.175	1.25	230	0.013 ± 0.003	0	0.415	1.9E-4	3.0E-3	3.0E-3

Table 3.12: Summary of the theoretical cross section (ThXsec), expected cross section limit at 95% CL (ExpXsec), and observed cross section limits at 95% CL (ObsXsec) for a range of modified Drell-Yan signal mass points for the Tracker+TOF analysis using 2015 data. The limits were produced using 2015 data and tight final selection. Included are the selection criteria (p_T, I_{as}, $1/\beta$, and Mass), as well as the signal efficiency (Seff), number of predicted background (Bckg. Pred), and observed data (obs) that pass the selection criteria. Shown are the modified DY $|Q| = 1e$ and $|Q| = 2e$ models.

Model	Mass (GeV)	$p_T >$ (GeV)	$I_{as} >$	$1/\beta >$	Mass> (GeV)	Bckg. Pred	Obs	Seff	ThXsec (pb)	ExpXsec (pb)	ObsXsec (pb)
DY $\|Q\| = 1e$	400	65	0.175	1.25	210	0018 $\pm$ 0.004	0	0.417	7.3E-3	3.1E-3	3.1E-3
DY $\|Q\| = 1e$	600	65	0.175	1.25	350	0.002 $\pm$ 0.000	0	0.461	1.2E-3	2.8E-3	2.8E-3
DY $\|Q\| = 1e$	800	65	0.175	1.25	480	0.001 $\pm$ 0.000	0	0.485	2.6E-4	2.6E-3	2.6E-3
DY $\|Q\| = 2e$	400	65	0.175	1.25	90	0.230 $\pm$ 0.188	0	0.409	2.3E-2	3.0E-3	3.0E-3
DY $\|Q\| = 2e$	600	65	0.175	1.25	200	0.021 $\pm$ 0.047	0	0.481	3.5E-3	2.7E-3	2.7E-3
DY $\|Q\| = 2e$	800	65	0.175	1.25	300	0.004 $\pm$ 0.004	0	0.487	8.0E-4	2.6E-3	2.6E-3

3.4.4 Limit Setting

The final step in the HSCP analysis involves setting limits on the various benchmark signal models. The tool used in the limit setting is known as the Higgs combined limit setting tool [57]. The Higgs combined limit setting tool takes as inputs the signal efficiency and its relative uncertainty, the background event estimate and its relative uncertainty, and the number of observed data that pass the final selection criteria. The final mass selection used for the background estimate, the observed data, and the MC signal simulation is calculated for each signal model as $\mu - 2\sigma$, where μ is the mean of the calculated mass distribution for the signal model simulation, and σ is the standard deviation.

The estimated background is obtained from the data-driven background procedure described earlier in Sec. 3.4.2, and the signal efficiency is obtained from the HSCP candidates extracted from the MC samples. The tool produces an expected and observed upper cross-section limit on the particular signal model. Figure 3.15 shows the observed upper cross section limits along with the theoretical cross sections for several benchmark signal types as functions of mass for the standard tracker-only and Tracker+TOF analysis. The limit setting tool places cross section limits at the 95% confidence level (CL) using the CL_s method [58, 59] where the statistical significance p-value is computed utilizing a profile likelihood technique [60]. The nuisance parameters in the likelihood technique are inputted as lognormal [61, 62], and correspond to the uncertainties on the integrated luminosity, the signal acceptance, and the background estimation. The HSCP multivariate analyses share several systematic uncertainties with the standard HSCP analyses, therefore the systematic uncertainties will be discussed in the following chapter. The upper cross section limits on different benchmark signal models are listed in Tables 3.9 to 3.12.

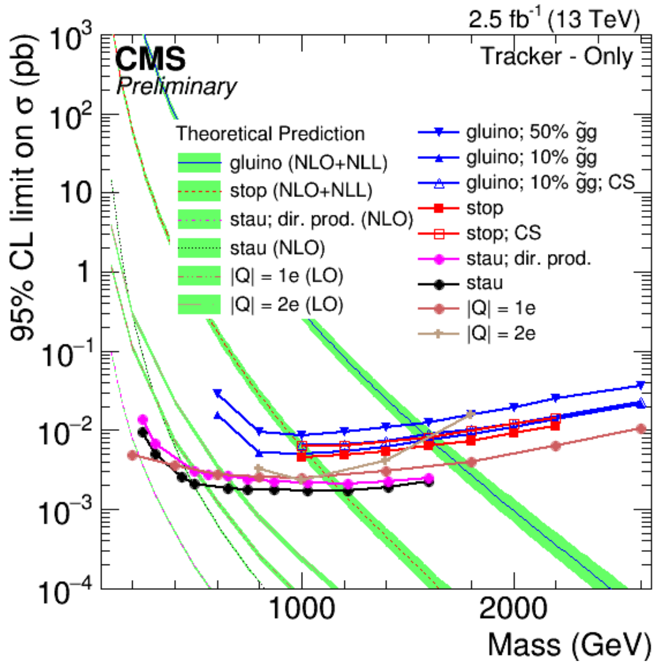

(a) 2015 tracker only

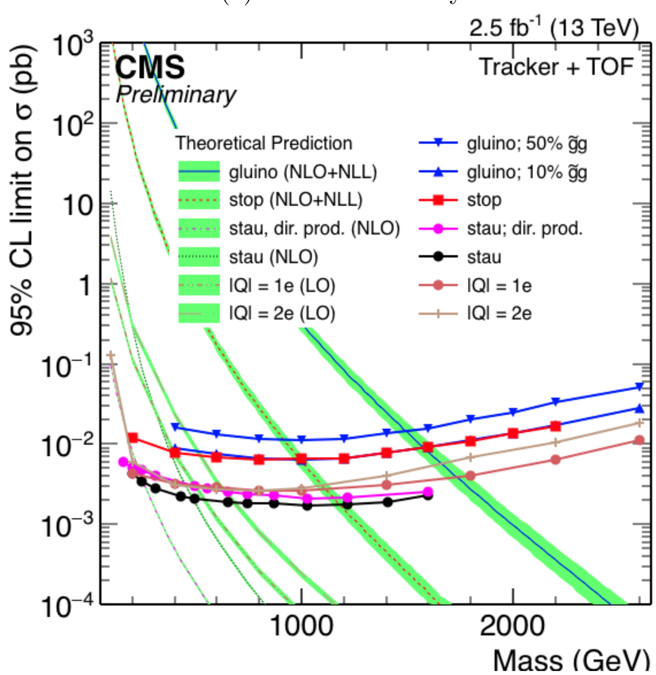

(b) 2015 Tracker+TOF

Figure 3.15: Observed (solid lines) cross section limits and theoretical (green uncertainty bands) cross sections as function of mass for several benchmark HSCP signal models. The cross sections from the tracker-only (a) and Tracker+TOF (b) analyses are presented.

CHAPTER 4

MULTIVARIATE HSCP ANALYSES

The HSCP multivariate based analyses use an artificial neural network in place of the calculated particle mass for data selection. The mass calculation only relies on the I_h and the reconstructed momentum. The average SM particle produces $I_h \sim 3$ MeV/cm for high momentum tracks. Yet normal fluctuations can allow for SM particles to produce I_h values more comparable to an HSCP, and cause a larger reconstructed mass. The motivation for an HSCP multivariate analysis is the ability to have multiple variables characterize the SM particles and HSCPs to make a search that is less sensitive to fluctuations in I_h. The development of the HSCP multivariate analyses utilized the 2015 data and the CMS software environment (CMSSW) version 7.4.15. The 2016 data was used as a final comparison test against the standard HSCP analyses and used CMSSW version 8.0.24.patch1. The multivariate versions of the tracker-only and Tracker+TOF analyses will be denoted as tracker-only+MVA and Tracker+TOF+MVA.

4.1 Artificial Neural Network

For the purposes of this research, the artificial neural network utilized exists in the ROOT data analysis framework. The specific artificial neural network used is the default TMlpANN and belongs to the MultiLayer Perceptron class of artificial neural network [63]. MultiLayer Perceptrons are feed forward networks meaning that the information from input nodes to hidden nodes to output node is only propagated in one direction, as opposed to recurrent networks which allow for the passing of information backwards within the hidden layers causing the organizational structure of the network to be dynamic. A properly trained artificial neural network with good background and signal discrimination will output a multivariate discriminant value with background at lower values and signal at larger values.

With respect to the structure of the artificial neural network used in this research, there are two variables that determine the behavior of the artificial neural network: the number of hidden layers, and the number of hidden nodes per layer. A single hidden layer is sufficient to approximate a given continuous correlation function to any precision, provided there are enough hidden nodes in that hidden layer [63]. The trade off of using a larger number of hidden nodes is the computation time required for training and utilization increases. Therefore, though a more optimal configuration may be possible, due to the relatively small number of inputs, a single hidden layer was chosen. A starting point is the use of 2-3 hidden nodes per input. As seen in Fig. 4.1, the difference in results due to training on an artificial neural network configured with 10, 15, or 20 hidden nodes was negligible. Therefore, while not optimized, 10 hidden nodes in 1 hidden layer were chosen as the artificial neural network configuration throughout the rest of the study. The Broyden-Fletcher-Goldfarb-Shannon method [64–67] was used for the training method.

4.2 Multivariate HSCP analysis

4.2.1 Artificial Neural Network Training and Testing

Training of the artificial neural network mappings to be incorporated in the HSCP multivariate analyses utilized a small subset of signal MC samples (Sec. 3.2) and a TOY background sample. For this research, TOY indicates that a background sample was produced from data events, and not generated via MC nor is raw collision data. The TOY background samples were created via a technique similar to the ABCD method the standard analysis utilizes to create the background prediction mass distribution. The TOY background samples were created from the entire 2.5 fb^{-1} 2015 dataset. The input variables to the artificial neural network were η, p_T, and I_{as} for the tracker-only+MVA analysis. The Tracker+TOF+MVA analysis used $1/\beta$ as an additional input. The input variables were separated into bins of η (bin width = 0.1), and randomly sampled within the respective η bin. Combinations from the sampling that fell into the D region were used to create a distribution that approximates the data.

Figures 4.2 and 4.3 show the agreement for the tracker only analysis between the TOY background and 2015 data for the input variables for the tracker-only+MVA and Tracker+TOF+MVA analyses respectively. Both background and data were required to pass the final loose selection. The primary benefit of utilizing the TOY data is that the training sample is no longer restrained to the number of data events, as well as reducing any bias the artificial neural network may develop due to the existence of true signal appearing in data. Furthermore, it allows testing the artificial neural network mappings on the true data without testing on the same sample that was used in

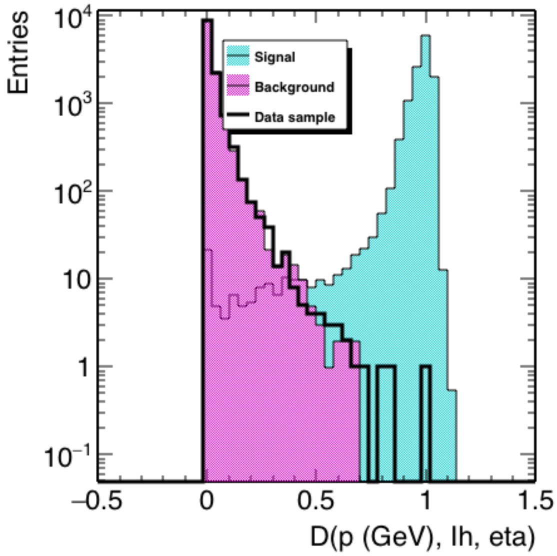

(a) 10 hidden nodes

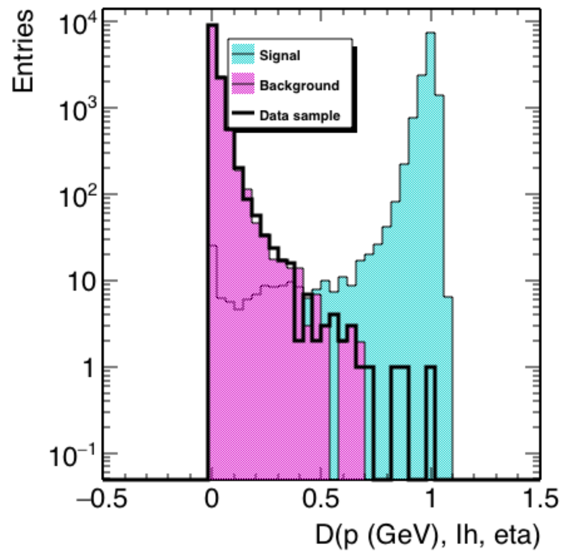

(b) 15 hidden nodes

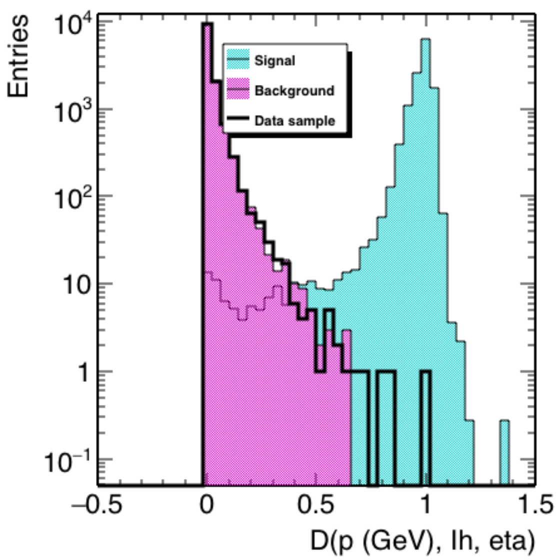

(c) 20 hidden nodes

Figure 4.1: Distributions of the tracker-only+MVA multivariate discriminant for different number of nodes in the artificial neural network. The artificial neural network was trained using a gluino mass = 1400 GeV signal and a TOY background sample. Distributions for a gluino mass = 1200 GeV signal (blue), TOY background (pink), and 2015 data passing the loose selection criteria (black line) are shown. All distributions are normalized to the number of data entries.

the training. Training of the artificial neural network was done on 10^4 events of TOY background and signal each.

Figure 4.4 shows a sample set of linear correlation matrices for the signal and background produced by an artificial neural network training. The correlation matrix indicates little to no correlation between I_h and p for the background, as should be the case (see Ch.3.4.2). By contrast, the signal correlation matrix indicates a much stronger correlation. Figure 4.5 shows the artificial neural network architecture that created the correlation matrix. The artificial neural network architecture illustration includes arrows representing the inputs and relative weights that each node assigned to the input variables.

The viability of a single artificial neural network mapping for a given signal type to be applied to different signal masses and still maintain signal to background discrimination was investigated. Figures 4.7 to 4.22 show the multivariate discriminant distributions of applying a mapping from one mass point to other signal mass points. Each analysis (tracker-only+MVA and Tracker+TOF+MVA) used a single (but not the same) TOY background sample for training all of the mappings for that analysis. Figures 4.7 to 4.22 show that when a lower mass trained mapping is applied to a larger mass point, the multivariate discriminant distributions remain well separated (e.g. Fig 4.7 (c)), and the signal multivariate discriminant distributions remain well peaked near 1. However when a mapping that was trained on a higher mass point is applied to a lower mass point, the multivariate discriminant distribution for the lower signal mass point increases the width of the peak near 1 (e.g. Fig 4.7 (a)). For most mappings tested, the background are heavily peaked near 0 and the signal are heavily peaked near 1, the exception being for mass points roughly 400 GeV or less as seen in case of the stau and DY signal types.

Overall the multivariate discriminant distributions outputted by the artificial neural network mappings show good signal to background separation, as the Receiver Operating Characteristic (ROC) curves in Figs. 4.8, 4.11, 4.14, 4.17, 4.20, and 4.23 show. In the ROC curves, the signal efficiency (S) versus background efficiency (B) for the same signal and background but with different mappings are shown with each point along a curve representing a selection value on the multivariate discriminant from 0 to 1.

An additional study on the significance versus discriminant selection value was conducted, with significance defined as $S/\sqrt{(S+B)}$. Figures.4.8, 4.11, 4.14, 4.17, 4.20, and 4.23 also include the sig-

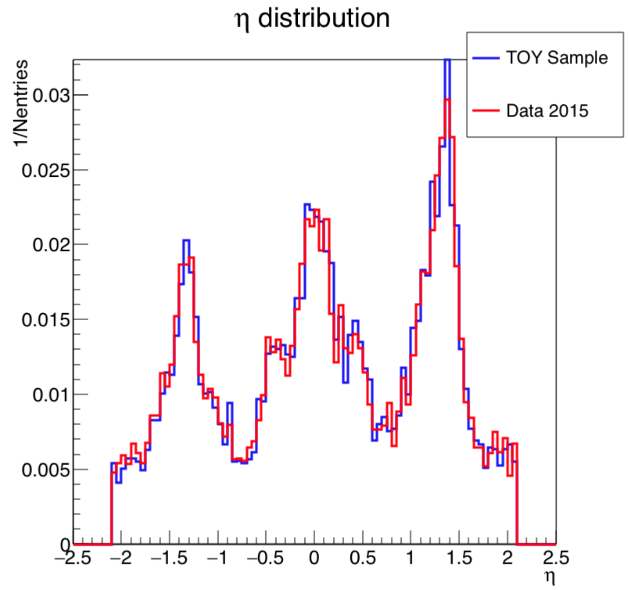

(a) η

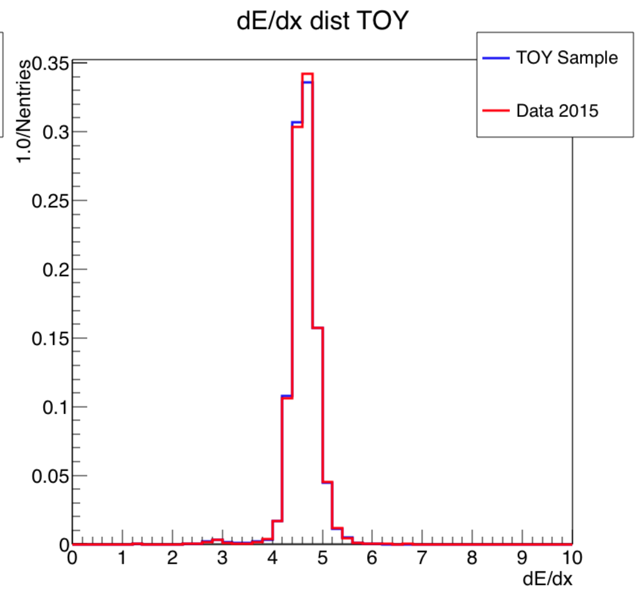

(b) dE/dx estimate

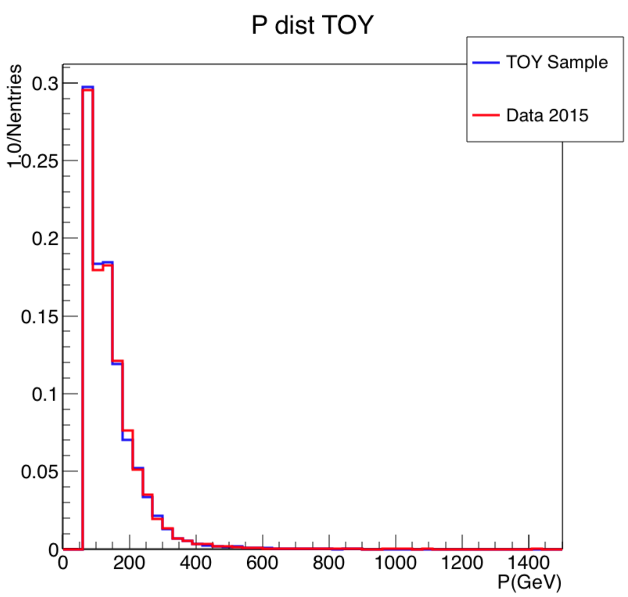

(c) p

Figure 4.2: Distributions of (a) eta, (b) I_h, and (c) p for a TOY background sample (blue) and 2015 data (red) for the tracker-only analysis. All of the distributions are normalized to unit area.

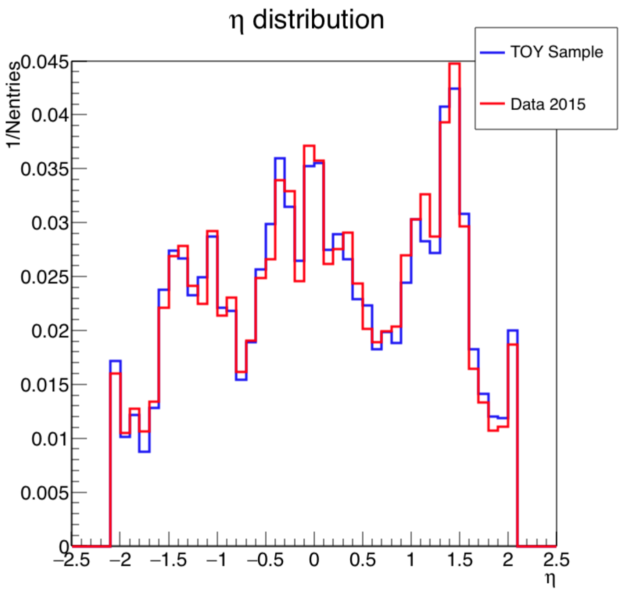

(a) η

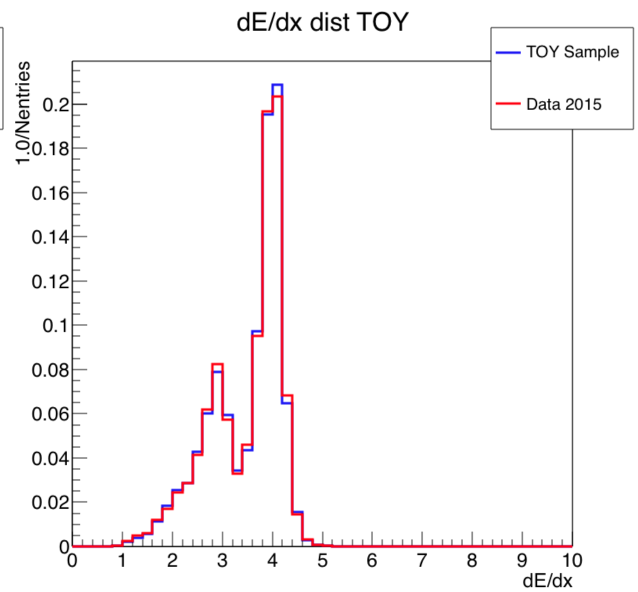

(b) dE/dx estimate

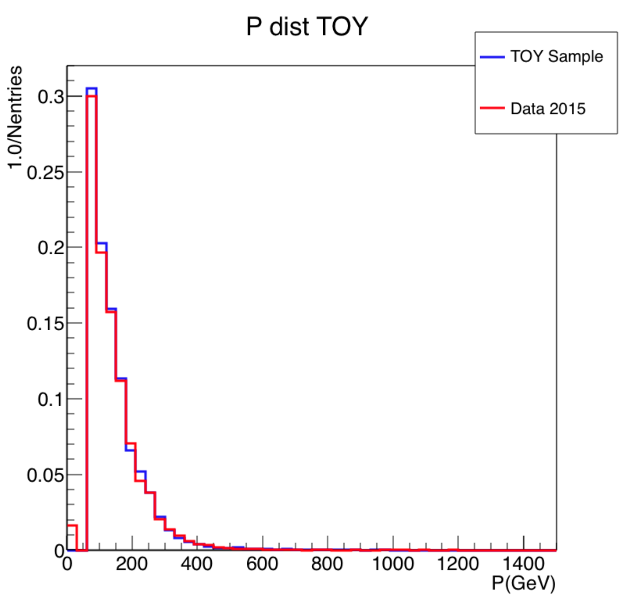

(c) p

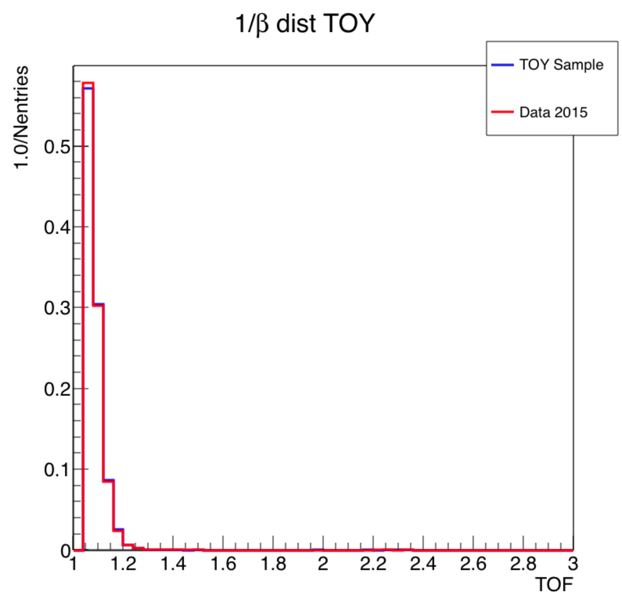

(d) $1/beta$

Figure 4.3: Distributions of (a) η, (b) I_h, (c) p, and (d) $1/\beta$ for a TOY background sample (blue) and 2015 data (red) for the Tracker+TOF analysis. All of the distributions are normalized to unit area.

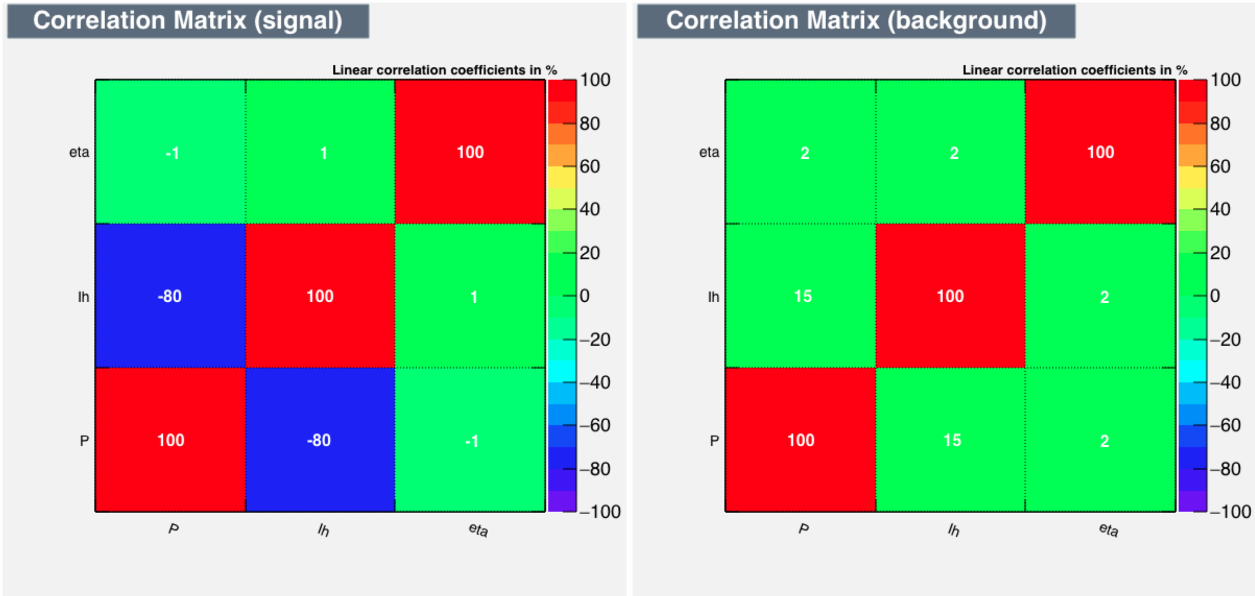

(a) Correlation matrix for signal

(b) Correlation matrix for TOY background

Figure 4.4: Linear correlation matrices after training the artificial neural network on a gluino mass = 800 GeV sample (left) and a TOY background sample (right) for the tracker-only+MVA analysis. The three inputs (p, I_h, and η) are indicated.

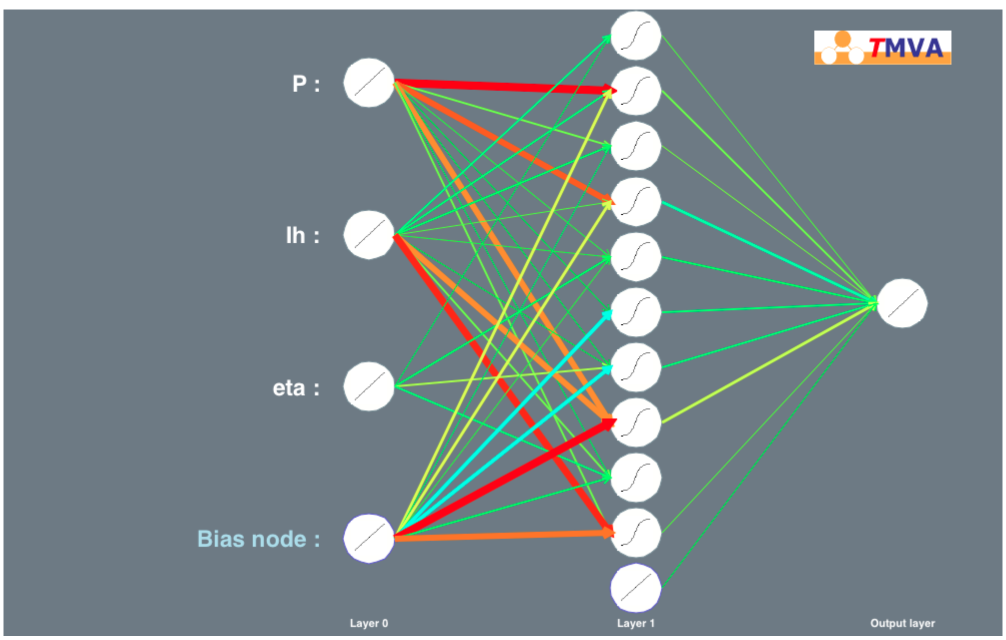

Figure 4.5: Diagram of the artificial neural network architecture with the input nodes, hidden nodes, and output nodes shown. The arrows indicate which inputs are being passed from node to node, with the arrow width correlated to the weight that node has assigned the given input.

nificance versus discriminant selection value for signal and background samples applied to different mappings. For the significance curves, the signals were scaled based on theoretical cross sections. The significance plots indicated in general that the larger mass trained mappings would reach a maximal value of significance at a lower selection value compared to the lower mass trained mappings. For Figs. 4.7 to 4.23 the hadron-like samples used mappings from the tracker-only+MVA analysis, whereas the plots showing lepton-like signals used mappings from the Tracker+TOF+MVA analysis.

In general the ROC curves indicate no significant difference between the different mappings for a given signal type. However, the significance plots show a trend for larger signal mass mappings to produce a higher significance value "sooner" (at lower selection values). In the case of very low masses (less than 500 GeV) the mappings were not able to attain the same level of signal significance as the mappings trained on higher masses. As previously mentioned, the mappings maintain signal to background discrimination when a mapping created from a lower mass point is applied to a higher mass point sample. However the larger the mass point used to train the mapping, the less likely the background is able to produce larger discriminant values thus increasing the background rejection. Therefore the mapping chosen to explore the signal type was chosen from the range of mass points excluded by previous CMS HSCP searches. The final mass points chosen for training the artificial neural networks were: gluino mass = 1400 GeV, stop mass = 1000 GeV, GMSB stau mass = 494 GeV, PP stau mass = 308 GeV, DY $|Q| = 1e$ mass = 600 GeV, DY $|Q| = 2e$ mass = 600 GeV (see Table 4.1).

For the HSCP multivariate analyses, the selection on the calculated mass from the standard analysis (Ch. 3) is replaced by a selection on the artificial neural network multivariate discriminant. Each of the signal type mappings are saved for the data and background prediction distributions to be used for discovery and limit setting. In similar fashion to the standard HSCP analyses, the HSCP multivariate analyses calculate the specific selection value on the multivariate discriminant used for limit setting at runtime. The selection value is taken to be that which maximizes the signal significance for selection values on the discriminant between 0.2 and 1. The limit setting becomes questionable for background uncertainties less than 10^{-2}, therefore the selection value on the multivariate discriminant is also required to have a background uncertainty no less than 10^{-2}. The result is a new source of systematic uncertainty related to the multivariate approach.

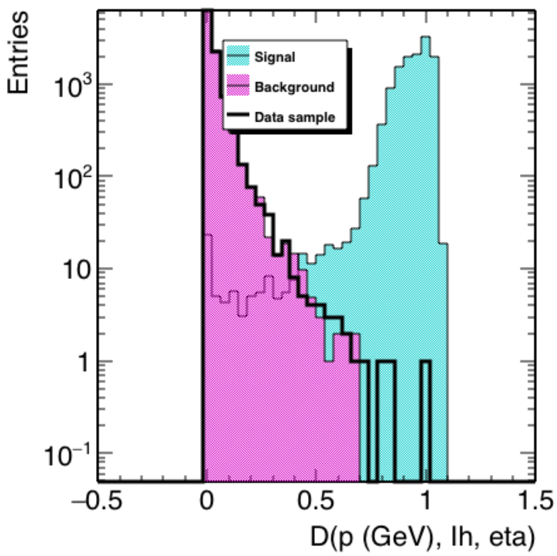

(a) gluino mass = 1000 GeV

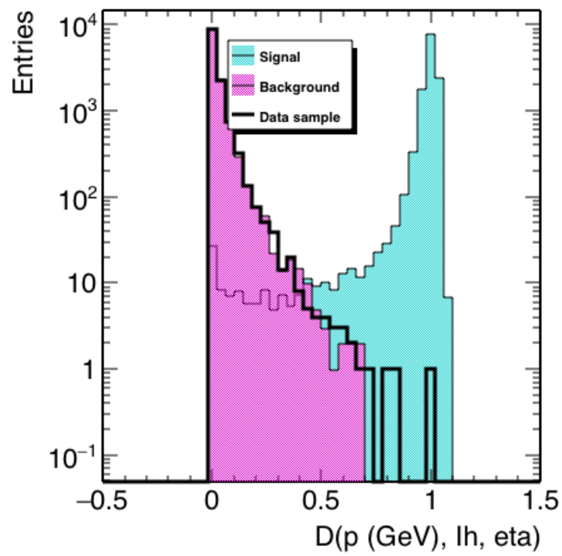

(b) gluino mass = 1400 GeV

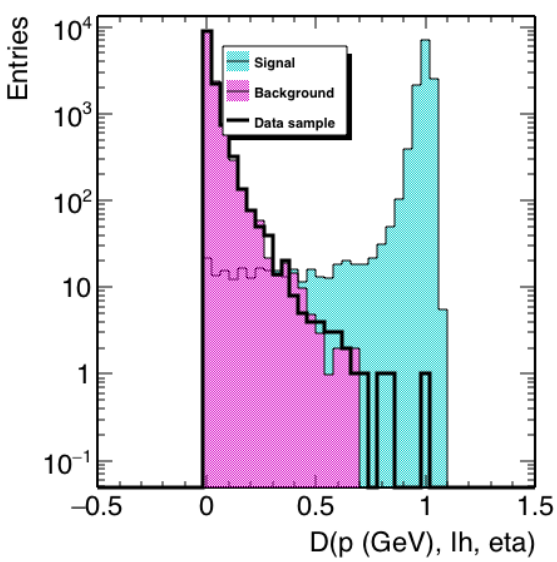

(c) gluino mass = 1800 GeV

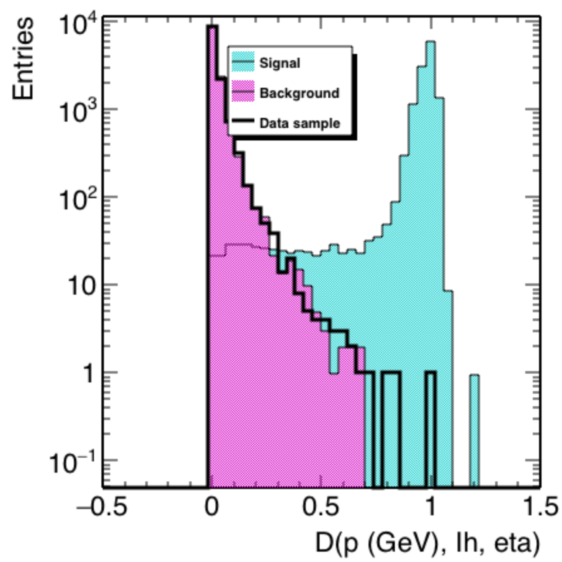

(d) gluino mass = 2200 GeV

Figure 4.6: Distributions of multivariate discriminant values for the tracker-only+MVA analysis after training with a gluino mass = 1400 GeV. The mapping was applied to samples of (a) gluino mass = 1000 GeV, (b) gluino mass = 1400 GeV, (c) gluino mass = 1800 GeV, (d) gluino mass = 2200 GeV signal samples (blue), a TOY background sample(pink), and 2015 data that pass the final loose selection (black lines). All distributions were normalized to the number of data passing the final loose selection.

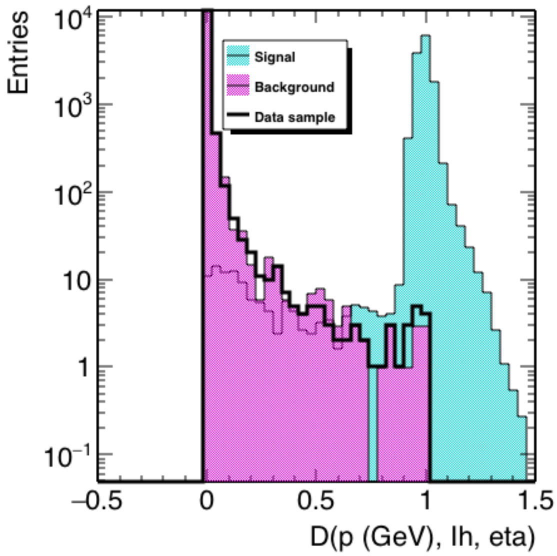

(a) gluino mass = 800 GeV training

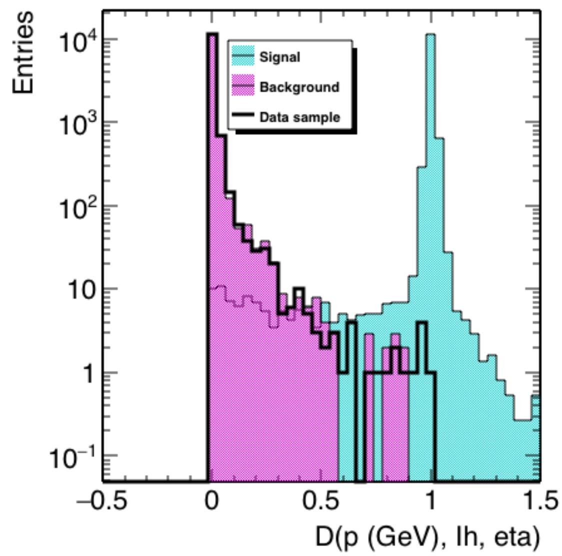

(b) gluino mass = 1000 GeV training

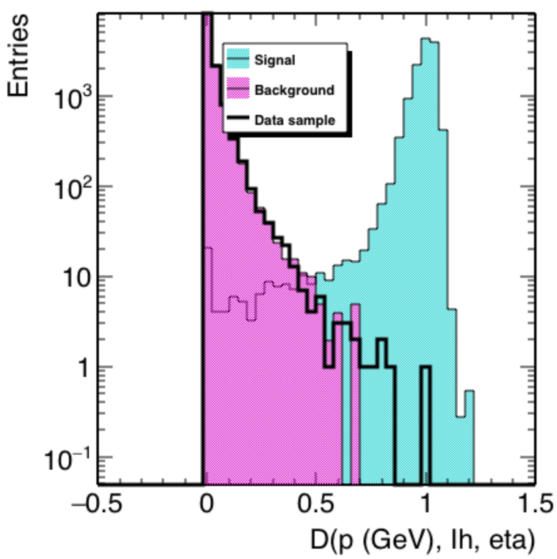

(c) gluino mass = 1200 GeV training

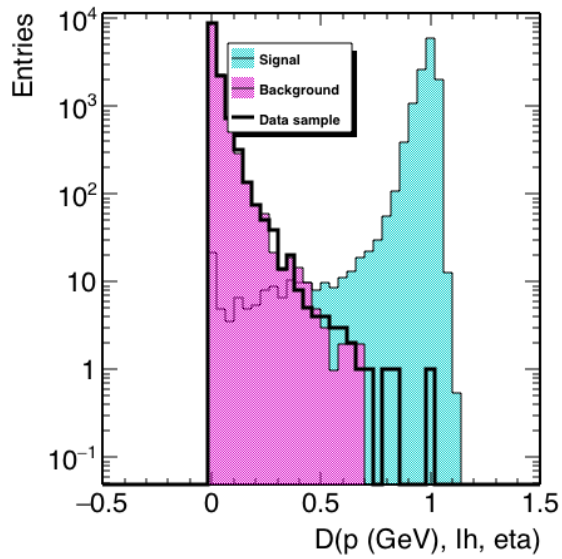

(d) gluino mass = 1400 GeV training

Figure 4.7: Distributions of multivariate discriminant values for the tracker-only+MVA analysis after training with (a) gluino mass = 800 GeV, (b) gluino mass = 1000 GeV, (c) gluino mass = 1200 GeV, and (d) gluino mass = 1400 GeV signal samples. For each mapping, the resulting distributions for the same gluino mass = 1200 GeV sample (blue), TOY distribution(pink), and 2015 data passing the final loose selection (black line) are shown. All distributions were normalized to the number of data passing the final loose selection.

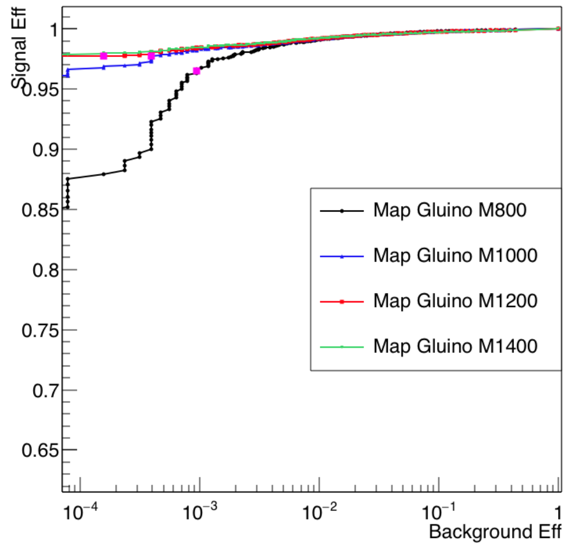

(a) gluino ROC curves

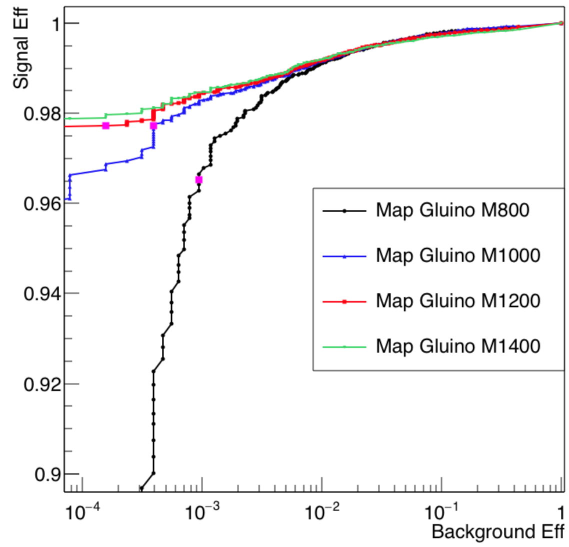

(b) gluino ROC curves zoomed

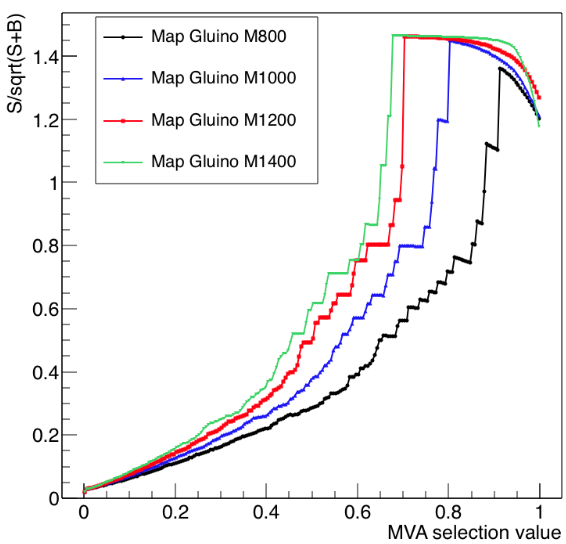

(c) gluino significance

Figure 4.8: The ROC (a)(b) and significance curves (c) for different mappings applied to a gluino mass = 1800 GeV signal. The discriminant selection of 0.7 is indicated in magenta on the ROC curves. For the gluino mass = 1400 GeV mapping, the TOY background discriminant distribution became 0 before the selection value of 0.7. Upper left: The ROC curves for the different mappings with the background efficiency on a log scale. Upper right: The same ROC curves with the y axis zoomed in. Lower left: Significance curves for the different mappings.

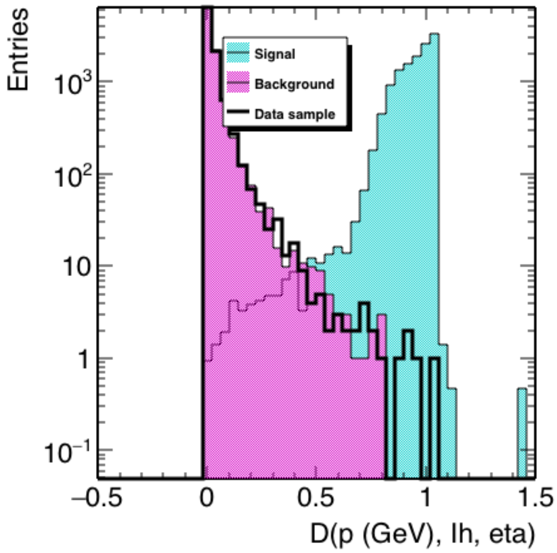

(a) stop mass = 800 GeV

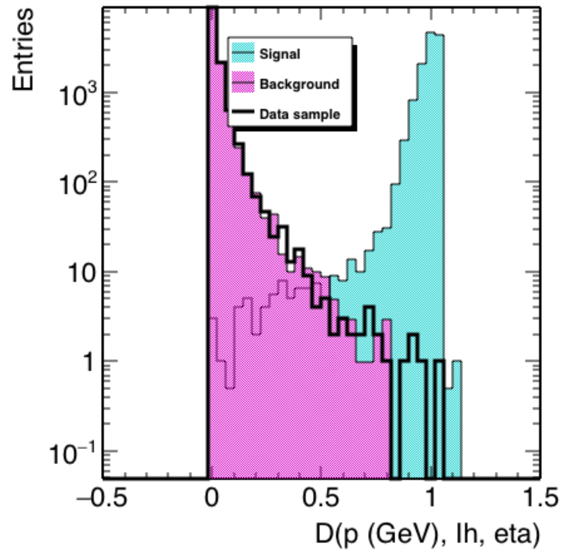

(b) stop mass = 1000 GeV

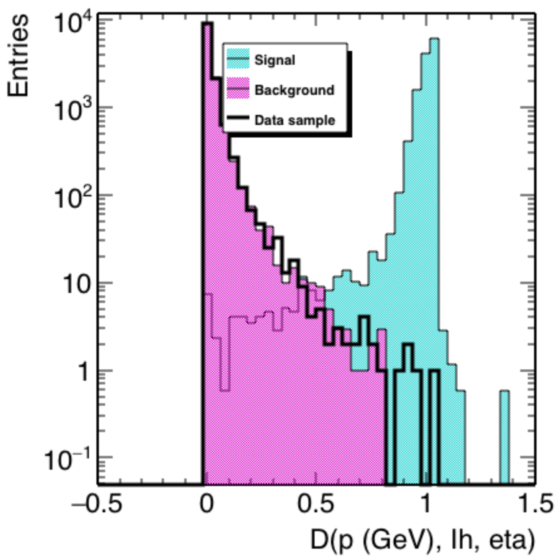

(c) stop mass = 1200 GeV

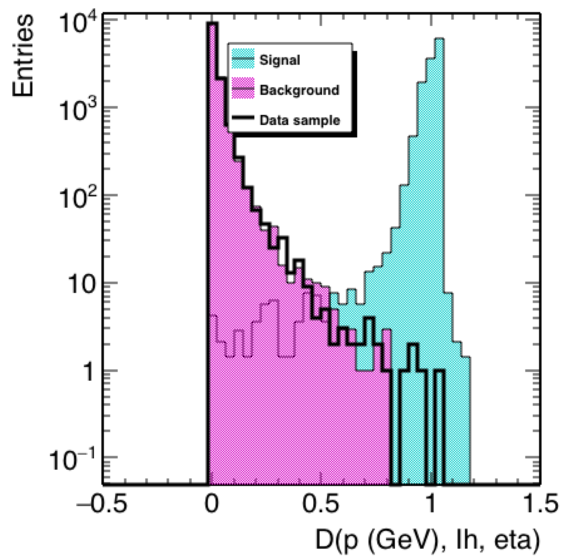

(d) stop mass = 1400 GeV

Figure 4.9: Distributions of multivariate discriminant values for the tracker-only+MVA analysis after training with a stop mass = 1000 GeV sample. The mapping was applied to samples of (a) stop mass = 800 GeV, (b) stop mass = 1000 GeV, (c) stop mass = 1200 GeV, (d) stop mass = 1400 GeV (blue), a TOY background sample (pink), and the 2015 data passing the final loose selection (black lines). All distributions were normalized to the number of data passing the final loose selection.

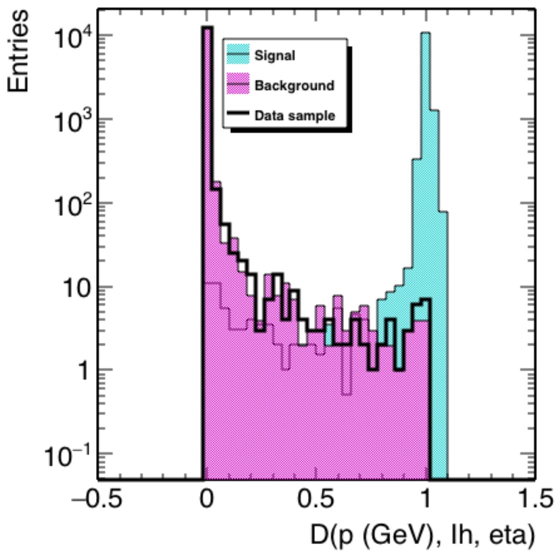

(a) Stop M800 GeV training

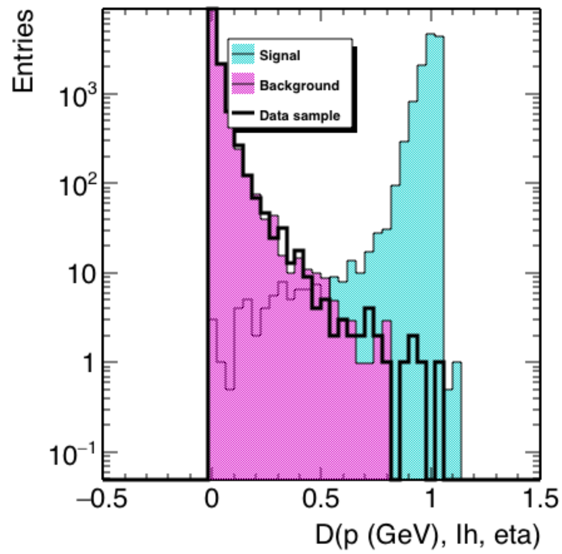

(b) Stop M1000 GeV training

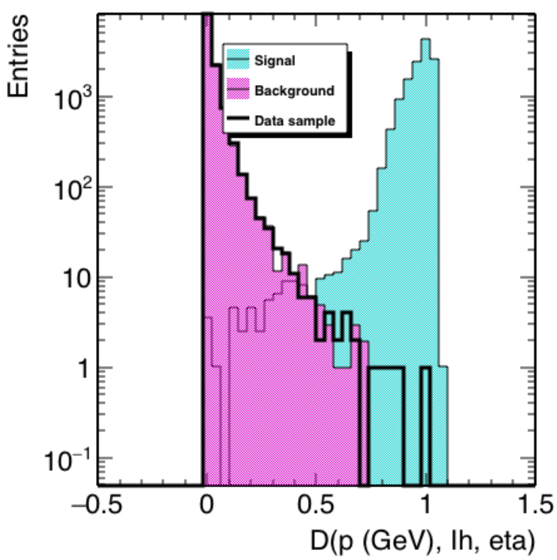

(c) Stop M1200 GeV training

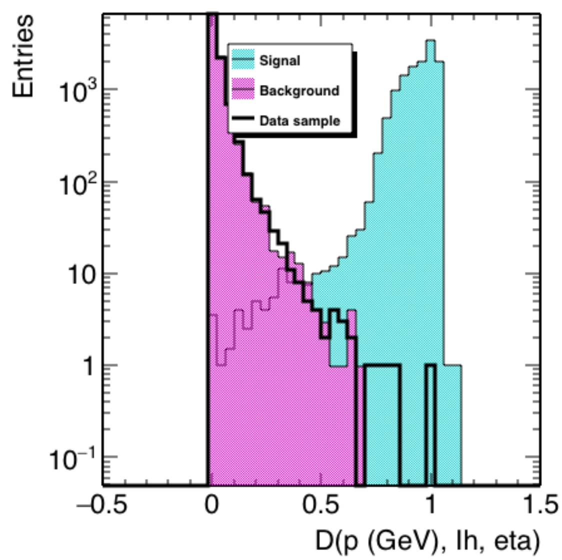

(d) Stop M1400 GeV training

Figure 4.10: Distributions of multivariate discriminant values for the tracker-only+MVA analysis after training with (a) stop mass = 800 GeV, (b) stop mass = 1000 GeV, (c) stop mass = 1200 GeV, and (d) stop mass = 1400 GeV signal samples. The mappings were applied to a stop mass = 1000 GeV (blue), a TOY background (pink), and 2015 data passing the final loose selection (black lines). All distributions were normalized to the number of data passing the final loose selection.

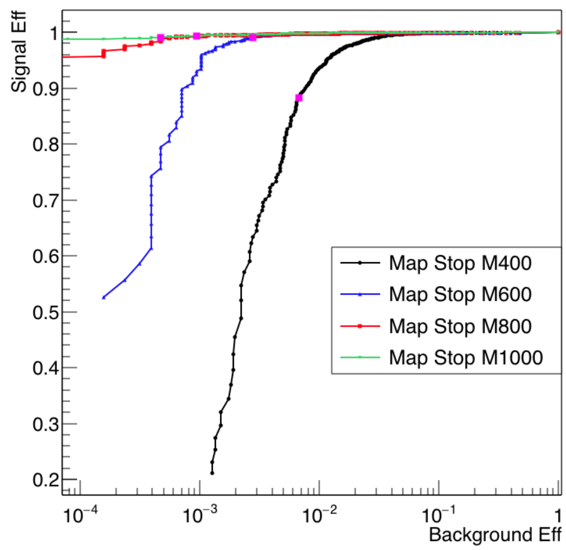

(a) stop ROC curves

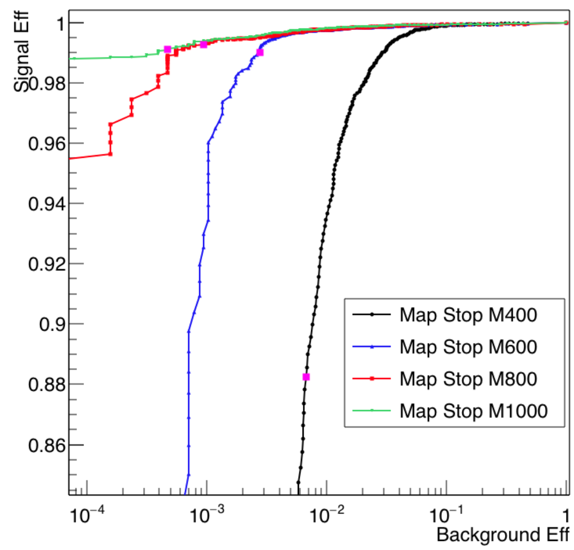

(b) stop ROC curves zoom

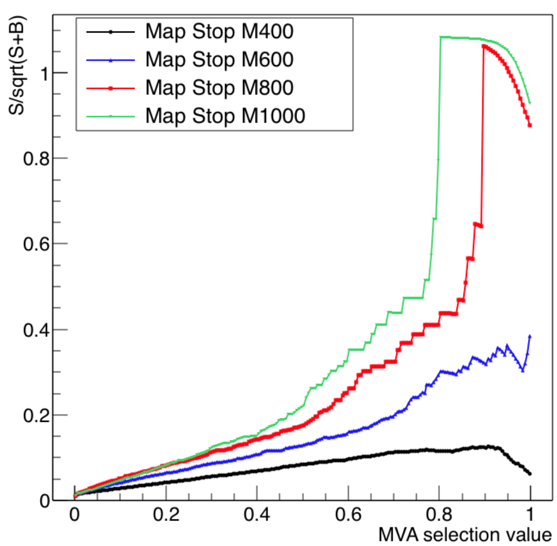

(c) stop significance

Figure 4.11: The ROC (a)(b) and significance curves (c) for different mappings applied to a stop mass = 800 GeV signal and TOY background sample. The discriminant selection of 0.7 is indicated in magenta on the ROC curves. Upper left: The ROC curves for the different mappings with the background efficiency on a log scale. Upper right: The same ROC curves with the y axis zoomed in. Lower left: Significance curves for the different mappings.

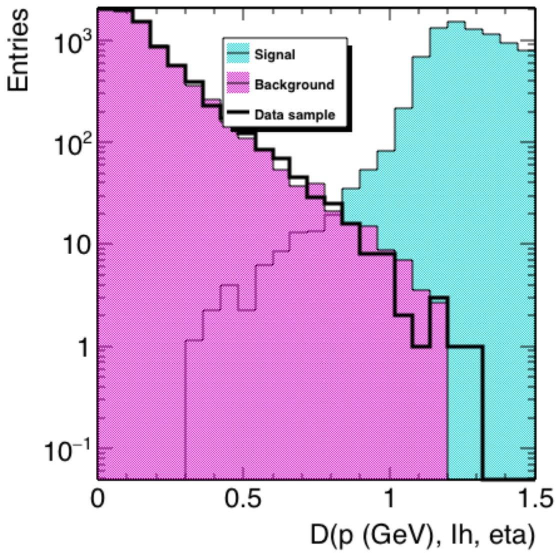

(a) GMSB stau mass = 247 GeV training

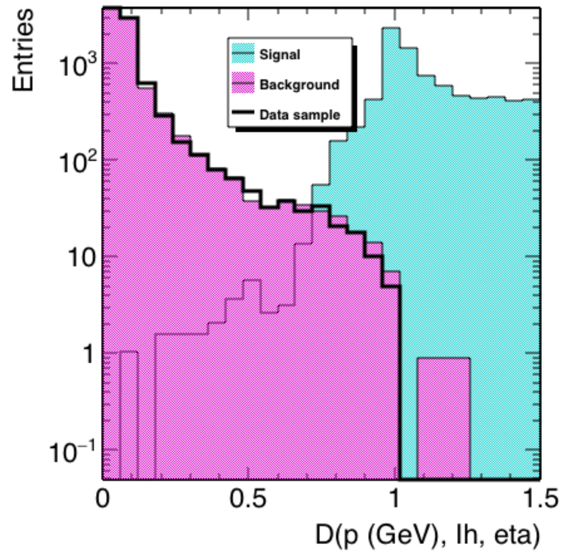

(b) GMSB stau mass = 308 GeV training

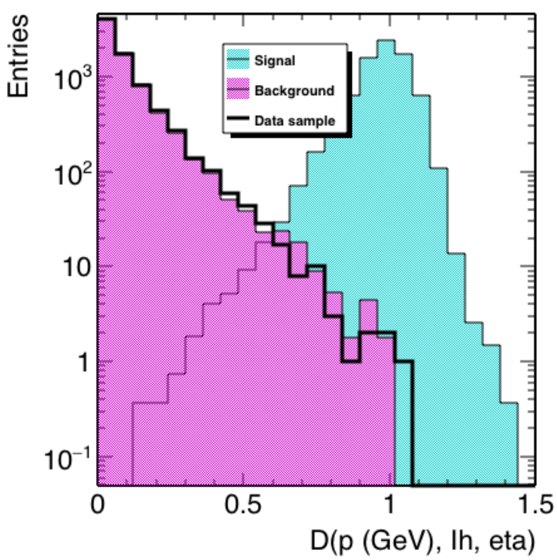

(c) GMSB stau mass = GeV training

Figure 4.12: Distributions of multivariate discriminant values for the Tracker+TOF+MVA analysis after training with (a)GMSB stau mass = 247 GeV, (b)GMSB stau mass = 308 GeV, and (c)GMSB stau mass = 494 GeV. The mappings were applied to a GMSB stau mass = 494 GeV (blue), a TOY background (pink), and 2015 data passing the final loose selection (black lines). All distributions were normalized to the number of data passing the final loose selection.

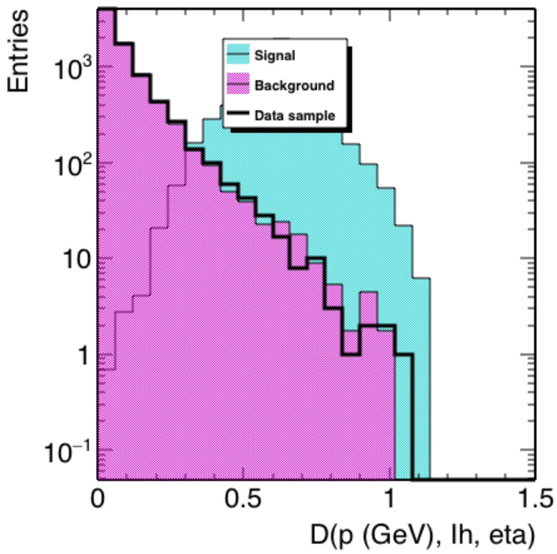

(a) GMSB stau mass = 247 GeV sample

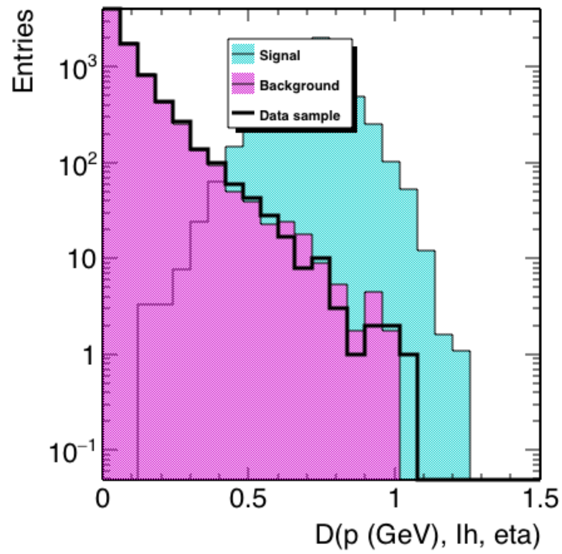

(b) GMSB stau mass = 308 GeV sample

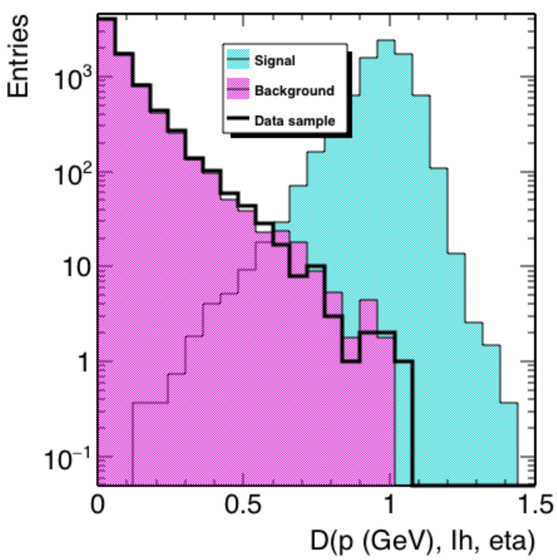

(c) GMSB stau mass = 494 GeV sample

Figure 4.13: Distributions of multivariate discriminant values for the Tracker+TOF+MVA analysis after training with a GMSB stau mass = 494 GeV sample. The mapping was applied samples of (a)GMSB stau mass = 247 GeV, (b)GMSB stau mass = 308 GeV, (c)GMSB stau mass = 494 GeV (blue), a TOY background (pink), and 2015 data passing the final loose selection (black lines).All distributions were normalized to the number of data passing the final loose selection.

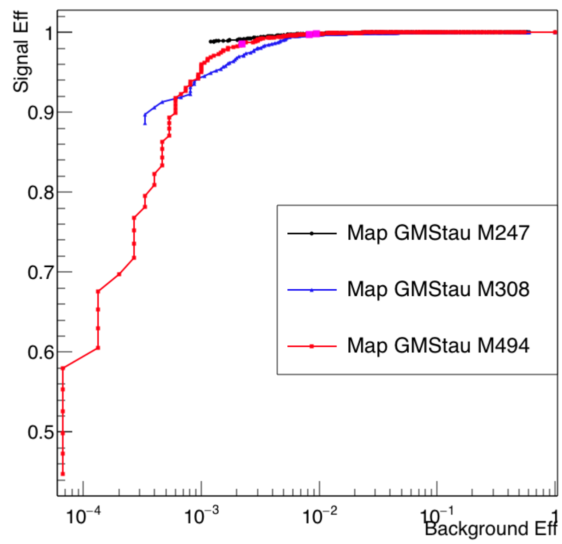

(a) gmstau ROC curves

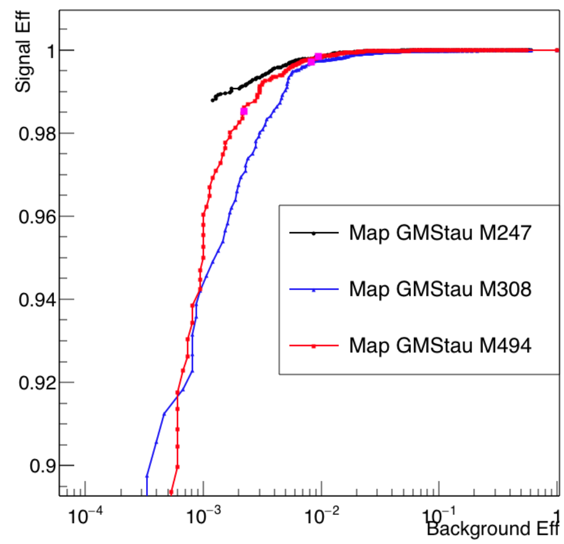

(b) gmstau ROC curves zoom

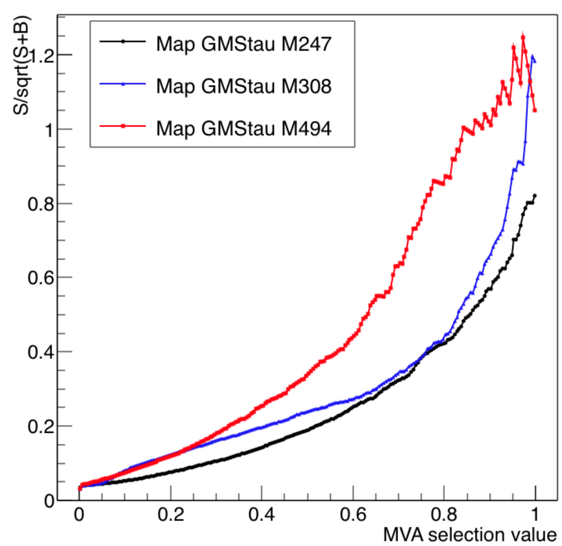

(c) gmstau significance

Figure 4.14: The ROC (a)(b) and significance curves (c) for different mappings applied to a GMSB stau mass = 494 GeV signal and TOY background sample. The discriminant selection of 0.7 is indicated in magenta on the ROC curves. Upper left: The ROC curves for the different mappings with the background efficiency on a log scale. Upper right: The same ROC curves with the y axis zoomed in. Lower left: Significance curves for the different mappings.

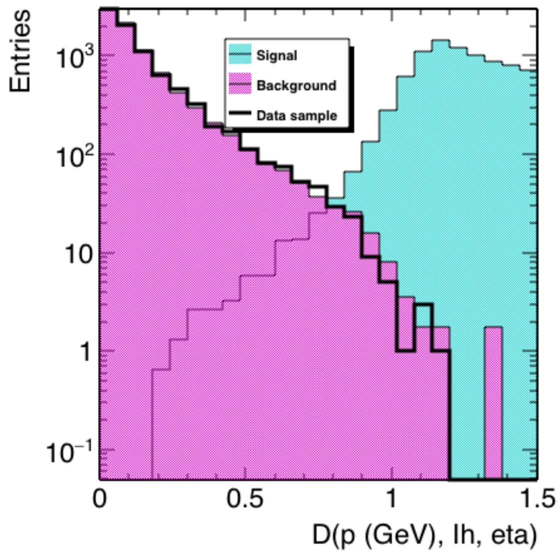

(a) PP stau mass = 247 GeV training

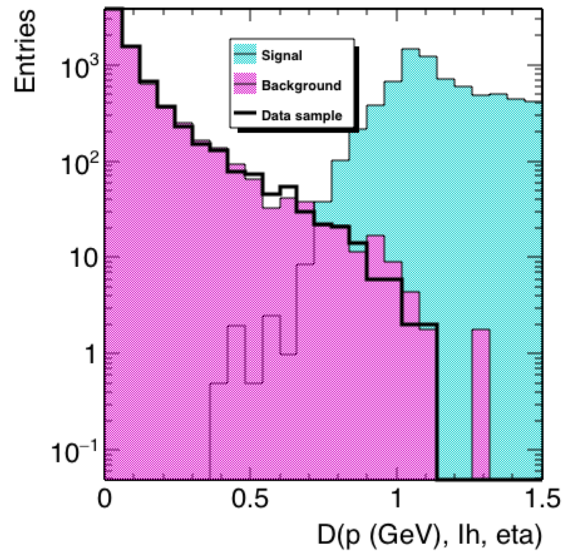

(b) PP stau mass = 308 GeV training

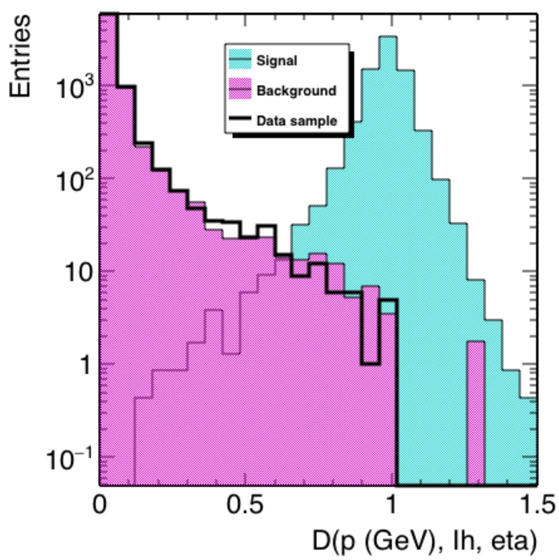

(c) PP stau mass = 494 GeV training

Figure 4.15: Distributions of multivariate discriminant values for the Tracker+TOF+MVA analysis after training with (a)PP stau mass = 247 GeV, (b)PP stau mass = 308 GeV, and (c)PP stau mass = 494 GeV. The mappings were applied to a PP stau mass = 494 GeV (blue), a TOY background (pink), and 2015 data passing the final loose selection (black lines). All distributions were normalized to the number of data passing the final loose selection.

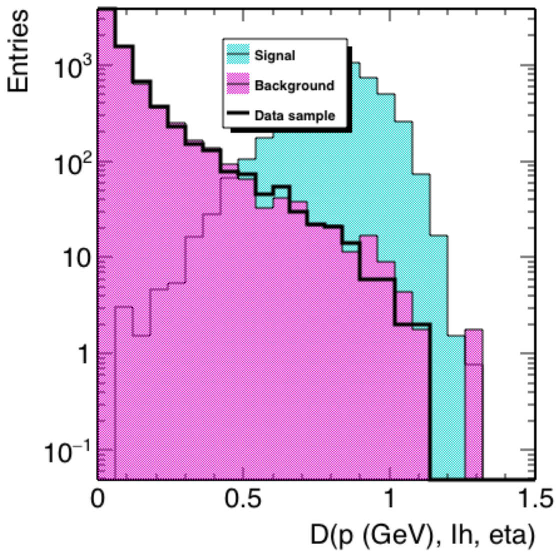

(a) PP stau mass = 247 GeV sample

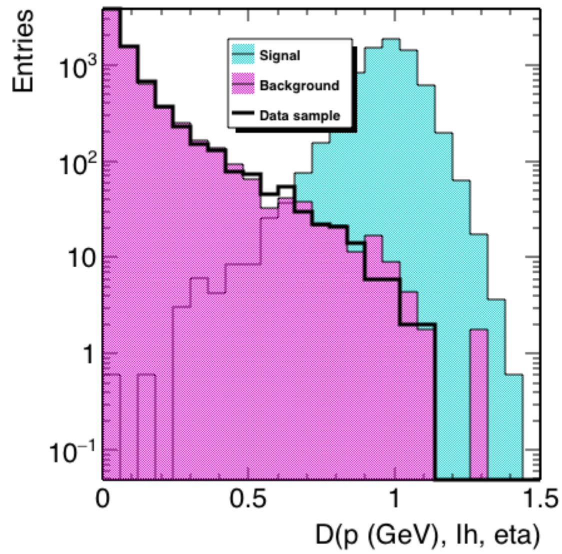

(b) PP stau mass = GeV sample

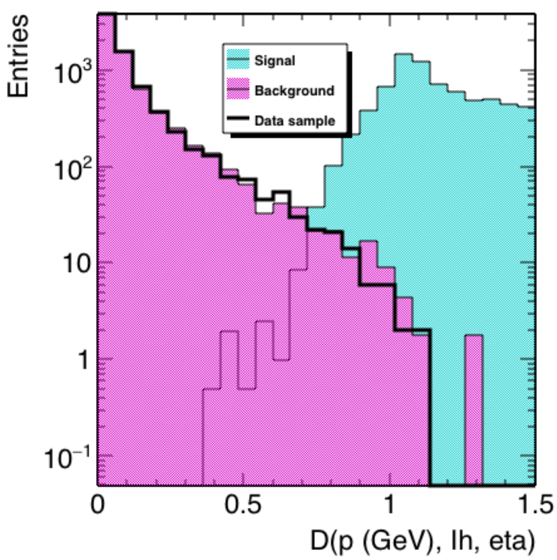

(c) PP stau mass = GeV sample

Figure 4.16: Distributions of multivariate discriminant values for the Tracker+TOF+MVA analysis after training with a PP stau mass = 494 GeV sample. The mapping was applied samples of (a)PP stau mass = 247 GeV, (b)PP stau mass = 308 GeV, (c)PP stau mass = 494 GeV (blue), a TOY background (pink), and 2015 data passing the final loose selection (black lines).All distributions were normalized to the number of data passing the final loose selection.

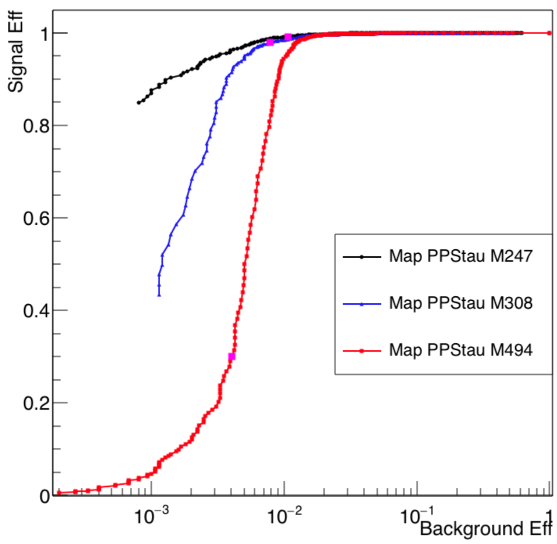

(a) PP stau ROC curves

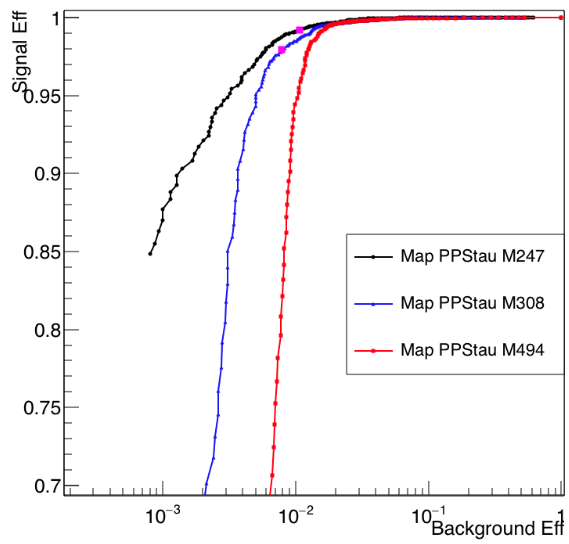

(b) PP stau ROC curves zoom

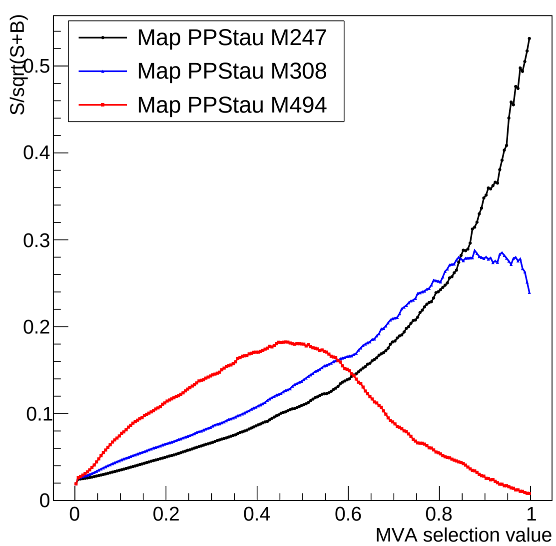

(c) PP stau significance

Figure 4.17: The ROC (a)(b) and significance curves (c) for different mappings applied to a PP stau mass = 308 GeV signal and TOY background sample. The discriminant selection of 0.7 is indicated in magenta on the ROC curves. Upper left: The ROC curves for the different mappings with the background efficiency on a log scale. Upper right: The same ROC curves with the y axis zoomed in. Lower left: Significance curves for the different mappings.

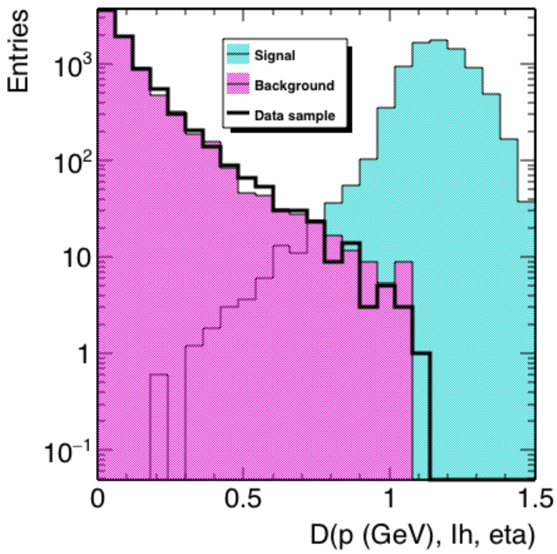

(a) DY $|Q| = 1e$ mass = 400 GeV training

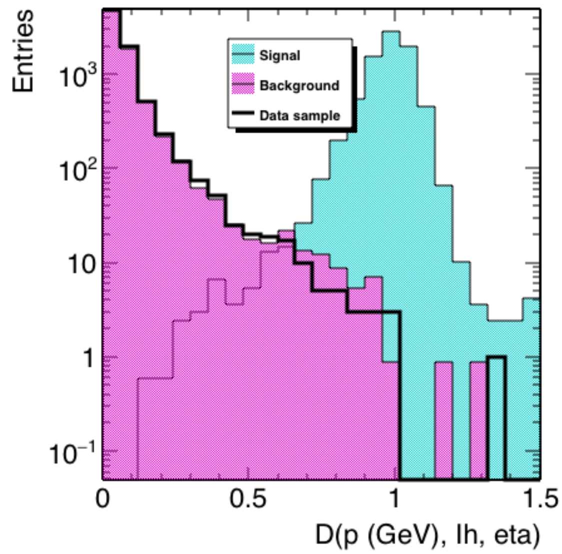

(b) DY $|Q| = 1e$ mass = 600 GeV training

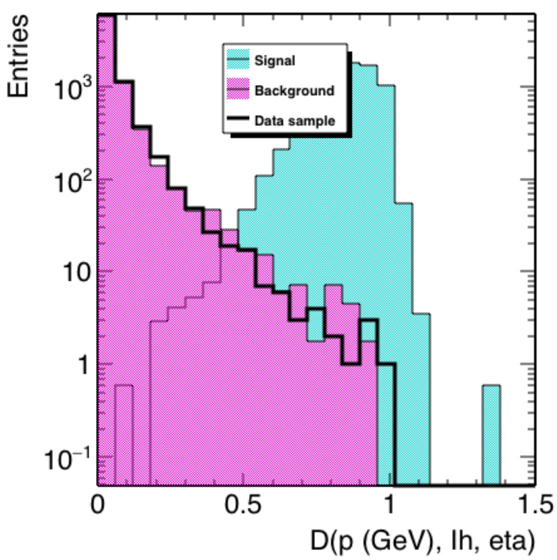

(c) DY $|Q| = 1e$ mass = 800 GeV training

Figure 4.18: Distributions of multivariate discriminant values for the Tracker+TOF+MVA analysis after training with (a) DY $|Q| = 1e$ mass = 400 GeV, (b)DY $|Q| = 1e$ mass = 600 GeV, and (c) DY $|Q| = 1e$ mass = 800 GeV. The mappings were applied to a DY $|Q| = 1e$ mass = 600 GeV (blue), a TOY background (pink), and 2015 data passing the final loose selection (black lines). All distributions were normalized to the number of data passing the final loose selection.

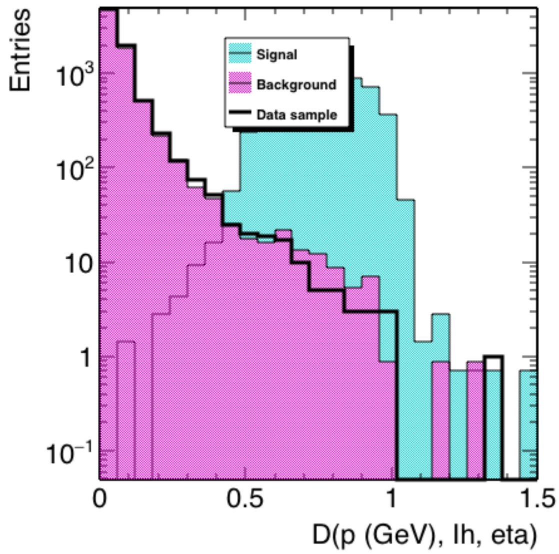

(a) DY $|Q| = 1e$ mass = 400 GeV sample

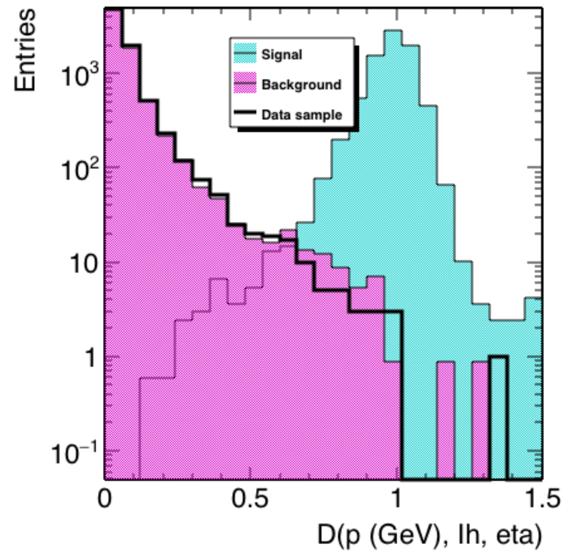

(b) DY $|Q| = 1e$ mass = 600 GeV sample

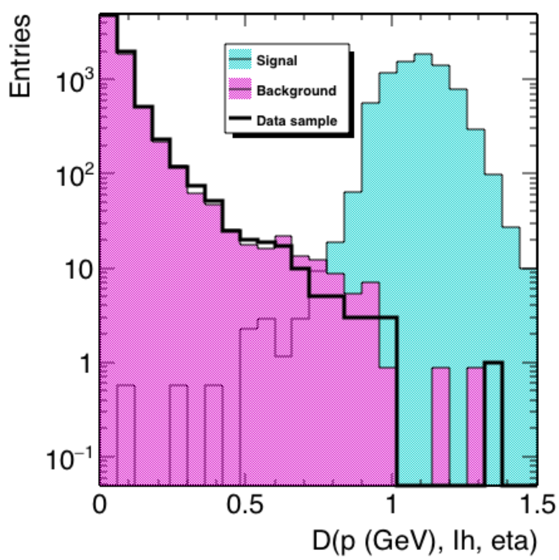

(c) DY $|Q| = 1e$ mass = 800 GeV sample

Figure 4.19: Distributions of multivariate discriminant values for the Tracker+TOF+MVA analysis after training with a DY $|Q| = 1e$ mass = 600 GeV. The mapping was applied samples of (a) DY $|Q| = 1e$ mass = 400 GeV, (b) DY $|Q| = 1e$ mass = 600 GeV, (c) DY $|Q| = 1e$ mass = 800 GeV (blue), a TOY background (pink), and 2015 data passing the final loose selection (black lines). All distributions were normalized to the number of data passing the final loose selection.

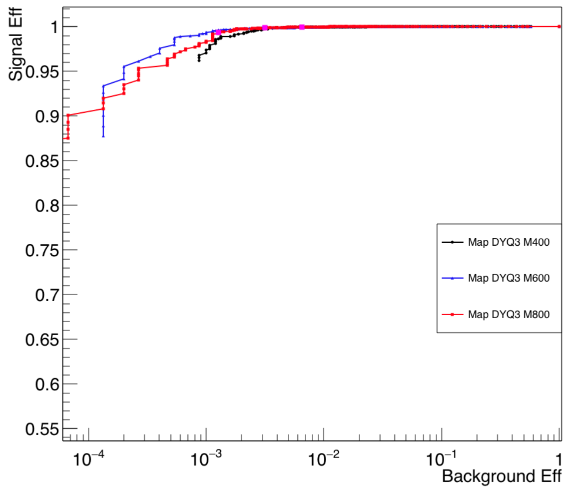

(a) DY $|Q| = 1e$ ROC curves

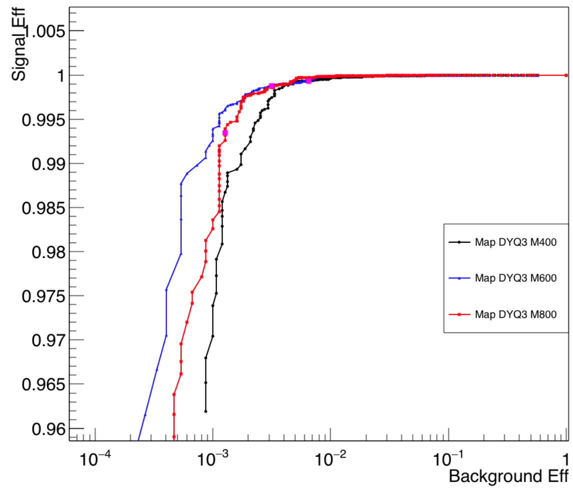

(b) DY $|Q| = 1e$ ROC curves zoom

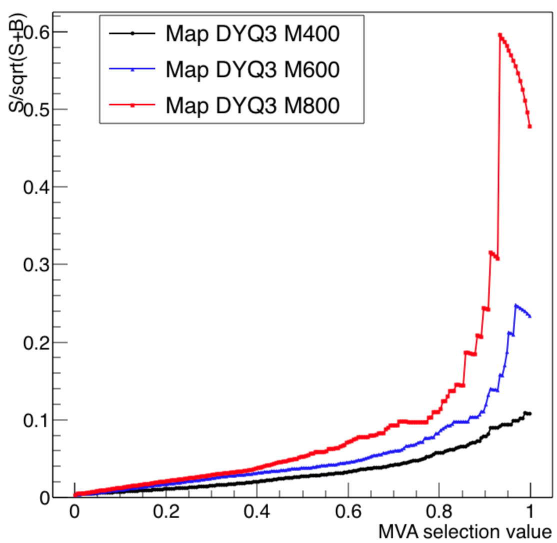

(c) DY $|Q| = 1e$ significance

Figure 4.20: The ROC (a)(b) and significance curves (c) for different mappings applied to a DY $|Q| = 1e$ mass = 600 GeV signal and TOY background sample. The discriminant selection of 0.7 is indicated in magenta on the ROC curves. Upper left: The ROC curves for the different mappings with the background efficiency on a log scale. Upper right: The same ROC curves with the y axis zoomed in. Lower left: Significance curves for the different mappings.

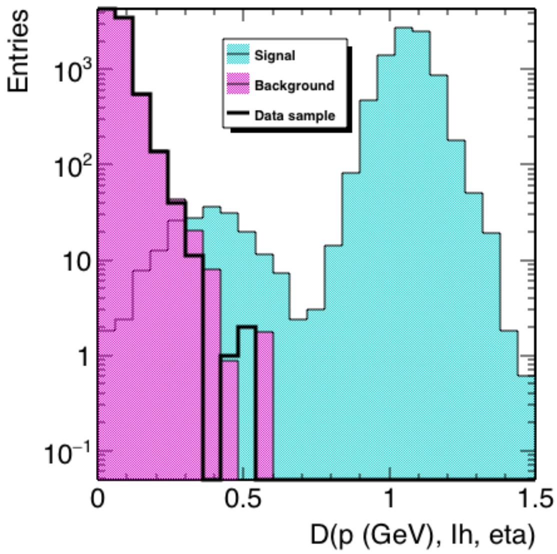

(a) DY $|Q| = 2e$ mass = 400 GeV training

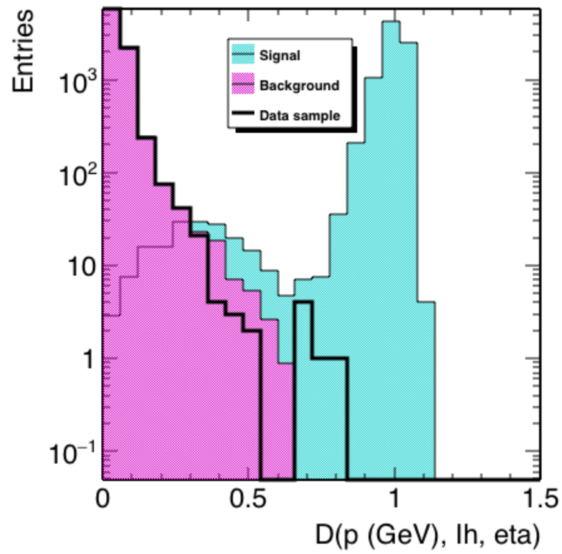

(b) DY $|Q| = 2e$ mass = 600 GeV training

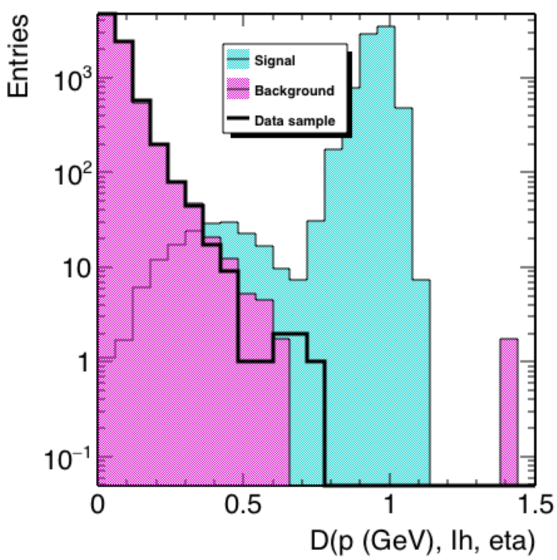

(c) DY $|Q| = 2e$ mass = 800 GeV training

Figure 4.21: Distributions of multivariate discriminant values for the Tracker+TOF+MVA analysis after training with (a) DY $|Q| = 2e$ mass = 400 GeV, (b)DY $|Q| = 2e$ mass = 600 GeV, and (c) DY $|Q| = 2e$ mass = 800 GeV. The mappings were applied to a DY $|Q| = 2e$ mass = 600 GeV (blue), a TOY background (pink), and 2015 data passing the final loose selection (black lines). All distributions were normalized to the number of data passing the final loose selection.

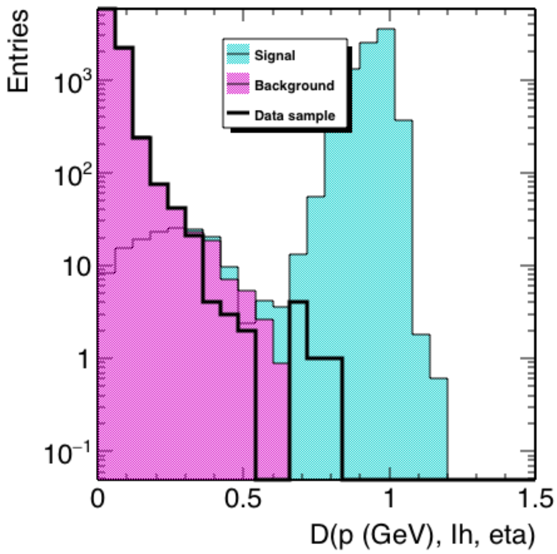

(a) DY $|Q| = 2e$ mass =400 GeV sample

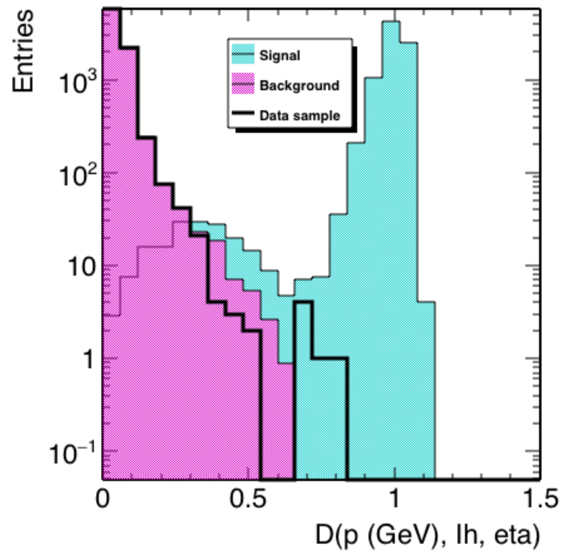

(b) DY $|Q| = 2e$ mass =600 GeV sample

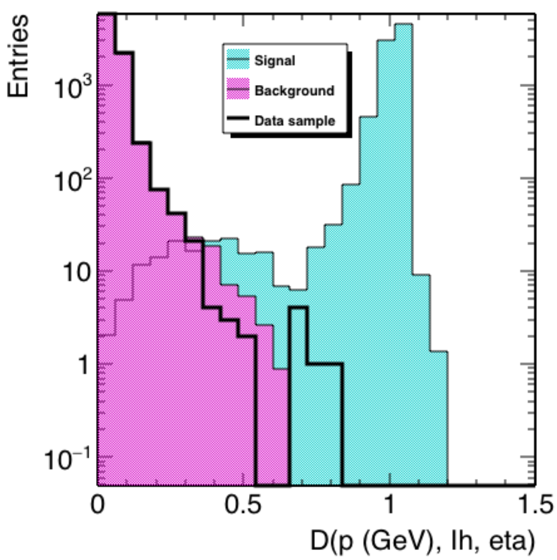

(c) DY $|Q| = 2e$ mass =800 GeV sample

Figure 4.22: Distributions of multivariate discriminant values for the Tracker+TOF+MVA analysis after training with a DY $|Q| = 2e$ mass = 600 GeV. The mapping was applied samples of (a) DY $|Q| = 2e$ mass = 400 GeV, (b) DY $|Q| = 2e$ mass = 600 GeV, (c) DY $|Q| = 2e$ mass = 800 GeV (blue), a TOY background (pink), and 2015 data passing the final loose selection (black lines).All distributions were normalized to the number of data passing the final loose selection.

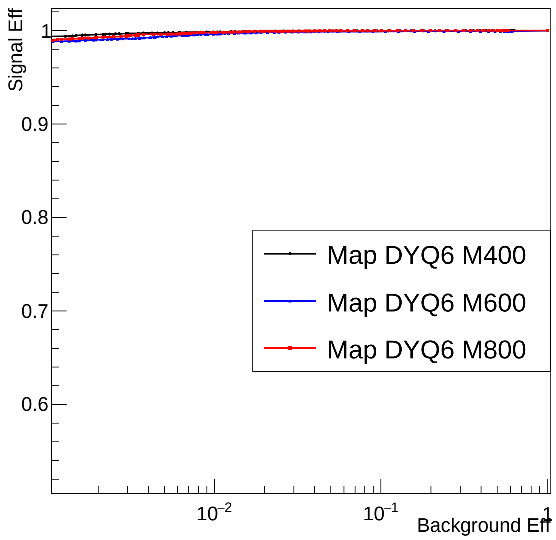

(a) DY $|Q| = 2e$ ROC curves

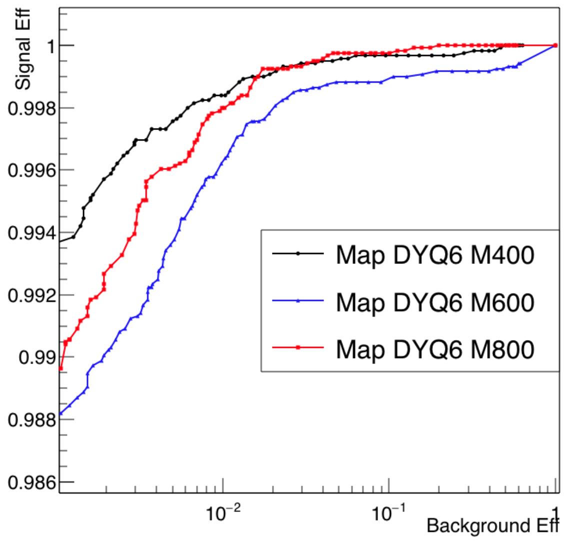

(b) DY $|Q| = 2e$ ROC curves zoom

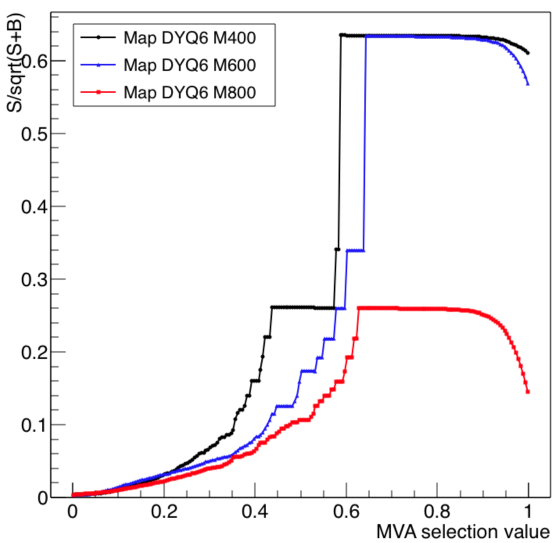

(c) DY $|Q| = 2e$ significance

Figure 4.23: The ROC (a)(b) and significance curves (c) for different mappings applied to a DY $|Q| = 2e$ mass = 600 GeV signal and TOY background sample. The discriminant selection of 0.7 is indicated in magenta on the ROC curves. Upper left: The ROC curves for the different mappings with the background efficiency on a log scale. Upper right: The same ROC curves with the y axis zoomed in. Lower left: Significance curves for the different mappings.

Table 4.1: The specific signal models used in training the artificial neural networks used to explore each signal type.

Signal Type	Trained Mass
Gluino	1400 GeV
Stop	1000 GeV
GMSB stau	494 GeV
PP Stau	308 GeV
DY $\lvert Q\rvert = 1e$	600 GeV
DY $\lvert Q\rvert = 2e$	600 GeV

4.3 Systematic Uncertainties

The systematic uncertainties considered for this analysis can be classified into one of three main categories: the integrated luminosity, the background prediction, or the signal acceptance. For the integrated luminosity, the uncertainty is given by CMS to be 2.3% at $\sqrt{s} = 13$ TeV [68].

The systematic uncertainty on the background prediction was obtained by looking at different combinations of background regions used to estimate the amount of background in the signal region, analogous to Eq. 3.8. As previously listed, in the case of the Tracker+TOF analysis, the inclusion of the extra dimension of inverse beta in selecting the signal region produces a total of 8 regions. Again, due to the independence of the variables, several ratios of the amount of data in different regions can be produced to obtain a background estimate in the signal region. The final systematic uncertainty was obtained by calculating the variance in the different background estimates and removing an estimate of the statistical contribution of said variance, as seen in Eqs.4.1 to 4.3.

$$V_N^{syst+stat} = \sqrt{\Sigma_i \frac{(x_i - \mu)^2}{(N-1)}} \tag{4.1}$$

$$V_N^{stat} = \sqrt{\Sigma_i \frac{{\sigma_i}^2}{N}} \tag{4.2}$$

$$V^{syst} = \sqrt{V_{syst+stat}^2 - V_{stat}^2} \tag{4.3}$$

here i represents the i-th independent background estimate, N represents the total number of independent background estimates, μ is the arithmetic mean value of the N independent background estimates, σ_i is the statistical uncertainty on the i-th background estimates, and the summations go from 1 to N. The systematic contribution to the variance of the background estimates is taken as the square root of the total variance squared minus the statistical contribution of the variance squared. The systematic uncertainty on the background prediction for the final selection criteria used is taken conservatively to be 20% after investigating the results of the Tracker+TOF+MVA ABCD method (see Fig. 4.24). Due to the lack of different independent background estimates for the tracker-only+MVA analysis, it is taken to have the same systematic uncertainty on the background prediction.

Several uncertainties contribute to the total systematic uncertainty on the signal acceptance. The trigger efficiency is dominated by the muon trigger as it is the dominant trigger (Ch. 3). By comparing the signal MC to data and shifting the arrival times of the simulated particles, the muon trigger timing is tested to evaluate how it changes with the possible slower arrival times of HSCPs. The difference in arrival times cause an uncertainty on the muon trigger efficiency of ~4% for most mass samples, with larger masses experiencing up to 8%. For the MET trigger, the change in trigger efficiency is found by adjusting the jet energy scale in the simulation of the HLT. This leads to an uncertainty of the MET trigger efficiency of less than 12% for all samples. When combined, the overall trigger uncertainty is found to be less than 13% for all samples. The inefficiencies of the muon triggers and MET trigger tend to compensate for one another.

For the offline reconstruction (Ch. 2) the track and muon reconstruction are almost fully efficient for the p_T ranges used in this search. Thus the signal acceptance uncertainty due to inefficiency in either the track and muon reconstruction is taken to be conservatively less than 2% . The position resolution for a reconstructed track is such that the uncertainties on the η value for the HSCP candidates in both signal MC and TOY background are found to be negligible ($\ll 1\%$) [44].

There is a contribution to the uncertainty on signal acceptance due to the uncertainty on the reconstructed momentum scale. This effect on the signal acceptance is estimated by shifting the momentum of tracks by the prescription given by the muon system experts as discussed in Ref. [69],

$$\frac{1}{p'_T} = \frac{1}{p_T} + \delta(q', \phi, \eta) \tag{4.4}$$

with

$$\delta(q', \phi, \eta) = A + B\eta^2 + q'C\sin(\phi - \phi_0) \tag{4.5}$$

where A = 0.236 TeV^{-1}, B = -0.135 TeV^{-1}, C = 0.282 TeV^{-1}, ϕ_0 = 1.337, and q' is the charge of the particle. A, B, C, and ϕ_0 are obtained by minimizing the difference between the invariant

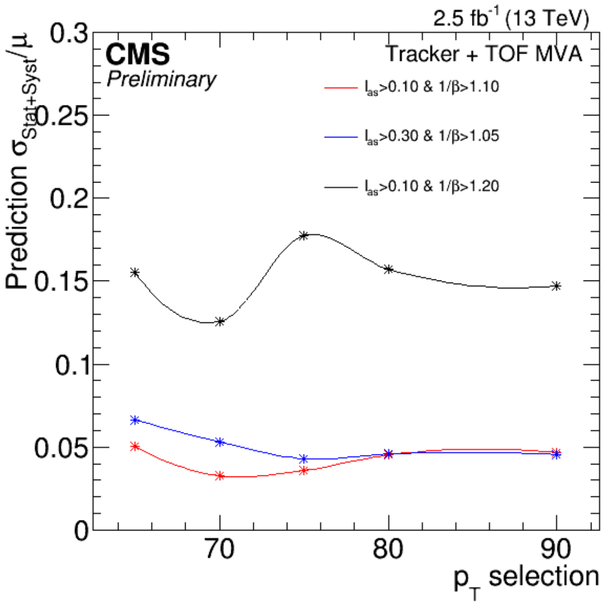

(a) Syst+Stat

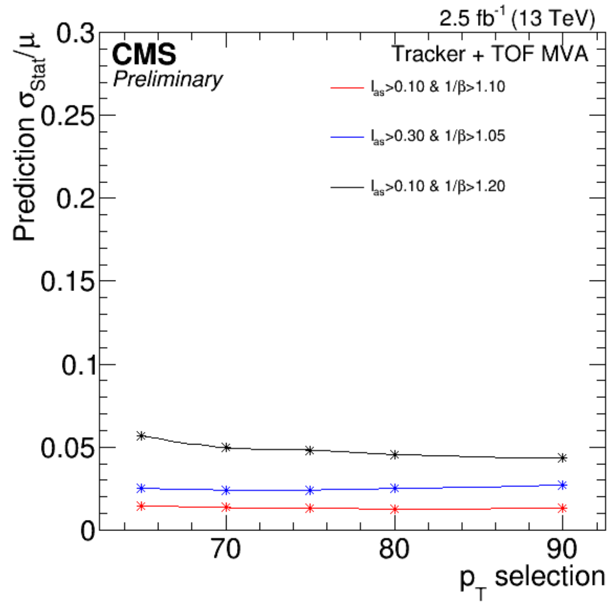

(b) Stat

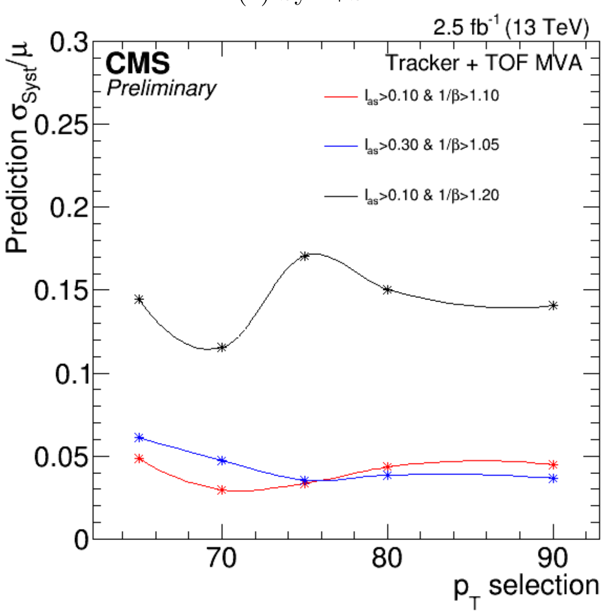

(c) Syst

Figure 4.24: (Left) Ratio of the total variance ($\sigma_{\text{syst+stat}}$) over the mean ($\mu$) for different background estimates (Eq.4.1). (Middle) Ratio of the statistical the quadratic mean of the background estimate statistical uncertainties (σ_{stat}) over the mean (μ) for different background estimates (Eq.4.2). (Right) Ratio of the square difference between the variance in the background estimates and the quadratic mean of the statistical uncertainties (σ_{stat}) and the mean (μ) for different estimates (Eq.4.3). All three plots are drawn for several combinations of I_{as} and $1/\beta$ selections (red, blue, black) versus different p_{T} selection using the 2015 data.

mass distributions from Z $\rightarrow \mu\mu$ events between data and MC simulation [69]. The resulting effect on the signal acceptance due to the p_T shift and the selection on p_T is less than 2%.

The uncertainty on calculated dE/dx in signal MC samples was determined by comparing SM MC tracks and data. The result shows that the MC simulation overestimates the value of dE/dx by as much as 5%, therefore a conservative value of 5% is chosen as the uncertainty on dE/dx. When applied to HSCP candidates, the change in signal acceptance due to passing the selection on I_{as} was found to be on average less than 5%, with some of the smaller mass models experiencing up to 20%.

The uncertainty on the $1/\beta$ estimate for signal MC was determined by comparing dimuon events between MC simulation and data. The MC simulations were found to overestimate $1/\beta$ by 1.5%. The overestimation led to a change in signal acceptance due to passing the selection on $1/\beta$ of less than 5% on average, with some of the smaller mass models experiencing up to 26% change in signal acceptance.

Beginning in 2015, a new source of systematic that may affect the signal acceptance was included. The source is from particles, predominantly low momenta hadrons, originating from the previous bunch crossing and interacting with the tracking layers. These particles, termed Highly Ionizing Particles (HIP), induce a very low charge collection in the track layers causing a drift in the voltage baseline of the tracker layers. The drift can cause a shift downward of the measured cluster charge to below MIP levels, and thus affect the overall estimate of dE/dx. The effect of the HIP induced baseline voltage drift is estimated by using signal MC simulations modified by increasing the rate of low dE/dx measurements. The effect of HIP background on signal acceptance due to passing I_{as} was found to be on average $< 1\%$ for most mass models, and at most 12% for the low mass models.

A source of systematic uncertainty on the signal acceptance that differs from the standard HSCP analysis arises from the use of the artificial neural network. The systematic uncertainty originates from how the uncertainties on the input variables affect the final multivariate discriminant values outputted by the artificial neural network mappings. The 5% overestimate is applied to the HSCP candidate dE/dx from MC signal samples entering the artificial neural network and the resulting difference can be seen in Fig. 4.25. The momentum scale uncertainty described above was applied to the HSCP candidates momenta for both MC and data. The resulting difference in multivariate discriminant distribution can be seen in Fig4.25. The combined effect of both the dE/dx uncertainty and the momentum scale was also studied as it is the combined affect that will change the multivariate discriminant distributions used for discovery and limit setting Fig. 4.25. A similar series of comparisons was done for the Tracker+TOF multivariate analysis including the uncertainty from $1/\beta$.

Overall, it can be seen that the combined dE/dx, momentum, and/or $1/\beta$ uncertainties do cause a slight shift to lower multivaraite discriminant values for some of the signal HSCP candidates, yet a similar shift also occurs to the TOY background discriminant distribution. Overall the discriminant distribution is still heavily peaked near 1 for the signal and near 0 for the TOY background distributions. The combined effect of the uncertainties on the input variables create a shift in the discriminant values and affect signal acceptance. The uncertainty on the signal acceptance due to the shift in multivariate discriminant values is found to be up to 18% for the tracker-only+MVA and up to 22% for the Tracker+TOF+MVA analyses in the lower mass regions. The shifts in discriminant values have less effect on signal acceptance at higher masses, with signal acceptance uncertainties less than 5% for the higher mass regions.

After processing all of the benchmark signal models and examining the impacts of the various sources of systematics on the signal acceptances, total uncertainties on signal acceptance are found to be less than 15% for the tracker-only+MVA and the Tracker+TOF+MVA analyses for most mass models. The dominant contribution to the total signal acceptance uncertainties in the larger mass region is the trigger efficiency. The total uncertainty on the signal acceptance was found to be up to 32% for the lower mass models in the tracker-only+MVA analysis, and up to 45% for the Tracker+TOF+MVA analysis. The larger uncertainties for the lower mass models in both analyses are due to choice of mass used for producing the artificial neural network mapping. As discussed in Sec. 4.2.2, the mappings produce less signal to background discrimination for lower mass points. In the larger mass models, the artificial neural network mappings are better able to discriminate between signal and background. Figure 4.26 show the relative uncertainties across the different masses for the gluino f = 10% and GMSB stau models as for both MVA analyses. Tables 4.2 to 4.7 list the sources of systematic uncertainties and their range of values across the different signal types for the tracker-only+MVA and the Tracker+TOF+MVA analyses.

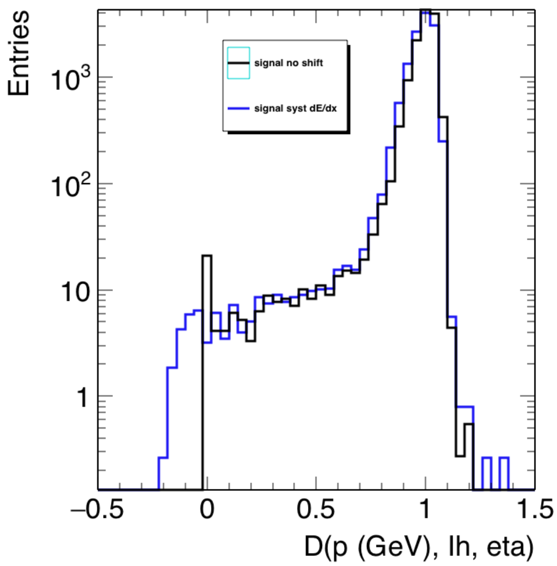

(a) dE/dx estimate

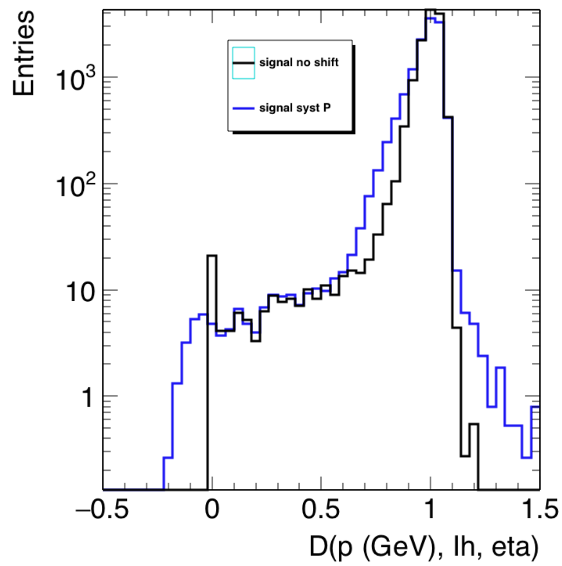

(b) momentum

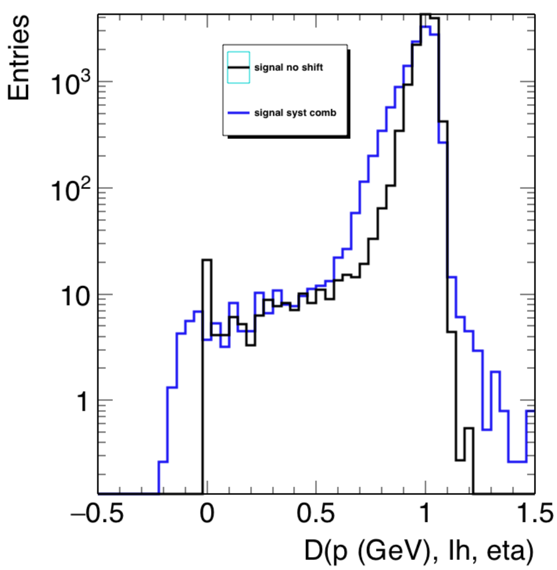

(c) combined

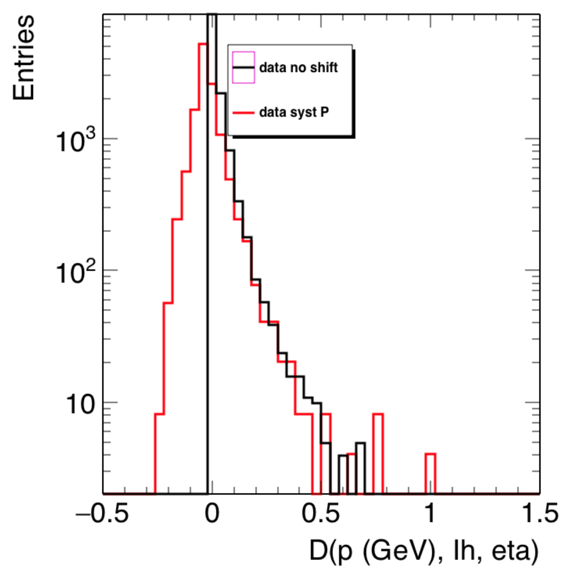

(d) combined

Figure 4.25: Distributions of the multivariate discriminant with (red) and without (blue) the inclusion of the uncertainty on an input variable for tracker-onlyanalysis for a gluino mass = 1200 GeV sample. Both dE/dx estimate (a) and momentum (b) are varied individually and their combined effect is shown as well (c). The inclusion of the uncertainty on momentum for the TOY background sample is also shown (d). All plots use the same gluino mass = 1400 GeV mapping and are normalized to the number of 2015 data passing the final loose selection.

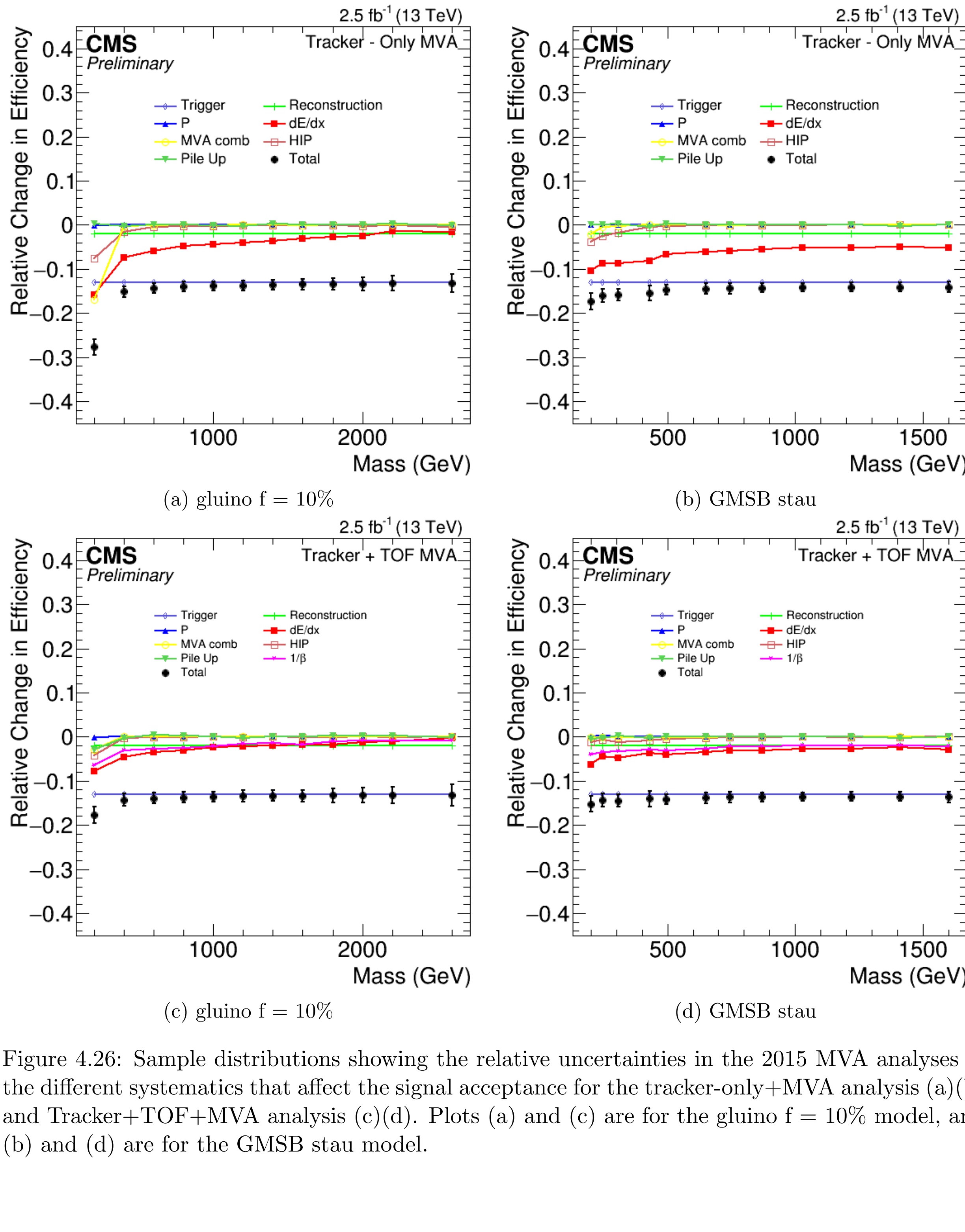

(a) gluino f = 10%

(b) GMSB stau

(c) gluino f = 10%

(d) GMSB stau

Figure 4.26: Sample distributions showing the relative uncertainties in the 2015 MVA analyses of the different systematics that affect the signal acceptance for the tracker-only+MVA analysis (a)(b) and Tracker+TOF+MVA analysis (c)(d). Plots (a) and (c) are for the gluino f = 10% model, and (b) and (d) are for the GMSB stau model.

Table 4.2: Sources of systematic uncertainties and their corresponding relative uncertainties on the gluino signal samples for the 2015 tracker-only+MVA and Tracker+TOF+MVA analyses.

Source	Relative Uncertainty (%)	
	tracker-only+MVA	Tk+TOF+MVA
Trigger efficiency	< 13	< 13
Track momentum scale	< 2	< 2
Track reconstruction	< 2	< 2
Ionization energy loss	< 15	< 8
HIP background effect	< 3	< 4
Time-of-flight	-	< 8
Muon reconstruction	-	2
Pileup contribution	< 1	< 5
MVA	< 10	< 5
Total signal acceptance uncertainty	< 25	< 18
Collision background uncertainty	20	20
Uncertainty on Luminosity	2.3	2.3

Table 4.3: Sources of systematic uncertainties and their corresponding relative uncertainties on the stop signal samples for the 2015 tracker-only+MVA and Tracker+TOF+MVA analyses.

Source	Relative Uncertainty (%)	
	tracker-only+MVA	Tk+TOF+MVA
Trigger efficiency	< 13	< 13
Track momentum scale	< 2	< 2
Track reconstruction	< 2	< 2
Ionization energy loss	< 6	< 10
HIP background effect	< 4	< 6
Time-of-flight	-	< 13
Muon reconstruction	-	2
Pileup contribution	< 1	< 6
MVA	< 6	< 10
Total signal acceptance uncertainty	< 18	< 25
Collision background uncertainty	20	20
Uncertainty on Luminosity	2.3	2.3

Table 4.4: Sources of systematic uncertainties and their corresponding relative uncertainties on the GMSB stau signal samples for the 2015 tracker-only+MVA and Tracker+TOF+MVA analyses.

Source	Relative Uncertainty (%)	
	tracker-only+MVA	Tk+TOF+MVA
Trigger efficiency	< 13	< 13
Track momentum scale	< 2	< 2
Track reconstruction	< 2	< 2
Ionization energy loss	< 12	< 8
HIP background effect	< 5	< 2
Time-of-flight	-	< 4
Muon reconstruction	-	2
Pileup contribution	< 1	< 1
MVA	< 6	< 2
Total signal acceptance uncertainty	< 18	< 16
Collision background uncertainty	20	20
Uncertainty on Luminosity	2.3	2.3

Table 4.5: Sources of systematic uncertainties and their corresponding relative uncertainties on the PP stau signal samples for the 2015 tracker-only+MVA and Tracker+TOF+MVA analyses.

Source	Relative Uncertainty (%)	
	tracker-only+MVA	Tk+TOF+MVA
Trigger efficiency	< 13	< 13
Track momentum scale	< 5	< 2
Track reconstruction	< 2	< 2
Ionization energy loss	< 18	< 10
HIP background effect	< 7	< 4
Time-of-flight	-	< 6
Muon reconstruction	-	2
Pileup contribution	< 1	< 1
MVA	< 15	< 2
Total signal acceptance uncertainty	< 28	< 18
Collision background uncertainty	20	20
Uncertainty on Luminosity	2.3	2.3

Table 4.6: Sources of systematic uncertainties and their corresponding relative uncertainties on the DY $|Q| = 1e$ signal samples for the 2015 tracker-only+MVA and Tracker+TOF+MVA analyses.

Source	Relative Uncertainty (%)	
	tracker-only+MVA	Tk+TOF+MVA
Trigger efficiency	< 13	< 13
Track momentum scale	< 2	< 2
Track reconstruction	< 2	< 2
Ionization energy loss	< 18	< 8
HIP background effect	< 12	< 8
Time-of-flight	-	< 21
Muon reconstruction	-	2
Pileup contribution	< 1	< 20
MVA	< 18	< 22
Total signal acceptance uncertainty	< 32	< 45
Collision background uncertainty	20	20
Uncertainty on Luminosity	2.3	2.3

Table 4.7: Sources of systematic uncertainties and their corresponding relative uncertainties on the DY $|Q| = 2e$ signal samples for the 2015 tracker-only+MVA and Tracker+TOF+MVA analyses.

Source	Relative Uncertainty (%)	
	tracker-only+MVA	Tk+TOF+MVA
Trigger efficiency	< 13	< 13
Track momentum scale	< 2	< 2
Track reconstruction	< 2	< 2
Ionization energy loss	< 2	< 2
HIP background effect	< 4	< 4
Time-of-flight	-	< 26
Muon reconstruction	-	2
Pileup contribution	< 1	< 4
MVA	< 2	< 2
Total signal acceptance uncertainty	< 14	< 35
Collision background uncertainty	20	20
Uncertainty on Luminosity	2.3	2.3

Table 4.8: The number of predicted and observed events in 2015 data for a range of selection values on the multivariate discriminant (MVA). Presented are the results from the gluino mapping.

Analysis	Selection				Number of events	
	p_T (GeV)	I_{as}	$1/\beta$	MVA	Predicted	Observed
tracker-only+MVA	60	0.1	—	0	11946.7± 2392.0	12544
	60	0.1	—	0.20	185.6± 37.1	184
	60	0.1	—	0.40	30.1± 6.0	31
	60	0.1	—	0.60	6.6± 1.4	9
	60	0.1	—	0.80	1.0± 0.2	1
	65	0.3	—	0	29.3± 6.1	24
	65	0.3	—	0.20	3.6± 0.8	0
	65	0.3	—	0.40	0.4± 0.1	0
	65	0.3	—	0.60	0.07± 0.02	0
	65	0.3	—	0.80	0.012± 0.003	0
Tracker+TOF+MVA	65	0.050	1.050	0	16644.9± 3329.8	16546
	65	0.050	1.050	0.20	664.9 ± 133.0	661
	65	0.050	1.050	0.40	103.0± 20.6	97
	65	0.050	1.050	0.60	20.3± 4.1	17
	65	0.050	1.050	0.80	2.1± 0.4	2
	65	0.175	1.250	0	0.85± 0.18	0
	65	0.175	1.250	0.20	0.05 ± 0.01	0
	65	0.175	1.250	0.40	0.003± 0.001	0
	65	0.175	1.250	0.60	0.001± 0.000	0
	65	0.175	1.250	0.80	0.000± 0.000	0

4.4 Multivariate Analyses Results with 2015 Data

The numbers of observed data for the 2015 dataset and background prediction were obtained using the same selections on I_{as}, p_T, and $1/\beta$ as the standard HSCP analyses with the multivariate discriminant replacing the selection on mass. No statistically significant excess was observed for different selection values on the multivariate discriminant as seen Tables 4.8 and 4.9 for either the tracker-only+MVA or the Tracker+TOF+MVA analyses. The final loose selection is also provided in the tables showing the agreement between the background prediction and the observed 2015 data. A table for each signal type listing the prediction versus observed data for the 2015 dataset can be found in Appendix A.

The Higgs tool was used to produce cross section limits as was done for the standard HSCP analyses. A summary of results from the Higgs tool for the multivariate analyses are presented in Tables

Table 4.9: The number of predicted and observed events in 2015 data for a range of selection values on the multivariate discriminant (MVA). Presented are the results from the GMSB stau mapping.

Analysis	Selection				Number of events	
	p_T (GeV)	I_{as}	$1/\beta$	MVA	Predicted	Observed
tracker-only+MVA	60	0.1	—	0	11946.7± 2392.3	12544
	60	0.1	—	0.2	206.5± 41.3	209
	60	0.1	—	0.4	47.0± 9.4	49
	60	0.1	—	0.6	13.9± 2.8	17
	60	0.1	—	0.8	3.9± 0.8	6
	65	0.3	—	0	29.3± 6.1	24
	65	0.3	—	0.20	2.9± 0.7	1
	65	0.3	—	0.40	0.4± 0.1	0
	65	0.3	—	0.60	0.1± 0.02	0
	65	0.3	—	0.80	0.03± 0.006	0
Tracker+TOF+MVA	65	0.050	1.050	0	16644.9± 3331.2	16546
	65	0.050	1.050	0.20	513.4 ± 102.7	484
	65	0.050	1.050	0.40	182.2± 36.5	164
	65	0.050	1.050	0.60	74.9± 15.0	73
	65	0.050	1.050	0.80	26.3± 5.3	22
	65	0.175	1.250	0	0.85 ± 0.18	0
	65	0.175	1.250	0.20	0.010± 0.002	0
	65	0.175	1.250	0.40	0.003± 0.001	0
	65	0.175	1.250	0.60	0.001± 0.000	0
	65	0.175	1.250	0.60	0.000± 0.000	0

4.10 to 4.13. The results were obtained using the same selection on p_T, I_{as}, and $1/\beta$ as the standard analyses, but with a selection on multivariate discriminant replacing the selection on mass. The range of selection values across all signal models for the multivariate discriminant varied between 0.2 to 0.98 for the tracker-only+MVA and between 0.2 to 0.54 for the Tracker+TOF+MVA analyses. The selection on multivariate discriminant was calculated for each signal model to maximize signal significance as discussed in Sec. 4.1. The Higgs tool placed upper limits at the 95% CL on the observed cross section that varied between 1.8×10^{-3} pb to 8.6×10^{-1} pb for the tracker-only+MVA analysis. For the Tracker+TOF+MVA analysis, the upper limits varied between 1.7×10^{-3} pb to 1.3×10^{-1} pb.

A comparison of the observed cross section limits produced by the Higgs tool and the theoretical cross sections allowed the estimation of lower mass limits for each signal type. Lower mass limits of 1610(1590) GeV for the gluino f = 10%, 1040(990) GeV for the stop, 490(490) GeV for the GMSB stau, 200(240) for the PP stau, 510(550) GeV for the DY $|Q| = 1e$, and 710(660) GeV for the DY $|Q| = 2e$ were calculated for the tracker-only+MVA(Tracker+TOF+MVA) analysis. The lower mass limits on the 2015 data for both standard and multivariate analyses are listed in Table 4.14.

When compared to the results of the standard analysis, the HSCP multivariate analyses showed an improvement in the expected and observed cross sections for some of the signal models, while the results for many models remained unchanged. The improvement was up to 10% in some cases. In general there was negligible improvement on the lower mass limits, with several of the mass limits only improving by $< 1\%$. However there was $\approx 5\%$ improvement for the modified DY signal types in the tracker-only+MVA analysis compared to the standard tracker-only analysis. Furthermore, the standard Tracker+TOF analysis was unable to place a lower mass limit on the PP stau, but the Tracker+TOF+MVA analysis was successful.

An investigation was also conducted on the robustness of the MVA upon relaxation of the selection criteria. By constraint, the selection on p_T was not allowed to be relaxed because the next lower value would be identical to the pre-selection criteria. Therefore the selections on I_{as} and/or $1/\beta$ were relaxed in an attempt to find a more optimal set of selection criteria. For the tracker-only+MVA analysis, the I_{as} was varied in 0.025 increments from 0.200 to 0.300, and the results of the Higgs tool were recorded. For the Tracker + TOF + MVA analysis, both the final

Table 4.10: Summary of the theoretical cross section (ThXsec), expected cross section limit at 95% CL (ExpXsec), and observed cross section limits at 95% CL (ObsXsec) for a range of gluino signal mass points for the tracker-only+MVA analysis using 2015 data. Included are the selection criteria (p_T, I_{as}, $1/\beta$, and MVA), as well as the signal efficiency (Seff), number of predicted background (Bckg. Pred), and observed data (obs) that pass the selection criteria. Shown are f = 10%,50% for gluino models including the the charged suppressed interaction models (denoted with an N).

Model	Mass (GeV)	$p_T >$ (GeV)	$I_{as} >$	$1/\beta >$	MVA>	Bckg. Pred	Obs	Seff	ThXsec (pb)	ExpXsec (pb)	ObsXsec (pb)	Signif
Gluino f = 0.1	1000	65	0.300	/	0.420	0.309 ± 0.068	0	0.233	3.2E-01	5.2E-03	5.2E-03	0.00
Gluino f = 0.1	1400	65	0.300	/	0.640	0.049 ± 0.011	0	0.199	2.5E-02	6.1E-03	6.1E-03	0.00
Gluino f = 0.1	1800	65	0.300	/	0.640	0.049 ± 0.011	0	0.143	2.7E-03	8.5E-03	8.5E-03	0.00
Gluino f = 0.1	2200	65	0.300	/	0.640	0.049 ± 0.011	0	0.094	3.6E-04	1.3E-02	1.3E-02	0.00
Gluino f = 0.5	1000	65	0.300	/	0.480	0.183 ± 0.040	0	0.136	3.2E-01	9.0E-03	9.0E-03	0.00
Gluino f = 0.5	1400	65	0.300	/	0.620	0.056 ± 0.012	0	0.114	2.5E-02	1.0E-02	1.0E-02	0.00
Gluino f = 0.5	1800	65	0.300	/	0.640	0.049 ± 0.011	0	0.080	2.7E-03	1.5E-02	1.5E-02	0.00
Gluino f = 0.5	2200	65	0.300	/	0.640	0.049 ± 0.011	0	0.052	3.6E-04	2.3E-02	2.3E-02	0.00
Gluino N f = 0.1	1200	65	0.300	/	0.460	0.215 ± 0.047	0	0.190	8.4E-02	6.4E-03	6.4E-03	0.00
Gluino N f = 0.1	1600	65	0.300	/	0.640	0.049 ± 0.011	0	0.148	8.0E-03	8.3E-03	8.3E-03	0.00
Gluino N f = 0.1	2000	65	0.300	/	0.640	0.049 ± 0.011	0	0.103	9.7E-04	1.2E-02	1.2E-02	0.00
Gluino N f = 0.5	1200	65	0.300	/	0.540	0.106 ± 0.023	0	0.146	8.4E-02	8.5E-03	8.5E-03	0.00
Gluino N f = 0.5	1600	65	0.300	/	0.640	0.049 ± 0.011	0	0.114	8.0E-03	1.1E-02	1.1E-02	0.00
Gluino N f = 0.5	2000	65	0.300	/	0.640	0.049 ± 0.011	0	0.079	9.7E-04	1.5E-02	1.5E-02	0.00

Table 4.11: Summary of the theoretical cross section (ThXsec), expected cross section limit at 95% CL (ExpXsec), and observed cross section limits at 95% CL (ObsXsec) for a range of stop signal mass points for the tracker-only+MVA analysis using 2015 data. Included are the selection criteria (p_T, I_{as}, $1/\beta$, and Mass), as well as the signal efficiency (Seff), number of predicted background (Bckg. Pred), and observed data (obs) that pass the selection criteria. Shown are stop models including the charged suppressed interaction models (denoted with an N).

Model	Mass (GeV)	$p_T >$ (GeV)	$I_{as} >$	$1/\beta >$	MVA>	Bckg. Pred	Obs	Seff	ThXsec (pb)	ExpXsec (pb)	ObsXsec (pb)	Signif
Stop	1000	65	0.300	/	0.700	0.052 ± 0.011	0	0.262	6.0E-03	4.6E-03	4.6E-03	0.00
Stop	1400	65	0.300	/	0.700	0.052 ± 0.011	0	0.229	4.5E-04	5.3E-03	5.3E-03	0.00
Stop	1800	65	0.300	/	0.700	0.052 ± 0.011	0	0.168	4.6E-05	7.2E-03	7.2E-03	0.00
Stop N	1000	65	0.300	/	0.700	0.052 ± 0.011	0	0.196	6.0E-03	6.2E-03	6.2E-03	0.00
Stop N	1600	65	0.300	/	0.700	0.052 ± 0.011	0	0.155	1.4E-04	7.8E-03	7.8E-03	0.00
Stop N	1800	65	0.300	/	0.700	0.052 ± 0.011	0	0.128	4.6E-05	9.3E-03	9.3E-03	0.00

Table 4.12: Summary of the theoretical cross section (ThXsec), expected cross section limit at 95% CL (ExpXsec), and observed cross section limits at 95% CL (ObsXsec) for a range of stau signal mass points for the Tracker+TOF+MVA analysis using 2015 data. Included are the selection criteria (p_T, I_{as}, $1/\beta$, and Mass), as well as the signal efficiency (Seff), number of predicted background (Bckg. Pred), and observed data (obs) that pass the selection criteria. Shown are the GMSB and PP stau production modes.

Model	Mass (GeV)	$p_T >$ (GeV)	$I_{as} >$	$1/\beta >$	MVA>	Bckg. Pred	Obs	Seff	ThXsec (pb)	ExpXsec (pb)	ObsXsec (pb)	Signif
GMSB stau	247	65	0.175	1.250	0.200	0.170 ± 0.034	0	0.365	8.8E-02	3.3E-03	3.3E-03	0.00
GMSB stau	308	65	0.175	1.250	0.260	0.082 ± 0.016	0	0.433	2.5E-02	2.9E-03	2.9E-03	0.00
GMSB stau	494	65	0.175	1.250	0.300	0.054 ± 0.011	0	0.595	1.9E-03	2.1E-03	2.1 E-03	0.00
PP stau	247	65	0.175	1.250	0.320	0.053 ± 0.011	0	0.271	3.7E-03	4.6E-03	4.6E-03	0.00
PP stau	308	65	0.175	1.250	0.320	0.053 ± 0.011	0	0.317	1.5E-03	3.9E-03	3.9E-03	0.00
PP stau	494	65	0.175	1.250	0.320	0.053 ± 0.011	0	0.418	1.9E-04	2.9E-03	2.9E-03	0.00

Table 4.13: Summary of the theoretical cross section (ThXsec), expected cross section limit at 95% CL (ExpXsec), and observed cross section limits at 95% CL (ObsXsec) for a range of modified Drell-Yan signal mass points for the Tracker+TOF+MVA analysis using 2015 data. Included are the selection criteria (p_T, I_{as}, $1/\beta$, and MVA), as well as the signal efficiency (Seff), number of predicted background (Bckg. Pred), and observed data (obs) that pass the selection criteria. Shown are the modified DY $|Q| = 1e$ and $|Q| = 2e$ models.

Model	Mass (GeV)	$p_T >$ (GeV)	$I_{as} >$	$1/\beta >$	MVA>	Bckg. Pred	Obs	Seff	ThXsec (pb)	ExpXsec (pb)	ObsXsec (pb)	Signif
DY $\|Q\| = 1e$	400	65	0.175	1.250	0.220	0.055 ± 0.011	0	0.420	7.3E-03	3.0E-03	3.0E-03	0.00
DY $\|Q\| = 1e$	600	65	0.175	1.250	0.220	0.055 ± 0.011	0	0.466	1.2E-03	2.7E-03	2.7E-03	0.00
DY $\|Q\| = 1e$	800	65	0.175	1.250	0.220	0.055 ± 0.011	0	0.488	2.6E-04	2.6E-03	2.6E-03	0.00
DY $\|Q\| = 2e$	400	65	0.175	1.250	0.200	0.026 ± 0.005	0	0.410	2.3E-02	3.1E-03	3.1E-03	0.00
DY $\|Q\| = 2e$	600	65	0.175	1.250	0.200	0.026 ± 0.005	0	0.482	3.5E-03	2.6E-03	2.6E-03	0.00
DY $\|Q\| = 2e$	800	65	0.175	1.250	0.200	0.026 ± 0.005	0	0.489	8.0E-04	2.6E-03	2.6E-03	0.00

Table 4.14: Lower mass limits for the 2015 data from both the standard HSCP analyses (tracker-only and Tracker+TOF) compared to the HSCP multivariate analyses (tracker-only+MVA and Tracker+TOF+MVA) for all 6 benchmark signal types. All analyses used the final tight selection.

	Lower mass limit			
	tracker-only		Tracker+TOF	
Signal Type	Mass selection	MVA selection	Mass selection	MVA selection
Gluino f = 0.1	1610	1620	1580	1590
Stop	1040	1040	990	990
GMSB Stau	490	490	480	490
PP Stau	240	240	—	240
DY $\|Q\|$ = 1e	510	540	550	550
DY $\|Q\|$ = 2e	680	710	660	660

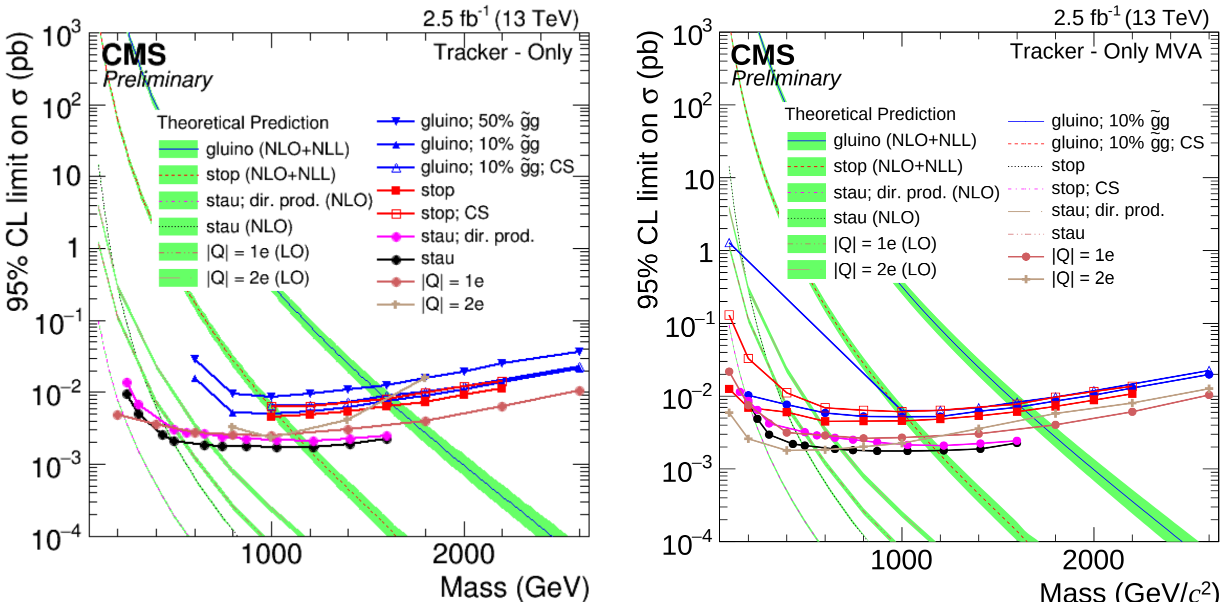

(a) Standard analysis (b) MVA

Figure 4.27: Theoretical cross section and the 95% CL upper limit on the observed cross section, both as a function of mass, using the final tight selection on 2015 data. The left plot shows the results from the standard HSCP tracker-only analysis, and the right plot shows the results from the tracker-only+MVA analysis.

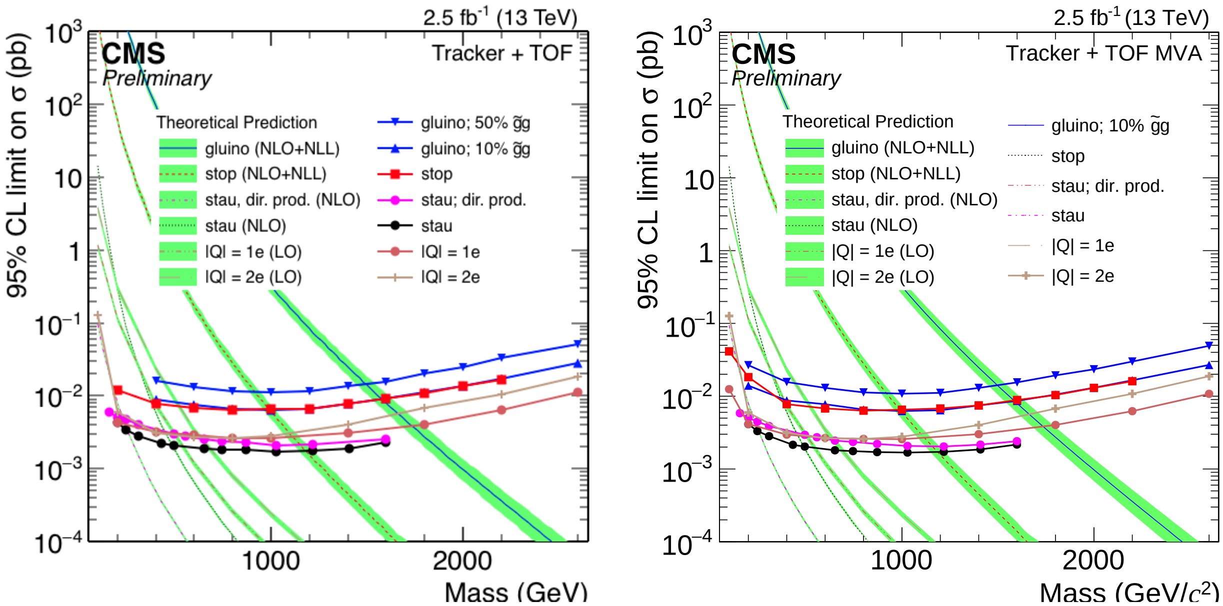

(a) Standard analysis (b) MVA

Figure 4.28: Theoretical cross section and the 95% CL upper limit on the observed cross section, both as a function of mass, using the final tight selection on 2015 data. The left plot shows the results from the standard HSCP tracker-only analysis, and the right plot shows the results from the Tracker+TOF+MVA analysis.

selection values on I_{as} and $1/\beta$ were relaxed between 0.175 to 0.150 for I_{as} and between 1.25 to 1.15 in $1/\beta$.

The combinations of relaxed final selection criteria were applied to a range of signal models in search of a potentially optimized selection over the final selection from the standard analyses. The determination of an improved final selection criteria was taken to be that which decreased the median value of the expected upper cross section limit while maintaining the $\pm\sigma$ range. Furthermore the chosen selection criteria was also required to maintain a $\pm 2\sigma$ range comparable to the results of the standard HSCP analysis. Tables 4.15 to 4.20 show the Higgs tool results of scanning through the different selection criteria.

The final selection criteria from the optimization scan to be tested were chosen to be $I_{as} > 0.250$ and $p_T > 65$ GeV for the tracker-only+MVA, and $I_{as} > 0.150$, $p_T > 65$ GeV, $1/\beta > 1.250$ for the Tracker+TOF+MVA analysis as seen in Table 4.21. The MVA selection during limit setting was again selected by maximizing the signal significance for MVA values between 0.2 and 1 for each signal model.

Using the final selections from the optimization scan, a comparison of the theoretical cross sections and the 95% CL upper limit on observed cross sections can be seen on the right in Fig. 4.29 for the tracker-only+MVA and Fig. 4.30 for the Tracker+TOF+MVA analysis. On the left of Figs. 4.29 and 4.30 are the standard HSCP analyses equivalent limit plots for the 2015 data. In Tables 4.22 to 4.25 are summaries of results for the signal benchmarks focusing on the hadron-like signals for the tracker-only+MVA analysis, and the lepton-like signals for the tracker+TOF+MVA analysis. A more inclusive summary can be found in Appendix B. The theoretical and upper limit on the observed cross section are used to place lower mass limits on the benchmark signal types. Table 4.26 shows the lower mass limits.

The final selection from the optimization scan did not produce a statistically significant excess of observed data over the background prediction. However, improvements were found in the cross section limits. Compared to the standard analyses, the upper limit on the expected and observed cross sections was up to $\approx 10\%$ lower than the results from the 2015 analysis. The lower mass limits remained relatively unchanged for many of the signal types between the 2015 standard analyses and the MVA analyses with the relaxed final selection from the scan. The results in both the cross section limits and the mass limits were consistent with the results obtained using the selection

Table 4.15: The table below show the results of varying the final selection criteria and the result produced by the Higgs tool when applied to a range of gluino signal models. Here, the central value of the upper expected cross section limit is denoted as μ_{exp}, and the uncertainty ranges are labeled as $\pm1\sigma_{exp}$ and $\pm2\sigma_{exp}$.

Model	$p_T >$ (GeV)	$I_{as} >$	MVA >	μ_{exp} (pb)	$+1\sigma_{exp}$ (pb)	$-1\sigma_{exp}$ (pb)	$+2\sigma_{exp}$ (pb)	$-2\sigma exp$ (pb)
Gluino f=0.1	65	0.300	0.58	0.005335	0.005335	0.005335	0.008307	0.005296
mass=1200 GeV	65	0.275	0.58	0.005298	0.005298	0.005298	0.008145	0.005096
	65	0.250	0.58	0.005167	0.005167	0.005167	0.008051	0.005060
	65	0.225	0.60	0.005088	0.008459	0.005088	0.009091	0.005023
	65	0.200	0.60	0.005098	0.005098	0.005098	0.008155	0.005138
Gluino f=0.1	65	0.300	0.64	0.008518	0.008518	0.008518	0.013470	0.008270
mass=1800 GeV	65	0.275	0.64	0.008428	0.008428	0.008428	0.013012	0.008332
	65	0.250	0.72	0.008312	0.008312	0.008312	0.013031	0.008095
	65	0.225	0.76	0.008315	0.008315	0.008315	0.012877	0.008126
	65	0.200	0.78	0.008024	0.008216	0.008024	0.012664	0.008019
Gluino f=0.1	65	0.300	0.64	0.013013	0.013013	0.013013	0.020035	0.012615
mass=2200 GeV	65	0.275	0.64	0.012789	0.012789	0.012789	0.020187	0.012662
	65	0.250	0.64	0.012881	0.012881	0.012881	0.020161	0.012699
	65	0.225	0.64	0.012753	0.012753	0.012753	0.019998	0.012647
	65	0.200	0.64	0.012535	0.013256	0.012426	0.019578	0.012330

Table 4.16: The table below show the results of varying the final selection criteria and the result produced by the Higgs tool when applied to a range of stop signal models. Here, the central value of the upper expected cross section limit is denoted as μ_{exp}, and the uncertainty ranges are labeled as $\pm 1\sigma_{exp}$ and $\pm 2\sigma_{exp}$.

Model	$p_T >$ (GeV)	$I_{as} >$	MVA >	μ_{exp} (pb)	$+1\sigma_{exp}$ (pb)	$-1\sigma_{exp}$ (pb)	$+2\sigma_{exp}$ (pb)	$-2\sigma exp$ (pb)
Stop	65	0.300	0.70	0.004584	0.004584	0.004584	0.007350	0.004564
mass = 1000 GeV	65	0.275	0.70	0.004671	0.004671	0.004671	0.007109	0.004550
	65	0.250	0.72	0.004558	0.004558	0.004558	0.006813	0.004334
	65	0.225	0.78	0.004508	0.004508	0.004508	0.006753	0.004315
	65	0.200	0.78	0.005167	0.005167	0.005167	0.008330	0.005164
Stop	65	0.300	0.70	0.005314	0.005314	0.005314	0.008269	0.005211
mass = 1400 GeV	65	0.275	0.70	0.005249	0.005249	0.005249	0.008087	0.005215
	65	0.250	0.72	0.005148	0.005148	0.005148	0.007983	0.005112
	65	0.225	0.72	0.005127	0.005127	0.005127	0.008029	0.004936
	65	0.200	0.74	0.005288	0.005288	0.005288	0.008431	0.005464
Stop	65	0.70	0.300	0.007194	0.007194	0.007194	0.011418	0.006971
mass = 1800 GeV	65	0.275	0.70	0.007106	0.007106	0.007106	0.011204	0.006979
	65	0.250	0.72	0.007034	0.007034	0.007034	0.010947	0.006960
	65	0.225	0.76	0.007624	0.007624	0.007624	0.011000	0.006911
	65	0.200	0.76	0.007574	0.007734	0.007210	0.011763	0.007204

Table 4.17: The table below show the results of varying the final selection criteria and the result produced by the Higgs tool when applied to a range of GMSB stau signal models for the Tracker+TOF+MVA analysis. Here, the central value of the upper expected cross section limit is denoted as μ_{exp}, and the uncertainty ranges are labeled as $\pm 1\sigma_{exp}$ and $\pm 2\sigma_{exp}$.

Model	$p_T >$ (GeV)	$I_{as} >$	$1/\beta >$	MVA >	μ_{exp} (pb)	$+1\sigma_{exp}$ (pb)	$-1\sigma_{exp}$ (pb)	$+2\sigma_{exp}$ (pb)	$-2\sigma exp$ (pb)
GMSB stau	65	0.175	1.25	0.26	0.002875	0.002875	0.002875	0.004302	0.002763
mass=308 GeV	65	0.175	1.20	0.26	0.002585	0.003928	0.002585	0.005143	0.002568
	65	0.175	1.15	0.26	0.003333	0.005375	0.002609	0.006856	0.002465
	65	0.150	1.25	0.26	0.002727	0.004134	0.002727	0.005613	0.002672
	65	0.150	1.20	0.26	0.003659	0.004933	0.002500	0.005933	0.002463
	65	0.150	1.15	0.26	0.004030	0.005791	0.003133	0.007894	0.002400
GMSB stau	65	0.175	1.25	0.30	0.002064	0.002064	0.002064	0.003181	0.002046
mass= 494 GeV	65	0.175	1.20	0.32	0.001951	0.001951	0.001951	0.003089	0.001897
	65	0.175	1.15	0.36	0.001934	0.002241	0.001934	0.002920	0.001873
	65	0.150	1.25	0.36	0.002038	0.002038	0.002038	0.003109	0.001979
	65	0.150	1.20	0.36	0.001886	0.001886	0.001886	0.002921	0.001873
	65	0.150	1.15	0.38	0.001835	0.002832	0.001835	0.003468	0.001827

Table 4.18: The table below show the results of varying the final selection criteria and the result produced by the Higgs tool when applied to a range of PP stau signal models for the Tracker+TOF+MVA analysis. Here, the central value of the upper expected cross section limit is denoted as μ_{exp}, and the uncertainty ranges are labeled as $\pm 1\sigma_{exp}$ and $\pm 2\sigma_{exp}$.

Model	$p_T >$ (GeV)	$I_{as} >$	$1/\beta >$	MVA >	μ_{exp} (pb)	$+1\sigma_{exp}$ (pb)	$-1\sigma_{exp}$ (pb)	$+2\sigma_{exp}$ (pb)	$-2\sigma exp$ (pb)
PP stau	65	0.175	1.25	0.32	0.003912	0.003912	0.003912	0.005983	0.003731
mass = 308 GeV	65	0.175	1.20	0.32	0.003545	0.003545	0.003545	0.005451	0.003548
	65	0.175	1.15	0.38	0.003516	0.005139	0.003516	0.007001	0.003482
	65	0.150	1.25	0.44	0.003818	0.003818	0.003818	0.005975	0.003775
	65	0.150	1.20	0.46	0.003348	0.005292	0.003340	0.006820	0.003326
	65	0.150	1.15	0.50	0.004535	0.006301	0.003544	0.008342	0.003342
PP stau	65	0.175	1.25	0.32	0.002913	0.002913	0.002913	0.004544	0.002905
mass = 494 GeV	65	0.175	1.20	0.32	0.002746	0.002746	0.002746	0.004217	0.002671
	65	0.175	1.15	0.36	0.002650	0.003539	0.002650	0.004070	0.002630
	65	0.150	1.25	0.44	0.002839	0.002839	0.002839	0.004375	0.002799
	65	0.150	1.20	0.48	0.002613	0.002613	0.002613	0.004131	0.002562
	65	0.150	1.15	0.48	0.002497	0.003693	0.002497	0.004939	0.002449

Table 4.19: The table below show the results of varying the final selection criteria and the result produced by the Higgs tool when applied to a range of DY $|Q| = 1e$ signal models for the Tracker+TOF+MVA analysis. Here, the central value of the upper expected cross section limit is denoted as μ_{exp}, and the uncertainty ranges are labeled as $\pm1\sigma_{exp}$ and $\pm2\sigma_{exp}$.

Model	$p_T >$ (GeV)	$I_{as} >$	$1/\beta >$	MVA >	μ_{exp} (pb)	$+1\sigma_{exp}$ (pb)	$-1\sigma_{exp}$ (pb)	$+2\sigma_{exp}$ (pb)	$-2\sigma exp$ (pb)
DY $\|Q\| = 1e$	65	0.175	1.25	0.22	0.003021	0.003021	0.003021	0.004660	0.002939
mass = 400 GeV	65	0.175	1.20	0.22	0.002804	0.002852	0.002804	0.004317	0.002765
	65	0.175	1.15	0.26	0.002740	0.004158	0.002740	0.005460	0.002729
	65	0.150	1.25	0.26	0.002915	0.002915	0.002915	0.004673	0.002888
	65	0.150	1.20	0.30	0.002804	0.004166	0.002804	0.005608	0.002720
	65	0.150	1.15	0.30	0.002693	0.003888	0.002653	0.006573	0.002631
DY $\|Q\| = 1e$	65	0.175	1.25	0.22	0.002718	0.002718	0.002718	0.004238	0.002633
mass = 600 GeV	65	0.175	1.20	0.22	0.002590	0.002590	0.002590	0.004082	0.002523
	65	0.175	1.15	0.28	0.002471	0.002471	0.002471	0.003937	0.002459
	65	0.150	1.25	0.26	0.002671	0.002671	0.002671	0.004194	0.002646
	65	0.150	1.20	0.26	0.002525	0.002525	0.002525	0.003912	0.002485
	65	0.150	1.15	0.32	0.002459	0.002478	0.002459	0.003790	0.002404

Table 4.20: The table below show the results of varying the final selection criteria and the result produced by the Higgs tool when applied to a range of DY $|Q| = 2e$ signal models for the Tracker+TOF+MVA analysis. Here, the central value of the upper expected cross section limit is denoted as μ_{exp}, and the uncertainty ranges are labeled as $\pm 1\sigma_{exp}$ and $\pm 2\sigma_{exp}$.

Model	$p_T >$ (GeV)	$I_{as} >$	$1/\beta >$	MVA $>$	μ_{exp} (pb)	$+1\sigma_{exp}$ (pb)	$-1\sigma_{exp}$ (pb)	$+2\sigma_{exp}$ (pb)	$-2\sigma exp$ (pb)
DY $\lvert Q\rvert = 2e$	65	0.175	1.25	0.20	0.003102	0.003102	0.003102	0.004713	0.003029
mass = 400 GeV	65	0.175	1.20		0.002602	0.002602	0.002602	0.004054	0.002545
	65	0.175	1.15		0.002292	0.003059	0.002292	0.003622	0.002240
	65	0.150	1.25		0.003098	0.003098	0.003098	0.004808	0.003077
	65	0.150	1.20		0.002615	0.002615	0.002615	0.004184	0.002527
	65	0.150	1.15		0.002343	0.003242	0.002343	0.004096	0.002193
DY $\lvert Q\rvert = 2e$	65	0.175	1.25	0.20	0.002659	0.002659	0.002659	0.004088	0.002602
mass = 600 GeV	65	0.175	1.20		0.002322	0.002322	0.002322	0.003659	0.002311
	65	0.175	1.15		0.002142	0.002142	0.002142	0.003362	0.002134
	65	0.150	1.25		0.002587	0.002587	0.002587	0.004096	0.002586
	65	0.150	1.20		0.002310	0.002310	0.002310	0.003625	0.002288
	65	0.150	1.15		0.002179	0.002179	0.002179	0.003401	0.002167

Table 4.21: Relaxed selection criteria for the MVA analyses not including MVA selection.

tracker-only+MVA	
Selection	value
p_T	65 GeV
I_{as}	0.250

Tracker + TOF + MVA	
Selection	value
p_T	65 GeV
I_{as}	1.50
$1/\beta$	1.25

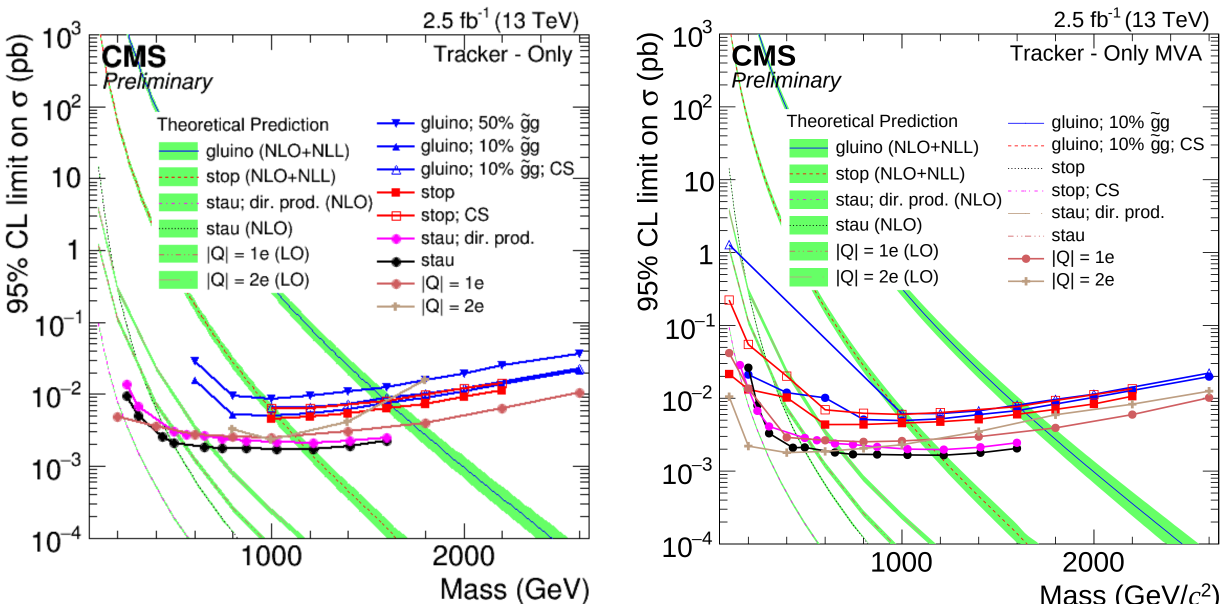

(a) Standard analysis (b) MVA

Figure 4.29: Theoretical and 95% CL upper limit on observed cross sections, both as a function of mass, using 2015 data. The left plot shows the results from the standard HSCP tracker-only analysis using the final tight selection. The right plot shows the results from the tracker-only+MVA analysis using the relaxed final selection.

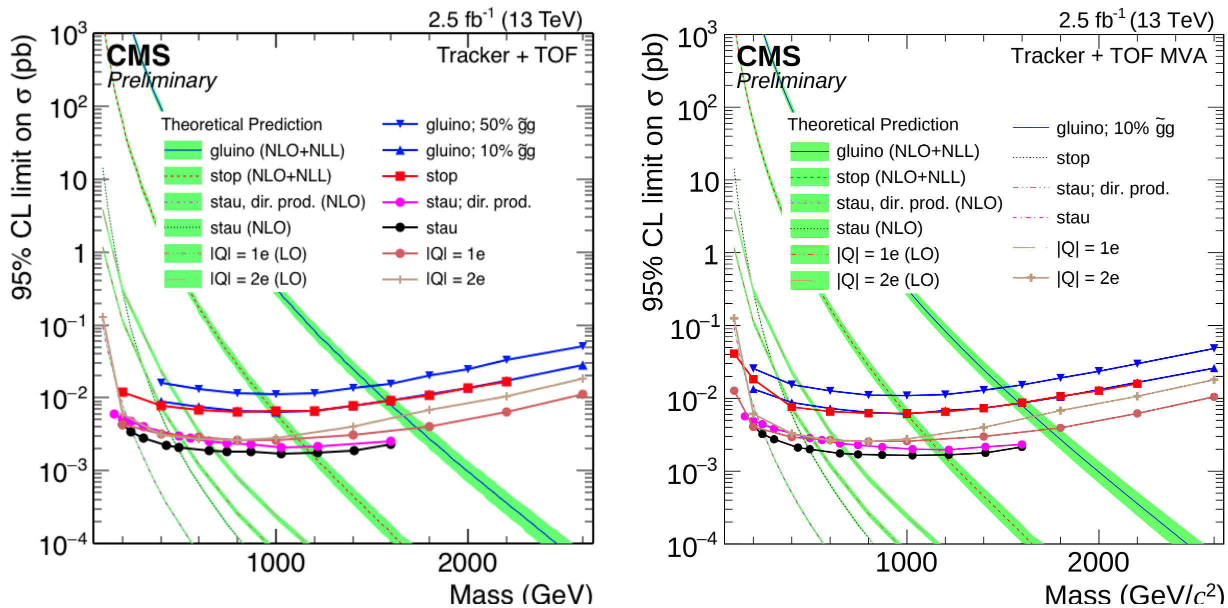

(a) Standard analysis (b) MVA

Figure 4.30: Theoretical and 95% CL upper limit on observed cross sections, both as a function of mass, using 2015 data. The left plot shows the results from the standard HSCP Tracker+TOF analysis using the final tight selection. The right plot shows the results from the Tracker+TOF+MVA analysis using the relaxed final selection.

Table 4.22: Summary of the theoretical cross section (ThXsec), expected cross section limit at 95% CL (ExpXsec), and observed cross section limits at 95% CL (ObsXsec) for a range of gluino signal mass points for the tracker-only+MVA analysis using 2015 data and relaxed final selection. Included are the selection criteria (p_T, I_{as}, $1/\beta$, and MVA), as well as the signal efficiency (Seff), number of predicted background (Bckg. Pred), and observed data (obs) that pass the selection criteria. Shown are f = 10%,50% for gluino models including the the charged suppressed interaction models (denoted with an N).

Model	Mass (GeV)	$p_T >$ (GeV)	$I_{as} >$	$1/\beta >$	MVA>	Bckg. Pred	Obs	Seff	ThXsec (pb)	ExpXsec (pb)	ObsXsec (pb)	Signif
Gluino f=0.1	1000	65	0.250	/	0.420	0.540 ± 0.112	0	0.242	3.2E-01	4.9E-03	4.9E-03	0.00
Gluino f=0.1	1600	65	0.250	/	0.640	0.091 ± 0.019	0	0.177	8.0E-03	6.8E-03	6.8E-03	0.00
Gluino f=0.1	1800	65	0.250	/	0.640	0.091 ± 0.019	0	0.146	2.7E-03	8.3E-03	8.3E-03	0.00
Gluino f=0.1	2200	65	0.250	/	0.640	0.091 ± 0.019	0	0.095	3.6E-04	1.3E-02	1.3E-02	0.00
Gluino f=0.5	1000	65	0.250	/	0.480	0.328 ± 0.068	0	0.142	3.2E-01	8.4E-03	8.4E-03	0.00
Gluino f=0.5	1400	65	0.250	/	0.640	0.091 ± 0.019	0	0.118	2.5E-02	1.0E-02	1.0E-02	0.00
Gluino f=0.5	1800	65	0.250	/	0.640	0.091 ± 0.019	0	0.083	2.7E-03	1.5E-02	1.5E-02	0.00
Gluino f=0.5	2200	65	0.250	/	0.640	0.091 ± 0.019	0	0.053	3.6E-04	2.3E-02	2.3E-02	0.00
GluinoN f10	1200	65	0.250	/	0.460	0.383 ± 0.079	0	0.195	8.4E-02	6.2E-03	6.2E-03	0.00
GluinoN f10	1600	65	0.250	/	0.640	0.091 ± 0.019	0	0.150	8.0E-03	8.0E-03	8.0E-03	0.00
GluinoN f10	2000	65	0.250	/	0.640	0.091 ± 0.019	0	0.104	9.7E-04	1.1E-02	1.1E-02	0.00
GluinoN f=0.5	1200	65	0.250	/	0.540	0.196 ± 0.040	0	0.150	8.4E-02	8.1E-03	8.1E-03	0.00
GluinoN f=0.5	1600	65	0.250	/	0.640	0.091 ± 0.019	0	0.116	8.0E-03	1.0E-02	1.0E-02	0.00
GluinoN f=0.5	2000	65	0.250	/	0.640	0.091 ± 0.019	0	0.079	9.7E-04	1.5E-02	1.5E-02	0.00

Table 4.23: Summary of the theoretical cross section (ThXsec), expected cross section limit at 95% CL (ExpXsec), and observed cross section limits at 95% CL (ObsXsec) for a range of stop signal mass points for the tracker-only+MVA analysis using 2015 data and relaxed final selection. Included are the selection criteria (p_T, I_{as}, $1/\beta$, and MVA), as well as the signal efficiency (Seff), number of predicted background (Bckg. Pred), and observed data (obs) that pass the selection criteria. Shown are both the stop models and the charge suppressed model (denoted with an N).

Model	Mass (GeV)	$p_T >$ (GeV)	$I_{as} >$	$1/\beta >$	MVA>	Bckg. Pred	Obs	Seff	ThXsec (pb)	ExpXsec (pb)	ObsXsec (pb)	Signif
Stop	1000	65	0.250	/	0.720	0.097 ± 0.020	0	0.270	6.0E-03	4.6E-03	4.6E-03	0.00
Stop	1400	65	0.250	/	0.720	0.097 ± 0.020	0	0.236	4.5E-04	5.1E-03	5.1E-03	0.00
Stop	1800	65	0.250	/	0.720	0.097 ± 0.020	0	0.172	4.6E-05	7.0E-03	7.0E-03	0.00
StopN	1000	65	0.250	/	0.720	0.097 ± 0.020	0	0.200	6.0E-03	6.0E-03	6.0E-03	0.00
StopN	1600	65	0.250	/	0.720	0.097 ± 0.020	0	0.157	1.4E-04	7.7E-03	7.7E-03	0.00
StopN	1800	65	0.250	/	0.720	0.097 ± 0.020	0	0.130	4.6E-05	9.3E-03	9.3E-03	0.00

Table 4.24: Summary of the theoretical cross section (ThXsec), expected cross section limit at 95% CL (ExpXsec), and observed cross section limits at 95% CL (ObsXsec) for a range of stau signal mass points for the Tracker+TOF+MVA analysis using 2015 data and relaxed final selection. Included are the selection criteria (p_T, I_{as}, $1/\beta$, and Mass), as well as the signal efficiency (Seff), number of predicted background (Bckg. Pred), and observed data (obs) that pass the selection criteria. Shown are the GMSB and PP stau production modes.

Model	Mass (GeV)	$p_T >$ (GeV)	$I_{as} >$	$1/\beta >$	MVA>	Bckg. Pred	Obs	Seff	ThXsec (pb)	ExpXsec (pb)	ObsXsec (pb)	Signif
GMSB stau	247	65	0.150	1.250	0.200	0.314 ± 0.063	0	0.372	8.8E-02	3.2E-03	3.2E-03	0.00
GMSB stau	308	65	0.150	1.250	0.200	0.314 ± 0.063	0	0.439	2.5E-02	2.7E-03	2.7E-03	0.00
GMSB stau	494	65	0.150	1.250	0.200	0.314 ± 0.063	0	0.603	1.9E-03	2.0E-03	2.0E-03	0.00
PP stau	247	65	0.150	1.250	0.200	0.297 ± 0.060	0	0.278	3.7E-03	4.4E-03	4.4E-03	0.00
PP stau	308	65	0.150	1.250	0.200	0.297 ± 0.060	0	0.325	1.5E-03	3.8E-03	3.8E-03	0.00
PP stau	494	65	0.150	1.250	0.200	0.297 ± 0.060	0	0.428	1.9E-04	2.8E-03	2.8E-03	0.00

Table 4.25: Summary of the theoretical cross section (ThXsec), expected cross section limit at 95% CL (ExpXsec), and observed cross section limits at 95% CL (ObsXsec) for a range of modified Drell-Yan signal mass points for the Tracker+TOF+MVA analysis using 2015 data. Included are the selection criteria (p_T, I_{as}, $1/\beta$, and MVA), as well as the signal efficiency (Seff), number of predicted background (Bckg. Pred), and observed data (obs) that pass the selection criteria. Shown are the modified DY $|Q| = 1e$ and $|Q| = 2e$ models.

Model	Mass (GeV)	$p_T >$ (GeV)	$I_{as} >$	$1/\beta >$	MVA>	Bckg. Pred	Obs	Seff	ThXsec (pb)	ExpXsec (pb)	ObsXsec (pb)	Signif
DY $|Q| = 1e$	400	65	0.150	1.250	0.200	0.143 ± 0.029	0	0.427	7.3E-03	2.9E-03	2.9E-03	0.00
DY $|Q| = 1e$	600	65	0.150	1.250	0.200	0.143 ± 0.029	0	0.471	1.2E-03	2.7E-03	2.7E-03	0.00
DY $|Q| = 1e$	800	65	0.150	1.250	0.200	0.143 ± 0.029	0	0.494	2.6E-04	2.6E-03	2.6E-03	0.00
DY $|Q| = 2e$	400	65	0.150	1.250	0.200	0.043 ± 0.009	0	0.410	2.3E-02	3.3E-03	3.3E-03	0.00
DY $|Q| = 2e$	600	65	0.150	1.250	0.200	0.043 ± 0.009	0	0.482	3.5E-03	2.6E-03	2.6E-03	0.00
DY $|Q| = 2e$	800	65	0.150	1.250	0.200	0.043 ± 0.009	0	0.489	8.0E-04	2.6E-03	2.6E-03	0.00

Table 4.26: Lower mass limits for the 2015 data from both the standard HSCP analyses (tracker-only and Tracker+TOF) compared to the HSCP multivariate analyses (tracker-only+MVA and Tracker+TOF+MVA) for all 6 benchmark signal types. The MVA analyses results shown used the relaxed final selection, and the standard analyses used the final tight selection.

	Lower mass limit			
	tracker-only		Tracker+TOF	
Signal Type	Mass selection	MVA selection	Mass selection	MVA selection
Gluino f = 0.1	1610	1630	1580	1590
Stop	1040	1040	480	490
GMSB Stau	490	490	480	490
PP Stau	240	240	—	240
DY $\|Q\| = 1$e	510	540	550	550
DY $\|Q\| = 2$e	680	710	660	670

criteria from the standard analyses over the majority of the signal types. The main reason for this was despite the an increase in the signal acceptance using the relaxed selection criteria versus the selection from the standard analyses ($\approx 10\%$ for some models), other models showed little to no increase in the signal acceptance. By contrast, the relaxation of the selection criteria increased the number of background prediction present ($\approx 2x$ in some models). The two effects offset each other when inputted into the Higgs tool resulting in cross sections that had little to no change for most of the signal models between the relaxed final selection and the final tight selection.

4.5 MVA Results with 2016 Data

The HSCP multivariate analyses developed on the 2015 collision data were applied to 2016 collision data. The analyzed 2016 collision data corresponded to 12.9 fb^{-1} covering Runs 273158 to 276811. The signal MC samples used were derived from the same signal MC samples used in the 2015 data analysis, with the amount of PU reweighted to match 2016 conditions.

The systematic uncertainty on the integrated luminosity was reported to be The methods of determining the systematic uncertainties for signal acceptance for the 2016 data were the same as those for the 2015 data. The systematic uncertainties for the 2016 MVA analyses are given in Tables 4.27 to 4.32 and were found to be largely the same as those found in the 2015 multivariate analyses.

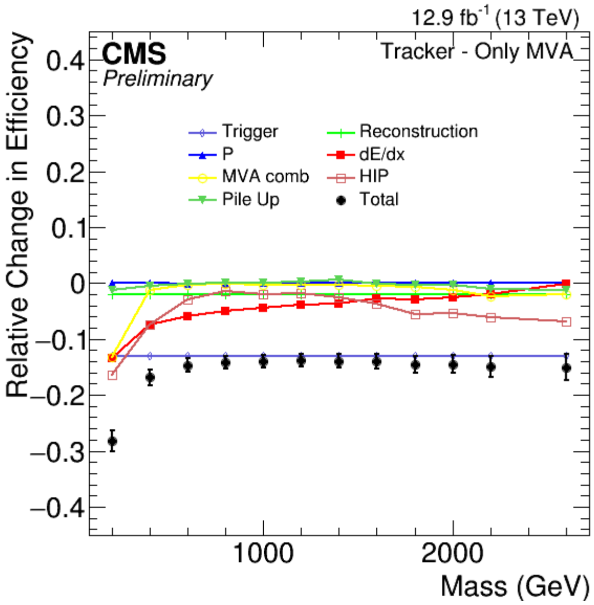

(a) Gluino f=0.1 tracker-only+MVA

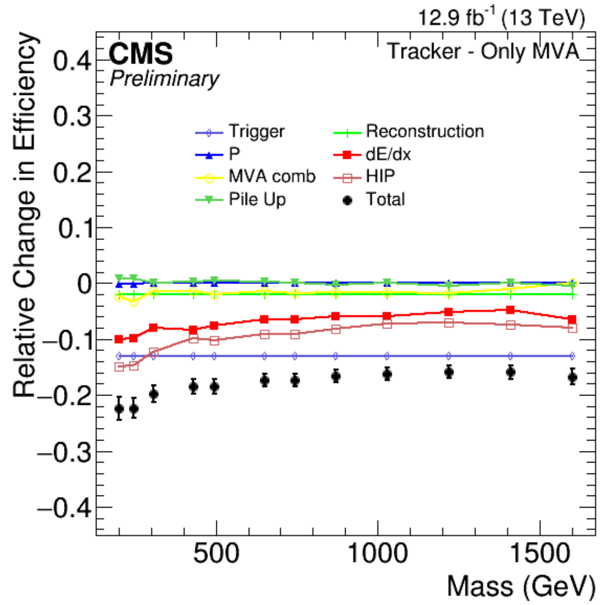

(b) GMSB stau tracker-only+MVA

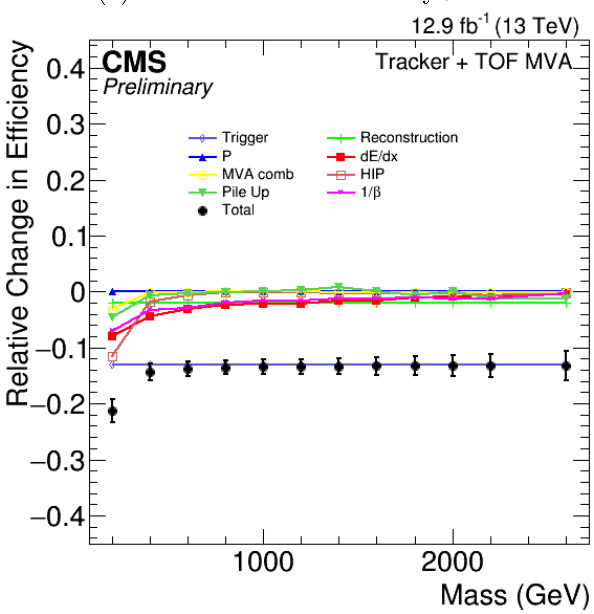

(c) Gluino f=0.1 Tracker+TOF+MVA

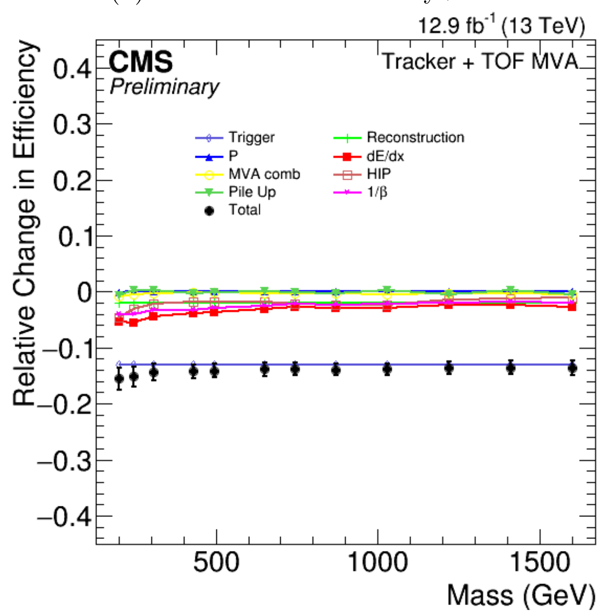

(d) GMSB stau Tracker+TOF+MVA

Figure 4.31: Sample distributions showing the relative uncertainties in the 2016 MVA analyses of the different systematics that affect the signal acceptance for the tracker-only+MVA analysis (a)(b) and Tracker+TOF+MVA analysis (c)(d). Plots (a) and (c) are for the gluino f = 10% model, and (b) and (d) are for the GMSB stau model.

Table 4.27: Sources of systematic uncertainties and their corresponding relative uncertainties on the gluino signal samples for the 2016 tracker-only+MVA and Tracker+TOF+MVA analyses.

Source	Relative Uncertainty (%)	
	tracker-only+MVA	Tk+TOF+MVA
Trigger efficiency	< 13	< 13
Track momentum scale	< 2	< 2
Track reconstruction	< 2	< 2
Ionization energy loss	< 15	< 8
HIP background effect	< 3	< 4
Time-of-flight	-	< 8
Muon reconstruction	-	2
Pileup contribution	< 1	< 5
MVA	< 10	< 5
Total signal acceptance uncertainty	< 25	< 18
Collision background uncertainty	20	20
Uncertainty on Luminosity	2.5	2.5

Table 4.28: Sources of systematic uncertainties and their corresponding relative uncertainties on the stop signal samples for the 2016 tracker-only+MVA and Tracker+TOF+MVA analyses.

Source	Relative Uncertainty (%)	
	tracker-only+MVA	Tk+TOF+MVA
Trigger efficiency	< 13	< 13
Track momentum scale	< 2	< 2
Track reconstruction	< 2	< 2
Ionization energy loss	< 6	< 10
HIP background effect	< 4	< 6
Time-of-flight	-	< 13
Muon reconstruction	-	2
Pileup contribution	< 1	< 6
MVA	< 6	< 10
Total signal acceptance uncertainty	< 18	< 25
Collision background uncertainty	20	20
Uncertainty on Luminosity	2.5	2.5

Table 4.29: Sources of systematic uncertainties and their corresponding relative uncertainties on the GMSB stau signal samples for the 2016 tracker-only+MVA and Tracker+TOF+MVA analyses.

Source	Relative Uncertainty (%)	
	tracker-only+MVA	Tk+TOF+MVA
Trigger efficiency	< 13	< 13
Track momentum scale	< 2	< 2
Track reconstruction	< 2	< 2
Ionization energy loss	< 12	< 8
HIP background effect	< 5	< 2
Time-of-flight	-	< 4
Muon reconstruction	-	2
Pileup contribution	< 1	< 1
MVA	< 6	< 2
Total signal acceptance uncertainty	< 18	< 16
Collision background uncertainty	20	20
Uncertainty on Luminosity	2.5	2.5

Table 4.30: Sources of systematic uncertainties and their corresponding relative uncertainties on the PP stau signal samples for the 2016 tracker-only+MVA and Tracker+TOF+MVA analyses.

Source	Relative Uncertainty (%)	
	tracker-only+MVA	Tk+TOF+MVA
Trigger efficiency	< 13	< 13
Track momentum scale	< 5	< 2
Track reconstruction	< 2	< 2
Ionization energy loss	< 18	< 10
HIP background effect	< 7	< 4
Time-of-flight	-	< 6
Muon reconstruction	-	2
Pileup contribution	< 1	< 1
MVA	< 15	< 2
Total signal acceptance uncertainty	< 28	< 18
Collision background uncertainty	20	20
Uncertainty on Luminosity	2.5	2.5

Table 4.31: Sources of systematic uncertainties and their corresponding relative uncertainties on the DY $|Q| = 1e$ signal samples for the 2016 tracker-only+MVA and Tracker+TOF+MVA analyses.

Source	Relative Uncertainty (%)	
	tracker-only+MVA	Tk+TOF+MVA
Trigger efficiency	< 13	< 13
Track momentum scale	< 2	< 2
Track reconstruction	< 2	< 2
Ionization energy loss	< 18	< 8
HIP background effect	< 12	< 8
Time-of-flight	-	< 21
Muon reconstruction	-	2
Pileup contribution	< 1	< 20
MVA	< 18	< 22
Total signal acceptance uncertainty	< 32	< 45
Collision background uncertainty	20	20
Uncertainty on Luminosity	2.5	2.5

Table 4.32: Sources of systematic uncertainties and their corresponding relative uncertainties on the DY $|Q| = 2e$ signal samples for the 2016 tracker-only+MVA and Tracker+TOF+MVA analyses.

Source	Relative Uncertainty (%)	
	tracker-only+MVA	Tk+TOF+MVA
Trigger efficiency	< 13	< 13
Track momentum scale	< 2	< 2
Track reconstruction	< 2	< 2
Ionization energy loss	< 2	< 2
HIP background effect	< 4	< 4
Time-of-flight	-	< 26
Muon reconstruction	-	2
Pileup contribution	< 1	< 4
MVA	< 2	< 2
Total signal acceptance uncertainty	< 14	< 35
Collision background uncertainty	20	20
Uncertainty on Luminosity	2.5	2.5

Table 4.33: The number of predicted and observed events in 2016 data for a range of MVA selection. Presented are the results from the Gluino MVA mapping

Analysis	Selection				Number of events	
	p_T (GeV)	I_{as}	$1/\beta$	MVA	Predicted	Observed
tracker-only+MVA	60	0.1	—	0	43436.5± 8689.5	44738
	60	0.1	—	0.20	489.0± 97.8	514
	60	0.1	—	0.40	65.4± 13.1	84
	60	0.1	—	0.60	17.9± 3.6	21
	65	0.3	—	0	87.4± 17.7	95
	65	0.3	—	0.20	6.4± 1.4	7
	65	0.3	—	0.40	0.5± 0.1	0
	65	0.3	—	0.60	0.1± 0.0	0
Tracker+TOF+MVA	65	0.050	1.050	0	72208.9± 12224.9	74343
	65	0.050	1.050	0.20	2030.2 ± 406.0	2216
	65	0.050	1.050	0.40	227.9± 55.6	310
	65	0.050	1.050	0.60	50.2± 10.0	58
	65	0.175	1.250	0	52.6± 10.5	50
	65	0.175	1.250	0.20	3.9 ± 0.8	3
	65	0.175	1.250	0.40	0.3± 0.1	1
	65	0.175	1.250	0.60	0.1± 0.0	1

As with the 2015 analyses, the dominant uncertainty on the signal acceptance was the overall trigger efficiency, with the systematic uncertainty on signal acceptance due to the artificial neural network becoming larger for the lower signal mass points. The total uncertainty on the signal acceptance was found to be less than 30% in the tracker-only+MVA and 20% in the Tracker+TOF+MVA analysis.

Tables 4.33 and 4.34 list the number of background prediction and observed data using the loose and tight selection criteria along with different selection on the multivariate discriminant. The systematic uncertainty on the background prediction was again taken to be conservatively 20%.

A summary of the 2016 results from the Higgs tool are given in Tables 4.35 to 4.38. Included are the 95% C.L upper limit on the observed and expected cross section limits.

In similar fashion to the 2015 analyses, the 2016 MVA analyses did result in lower mass limits comparable to the standard analyses. The improvement was again minimal ($< 2\%$) for most of the

Table 4.34: The number of predicted and observed events in 2016 data for a range of MVA selection. Presented are the results from the GMSB stau MVA mapping.

Analysis	Selection				Number of events	
	p_T (GeV)	I_{as}	$1/\beta$	MVA	Predicted	Observed
tracker-only+MVA	60	0.1	—	0	43436.5± 8689.5	44738
	60	0.1	—	0.20	2058.6± 411.8	2155
	60	0.1	—	0.40	565.8± 113.2	586
	60	0.1	—	0.60	226.4± 45.3	253
	65	0.3	—	0	87.4± 17.7	95
	65	0.3	—	0.25	45.5 ± 9.3	60
	65	0.3	—	0.50	4.1± 0.8	4
	65	0.3	—	0.75	1.1± 0.2	1
Tracker+TOF+MVA	65	0.050	1.050	0	72208.9± 12224.9	74343
	65	0.050	1.050	0.20	6702.7 ± 1240.6	6879
	65	0.050	1.050	0.40	1263.4± 252.7	1352
	65	0.050	1.050	0.60	309.7± 61.9	344
	65	0.175	1.250	0	52.6± 10.5	50
	65	0.175	1.250	0.20	13.5± 2.7	11
	65	0.175	1.250	0.40	1.7± 0.3	1
	65	0.175	1.250	0.60	0.4± 0.1	1

Table 4.35: Summary of the theoretical cross section (ThXsec), expected cross section limit at 95% CL (ExpXsec), and observed cross section limits at 95% CL (ObsXsec) for a range of gluino signal mass points for the tracker-only+MVA analysis using 2016 data. Included are the selection criteria (p_T, I_{as}, $1/\beta$, and MVA), as well as the signal efficiency (Seff), number of predicted background (Bckg. Pred), and observed data (obs) that pass the selection criteria. Shown are f = 10%,50% for gluino models including the the charged suppressed interaction models (denoted with an N).

Model	Mass (GeV)	$p_T >$ (GeV)	$I_{as} >$	$1/\beta >$	MVA>	Bckg. Pred	Obs	Seff	ThXsec (pb)	ExpXsec (pb)	ObsXsec (pb)	Signif
Gluino f=0.1	1000	65	0.250	/	0.280	4.630 ± 0.933	4	0.222	3.2E-01	2.1E-03	2.0E-03	0.00
Gluino f=0.1	1400	65	0.250	/	0.500	0.489 ± 0.098	0	0.188	2.5E-02	1.2E-03	1.2E-03	0.00
Gluino f=0.1	1800	65	0.250	/	0.760	0.053 ± 0.011	0	0.130	2.7E-03	1.8E-03	1.8E-03	0.00
Gluino f=0.1	2200	65	0.250	/	0.760	0.053 ± 0.011	0	0.087	3.6E-04	2.8E-03	2.8E-03	0.00
Gluino f=0.5	1000	65	0.250	/	0.340	2.280 ± 0.460	2	0.129	3.2E-01	2.9E-03	2.9E-03	0.00
Gluino f=0.5	1400	65	0.250	/	0.580	0.259 ± 0.052	0	0.108	2.5E-02	2.1E-03	2.1E-03	0.00
Gluino f=0.5	1800	65	0.250	/	0.760	0.053 ± 0.011	0	0.074	2.7E-03	3.2E-03	3.2E-03	0.00
Gluino f=0.5	2200	65	0.250	/	0.760	0.053 ± 0.011	0	0.049	3.6E-04	4.9E-03	4.9E-03	0.00
GluinoN f=0.1	1200	65	0.250	/	0.400	1.240 ± 0.249	0	0.189	8.4E-02	1.7E-03	1.3E-03	0.00
GluinoN f=0.1	1600	65	0.250	/	0.600	0.207 ± 0.042	0	0.148	8.0E-03	1.6E-03	1.6E-03	0.00
GluinoN f=0.1	2000	65	0.250	/	0.760	0.053 ± 0.011	0	0.100	9.7E-04	2.3E-03	2.3E-03	0.00
GluinoN f=0.5	1200	65	0.250	/	0.440	0.835 ± 0.168	0	0.144	8.4E-02	2.3E-03	1.6E-03	0.00
GluinoN f=0.5	1600	65	0.250	/	0.640	0.148 ± 0.030	0	0.111	8.0E-03	2.1E-03	2.1E-03	0.00
GluinoN f=0.5	2000	65	0.250	/	0.760	0.053 ± 0.011	0	0.073	9.7E-04	3.2E-03	3.2E-03	0.00

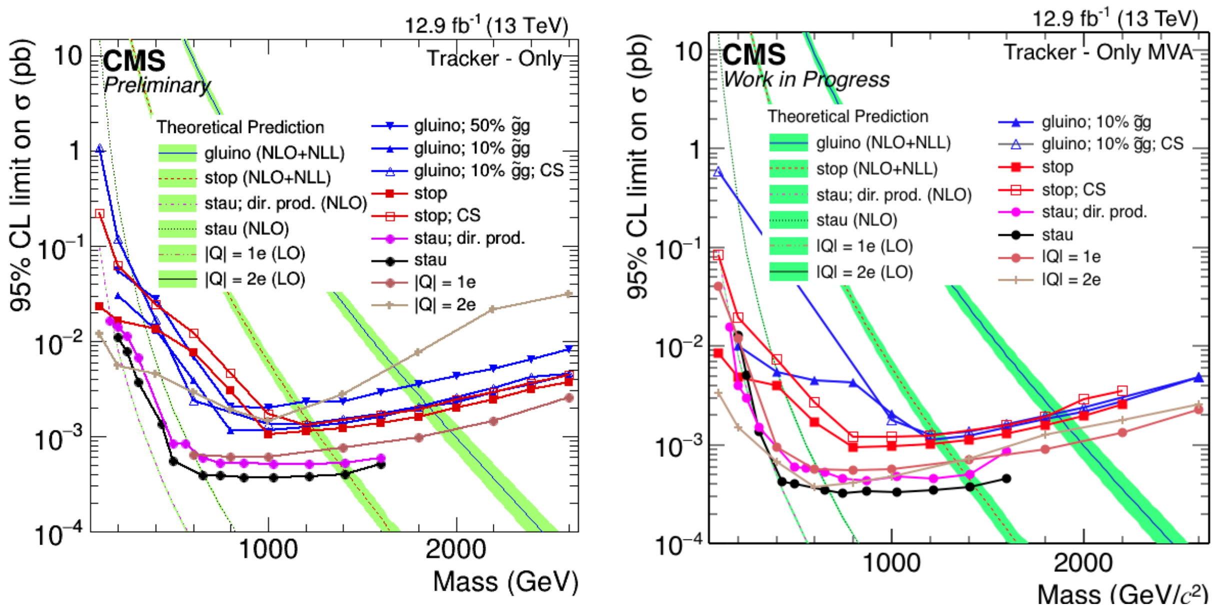

(a) standard tracker-only

(b) tracker-only+MVA

Figure 4.32: Theoretical and 95% CL upper limit on observed cross sections, both as a function of mass, using 2016 data. The left plot shows the results from the standard HSCP tracker-only analysis using the final tight selection. The right plot shows the results from the tracker-only+MVA analysis using the relaxed final selection.

Table 4.36: Summary of the theoretical cross section (ThXsec), expected cross section limit at 95% CL (ExpXsec), and observed cross section limits at 95% CL (ObsXsec) for a range of stop signal mass points for the tracker-only+MVA analysis using 2016 data. Included are the selection criteria (p_T, I_{as}, $1/\beta$, and Mass), as well as the signal efficiency (Seff), number of predicted background (Bckg. Pred), and observed data (obs) that pass the selection criteria. Shown are stop models including the charged suppressed interaction models (denoted with an N).

Model	Mass (GeV)	$p_T >$ (GeV)	$I_{as} >$	$1/\beta >$	MVA>	Bckg. Pred	Obs	Seff	ThXsec (pb)	ExpXsec (pb)	ObsXsec (pb)	Signif
Stop	1000	65	0.300	/	0.520	0.211 ± 0.043	0	0.237	6.0E-03	9.9E-04	9.9E-04	0.00
Stop	1400	65	0.300	/	0.840	0.022 ± 0.004	0	0.204	4.5E-04	1.2E-03	1.2E-03	0.00
Stop	1800	65	0.300	/	0.900	0.012 ± 0.003	0	0.155	4.6E-05	1.5E-03	1.5E-03	0.00
Stop N	1000	65	0.300	/	0.500	0.244 ± 0.050	0	0.192	6.0E-03	1.2E-03	1.2E-03	0.00
Stop N	1200	65	0.300	/	0.700	0.061 ± 0.013	0	0.187	1.6E-03	1.3E-03	1.3E-03	0.00
Stop N	1600	65	0.300	/	0.860	0.018 ± 0.004	0	0.146	1.4E-04	1.6E-03	1.6E-03	0.00

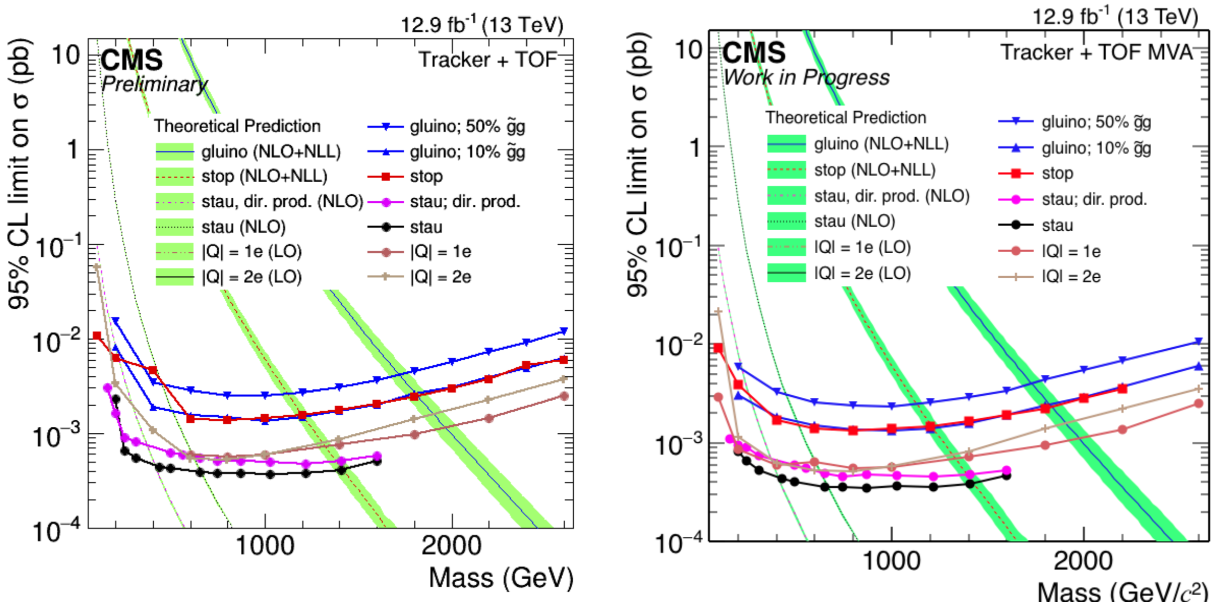

(a) standard Tracker+TOF

(b) Tracker+TOF+MVA

Figure 4.33: Theoretical and 95% CL upper limit on observed cross sections, both as a function of mass, using 2016 data. The left plot shows the results from the standard HSCP Tracker+TOF analysis using the final tight selection. The right plot shows the results from the Tracker+TOF+MVA analysis using the relaxed final selection.

Table 4.37: Summary of the theoretical cross section (ThXsec), expected cross section limit at 95% CL (ExpXsec), and observed cross section limits at 95% CL (ObsXsec) for a range of stau signal mass points for the Tracker+TOF+MVA analysis using 2016 data. Included are the selection criteria (p_T, I_{as}, $1/\beta$, and Mass), as well as the signal efficiency (Seff), number of predicted background (Bckg. Pred), and observed data (obs) that pass the selection criteria. Shown are the GMSB and PP stau production modes.

Model	Mass (GeV)	$p_T >$ (GeV)	$I_{as} >$	$1/\beta >$	MVA>	Bckg. Pred	Obs	Seff	ThXsec (pb)	ExpXsec (pb)	ObsXsec (pb)	Signif
GMSB stau	247	65	0.175	1.250	0.200	0.622 ± 0.125	0	0.363	8.8E-02	6.6E-04	6.3E-04	0.00
GMSB stau	308	65	0.175	1.250	0.220	0.483 ± 0.097	0	0.435	2.5E-02	5.3E-04	5.3E-04	0.00
GMSB stau	494	65	0.175	1.250	0.400	0.072 ± 0.014	0	0.584	1.9E-03	4.0E-04	4.0E-04	0.00
PP stau	247	65	0.175	1.250	0.280	0.254 ± 0.051	0	0.262	3.7E-03	9.0E-04	9.0E-04	0.00
PP stau	308	65	0.175	1.250	0.360	0.136 ± 0.027	0	0.298	1.5E-03	7.9E-04	7.9E-04	0.00
PP stau	494	65	0.175	1.250	0.740	0.020 ± 0.004	0	0.394	1.9E-04	6.0E-04	6.0E-04	0.00

Table 4.38: Summary of the theoretical cross section (ThXsec), expected cross section limit at 95% CL (ExpXsec), and observed cross section limits at 95% CL (ObsXsec) for a range of modified Drell-Yan signal mass points for the Tracker+TOF+MVA analysis using 2016 data. Included are the selection criteria (p_T, I_{as}, $1/\beta$, and MVA), as well as the signal efficiency (Seff), number of predicted background (Bckg. Pred), and observed data (obs) that pass the selection criteria. Shown are the modified DY $|Q| = 1e$ and $|Q| = 2e$ models.

Model	Mass (GeV)	$p_T >$ (GeV)	$I_{as} >$	$1/\beta >$	MVA>	Bckg. Pred	Obs	Seff	ThXsec (pb)	ExpXsec (pb)	ObsXsec (pb)	Signif
DY Q1	400	65	0.175	1.250	0.260	0.108 ± 0.022	0	0.397	7.3E-03	6.1E-04	6.1E-04	0.00
DY Q1	600	65	0.175	1.250	0.360	0.033 ± 0.007	0	0.424	1.2E-03	6.5E-04	6.5E-04	0.00
DY Q1	800	65	0.175	1.250	0.540	0.008 ± 0.002	0	0.446	2.6E-04	5.4E-04	5.4E-04	0.00
DY Q2	400	65	0.175	1.250	0.200	0.115 ± 0.023	0	0.396	2.3E-02	6.1E-04	6.1E-04	0.00
DY Q2	600	65	0.175	1.250	0.200	0.115 ± 0.023	0	0.463	3.5E-03	5.3E-04	5.3E-04	0.00
DY Q2	800	65	0.175	1.250	0.240	0.035 ± 0.007	0	0.465	8.0E-04	5.3E-04	5.3E-04	0.00

Table 4.39: Lower mass limits for the 2016 data from both the standard HSCP analyses (tracker-only and Tracker+TOF) compared to the HSCP multivariate analyses (tracker-only+MVA and Tracker+TOF+MVA) for several benchmark signal types. The MVA analyses used the same final selection as the standard analyses.

	Lower mass limit			
	tracker-only		Tracker+TOF	
Signal Type	Mass selection	MVA selection	Mass selection	MVA selection
Gluino f = 0.1	1850	1870	1810	1820
Stop	1250	1260	1200	1210
GMSB Stau	660	680	660	670
PP Stau	170	340	360	370
DY $|Q|$ = 1e	720	730	730	750
DY $|Q|$ = 2e	670	700	890	910

signal types, with slightly better improvements on the lepton signal types. The lower mass limits for the standard and MVA analyses on 2016 data are listed in Table 4.39.

As was done for the 2015 data, the final selection criteria for the 2016 data were relaxed for the MVA analyses to observe the effects on the final limits. In Tables 4.40 to 4.43 are summaries of the Higgs tools results using the relaxed final selection. A mored detailed listing of results can be found in Appendix B. Overall the relaxation of the final selection criteria for the 2016 data resulted in improvements on the cross section limits in some models, with improvements as high as ≈ 30%.

Using the relaxed final selection for the MVA analyses on 2016 data produced lower mass limits nearly identical to the final tight selection MVA analyses as seen in Table 4.44.

Table 4.40: Summary of the theoretical cross section (ThXsec), expected cross section limit at 95% CL (ExpXsec), and observed cross section limits at 95% CL (ObsXsec) for a range of gluino signal mass points for the tracker-only+MVA analysis using 2016 data and relaxed final selection. Included are the selection criteria (p_T, I_{as}, $1/\beta$, and MVA), as well as the signal efficiency (Seff), number of predicted background (Bckg. Pred), and observed data (obs) that pass the selection criteria. Shown are f = 10%,50% for gluino models including the the charged suppressed interaction models (denoted with an N).

Model	Mass (GeV)	$p_T >$ (GeV)	$I_{as} >$	$1/\beta >$	MVA>	Bckg. Pred	Obs	Seff	ThXsec (pb)	ExpXsec (pb)	ObsXsec (pb)	Signif
Gluino f=0.1	1000	65	0.250	/	0	4.630 ± 0.933	4	0.222	3.2E-01	2.1E-03	2.0E-03	0.00
Gluino f=0.1	1400	65	0.250	/	0	0.489 ± 0.098	0	0.188	2.5E-02	1.2E-03	1.2E-03	0.00
Gluino f=0.1	1800	65	0.250	/	0	0.043 ± 0.009	0	0.130	2.7E-03	1.8E-03	1.8E-03	0.00
Gluino f=0.1	2200	65	0.250	/	0	0.017 ± 0.003	0	0.087	3.6E-04	2.7E-03	2.7E-03	0.00
Gluino f=0.5	1000	65	0.250	/	0	2.280 ± 0.460	2	0.129	3.2E-01	2.9E-03	2.9E-03	0.00
Gluino f=0.5	1400	65	0.250	/	0	0.259 ± 0.052	0	0.108	2.5E-02	2.1E-03	2.1E-03	0.00
Gluino f=0.5	1800	65	0.250	/	0	0.028 ± 0.006	0	0.074	2.7E-03	3.2E-03	3.2E-03	0.00
Gluino f=0.5	2200	65	0.250	/	0	0.013 ± 0.003	0	0.048	3.6E-04	5.0E-03	5.0E-03	0.00
GluinoN f10	1200	65	0.250	/	0	1.240 ± 0.249	1	0.189	8.4E-02	1.7E-03	1.3E-03	0.00
GluinoN f10	1600	65	0.250	/	0	0.207 ± 0.042	0	0.148	8.0E-03	1.6E-03	1.6E-03	0.00
GluinoN f10	2000	65	0.250	/	0	0.017 ± 0.003	0	0.100	9.7E-04	2.4E-03	2.4E-03	0.00
GluinoN f=0.5	1200	65	0.250	/	0	0.835 ± 0.168	0	0.144	8.4E-02	2.3E-03	1.6E-03	0.00
GluinoN f=0.5	1600	65	0.250	/	0	0.148 ± 0.030	0	0.111	8.0E-03	2.1E-03	2.1E-03	0.00
GluinoN f=0.5	2000	65	0.250	/	0	0.022 ± 0.005	0	0.072	9.7E-04	3.3E-03	3.3E-03	0.00

Table 4.41: Summary of the theoretical cross section (ThXsec), expected cross section limit at 95% CL (ExpXsec), and observed cross section limits at 95% CL (ObsXsec) for a range of stop signal mass points for the tracker-only+MVA analysis using 2016 data and relaxed final selection. Included are the selection criteria (p_T, I_{as}, $1/\beta$, and Mass), as well as the signal efficiency (Seff), number of predicted background (Bckg. Pred), and observed data (obs) that pass the selection criteria. Shown are stop models including the charged suppressed interaction models (denoted with an N).

Model	Mass (GeV)	$p_T >$ (GeV)	$I_{as} >$	$1/\beta >$	MVA>	Bckg. Pred	Obs	Seff	ThXsec (pb)	ExpXsec (pb)	ObsXsec (pb)	Signif
Stop	1000	65	0.250	/	0.640	0.281 ± 0.056	0	0.244	6.0E-03	9.6E-04	9.6E-04	0.00
Stop	1400	65	0.250	/	0.860	0.058 ± 0.012	0	0.209	4.5E-04	1.1E-03	1.1E-03	0.00
Stop	1800	65	0.250	/	0.860	0.058 ± 0.012	0	0.158	4.6E-05	1.5E-03	1.5E-03	0.00
StopN	1000	65	0.250	/	0.640	0.281 ± 0.056	0	0.196	6.0E-03	1.2E-03	1.2E-03	0.00
StopN	1600	65	0.250	/	0.860	0.058 ± 0.012	0	0.148	1.4E-04	1.6E-03	1.6E-03	0.00
StopN	1800	65	0.250	/	0.860	0.058 ± 0.012	0	0.129	4.6E-05	1.9E-03	1.9E-03	0.00

Table 4.42: Summary of the theoretical cross section (ThXsec), expected cross section limit at 95% CL (ExpXsec), and observed cross section limits at 95% CL (ObsXsec) for a range of stau signal mass points for the Tracker+TOF+MVA analysis using 2016 data and relaxed final selection. Included are the selection criteria (p_T, I_{as}, $1/\beta$, and Mass), as well as the signal efficiency (Seff), number of predicted background (Bckg. Pred), and observed data (obs) that pass the selection criteria. Shown are the GMSB and PP stau production modes.

Model	Mass (GeV)	$p_T >$ (GeV)	$I_{as} >$	$1/\beta >$	MVA>	Bckg. Pred	Obs	Seff	ThXsec (pb)	ExpXsec (pb)	ObsXsec (pb)	Signif
GMSB stau	247	65	0.150	1.250	0.200	1.160 ± 0.233	0	0.369	8.8E-02	9.1E-04	6.5E-04	0.00
GMSB stau	308	65	0.150	1.250	0.220	0.905 ± 0.181	0	0.442	2.5E-02	7.6E-04	5.3E-04	0.00
GMSB stau	494	65	0.150	1.250	0.420	0.114 ± 0.023	0	0.594	1.9E-03	4.0E-04	4.0E-04	0.00
PP stau	247	65	0.150	1.250	0.320	0.343 ± 0.069	0	0.270	3.7E-03	9.0E-04	9.0E-04	0.00
PP stau	308	65	0.150	1.250	0.440	0.154 ± 0.031	0	0.305	1.5E-03	7.4E-04	7.4E-04	0.00
PP stau	494	65	0.150	1.250	0.660	0.051 ± 0.010	0	0.403	1.9E-04	5.9E-04	5.9E-04	0.00

Table 4.43: Summary of the theoretical cross section (ThXsec), expected cross section limit at 95% CL (ExpXsec), and observed cross section limits at 95% CL (ObsXsec) for a range of modified Drell-Yan signal mass points for the Tracker+TOF+MVA analysis using 2016 data and relaxed final selection. Included are the selection criteria (p_T, I_{as}, $1/\beta$, and MVA), as well as the signal efficiency (Seff), number of predicted background (Bckg. Pred), and observed data (obs) that pass the selection criteria. Shown are the modified DY $|Q| = 1e$ and $|Q| = 2e$ models.

Model	Mass (GeV)	$p_T >$ (GeV)	$I_{as} >$	$1/\beta >$	MVA>	Bckg. Pred	Obs	Seff	ThXsec (pb)	ExpXsec (pb)	ObsXsec (pb)	Signif
DY $\|Q\| = 1e$	400	65	0.150	1.250	0.260	0.197 ± 0.039	0	0.402	7.3E-03	6.0E-04	6.0E-04	0.00
DY $\|Q\| = 1e$	600	65	0.150	1.250	0.360	0.062 ± 0.012	0	0.429	1.2E-03	5.7E-04	5.7E-04	0.00
DY $\|Q\| = 1e$	800	65	0.150	1.250	0.380	0.051 ± 0.010	0	0.451	2.6E-04	5.4E-04	5.4E-04	0.00
DY $\|Q\| = 2e$	400	65	0.150	1.250	0.200	0.164 ± 0.033	0	0.396	2.3E-02	6.2E-04	6.2E-04	0.00
DY $\|Q\| = 2e$	600	65	0.150	1.250	0.200	0.164 ± 0.033	0	0.463	3.5E-03	5.3E-04	5.3E-04	0.00
DY $\|Q\| = 2e$	800	65	0.150	1.250	0.240	0.053 ± 0.011	0	0.465	8.0E-04	5.2E-04	5.2E-04	0.00

Table 4.44: Lower mass limits for the 2016 data from both the standard HSCP analyses (tracker-only and Tracker+TOF) compared to the HSCP multivariate analyses (tracker-only+MVA and Tracker+TOF+MVA) for several benchmark signal types. The standard analyses used the final tight selection and the MVA analyses used the relaxed final selection.

	Lower mass limit			
	tracker-only		Tracker+TOF	
Signal Type	Mass selection	MVA selection	Mass selection	MVA selection
Gluino f = 0.1	1850	1870	1810	1820
Stop	1250	1260	1200	1210
GMSB Stau	660	680	660	670
PP Stau	170	340	360	370
DY $\|Q\|$ = 1e	720	730	730	750
DY $\|Q\|$ = 2e	670	700	890	910

CHAPTER 5

CONCLUSION

Particle physics has been successful in describing all of the observed fundamental particles and the mechanisms that govern them, culminating in the Standard Model of particle physics. However, there exist several open questions. Many theories seek to answer these questions, and the Large Hadron Collider searches for new physics in order to shed light on which theory (or theories) may provide answers.

A direct way of probing the realm of new physics is the search for heavy stable charged particles. HSCPs provide a unique detector signature due to their anomalous dE/dx and larger time-of-flight compared to SM particles, providing a way to distinguish HSCPs with small background from SM particles. Any particle satisfying the basic description of an HSCP will produce such a signature, making the HSCP search a means of searching for new physics without necessarily being associated to a specific theoretical model. Since HSCPs do manifest in several theories beyond the Standard Model, this search also provides important restrictions on theoretical models.

This dissertation investigated the possibility of utilizing a multivariate approach in searching for HSCPs using data recorded by the Compact Muon Solenoid detector. The data collected in 2015 corresponded to 2.5 fb^{-1} and were used to develop and test the multivariate approach. Data collected in 2016 were used as a means of final comparison to previous HSCP search techniques and corresponded to 12.9 fb^{-1}. Benchmark signal models were utilized via Monte-Carlo simulations and included gluinos, stops, staus, and modified Drell-Yan (DY) fermions. Furthermore the gluinos included different fractions of neutral R-hadrons created at hadronization (f = 10% and f = 50%), and both the gluino and stop included an extra interaction model (charged suppressed). The staus modeled two different production modes, decay-chain (GMSB stau) and direct pair production (PP stau). The modified DY models included two different charges ($|Q| = 1e$ and $|Q| = 2e$). The 2015 and 2016 searches were carried out for the tracker-only, Tracker+TOF, tracker-only+MVA, and Tracker+TOF+MVA analyses.

The multivariate technique utilized an artificial neural network that produced a multivariate discriminant. The artificial neural network was trained on signal MC samples and TOY background samples to produce unique mappings for each of the benchmark signal types. Studies were made to examine the result of applying a mapping from one mass point to other mass points for a given signal type. It was observed that a mapping trained on a lower mass point retained signal to background discrimination for higher mass points. The mappings trained on a higher mass point were shown to lose discriminating power when applied to lower mass points, but provided greater background rejection than the mappings trained on lower mass points. The final determination of the mass points for each signal type was chosen to be the highest mass point excluded from the previous 2015 HSCP search.

The standard HSCP analyses and the HSCP multivariate analyses shared many of the same systematics and were studied using the same methodologies. In the multivariate analyses, there was a systematic uncertainty related to signal acceptance due to the artificial neural network. The uncertainties on the inputs to the artificial neural network (I_h, p, $1/\beta$) were included and the change in signal acceptance was calculated. The systematic uncertainty on the signal acceptance due to the shift in the multivariate discriminant values was small on average ($< 5\%$), with lower mass points having up to 20%. The increase of systematic uncertainty at lower mass points was due to the mappings being trained on higher mass points.

Using the artificial neural network mappings there was good agreement between the data based background prediction and data for the final loose selection; evidence that the background estimation was reliable. When the final tight selection criteria were applied, no statistically significant excess was found in observed data over background in either 2015 or 2016 data. Therefore no claim of evidence for HSCPs is made.

Limits were set on the expected cross sections, observed cross sections, and masses for the different signal models investigated. Based upon comparisons of the upper cross section limits and lower mass limits for the 2015 and 2016 datasets, the HSCP multivariate analyses produced $\approx 5\%$ improvements over the standard HSCP analyses in many of the signal models. This was due to decreased systematic uncertainties, increased background rejection, and increases in signal acceptance. The lower mass limits for the 2015 and 2016 data resulted in slight improvement for the hadron-like signals ($< 2\%$) and resulted in $< 5\%$ improvement for the lepton-like signals.

An application of the HSCP multivariate approach that was not explored would be the utilization of the multivariate approach to the multiply or fractionally charged HSCP searches. During reconstruction, particle momentum is calculated based on the assumption of unit charge. This leads to an underestimate in the case of multiply charged particles and an overestimate in the particle momentum in the case of fractionally charged particles. The mass calculation that is currently in use by the HSCP analyses relies heavily on the momentum (see Eq.3.7), and thus the HSCP searches for multiply or fractionally charged particles are affected by the incorrect reconstructed momentum. However, in the case of a multivariate approach, a properly trained mapping should allow for discrimination between signal and background without the need to recompute the particle momentum. The artificial neural network will rely on the relationships of all of the input variables and be less susceptible to the mismeasurement of momentum. A future analysis of the multivariate approach applied to the entire 2016 dataset collected by the CMS detector would also be of interest to see if the increased amount of data leads to evidence of HSCPs.

The search for HSCPs can probe for new physics without being tied to a specific model making it a versatile tool to search for new phenomena beyond the Standard Model. HSCPs are predicted in multiple theories and the search for HSCPs place important theoretical restrictions. The use of a multivariate approach has been found to be plausible and furthermore produced improved limits when compared to the standard HSCP analyses.

APPENDIX A

BACKGROUND PREDICTION VERSUS OBSERVED DATA

Table A.1: The number of predicted and observed events in 2015 data for a range of MVA selections using the gluino MVA mapping

Analysis	Selection				Number of events	
	p_T (GeV)	I_{as}	$1/\beta$	MVA	Predicted	Observed
tracker-only+MVA	60	0.1	——	0	11946.7± 2392.0	12544
	60	0.1	——	0.20	185.6± 37.1	184
	60	0.1	——	0.40	30.1± 6.0	31
	60	0.1	——	0.60	6.6± 1.4	9
	60	0.1	——	0.80	1.0± 0.2	1
	65	0.3	——	0	29.3± 6.1	24
	65	0.3	——	0.20	3.6± 0.8	0
	65	0.3	——	0.40	0.4± 0.1	0
	65	0.3	——	0.60	0.07± 0.02	0
	65	0.3	——	0.80	0.012± 0.003	0
Tracker+TOF+MVA	65	0.050	1.050	0	16644.9± 3329.8	16546
	65	0.050	1.050	0.20	664.9 ± 133.0	661
	65	0.050	1.050	0.40	103.0± 20.6	97
	65	0.050	1.050	0.60	20.3± 4.1	17
	65	0.050	1.050	0.80	2.1 ± 0.4	2
	65	0.175	1.250	0	0.85 ± 0.18	0
	65	0.175	1.250	0.20	0.05 ± 0.01	0
	65	0.175	1.250	0.40	0.003± 0.001	0
	65	0.175	1.250	0.60	0.001± 0.000	0
	65	0.175	1.250	0.80	0.000± 0.000	0

Table A.2: The number of predicted and observed events in 2015 data for a range of MVA selections using the stop MVA mapping

Analysis	Selection				Number of events	
	p_T (GeV)	I_{as}	$1/\beta$	MVA	Predicted	Observed
tracker-only+MVA	60	0.1	——	0	11946.7± 2392.3	12544
	60	0.1	——	0.2	206.5± 41.3	209
	60	0.1	——	0.4	47.0± 9.4	49
	60	0.1	——	0.6	13.9± 2.8	17
	60	0.1	——	0.8	3.9± 0.8	6
	65	0.3	——	0	29.3± 6.1	24
	65	0.3	——	0.20	2.9± 0.7	1
	65	0.3	——	0.40	0.4± 0.1	0
	65	0.3	——	0.60	0.1± 0.02	0
	65	0.3	——	0.80	0.03± 0.006	0
Tracker+TOF+MVA	65	0.050	1.050	0	16644.9± 3331.2	16546
	65	0.050	1.050	0.20	513.4 ± 102.7	484
	65	0.050	1.050	0.40	182.2± 36.5	164
	65	0.050	1.050	0.60	74.9± 15.0	73
	65	0.050	1.050	0.80	26.3± 5.3	22
	65	0.175	1.250	0	0.85 ± 0.18	0
	65	0.175	1.250	0.20	0.010± 0.002	0
	65	0.175	1.250	0.40	0.003± 0.001	0
	65	0.175	1.250	0.60	0.001± 0.000	0
	65	0.175	1.250	0.60	0.000± 0.000	0

Table A.3: The number of predicted and observed events in 2015 data for a range of MVA selections using the GMSB stau MVA mapping

Analysis	Selection				Number of events	
	p_T (GeV)	I_{as}	$1/\beta$	MVA	Predicted	Observed
tracker-only+MVA	60	0.1	—	0	11946.7± 2391.9	12544
	60	0.1	—	0.20	743.4± 148.7	741
	60	0.1	—	0.40	255.3± 51.1	243
	60	0.1	—	0.60	108.6± 21.7	119
	60	0.1	—	0.80	44.9± 9.0	48
	65	0.3	—	0	29.3± 6.1	24
	65	0.3	—	0.20	12.9± 2.8	7
	65	0.3	—	0.40	2.5± 0.5	1
	65	0.3	—	0.60	0.8± 0.2	0
	65	0.3	—	0.80	0.32± 0.07	0
Tracker+TOF+MVA	65	0.050	1.050	0	16644.9± 3329.7	16546
	65	0.050	1.050	0.20	2022.8 ± 404.6	1979
	65	0.050	1.050	0.40	444.1± 88.8	434
	65	0.050	1.050	0.60	120.3± 24.1	108
	65	0.050	1.050	0.80	31.3± 6.3	28
	65	0.175	1.250	0	0.85 ± 0.18	0
	65	0.175	1.250	0.20	0.17± 0.03	0
	65	0.175	1.250	0.40	0.021± 0.004	0
	65	0.175	1.250	0.60	0.004± 0.001	0
	65	0.175	1.250	0.80	0.001± 0.000	0

Table A.4: The number of predicted and observed events in 2015 data for a range of MVA selections using the PP stau MVA mapping

Analysis	Selection				Number of events	
	p_T (GeV)	I_{as}	$1/\beta$	MVA	Predicted	Observed
tracker-only+MVA	60	0.1	—	0	11946.7± 2391.6	12544
	60	0.1	—	0.20	1425.5± 285.2	1470
	60	0.1	—	0.40	529.4± 105.9	528
	60	0.1	—	0.60	223.3± 44.7	219
	60	0.1	—	0.80	90.4± 18.1	99
	65	0.3	—	0	29.3± 6.1	24
	65	0.3	—	0.20	15.3± 3.2	9
	65	0.3	—	0.40	4.4± 0.9	3
	65	0.3	—	0.60	1.7± 0.4	1
	65	0.3	—	0.80	0.8± 0.2	0
Tracker+TOF+MVA	65	0.050	1.050	0	16644.9± 3329.8	16546
	65	0.050	1.050	0.20	2339.6 ± 468.0	2241
	65	0.050	1.050	0.40	846.6± 169.3	826
	65	0.050	1.050	0.60	368.0± 73.6	340
	65	0.050	1.050	0.80	129.5± 25.9	113
	65	0.175	1.250	0	0.85 ± 0.18	0
	65	0.175	1.250	0.20	0.16± 0.03	0
	65	0.175	1.250	0.40	0.03± 0.006	0
	65	0.175	1.250	0.60	0.012± 0.002	0
	65	0.175	1.250	0.80	0.005± 0.001	0

Table A.5: The number of predicted and observed events in 2015 data for a range of MVA selections using the DY $|Q| = 1e$ MVA mapping

Analysis	Selection				Number of events	
	p_T (GeV)	I_{as}	$1/\beta$	MVA	Predicted	Observed
tracker-only+MVA	60	0.1	—	0	11946.7± 2391.6	12544
	60	0.1	—	0.20	399.7± 80.0	382
	60	0.1	—	0.40	120.3± 24.1	126
	60	0.1	—	0.60	47.4± 9.5	49
	60	0.1	—	0.80	17.7± 3.5	21
	65	0.3	—	0	29.3± 6.2	24
	65	0.3	—	0.20	7.8± 1.8	4
	65	0.3	—	0.40	1.0± 0.2	0
	65	0.3	—	0.60	0.3± 0.06	0
	65	0.3	—	0.80	0.1± 0.02	0
Tracker+TOF+MVA	65	0.050	1.050	0	16644.9± 3329.8	16546
	65	0.050	1.050	0.20	1059.3 ± 211.9	1043
	65	0.050	1.050	0.40	258.1± 51.6	236
	65	0.050	1.050	0.60	96.4± 19.3	86
	65	0.050	1.050	0.80	36.3± 7.3	31
	65	0.175	1.250	0	0.85 ± 0.18	0
	65	0.175	1.250	0.20	0.08± 0.2	0
	65	0.175	1.250	0.40	0.008± 0.002	0
	65	0.175	1.250	0.60	0.002± 0.000	0
	65	0.175	1.250	0.80	0.001± 0.0	0

Table A.6: The number of predicted and observed events in 2015 data for a range of MVA selections using the DY $|Q| = 2e$ MVA mapping

Analysis	Selection				Number of events	
	p_T (GeV)	I_{as}	$1/\beta$	MVA	Predicted	Observed
tracker-only+MVA	60	0.1	—	0	11946.7± 2391.6	12544
	60	0.1	—	0.20	161.9 ± 32.4	172
	60	0.1	—	0.40	20.7± 4.1	24
	60	0.1	—	0.60	3.3± 0.7	3
	60	0.1	—	0.80	0.2± 0.04	0
	65	0.3	—	0	29.3± 6.1	24
	65	0.3	—	0.20	3.0± 0.7	1
	65	0.3	—	0.40	0.3± 0.1	0
	65	0.3	—	0.60	0.05± 0.01	0
	65	0.3	—	0.80	0.006± 0.002	0
Tracker+TOF+MVA	65	0.050	1.050	0	16644.9± 3329.8	16546
	65	0.050	1.050	0.20	313.7 ± 62.8	297
	65	0.050	1.050	0.40	32.0± 6.4	29
	65	0.050	1.050	0.60	4.6± 0.9	11
	65	0.050	1.050	0.80	0.03± 0.01	3
	65	0.175	1.250	0	0.85 ± 0.18	0
	65	0.175	1.250	0.20	0.03± 0.005	0
	65	0.175	1.250	0.40	0.000± 0.000	0
	65	0.175	1.250	0.60	0.000± 0.000	0
	65	0.175	1.250	0.80	0.000± 0.000	0

Table A.7: The number of predicted and observed events in 2016 data for a range of MVA selections using the gluino MVA mapping

Analysis	Selection				Number of events	
	p_T (GeV)	I_{as}	$1/\beta$	MVA	Predicted	Observed
tracker-only+MVA	60	0.1	——	0	43436.5± 8689.5	44738
	60	0.1	——	0.20	489.0 ± 97.8	514
	60	0.1	——	0.40	65.4± 13.1	84
	60	0.1	——	0.60	12.9± 2.6	21
	60	0.1	——	0.80	2.0± 0.4	5
	65	0.3	——	0	87.4± 17.7	95
	65	0.3	——	0.20	6.4± 1.4	7
	65	0.3	——	0.40	0.5± 0.1	0
	65	0.3	——	0.60	0.07± 0.02	0
	65	0.3	——	0.80	0.01± 0.002	0
Tracker+TOF+MVA	65	0.050	1.050	0	72208.9± 14442.9	74343
	65	0.050	1.050	0.20	2030.2 ± 406.0	2116
	65	0.050	1.050	0.40	227.8± 55.6	310
	65	0.050	1.050	0.60	50.2± 10.0	58
	65	0.050	1.050	0.80	5.3± 1.1	14
	65	0.175	1.250	0	2.6± 0.5	5
	65	0.175	1.250	0.20	0.18 ± 0.04	0
	65	0.175	1.250	0.40	0.011± 0.002	0
	65	0.175	1.250	0.60	0.001± 0.000	0
	65	0.175	1.250	0.80	0.000± 0.000	0

Table A.8: The number of predicted and observed events in 2016 data for a range of MVA selections using the stop MVA mapping

Analysis	Selection				Number of events	
	p_T (GeV)	I_{as}	$1/\beta$	MVA	Predicted	Observed
tracker-only+MVA	60	0.1	——	0	43436.5± 8689.5	44738
	60	0.1	——	0.20	515.9 ± 103.2	544
	60	0.1	——	0.40	97.3± 19.5	117
	60	0.1	——	0.60	28.0± 5.4	38
	60	0.1	——	0.80	9.2± 1.4	11
	65	0.3	——	0	29.3± 17.7	95
	65	0.3	——	0.20	4.7± 1.0	6
	65	0.3	——	0.40	0.5± 0.1	0
	65	0.3	——	0.60	0.24± 0.05	0
	65	0.3	——	0.80	0.06± 0.01	0
Tracker+TOF+MVA	65	0.050	1.050	0	72208.9± 14442.9	74343
	65	0.050	1.050	0.20	1396.2 ± 279.3	1451
	65	0.050	1.050	0.40	499.1± 99.8	531
	65	0.050	1.050	0.60	206.9± 41.4	234
	65	0.050	1.050	0.80	70.9± 14.2	98
	65	0.175	1.250	0	2.6± 0.5	5
	65	0.175	1.250	0.20	0.025± 0.005	0
	65	0.175	1.250	0.40	0.007± 0.001	0
	65	0.175	1.250	0.60	0.002± 0.000	0
	65	0.175	1.250	0.80	0.001± 0.000	0

Table A.9: The number of predicted and observed events in 2016 data for a range of MVA selections using the GMSB stau MVA mapping

Analysis	Selection				Number of events	
	p_T (GeV)	I_{as}	$1/\beta$	MVA	Predicted	Observed
tracker-only+MVA	60	0.1	——	0	43436.5± 8689.5	44738
	60	0.1	——	0.20	2058.6 ± 411.8	2155
	60	0.1	——	0.40	565.8± 113.2	586
	60	0.1	——	0.60	226.4± 45.3	253
	60	0.1	——	0.80	93.1± 18.6	110
	65	0.3	——	0	87.4± 17.7	95
	65	0.3	——	0.20	45.3± 9.3	60
	65	0.3	——	0.40	4.1± 0.8	4
	65	0.3	——	0.60	1.1± 0.2	1
	65	0.3	——	0.80	0.45± 0.09	0
Tracker+TOF+MVA	65	0.050	1.050	0	72208.9± 14442.9	74343
	65	0.050	1.050	0.20	6702.7 ± 1340.6	6879
	65	0.050	1.050	0.40	1263.4± 252.7	1352
	65	0.050	1.050	0.60	309.7± 61.9	344
	65	0.050	1.050	0.80	71.1± 14.2	88
	65	0.175	1.250	0	2.6± 0.5	5
	65	0.175	1.250	0.20	0.6± 0.1	1
	65	0.175	1.250	0.40	0.07± 0.01	0
	65	0.175	1.250	0.60	0.01± 0.003	0
	65	0.175	1.250	0.80	0.003± 0.001	0

Table A.10: The number of predicted and observed events in 2016 data for a range of MVA selections using the PP stau MVA mapping

Analysis	Selection				Number of events	
	p_T (GeV)	I_{as}	$1/\beta$	MVA	Predicted	Observed
tracker-only+MVA	60	0.1	—	0	43436.5± 8689.5	44738
	60	0.1	—	0.20	4591.0 ± 918.3	4715
	60	0.1	—	0.40	1465.7± 293.1	1545
	60	0.1	—	0.60	575.1± 115.0	601
	60	0.1	—	0.80	231.4± 46.3	254
	65	0.3	—	0	87.4± 17.9	95
	65	0.3	—	0.20	48.0± 9.8	59
	65	0.3	—	0.40	10.0± 2.0	17
	65	0.3	—	0.60	3.3± 0.7	2
	65	0.3	—	0.80	1.4± 0.3	1
Tracker+TOF+MVA	65	0.050	1.050	0	72208.9± 14442.9	74343
	65	0.050	1.050	0.20	6959.0 ± 1391.8	7083
	65	0.050	1.050	0.40	2182.4± 436.5	2251
	65	0.050	1.050	0.60	875.4± 175.1	956
	65	0.050	1.050	0.80	327.1± 65.4	359
	65	0.175	1.250	0	2.6± 0.5	5
	65	0.175	1.250	0.20	0.6± 0.1	0
	65	0.175	1.250	0.40	0.11± 0.02	0
	65	0.175	1.250	0.60	0.036± 0.007	0
	65	0.175	1.250	0.80	0.015± 0.003	0

Table A.11: The number of predicted and observed events in 2016 data for a range of MVA selections using the DY $|Q| = 1e$ MVA mapping

Analysis	Selection				Number of events	
	p_T (GeV)	I_{as}	$1/\beta$	MVA	Predicted	Observed
tracker-only+MVA	60	0.1	—	0	43436.5± 8689.5	44738
	60	0.1	—	0.20	4591.0 ± 918.3	1011
	60	0.1	—	0.40	1465.7± 293.1	269
	60	0.1	—	0.60	575.1± 115.0	113
	60	0.1	—	0.80	231.4± 46.3	38
	65	0.3	—	0	87.4± 17.9	95
	65	0.3	—	0.20	20.9± 4.4	34
	65	0.3	—	0.40	1.3± 0.3	1
	65	0.3	—	0.60	0.38± 0.08	0
	65	0.3	—	0.80	0.14± 0.03	0
Tracker+TOF+MVA	65	0.050	1.050	0	72208.9± 14442.9	74343
	65	0.050	1.050	0.20	3135.0 ± 627.0	3240
	65	0.050	1.050	0.40	675.5± 135.1	735
	65	0.050	1.050	0.60	238.4± 47.7	277
	65	0.050	1.050	0.80	80.1± 16.0	105
	65	0.175	1.250	0	2.6± 0.5	5
	65	0.175	1.250	0.20	0.31± 0.06	0
	65	0.175	1.250	0.40	0.02± 0.005	0
	65	0.175	1.250	0.60	0.006± 0.001	0
	65	0.175	1.250	0.80	0.002± 0.000	0

Table A.12: The number of predicted and observed events in 2016 data for a range of MVA selections using the DY $|Q| = 2e$ MVA mapping

Analysis	Selection				Number of events	
	p_T (GeV)	I_{as}	$1/\beta$	MVA	Predicted	Observed
tracker-only+MVA	60	0.1	—	0	43436.5± 8689.5	44738
	60	0.1	—	0.20	470.2 ± 94.0	498
	60	0.1	—	0.40	49.9± 10.0	62
	60	0.1	—	0.60	6.9± 1.4	9
	60	0.1	—	0.80	0.42± 0.08	2
	65	0.3	—	0	87.4± 17.7	95
	65	0.3	—	0.20	4.9± 1.0	5
	65	0.3	—	0.40	0.37± 0.08	0
	65	0.3	—	0.60	0.05± 0.01	0
	65	0.3	—	0.80	0.004± 0.001	0
Tracker+TOF+MVA	65	0.050	1.050	0	72208.9± 14442.9	74343
	65	0.050	1.050	0.20	789.6 ± 157.9	868
	65	0.050	1.050	0.40	68.2± 13.6	81
	65	0.050	1.050	0.60	9.7± 1.9	22
	65	0.050	1.050	0.80	0.12± 0.03	3
	65	0.175	1.250	0	2.6± 0.5	5
	65	0.175	1.250	0.20	0.12± 0.02	0
	65	0.175	1.250	0.40	0.002± 0.000	0
	65	0.175	1.250	0.60	0.000± 0.000	0
	65	0.175	1.250	0.80	0.000± 0.000	0

APPENDIX B

FULL RESULTS

Table B.1: Tracker-only+MVA results using 2015 data with the same final selection as the standard analysis.

Model	Mass (GeV)	$p_T >$ (GeV)	$I_{as} >$	$1/\beta >$	MVA>	Bckg. Pred	Obs	SigEff	ThXsec (pb)	ExpXsec (pb)	ObsXsec (pb)	Signif
Gluino f=0.1	200	65	0.300	/	0.200	3.580 ± 0.797	0	0.102	3.4E+03	2.0E-02	1.0E-02	0.00
Gluino f=0.1	400	65	0.300	/	0.200	3.580 ± 0.797	0	0.167	9.5E+01	1.3E-02	7.6E-03	0.00
Gluino f=0.1	600	65	0.300	/	0.200	3.580 ± 0.797	0	0.201	9.1E+00	1.1E-02	5.9E-03	0.00
Gluino f=0.1	800	65	0.300	/	0.320	0.894 ± 0.201	0	0.225	1.5E+00	7.5E-03	4.9E-03	0.00
Gluino f=0.1	1000	65	0.300	/	0.420	0.309 ± 0.068	0	0.233	3.2E-01	5.2E-03	5.2E-03	0.00
Gluino f=0.1	1200	65	0.300	/	0.580	0.080 ± 0.017	0	0.226	8.4E-02	5.3E-03	5.3E-03	0.00
Gluino f=0.1	1400	65	0.300	/	0.640	0.049 ± 0.011	0	0.199	2.5E-02	6.1E-03	6.1E-03	0.00
Gluino f=0.1	1600	65	0.300	/	0.640	0.049 ± 0.011	0	0.173	8.0E-03	7.0E-03	7.0E-03	0.00
Gluino f=0.1	1800	65	0.300	/	0.640	0.049 ± 0.011	0	0.143	2.7E-03	8.5E-03	8.5E-03	0.00
Gluino f=0.1	2000	65	0.300	/	0.640	0.049 ± 0.011	0	0.117	9.7E-04	1.0E-02	1.0E-02	0.00
Gluino f=0.1	2200	65	0.300	/	0.640	0.049 ± 0.011	0	0.094	3.6E-04	1.3E-02	1.3E-02	0.00
Gluino f=0.1	2600	65	0.300	/	0.640	0.049 ± 0.011	0	0.060	5.0E-05	2.1E-02	2.1E-02	0.00
GluinoN f=0.1	100	65	0.300	/	0.200	3.580 ± 0.797	0	0.002	8.2E+04	1.3E+00	7.4E-01	0.00
GluinoN f=0.1	1000	65	0.300	/	0.400	0.373 ± 0.082	0	0.189	3.2E-01	6.5E-03	6.5E-03	0.00
GluinoN f=0.1	1200	65	0.300	/	0.460	0.215 ± 0.047	0	0.190	8.4E-02	6.4E-03	6.4E-03	0.00
GluinoN f=0.1	1400	65	0.300	/	0.600	0.067 ± 0.015	0	0.174	2.5E-02	7.1E-03	7.1E-03	0.00
GluinoN f=0.1	1600	65	0.300	/	0.640	0.049 ± 0.011	0	0.148	8.0E-03	8.3E-03	8.3E-03	0.00
GluinoN f=0.1	1800	65	0.300	/	0.640	0.049 ± 0.011	0	0.125	2.7E-03	9.8E-03	9.8E-03	0.00
GluinoN f=0.1	2000	65	0.300	/	0.640	0.049 ± 0.011	0	0.103	9.7E-04	1.2E-02	1.2E-02	0.00
GluinoN f=0.1	2600	65	0.300	/	0.640	0.049 ± 0.011	0	0.054	5.0E-05	2.2E-02	2.2E-02	0.00
Gluino f=0.5	200	65	0.300	/	0.200	3.580 ± 0.797	0	0.052	3.4E+03	4.4E-02	2.2E-02	0.00
Gluino f=0.5	400	65	0.300	/	0.200	3.580 ± 0.797	0	0.094	9.5E+01	2.2E-02	1.0E-02	0.00
Gluino f=0.5	600	65	0.300	/	0.200	3.580 ± 0.797	0	0.116	9.1E+00	2.0E-02	1.1E-02	0.00
Gluino f=0.5	800	65	0.300	/	0.300	1.140 ± 0.259	0	0.131	1.5E+00	1.3E-02	9.0E-03	0.00
Gluino f=0.5	1000	65	0.300	/	0.480	0.183 ± 0.040	0	0.136	3.2E-01	9.0E-03	9.0E-03	0.00
Gluino f=0.5	1200	65	0.300	/	0.560	0.091 ± 0.020	0	0.131	8.4E-02	9.4E-03	9.4E-03	0.00
Gluino f=0.5	1400	65	0.300	/	0.620	0.056 ± 0.012	0	0.114	2.5E-02	1.0E-02	1.0E-02	0.00
Gluino f=0.5	1600	65	0.300	/	0.640	0.049 ± 0.011	0	0.100	8.0E-03	1.2E-02	1.2E-02	0.00
Gluino f=0.5	1800	65	0.300	/	0.640	0.049 ± 0.011	0	0.080	2.7E-03	1.5E-02	1.5E-02	0.00
Gluino f=0.5	2000	65	0.300	/	0.640	0.049 ± 0.011	0	0.066	9.7E-04	1.8E-02	1.8E-02	0.00
Gluino f=0.5	2200	65	0.300	/	0.640	0.049 ± 0.011	0	0.052	3.6E-04	2.3E-02	2.3E-02	0.00
Gluino f=0.5	2600	65	0.300	/	0.640	0.049 ± 0.011	0	0.034	5.0E-05	3.5E-02	3.5E-02	0.00
GluinoN f=0.5	100	65	0.300	/	0.200	3.580 ± 0.797	0	0.002	8.2E+04	1.6E+00	8.6E-01	0.00
GluinoN f=0.5	1000	65	0.300	/	0.420	0.309 ± 0.068	0	0.146	3.2E-01	8.3E-03	8.3E-03	0.00
GluinoN f=0.5	1200	65	0.300	/	0.540	0.106 ± 0.023	0	0.146	8.4E-02	8.5E-03	8.5E-03	0.00
GluinoN f=0.5	1400	65	0.300	/	0.580	0.080 ± 0.017	0	0.136	2.5E-02	9.0E-03	9.0E-03	0.00
GluinoN f=0.5	1600	65	0.300	/	0.640	0.049 ± 0.011	0	0.114	8.0E-03	1.1E-02	1.1E-02	0.00
GluinoN f=0.5	1800	65	0.300	/	0.640	0.049 ± 0.011	0	0.096	2.7E-03	1.3E-02	1.3E-02	0.00
GluinoN f=0.5	2000	65	0.300	/	0.640	0.049 ± 0.011	0	0.079	9.7E-04	1.5E-02	1.5E-02	0.00
GluinoN f=0.5	2600	65	0.300	/	0.640	0.049 ± 0.011	0	0.042	5.0E-05	2.9E-02	2.9E-02	0.00
Stop	100	65	0.300	/	0.200	2.950 ± 0.655	1	0.120	1.4E+03	1.8E-02	1.3E-02	0.00
Stop	200	65	0.300	/	0.200	2.950 ± 0.655	1	0.195	6.1E+01	1.2E-02	6.9E-03	0.00
Stop	400	65	0.300	/	0.200	2.950 ± 0.655	1	0.246	1.8E+00	9.0E-03	6.0E-03	0.00
Stop	600	65	0.300	/	0.340	0.650 ± 0.141	0	0.267	1.7E-01	5.3E-03	4.5E-03	0.00
Stop	800	65	0.300	/	0.560	0.124 ± 0.027	0	0.270	2.8E-02	4.5E-03	4.5E-03	0.00
Stop	1000	65	0.300	/	0.700	0.052 ± 0.011	0	0.262	6.0E-03	4.6E-03	4.6E-03	0.00

Continued on next page

Table B.1 – continued from previous page

Model	Mass (GeV)	$p_T >$ (GeV)	$I_{as} >$	$1/\beta >$	MVA>	Bckg. Pred	Obs	SigEff	ThXsec (pb)	ExpXsec (pb)	ObsXsec (pb)	Signif
Stop	1200	65	0.300	/	0.700	0.052 ± 0.011	0	0.250	1.6E-03	4.8E-03	4.8E-03	0.00
Stop	1400	65	0.300	/	0.700	0.052 ± 0.011	0	0.229	4.5E-04	5.3E-03	5.3E-03	0.00
Stop	1600	65	0.300	/	0.700	0.052 ± 0.011	0	0.197	1.4E-04	6.1E-03	6.1E-03	0.00
Stop	1800	65	0.300	/	0.700	0.052 ± 0.011	0	0.168	4.6E-05	7.2E-03	7.2E-03	0.00
Stop	2000	65	0.300	/	0.700	0.052 ± 0.011	0	0.138	1.6E-05	8.9E-03	8.9E-03	0.00
Stop	2200	65	0.300	/	0.700	0.052 ± 0.011	0	0.112	6.0E-06	1.1E-02	1.1E-02	0.00
StopN	100	65	0.300	/	0.200	2.950 ± 0.655	1	0.012	1.4E+03	1.9E-01	1.3E-01	0.00
StopN	200	65	0.300	/	0.200	2.950 ± 0.655	1	0.046	6.1E+01	4.9E-02	3.3E-02	0.00
StopN	400	65	0.300	/	0.200	2.950 ± 0.655	1	0.123	1.8E+00	1.8E-02	1.1E-02	0.00
StopN	600	65	0.300	/	0.340	0.650 ± 0.141	0	0.169	1.7E-01	9.4E-03	6.9E-03	0.00
StopN	800	65	0.300	/	0.620	0.086 ± 0.019	0	0.189	2.8E-02	6.5E-03	6.5E-03	0.00
StopN	1000	65	0.300	/	0.700	0.052 ± 0.011	0	0.196	6.0E-03	6.2E-03	6.2E-03	0.00
StopN	1200	65	0.300	/	0.700	0.052 ± 0.011	0	0.189	1.6E-03	6.3E-03	6.3E-03	0.00
StopN	1600	65	0.300	/	0.700	0.052 ± 0.011	0	0.155	1.4E-04	7.8E-03	7.8E-03	0.00
StopN	1800	65	0.300	/	0.700	0.052 ± 0.011	0	0.128	4.6E-05	9.3E-03	9.3E-03	0.00
StopN	2000	65	0.300	/	0.700	0.052 ± 0.011	0	0.106	1.6E-05	1.1E-02	1.1E-02	0.00
StopN	2200	65	0.300	/	0.700	0.052 ± 0.011	0	0.089	6.0E-06	1.4E-02	1.4E-02	0.00
GMSB stau	200	65	0.300	/	0.200	12.900 ± 2.760	7	0.271	2.8E-01	1.4E-02	8.5E-03	0.00
GMSB stau	247	65	0.300	/	0.340	3.910 ± 0.853	2	0.352	8.8E-02	6.8E-03	4.9E-03	0.00
GMSB stau	308	65	0.300	/	0.460	1.650 ± 0.360	0	0.418	2.5E-02	4.5E-03	3.0E-03	0.00
GMSB stau	432	65	0.300	/	0.720	0.440 ± 0.094	0	0.555	3.9E-03	2.2E-03	2.2E-03	0.00
GMSB stau	494	65	0.300	/	0.840	0.268 ± 0.057	0	0.584	1.9E-03	2.1E-03	2.1E-03	0.00
GMSB stau	651	65	0.300	/	0.980	0.147 ± 0.032	0	0.660	4.1E-04	1.9E-03	1.9E-03	0.00
GMSB stau	745	65	0.300	/	0.980	0.147 ± 0.032	0	0.677	1.9E-04	1.8E-03	1.8E-03	0.00
GMSB stau	871	65	0.300	/	0.980	0.147 ± 0.032	0	0.697	6.9E-05	1.8E-03	1.8E-03	0.00
GMSB stau	1029	65	0.300	/	0.980	0.147 ± 0.032	0	0.703	2.2E-05	1.8E-03	1.8E-03	0.00
GMSB stau	1218	65	0.300	/	0.980	0.147 ± 0.032	0	0.696	6.0E-06	1.8E-03	1.8E-03	0.00
GMSB stau	1409	65	0.300	/	0.980	0.147 ± 0.032	0	0.653	2.0E-06	1.9E-03	1.9E-03	0.00
GMSB stau	1599	65	0.300	/	0.980	0.147 ± 0.032	0	0.547	1.0E-06	2.3E-03	2.3E-03	0.00
PP stau	156	65	0.300	/	0.360	5.580 ± 1.170	4	0.184	2.0E-02	1.7E-02	1.3E-02	0.00
PP stau	200	65	0.300	/	0.480	2.920 ± 0.612	2	0.221	8.0E-03	1.1E-02	8.6E-03	0.00
PP stau	247	65	0.300	/	0.620	1.570 ± 0.329	1	0.252	3.7E-03	6.7E-03	6.7E-03	0.00
PP stau	308	65	0.300	/	0.800	0.772 ± 0.163	0	0.291	1.5E-03	5.9E-03	4.3E-03	0.00
PP stau	494	65	0.300	/	0.980	0.371 ± 0.079	0	0.380	1.9E-04	3.2E-03	3.2E-03	0.00
PP stau	557	65	0.300	/	0.980	0.371 ± 0.079	0	0.413	1.1E-04	2.9E-03	2.9E-03	0.00
PP stau	651	65	0.300	/	0.980	0.371 ± 0.079	0	0.456	4.9E-05	2.7E-03	2.7E-03	0.00
PP stau	745	65	0.300	/	0.980	0.371 ± 0.079	0	0.486	2.4E-05	2.5E-03	2.5E-03	0.00
PP stau	871	65	0.300	/	0.980	0.371 ± 0.079	0	0.520	1.0E-05	2.3E-03	2.3E-03	0.00
PP stau	1029	65	0.300	/	0.980	0.371 ± 0.079	0	0.564	4.0E-06	2.1E-03	2.1E-03	0.00
PP stau	1218	65	0.300	/	0.980	0.371 ± 0.079	0	0.575	1.0E-06	2.1E-03	2.1E-03	0.00
PP stau	1409	65	0.300	/	0.980	0.371 ± 0.079	0	0.542	0.0E+00	2.2E-03	2.2E-03	0.00
PP stau	1599	65	0.300	/	0.920	0.477 ± 0.101	0	0.486	0.0E+00	2.4E-03	2.4E-03	0.00
DY $\|Q\| = 1e$	100	65	0.300	/	0.200	7.810 ± 1.780	4	0.101	1.2E+00	3.4E-02	2.2E-02	0.00
DY $\|Q\| = 1e$	200	65	0.300	/	0.200	7.810 ± 1.780	4	0.284	1.1E-01	1.2E-02	7.5E-03	0.00
DY $\|Q\| = 1e$	400	65	0.300	/	0.480	0.554 ± 0.119	0	0.401	7.3E-03	3.3E-03	3.2E-03	0.00
DY $\|Q\| = 1e$	600	65	0.300	/	0.760	0.132 ± 0.028	0	0.442	1.2E-03	2.9E-03	2.9E-03	0.00
DY $\|Q\| = 1e$	800	65	0.300	/	0.980	0.047 ± 0.010	0	0.476	2.6E-04	2.8E-03	2.8E-03	0.00
DY $\|Q\| = 1e$	1000	65	0.300	/	0.980	0.047 ± 0.010	0	0.480	7.6E-05	2.7E-03	2.7E-03	0.00
DY $\|Q\| = 1e$	1400	65	0.300	/	0.980	0.047 ± 0.010	0	0.415	9.0E-06	3.1E-03	3.1E-03	0.00
DY $\|Q\| = 1e$	1800	65	0.300	/	0.980	0.047 ± 0.010	0	0.315	1.0E-06	4.1E-03	4.1E-03	0.00
DY $\|Q\| = 1e$	2200	65	0.300	/	0.980	0.047 ± 0.010	0	0.203	0.0E+00	6.2E-03	6.2E-03	0.00
DY $\|Q\| = 1e$	2600	65	0.300	/	0.980	0.047 ± 0.010	0	0.123	0.0E+00	1.0E-02	1.0E-02	0.00
DY $\|Q\| = 2e$	100	65	0.300	/	0.200	3.050 ± 0.678	1	0.259	3.8E+00	8.5E-03	5.9E-03	0.00
DY $\|Q\| = 2e$	200	65	0.300	/	0.340	0.521 ± 0.114	0	0.585	3.0E-01	2.1E-03	2.1E-03	0.00
DY $\|Q\| = 2e$	400	65	0.300	/	0.500	0.111 ± 0.024	0	0.699	2.3E-02	1.8E-03	1.8E-03	0.00
DY $\|Q\| = 2e$	600	65	0.300	/	0.600	0.049 ± 0.011	0	0.676	3.5E-03	1.8E-03	1.8E-03	0.00
DY $\|Q\| = 2e$	800	65	0.300	/	0.600	0.049 ± 0.011	0	0.614	8.0E-04	2.0E-03	2.0E-03	0.00
DY $\|Q\| = 2e$	1000	65	0.300	/	0.600	0.049 ± 0.011	0	0.544	2.4E-04	2.3E-03	2.3E-03	0.00
DY $\|Q\| = 2e$	1400	65	0.300	/	0.600	0.049 ± 0.011	0	0.364	2.7E-05	3.5E-03	3.5E-03	0.00
DY $\|Q\| = 2e$	1800	65	0.300	/	0.600	0.049 ± 0.011	0	0.217	4.0E-06	5.9E-03	5.9E-03	0.00

Continued on next page

Table B.1 – continued from previous page

Model	Mass (GeV)	$p_T >$ (GeV)	$I_{as} >$	$1/\beta >$	MVA>	Bckg. Pred	Obs	SigEff	ThXsec (pb)	ExpXsec (pb)	ObsXsec (pb)	Signif
DY $\|Q\| = 2e$	2200	65	0.300	/	0.600	0.049 ± 0.011	0	0.154	1.0E-06	8.2E-03	8.2E-03	0.00
DY $\|Q\| = 2e$	2600	65	0.300	/	0.600	0.049 ± 0.011	0	0.101	0.0E+00	1.3E-02	1.3E-02	0.00

Table B.2: Tracker+TOF+MVA results using 2015 data with the same final selection as the standard analysis.

Model	Mass (GeV)	$p_T >$ (GeV)	$I_{as} >$	$1/\beta >$	MVA>	Bckg. Pred	Obs	SigEff	ThXsec (pb)	ExpXsec (pb)	ObsXsec (pb)	Signif
Gluino f=0.1	200	65	0.175	1.250	0.200	0.046 ± 0.009	0	0.090	3.4E+03	1.4E-02	1.4E-02	0.00
Gluino f=0.1	400	65	0.175	1.250	0.200	0.046 ± 0.009	0	0.138	9.5E+01	8.7E-03	8.7E-03	0.00
Gluino f=0.1	600	65	0.175	1.250	0.200	0.046 ± 0.009	0	0.167	9.1E+00	7.8E-03	7.8E-03	0.00
Gluino f=0.1	800	65	0.175	1.250	0.200	0.046 ± 0.009	0	0.188	1.5E+00	6.6E-03	6.6E-03	0.00
Gluino f=0.1	1000	65	0.175	1.250	0.200	0.046 ± 0.009	0	0.196	3.2E-01	6.3E-03	6.3E-03	0.00
Gluino f=0.1	1200	65	0.175	1.250	0.200	0.046 ± 0.009	0	0.189	8.4E-02	6.4E-03	6.4E-03	0.00
Gluino f=0.1	1400	65	0.175	1.250	0.200	0.046 ± 0.009	0	0.163	2.5E-02	7.5E-03	7.5E-03	0.00
Gluino f=0.1	1600	65	0.175	1.250	0.200	0.046 ± 0.009	0	0.138	8.0E-03	8.6E-03	8.6E-03	0.00
Gluino f=0.1	1800	65	0.175	1.250	0.200	0.046 ± 0.009	0	0.114	2.7E-03	1.1E-02	1.1E-02	0.00
Gluino f=0.1	2000	65	0.175	1.250	0.200	0.046 ± 0.009	0	0.092	9.7E-04	1.3E-02	1.3E-02	0.00
Gluino f=0.1	2200	65	0.175	1.250	0.200	0.046 ± 0.009	0	0.072	3.6E-04	1.7E-02	1.7E-02	0.00
Gluino f=0.1	2600	65	0.175	1.250	0.200	0.046 ± 0.009	0	0.046	5.0E-05	2.7E-02	2.7E-02	0.00
Gluino f=0.5	200	65	0.175	1.250	0.200	0.046 ± 0.009	0	0.047	3.4E+03	2.7E-02	2.7E-02	0.00
Gluino f=0.5	400	65	0.175	1.250	0.200	0.046 ± 0.009	0	0.077	9.5E+01	1.6E-02	1.6E-02	0.00
Gluino f=0.5	600	65	0.175	1.250	0.200	0.046 ± 0.009	0	0.095	9.1E+00	1.3E-02	1.3E-02	0.00
Gluino f=0.5	800	65	0.175	1.250	0.200	0.046 ± 0.009	0	0.108	1.5E+00	1.1E-02	1.1E-02	0.00
Gluino f=0.5	1000	65	0.175	1.250	0.200	0.046 ± 0.009	0	0.113	3.2E-01	1.1E-02	1.1E-02	0.00
Gluino f=0.5	1200	65	0.175	1.250	0.200	0.046 ± 0.009	0	0.108	8.4E-02	1.1E-02	1.1E-02	0.00
Gluino f=0.5	1400	65	0.175	1.250	0.200	0.046 ± 0.009	0	0.092	2.5E-02	1.3E-02	1.3E-02	0.00
Gluino f=0.5	1600	65	0.175	1.250	0.200	0.046 ± 0.009	0	0.079	8.0E-03	1.5E-02	1.5E-02	0.00
Gluino f=0.5	1800	65	0.175	1.250	0.200	0.046 ± 0.009	0	0.063	2.7E-03	1.9E-02	1.9E-02	0.00
Gluino f=0.5	2000	65	0.175	1.250	0.200	0.046 ± 0.009	0	0.052	9.7E-04	2.3E-02	2.3E-02	0.00
Gluino f=0.5	2200	65	0.175	1.250	0.200	0.046 ± 0.009	0	0.040	3.6E-04	3.0E-02	3.0E-02	0.00
Gluino f=0.5	2600	65	0.175	1.250	0.200	0.046 ± 0.009	0	0.025	5.0E-05	4.9E-02	4.9E-02	0.00
Stop	100	65	0.175	1.250	0.200	0.010 ± 0.002	0	0.030	1.4E+03	4.1E-02	4.1E-02	0.00
Stop	200	65	0.175	1.250	0.200	0.010 ± 0.002	0	0.069	6.1E+01	1.8E-02	1.8E-02	0.00
Stop	400	65	0.175	1.250	0.200	0.010 ± 0.002	0	0.156	1.8E+00	7.8E-03	7.8E-03	0.00
Stop	600	65	0.175	1.250	0.200	0.010 ± 0.002	0	0.180	1.7E-01	6.8E-03	6.8E-03	0.00
Stop	800	65	0.175	1.250	0.200	0.010 ± 0.002	0	0.192	2.8E-02	6.3E-03	6.3E-03	0.00
Stop	1000	65	0.175	1.250	0.200	0.010 ± 0.002	0	0.192	6.0E-03	6.5E-03	6.5E-03	0.00
Stop	1200	65	0.175	1.250	0.200	0.010 ± 0.002	0	0.184	1.6E-03	6.8E-03	6.8E-03	0.00
Stop	1400	65	0.175	1.250	0.200	0.010 ± 0.002	0	0.163	4.5E-04	7.5E-03	7.5E-03	0.00
Stop	1600	65	0.175	1.250	0.200	0.010 ± 0.002	0	0.138	1.4E-04	8.9E-03	8.9E-03	0.00
Stop	1800	65	0.175	1.250	0.200	0.010 ± 0.002	0	0.116	4.6E-05	1.0E-02	1.0E-02	0.00
Stop	2000	65	0.175	1.250	0.200	0.010 ± 0.002	0	0.095	1.6E-05	1.3E-02	1.3E-02	0.00
Stop	2200	65	0.175	1.250	0.200	0.010 ± 0.002	0	0.076	6.0E-06	1.6E-02	1.6E-02	0.00
GMSB stau	200	65	0.175	1.250	0.200	0.170 ± 0.034	0	0.291	2.8E-01	4.1E-03	4.1E-03	0.00
GMSB stau	247	65	0.175	1.250	0.200	0.170 ± 0.034	0	0.365	8.8E-02	3.3E-03	3.3E-03	0.00
GMSB stau	308	65	0.175	1.250	0.260	0.082 ± 0.016	0	0.433	2.5E-02	2.9E-03	2.9E-03	0.00
GMSB stau	432	65	0.175	1.250	0.300	0.054 ± 0.011	0	0.564	3.9E-03	2.1E-03	2.1E-03	0.00
GMSB stau	494	65	0.175	1.250	0.300	0.054 ± 0.011	0	0.595	1.9E-03	2.1E-03	2.1E-03	0.00
GMSB stau	651	65	0.175	1.250	0.300	0.054 ± 0.011	0	0.667	4.1E-04	1.9E-03	1.9E-03	0.00
GMSB stau	745	65	0.175	1.250	0.300	0.054 ± 0.011	0	0.691	1.9E-04	1.7E-03	1.7E-03	0.00
GMSB stau	871	65	0.175	1.250	0.300	0.054 ± 0.011	0	0.706	6.9E-05	1.7E-03	1.7E-03	0.00
GMSB stau	1029	65	0.175	1.250	0.300	0.054 ± 0.011	0	0.716	2.2E-05	1.7E-03	1.7E-03	0.00
GMSB stau	1218	65	0.175	1.250	0.300	0.054 ± 0.011	0	0.704	6.0E-06	1.8E-03	1.8E-03	0.00
GMSB stau	1409	65	0.175	1.250	0.300	0.054 ± 0.011	0	0.658	2.0E-06	1.9E-03	1.9E-03	0.00
GMSB stau	1599	65	0.175	1.250	0.300	0.054 ± 0.011	0	0.555	1.0E-06	2.2E-03	2.2E-03	0.00
PP stau	156	65	0.175	1.250	0.200	0.156 ± 0.031	0	0.209	2.0E-02	5.8E-03	5.8E-03	0.00

Continued on next page

Table B.2 – continued from previous page

Model	Mass (GeV)	$p_T >$ (GeV)	$I_{as} >$	$1/\beta >$	MVA>	Bckg. Pred	Obs	SigEff	ThXsec (pb)	ExpXsec (pb)	ObsXsec (pb)	Signif
PP stau	200	65	0.175	1.250	0.260	0.085 ± 0.017	0	0.243	8.0E-03	5.0E-03	5.0E-03	0.00
PP stau	247	65	0.175	1.250	0.320	0.053 ± 0.011	0	0.271	3.7E-03	4.6E-03	4.6E-03	0.00
PP stau	308	65	0.175	1.250	0.320	0.053 ± 0.011	0	0.317	1.5E-03	3.9E-03	3.9E-03	0.00
PP stau	494	65	0.175	1.250	0.320	0.053 ± 0.011	0	0.418	1.9E-04	2.9E-03	2.9E-03	0.00
PP stau	557	65	0.175	1.250	0.320	0.053 ± 0.011	0	0.448	1.1E-04	2.7E-03	2.7E-03	0.00
PP stau	651	65	0.175	1.250	0.320	0.053 ± 0.011	0	0.499	4.9E-05	2.4E-03	2.4E-03	0.00
PP stau	745	65	0.175	1.250	0.320	0.053 ± 0.011	0	0.522	2.4E-05	2.4E-03	2.4E-03	0.00
PP stau	871	65	0.175	1.250	0.320	0.053 ± 0.011	0	0.557	1.0E-05	2.2E-03	2.2E-03	0.00
PP stau	1029	65	0.175	1.250	0.320	0.053 ± 0.011	0	0.595	4.0E-06	2.1E-03	2.1E-03	0.00
PP stau	1218	65	0.175	1.250	0.320	0.053 ± 0.011	0	0.603	1.0E-06	2.0E-03	2.0E-03	0.00
PP stau	1409	65	0.175	1.250	0.540	0.053 ± 0.011	0	0.569	0.0E+00	2.2E-03	2.2E-03	0.00
PP stau	1599	65	0.175	1.250	0.320	0.053 ± 0.011	0	0.509	0.0E+00	2.4E-03	2.4E-03	0.00
DY $\|Q\| = 1e$	100	65	0.175	1.250	0.200	0.079 ± 0.016	0	0.110	1.2E+00	1.2E-02	1.2E-02	0.00
DY $\|Q\| = 1e$	200	65	0.175	1.250	0.200	0.079 ± 0.016	0	0.305	1.1E-01	4.1E-03	4.1E-03	0.00
DY $\|Q\| = 1e$	400	65	0.175	1.250	0.220	0.055 ± 0.011	0	0.420	7.3E-03	3.0E-03	3.0E-03	0.00
DY $\|Q\| = 1e$	600	65	0.175	1.250	0.220	0.055 ± 0.011	0	0.466	1.2E-03	2.7E-03	2.7E-03	0.00
DY $\|Q\| = 1e$	800	65	0.175	1.250	0.220	0.055 ± 0.011	0	0.488	2.6E-04	2.6E-03	2.6E-03	0.00
DY $\|Q\| = 1e$	1000	65	0.175	1.250	0.220	0.055 ± 0.011	0	0.489	7.6E-05	2.6E-03	2.6E-03	0.00
DY $\|Q\| = 1e$	1400	65	0.175	1.250	0.220	0.055 ± 0.011	0	0.422	9.0E-06	3.0E-03	3.0E-03	0.00
DY $\|Q\| = 1e$	1800	65	0.175	1.250	0.220	0.055 ± 0.011	0	0.317	1.0E-06	4.1E-03	4.1E-03	0.00
DY $\|Q\| = 1e$	2200	65	0.175	1.250	0.220	0.055 ± 0.011	0	0.200	0.0E+00	6.3E-03	6.3E-03	0.00
DY $\|Q\| = 1e$	2600	65	0.175	1.250	0.220	0.055 ± 0.011	0	0.118	0.0E+00	1.1E-02	1.1E-02	0.00
DY $\|Q\| = 2e$	100	65	0.175	1.250	0.200	0.026 ± 0.005	0	0.011	3.8E+00	1.3E-01	1.3E-01	0.00
DY $\|Q\| = 2e$	200	65	0.175	1.250	0.200	0.026 ± 0.005	0	0.212	3.0E-01	6.0E-03	6.0E-03	0.00
DY $\|Q\| = 2e$	400	65	0.175	1.250	0.200	0.026 ± 0.005	0	0.410	2.3E-02	3.1E-03	3.1E-03	0.00
DY $\|Q\| = 2e$	600	65	0.175	1.250	0.200	0.026 ± 0.005	0	0.482	3.5E-03	2.6E-03	2.6E-03	0.00
DY $\|Q\| = 2e$	800	65	0.175	1.250	0.200	0.026 ± 0.005	0	0.489	8.0E-04	2.6E-03	2.6E-03	0.00
DY $\|Q\| = 2e$	1000	65	0.175	1.250	0.200	0.026 ± 0.005	0	0.452	2.4E-04	2.8E-03	2.8E-03	0.00
DY $\|Q\| = 2e$	1400	65	0.175	1.250	0.200	0.026 ± 0.005	0	0.313	2.7E-05	4.0E-03	4.0E-03	0.00
DY $\|Q\| = 2e$	1800	65	0.175	1.250	0.200	0.026 ± 0.005	0	0.184	4.0E-06	6.7E-03	6.7E-03	0.00
DY $\|Q\| = 2e$	2200	65	0.175	1.250	0.200	0.026 ± 0.005	0	0.120	1.0E-06	1.1E-02	1.1E-02	0.00
DY $\|Q\| = 2e$	2600	65	0.175	1.250	0.200	0.026 ± 0.005	0	0.069	0.0E+00	1.9E-02	1.9E-02	0.00

Table B.3: Tracker-only+MVA results using 2015 data with the relaxed final selection.

Model	Mass (GeV)	$p_T >$ (GeV)	$I_{as} >$	$1/\beta >$	MVA>	Bckg. Pred	Obs	SigEff	ThXsec (pb)	ExpXsec (pb)	ObsXsec (pb)	Signif
Gluino f=0.1	200	65	0.250	/	0.200	5.770 ± 1.200	4	0.106	3.4E+03	2.8E-02	2.1E-02	0.00
Gluino f=0.1	400	65	0.250	/	0.200	5.770 ± 1.200	4	0.178	9.5E+01	1.4E-02	1.2E-02	0.00
Gluino f=0.1	600	65	0.250	/	0.200	5.770 ± 1.200	4	0.212	9.1E+00	1.4E-02	1.0E-02	0.00
Gluino f=0.1	800	65	0.250	/	0.320	1.450 ± 0.304	0	0.235	1.5E+00	6.9E-03	5.1E-03	0.00
Gluino f=0.1	1000	65	0.250	/	0.440	0.455 ± 0.094	0	0.242	3.2E-01	5.0E-03	5.0E-03	0.00
Gluino f=0.1	1200	65	0.250	/	0.580	0.149 ± 0.031	0	0.234	8.4E-02	5.2E-03	5.2E-03	0.00
Gluino f=0.1	1400	65	0.250	/	0.680	0.065 ± 0.014	0	0.206	2.5E-02	5.9E-03	5.9E-03	0.00
Gluino f=0.1	1600	65	0.250	/	0.720	0.048 ± 0.010	0	0.177	8.0E-03	6.6E-03	6.6E-03	0.00
Gluino f=0.1	1800	65	0.250	/	0.720	0.048 ± 0.010	0	0.146	2.7E-03	8.4E-03	8.4E-03	0.00
Gluino f=0.1	2000	65	0.250	/	0.720	0.048 ± 0.010	0	0.120	9.7E-04	1.0E-02	1.0E-02	0.00
Gluino f=0.1	2200	65	0.250	/	0.720	0.048 ± 0.010	0	0.095	3.6E-04	1.3E-02	1.3E-02	0.00
Gluino f=0.1	2600	65	0.250	/	0.720	0.048 ± 0.010	0	0.061	5.0E-05	1.9E-02	1.9E-02	0.00
GluinoN f=0.1	100	65	0.250	/	0.200	5.770 ± 1.200	4	0.002	8.2E+04	1.8E+00	1.3E+00	0.00
GluinoN f=0.1	1000	65	0.250	/	0.440	0.455 ± 0.094	0	0.194	3.2E-01	6.1E-03	6.1E-03	0.00
GluinoN f=0.1	1200	65	0.250	/	0.520	0.234 ± 0.048	0	0.195	8.4E-02	6.2E-03	6.2E-03	0.00
GluinoN f=0.1	1400	65	0.250	/	0.720	0.048 ± 0.010	0	0.178	2.5E-02	6.9E-03	6.9E-03	0.00
GluinoN f=0.1	1600	65	0.250	/	0.720	0.048 ± 0.010	0	0.150	8.0E-03	8.0E-03	8.0E-03	0.00
GluinoN f=0.1	1800	65	0.250	/	0.720	0.048 ± 0.010	0	0.127	2.7E-03	9.5E-03	9.5E-03	0.00
GluinoN f=0.1	2000	65	0.250	/	0.720	0.048 ± 0.010	0	0.104	9.7E-04	1.2E-02	1.2E-02	0.00
GluinoN f=0.1	2600	65	0.250	/	0.720	0.048 ± 0.010	0	0.055	5.0E-05	2.2E-02	2.2E-02	0.00

Continued on next page

Table B.3 – continued from previous page

Model	Mass (GeV)	$p_T >$ (GeV)	$I_{as} >$	$1/\beta >$	MVA>	Bckg. Pred	Obs	SigEff	ThXsec (pb)	ExpXsec (pb)	ObsXsec (pb)	Signif
Gluino f=0.5	200	65	0.250	/	0.200	5.770 ± 1.200	4	0.054	3.4E+03	5.4E-02	4.3E-02	0.00
Gluino f=0.5	400	65	0.250	/	0.200	5.770 ± 1.200	4	0.101	9.5E+01	2.9E-02	2.2E-02	0.00
Gluino f=0.5	600	65	0.250	/	0.220	4.610 ± 0.965	3	0.123	9.1E+00	2.0E-02	1.6E-02	0.00
Gluino f=0.5	800	65	0.250	/	0.340	1.180 ± 0.245	0	0.137	1.5E+00	1.2E-02	8.1E-03	0.00
Gluino f=0.5	1000	65	0.250	/	0.480	0.328 ± 0.068	0	0.142	3.2E-01	8.4E-03	8.4E-03	0.00
Gluino f=0.5	1200	65	0.250	/	0.620	0.105 ± 0.022	0	0.136	8.4E-02	8.9E-03	8.9E-03	0.00
Gluino f=0.5	1400	65	0.250	/	0.720	0.048 ± 0.010	0	0.118	2.5E-02	1.0E-02	1.0E-02	0.00
Gluino f=0.5	1600	65	0.250	/	0.720	0.048 ± 0.010	0	0.103	8.0E-03	1.2E-02	1.2E-02	0.00
Gluino f=0.5	1800	65	0.250	/	0.720	0.048 ± 0.010	0	0.083	2.7E-03	1.4E-02	1.4E-02	0.00
Gluino f=0.5	2000	65	0.250	/	0.720	0.048 ± 0.010	0	0.068	9.7E-04	1.8E-02	1.8E-02	0.00
Gluino f=0.5	2200	65	0.250	/	0.720	0.048 ± 0.010	0	0.053	3.6E-04	2.3E-02	2.3E-02	0.00
Gluino f=0.5	2600	65	0.250	/	0.720	0.048 ± 0.010	0	0.035	5.0E-05	3.5E-02	3.5E-02	0.00
GluinoN f=0.5	100	65	0.250	/	0.200	5.770 ± 1.200	4	0.002	8.2E+04	2.0E+00	1.5E+00	0.00
GluinoN f=0.5	1000	65	0.250	/	0.440	0.455 ± 0.094	0	0.150	3.2E-01	7.9E-03	7.9E-03	0.00
GluinoN f=0.5	1200	65	0.250	/	0.580	0.149 ± 0.031	0	0.150	8.4E-02	8.0E-03	8.0E-03	0.00
GluinoN f=0.5	1400	65	0.250	/	0.720	0.048 ± 0.010	0	0.139	2.5E-02	8.7E-03	8.7E-03	0.00
GluinoN f=0.5	1600	65	0.250	/	0.720	0.048 ± 0.010	0	0.116	8.0E-03	1.1E-02	1.1E-02	0.00
GluinoN f=0.5	1800	65	0.250	/	0.720	0.048 ± 0.010	0	0.098	2.7E-03	1.2E-02	1.2E-02	0.00
GluinoN f=0.5	2000	65	0.250	/	0.720	0.048 ± 0.010	0	0.079	9.7E-04	1.6E-02	1.6E-02	0.00
GluinoN f=0.5	2600	65	0.250	/	0.720	0.048 ± 0.010	0	0.043	5.0E-05	2.9E-02	2.9E-02	0.00
Stop	100	65	0.250	/	0.200	5.120 ± 1.060	5	0.120	1.4E+03	2.2E-02	2.2E-02	0.00
Stop	200	65	0.250	/	0.200	5.120 ± 1.060	5	0.201	6.1E+01	1.3E-02	1.3E-02	0.00
Stop	400	65	0.250	/	0.220	4.000 ± 0.827	3	0.252	1.8E+00	9.6E-03	8.0E-03	0.00
Stop	600	65	0.250	/	0.400	0.781 ± 0.160	0	0.273	1.7E-01	6.3E-03	4.4E-03	0.00
Stop	800	65	0.250	/	0.640	0.160 ± 0.033	0	0.279	2.8E-02	4.4E-03	4.4E-03	0.00
Stop	1000	65	0.250	/	0.780	0.064 ± 0.013	0	0.270	6.0E-03	4.5E-03	4.5E-03	0.00
Stop	1200	65	0.250	/	0.820	0.049 ± 0.010	0	0.258	1.6E-03	4.7E-03	4.7E-03	0.00
Stop	1400	65	0.250	/	0.820	0.049 ± 0.010	0	0.236	4.5E-04	5.2E-03	5.2E-03	0.00
Stop	1600	65	0.250	/	0.820	0.049 ± 0.010	0	0.202	1.4E-04	6.0E-03	6.0E-03	0.00
Stop	1800	65	0.250	/	0.820	0.049 ± 0.010	0	0.172	4.6E-05	7.3E-03	7.3E-03	0.00
Stop	2000	65	0.250	/	0.820	0.049 ± 0.010	0	0.141	1.6E-05	8.6E-03	8.6E-03	0.00
Stop	2200	65	0.250	/	0.820	0.049 ± 0.010	0	0.115	6.0E-06	1.0E-02	1.0E-02	0.00
StopN	100	65	0.250	/	0.200	5.120 ± 1.060	5	0.012	1.4E+03	2.2E-01	2.2E-01	0.00
StopN	200	65	0.250	/	0.200	5.120 ± 1.060	5	0.047	6.1E+01	5.5E-02	5.5E-02	0.00
StopN	400	65	0.250	/	0.260	2.600 ± 0.535	0	0.126	1.8E+00	1.6E-02	9.6E-03	0.00
StopN	600	65	0.250	/	0.500	0.385 ± 0.079	0	0.172	1.7E-01	7.0E-03	7.0E-03	0.00
StopN	800	65	0.250	/	0.660	0.141 ± 0.029	0	0.193	2.8E-02	6.3E-03	6.3E-03	0.00
StopN	1000	65	0.250	/	0.820	0.049 ± 0.010	0	0.200	6.0E-03	6.0E-03	6.0E-03	0.00
StopN	1200	65	0.250	/	0.820	0.049 ± 0.010	0	0.193	1.6E-03	6.4E-03	6.4E-03	0.00
StopN	1600	65	0.250	/	0.820	0.049 ± 0.010	0	0.157	1.4E-04	7.9E-03	7.9E-03	0.00
StopN	1800	65	0.250	/	0.820	0.049 ± 0.010	0	0.130	4.6E-05	9.6E-03	9.6E-03	0.00
StopN	2000	65	0.250	/	0.820	0.049 ± 0.010	0	0.108	1.6E-05	1.1E-02	1.1E-02	0.00
StopN	2200	65	0.250	/	0.820	0.049 ± 0.010	0	0.090	6.0E-06	1.3E-02	1.3E-02	0.00
GMSB stau	200	65	0.250	/	0.240	16.400 ± 3.360	17	0.297	2.8E-01	1.6E-02	1.6E-02	0.12
GMSB stau	247	65	0.250	/	0.340	6.980 ± 1.440	7	0.379	8.8E-02	8.0E-03	8.0E-03	0.00
GMSB stau	308	65	0.250	/	0.480	2.910 ± 0.596	1	0.450	2.5E-02	5.1E-03	3.4E-03	0.00
GMSB stau	432	65	0.250	/	0.760	0.809 ± 0.165	0	0.588	3.9E-03	2.9E-03	2.1E-03	0.00
GMSB stau	494	65	0.250	/	0.860	0.527 ± 0.108	0	0.615	1.9E-03	2.0E-03	2.0E-03	0.00
GMSB stau	651	65	0.250	/	0.980	0.302 ± 0.062	0	0.688	4.1E-04	1.8E-03	1.8E-03	0.00
GMSB stau	745	65	0.250	/	0.980	0.302 ± 0.062	0	0.705	1.9E-04	1.7E-03	1.7E-03	0.00
GMSB stau	871	65	0.250	/	0.980	0.302 ± 0.062	0	0.722	6.9E-05	1.7E-03	1.7E-03	0.00
GMSB stau	1029	65	0.250	/	0.980	0.302 ± 0.062	0	0.730	2.2E-05	1.7E-03	1.7E-03	0.00
GMSB stau	1218	65	0.250	/	0.980	0.302 ± 0.062	0	0.723	6.0E-06	1.7E-03	1.7E-03	0.00
GMSB stau	1409	65	0.250	/	0.980	0.302 ± 0.062	0	0.675	2.0E-06	1.8E-03	1.8E-03	0.00
GMSB stau	1599	65	0.250	/	0.980	0.302 ± 0.062	0	0.567	1.0E-06	2.0E-03	2.0E-03	0.00
PP stau	156	65	0.250	/	0.360	12.500 ± 2.540	15	0.207	2.0E-02	2.3E-02	2.6E-02	0.55
PP stau	200	65	0.250	/	0.480	6.750 ± 1.370	7	0.245	8.0E-03	1.2E-02	1.3E-02	0.09
PP stau	247	65	0.250	/	0.620	3.640 ± 0.737	2	0.276	3.7E-03	8.7E-03	6.7E-03	0.00
PP stau	308	65	0.250	/	0.820	1.590 ± 0.322	0	0.324	1.5E-03	5.4E-03	4.2E-03	0.00
PP stau	494	65	0.250	/	0.980	0.791 ± 0.161	0	0.416	1.9E-04	3.7E-03	2.9E-03	0.00

Continued on next page

Table B.3 – continued from previous page

Model	Mass (GeV)	$p_T >$ (GeV)	$I_{as} >$	$1/\beta >$	MVA>	Bckg. Pred	Obs	SigEff	ThXsec (pb)	ExpXsec (pb)	ObsXsec (pb)	Signif
PP stau	557	65	0.250	/	0.980	0.791 ± 0.161	0	0.454	1.1E-04	3.9E-03	2.7E-03	0.00
PP stau	651	65	0.250	/	0.980	0.791 ± 0.161	0	0.499	4.9E-05	3.1E-03	2.4E-03	0.00
PP stau	745	65	0.250	/	0.980	0.791 ± 0.161	0	0.526	2.4E-05	3.3E-03	2.3E-03	0.00
PP stau	871	65	0.250	/	0.980	0.791 ± 0.161	0	0.563	1.0E-05	2.5E-03	2.1E-03	0.00
PP stau	1029	65	0.250	/	0.980	0.791 ± 0.161	0	0.603	4.0E-06	2.9E-03	2.0E-03	0.00
PP stau	1218	65	0.250	/	0.980	0.791 ± 0.161	0	0.609	1.0E-06	2.8E-03	2.0E-03	0.00
PP stau	1409	65	0.250	/	0.980	0.791 ± 0.161	0	0.572	0.0E+00	2.6E-03	2.1E-03	0.00
PP stau	1599	65	0.250	/	0.920	1.040 ± 0.210	0	0.509	0.0E+00	3.3E-03	2.4E-03	0.00
DY $\|Q\| = 1e$	100	65	0.250	/	0.200	12.200 ± 2.570	12	0.101	1.2E+00	4.2E-02	4.2E-02	0.00
DY $\|Q\| = 1e$	200	65	0.250	/	0.200	12.200 ± 2.570	12	0.311	1.1E-01	1.4E-02	1.4E-02	0.00
DY $\|Q\| = 1e$	400	65	0.250	/	0.480	1.150 ± 0.234	0	0.426	7.3E-03	4.2E-03	3.0E-03	0.00
DY $\|Q\| = 1e$	600	65	0.250	/	0.780	0.264 ± 0.054	0	0.473	1.2E-03	2.7E-03	2.7E-03	0.00
DY $\|Q\| = 1e$	800	65	0.250	/	0.980	0.093 ± 0.019	0	0.499	2.6E-04	2.5E-03	2.5E-03	0.00
DY $\|Q\| = 1e$	1000	65	0.250	/	0.980	0.093 ± 0.019	0	0.502	7.6E-05	2.6E-03	2.6E-03	0.00
DY $\|Q\| = 1e$	1400	65	0.250	/	0.980	0.093 ± 0.019	0	0.433	9.0E-06	3.0E-03	3.0E-03	0.00
DY $\|Q\| = 1e$	1800	65	0.250	/	0.980	0.093 ± 0.019	0	0.327	1.0E-06	3.9E-03	3.9E-03	0.00
DY $\|Q\| = 1e$	2200	65	0.250	/	0.980	0.093 ± 0.019	0	0.210	0.0E+00	6.0E-03	6.0E-03	0.00
DY $\|Q\| = 1e$	2600	65	0.250	/	0.980	0.093 ± 0.019	0	0.126	0.0E+00	1.0E-02	1.0E-02	0.00
DY $\|Q\| = 2e$	100	65	0.250	/	0.200	4.900 ± 1.020	5	0.259	3.8E+00	1.1E-02	1.1E-02	0.04
DY $\|Q\| = 2e$	200	65	0.250	/	0.380	0.590 ± 0.122	0	0.585	3.0E-01	2.2E-03	2.1E-03	0.00
DY $\|Q\| = 2e$	400	65	0.250	/	0.640	0.055 ± 0.012	0	0.699	2.3E-02	1.8E-03	1.8E-03	0.00
DY $\|Q\| = 2e$	600	65	0.250	/	0.640	0.055 ± 0.012	0	0.676	3.5E-03	1.8E-03	1.8E-03	0.00
DY $\|Q\| = 2e$	800	65	0.250	/	0.640	0.055 ± 0.012	0	0.614	8.0E-04	2.0E-03	2.0E-03	0.00
DY $\|Q\| = 2e$	1000	65	0.250	/	0.640	0.055 ± 0.012	0	0.544	2.4E-04	2.3E-03	2.3E-03	0.00
DY $\|Q\| = 2e$	1400	65	0.250	/	0.640	0.055 ± 0.012	0	0.364	2.7E-05	3.4E-03	3.4E-03	0.00
DY $\|Q\| = 2e$	1800	65	0.250	/	0.640	0.055 ± 0.012	0	0.217	4.0E-06	5.8E-03	5.8E-03	0.00
DY $\|Q\| = 2e$	2200	65	0.250	/	0.640	0.055 ± 0.012	0	0.154	1.0E-06	8.2E-03	8.2E-03	0.00
DY $\|Q\| = 2e$	2600	65	0.250	/	0.640	0.055 ± 0.012	0	0.101	0.0E+00	1.3E-02	1.3E-02	0.00

Table B.4: Tracker+TOF+MVA results using 2015 data with the relaxed final selection.

Model	Mass (GeV)	$p_T >$ (GeV)	$I_{as} >$	$1/\beta >$	MVA>	Bckg. Pred	Obs	SigEff	ThXsec (pb)	ExpXsec (pb)	ObsXsec (pb)	Signif
Gluino f=0.1	200	65	0.150	1.250	0.200	0.085 ± 0.017	0	0.092	3.4E+03	1.3E-02	1.3E-02	0.00
Gluino f=0.1	400	65	0.150	1.250	0.200	0.085 ± 0.017	0	0.140	9.5E+01	8.8E-03	8.8E-03	0.00
Gluino f=0.1	600	65	0.150	1.250	0.200	0.085 ± 0.017	0	0.170	9.1E+00	7.3E-03	7.3E-03	0.00
Gluino f=0.1	800	65	0.150	1.250	0.220	0.060 ± 0.012	0	0.190	1.5E+00	6.6E-03	6.6E-03	0.00
Gluino f=0.1	1000	65	0.150	1.250	0.220	0.060 ± 0.012	0	0.197	3.2E-01	5.9E-03	5.9E-03	0.00
Gluino f=0.1	1200	65	0.150	1.250	0.220	0.060 ± 0.012	0	0.191	8.4E-02	6.3E-03	6.3E-03	0.00
Gluino f=0.1	1400	65	0.150	1.250	0.220	0.060 ± 0.012	0	0.164	2.5E-02	7.4E-03	7.4E-03	0.00
Gluino f=0.1	1600	65	0.150	1.250	0.220	0.060 ± 0.012	0	0.139	8.0E-03	8.8E-03	8.8E-03	0.00
Gluino f=0.1	1800	65	0.150	1.250	0.220	0.060 ± 0.012	0	0.115	2.7E-03	1.0E-02	1.0E-02	0.00
Gluino f=0.1	2000	65	0.150	1.250	0.220	0.060 ± 0.012	0	0.093	9.7E-04	1.3E-02	1.3E-02	0.00
Gluino f=0.1	2200	65	0.150	1.250	0.220	0.060 ± 0.012	0	0.073	3.6E-04	1.7E-02	1.7E-02	0.00
Gluino f=0.1	2600	65	0.150	1.250	0.220	0.060 ± 0.012	0	0.046	5.0E-05	2.6E-02	2.6E-02	0.00
Gluino f=0.5	200	65	0.150	1.250	0.200	0.085 ± 0.017	0	0.048	3.4E+03	2.6E-02	2.6E-02	0.00
Gluino f=0.5	400	65	0.150	1.250	0.200	0.085 ± 0.017	0	0.078	9.5E+01	1.5E-02	1.5E-02	0.00
Gluino f=0.5	600	65	0.150	1.250	0.200	0.085 ± 0.017	0	0.097	9.1E+00	1.3E-02	1.3E-02	0.00
Gluino f=0.5	800	65	0.150	1.250	0.220	0.060 ± 0.012	0	0.109	1.5E+00	1.2E-02	1.2E-02	0.00
Gluino f=0.5	1000	65	0.150	1.250	0.220	0.060 ± 0.012	0	0.114	3.2E-01	1.1E-02	1.1E-02	0.00
Gluino f=0.5	1200	65	0.150	1.250	0.220	0.060 ± 0.012	0	0.109	8.4E-02	1.1E-02	1.1E-02	0.00
Gluino f=0.5	1400	65	0.150	1.250	0.220	0.060 ± 0.012	0	0.093	2.5E-02	1.3E-02	1.3E-02	0.00
Gluino f=0.5	1600	65	0.150	1.250	0.220	0.060 ± 0.012	0	0.079	8.0E-03	1.5E-02	1.5E-02	0.00
Gluino f=0.5	1800	65	0.150	1.250	0.220	0.060 ± 0.012	0	0.064	2.7E-03	1.9E-02	1.9E-02	0.00
Gluino f=0.5	2000	65	0.150	1.250	0.220	0.060 ± 0.012	0	0.052	9.7E-04	2.4E-02	2.4E-02	0.00
Gluino f=0.5	2200	65	0.150	1.250	0.220	0.060 ± 0.012	0	0.040	3.6E-04	3.0E-02	3.0E-02	0.00
Gluino f=0.5	2600	65	0.150	1.250	0.220	0.060 ± 0.012	0	0.026	5.0E-05	4.8E-02	4.8E-02	0.00

Continued on next page

Table B.4 – continued from previous page

Model	Mass (GeV)	$p_T >$ (GeV)	$I_{as} >$	$1/\beta >$	MVA>	Bckg. Pred	Obs	SigEff	ThXsec (pb)	ExpXsec (pb)	ObsXsec (pb)	Signif
Stop	100	65	0.150	1.250	0.200	0.023 ± 0.005	0	0.030	1.4E+03	4.1E-02	4.1E-02	0.00
Stop	200	65	0.150	1.250	0.200	0.023 ± 0.005	0	0.069	6.1E+01	1.8E-02	1.8E-02	0.00
Stop	400	65	0.150	1.250	0.200	0.023 ± 0.005	0	0.157	1.8E+00	7.6E-03	7.6E-03	0.00
Stop	600	65	0.150	1.250	0.200	0.023 ± 0.005	0	0.181	1.7E-01	6.6E-03	6.6E-03	0.00
Stop	800	65	0.150	1.250	0.200	0.023 ± 0.005	0	0.194	2.8E-02	6.2E-03	6.2E-03	0.00
Stop	1000	65	0.150	1.250	0.200	0.023 ± 0.005	0	0.194	6.0E-03	6.2E-03	6.2E-03	0.00
Stop	1200	65	0.150	1.250	0.200	0.023 ± 0.005	0	0.186	1.6E-03	6.5E-03	6.5E-03	0.00
Stop	1400	65	0.150	1.250	0.200	0.023 ± 0.005	0	0.164	4.5E-04	7.3E-03	7.3E-03	0.00
Stop	1600	65	0.150	1.250	0.200	0.023 ± 0.005	0	0.139	1.4E-04	8.7E-03	8.7E-03	0.00
Stop	1800	65	0.150	1.250	0.200	0.023 ± 0.005	0	0.116	4.6E-05	1.1E-02	1.1E-02	0.00
Stop	2000	65	0.150	1.250	0.200	0.023 ± 0.005	0	0.095	1.6E-05	1.3E-02	1.3E-02	0.00
Stop	2200	65	0.150	1.250	0.200	0.023 ± 0.005	0	0.076	6.0E-06	1.6E-02	1.6E-02	0.00
GMSB stau	200	65	0.150	1.250	0.200	0.314 ± 0.063	0	0.297	2.8E-01	4.1E-03	4.1E-03	0.00
GMSB stau	247	65	0.150	1.250	0.200	0.314 ± 0.063	0	0.372	8.8E-02	3.2E-03	3.2E-03	0.00
GMSB stau	308	65	0.150	1.250	0.300	0.102 ± 0.021	0	0.439	2.5E-02	2.7E-03	2.7E-03	0.00
GMSB stau	432	65	0.150	1.250	0.360	0.058 ± 0.012	0	0.571	3.9E-03	2.2E-03	2.2E-03	0.00
GMSB stau	494	65	0.150	1.250	0.360	0.058 ± 0.012	0	0.603	1.9E-03	2.0E-03	2.0E-03	0.00
GMSB stau	651	65	0.150	1.250	0.360	0.058 ± 0.012	0	0.674	4.1E-04	1.8E-03	1.8E-03	0.00
GMSB stau	745	65	0.150	1.250	0.360	0.058 ± 0.012	0	0.698	1.9E-04	1.8E-03	1.8E-03	0.00
GMSB stau	871	65	0.150	1.250	0.360	0.058 ± 0.012	0	0.712	6.9E-05	1.7E-03	1.7E-03	0.00
GMSB stau	1029	65	0.150	1.250	0.360	0.058 ± 0.012	0	0.722	2.2E-05	1.7E-03	1.7E-03	0.00
GMSB stau	1218	65	0.150	1.250	0.360	0.058 ± 0.012	0	0.709	6.0E-06	1.7E-03	1.7E-03	0.00
GMSB stau	1409	65	0.150	1.250	0.360	0.058 ± 0.012	0	0.662	2.0E-06	1.9E-03	1.9E-03	0.00
GMSB stau	1599	65	0.150	1.250	0.360	0.058 ± 0.012	0	0.559	1.0E-06	2.2E-03	2.2E-03	0.00
PP stau	156	65	0.150	1.250	0.200	0.297 ± 0.060	0	0.216	2.0E-02	5.7E-03	5.7E-03	0.00
PP stau	200	65	0.150	1.250	0.280	0.143 ± 0.029	0	0.249	8.0E-03	4.9E-03	4.9E-03	0.00
PP stau	247	65	0.150	1.250	0.400	0.065 ± 0.013	0	0.278	3.7E-03	4.4E-03	4.4E-03	0.00
PP stau	308	65	0.150	1.250	0.440	0.052 ± 0.010	0	0.325	1.5E-03	3.7E-03	3.7E-03	0.00
PP stau	494	65	0.150	1.250	0.440	0.052 ± 0.010	0	0.428	1.9E-04	2.9E-03	2.9E-03	0.00
PP stau	557	65	0.150	1.250	0.440	0.052 ± 0.010	0	0.459	1.1E-04	2.7E-03	2.7E-03	0.00
PP stau	651	65	0.150	1.250	0.440	0.052 ± 0.010	0	0.509	4.9E-05	2.4E-03	2.4E-03	0.00
PP stau	745	65	0.150	1.250	0.440	0.052 ± 0.010	0	0.530	2.4E-05	2.3E-03	2.3E-03	0.00
PP stau	871	65	0.150	1.250	0.440	0.052 ± 0.010	0	0.567	1.0E-05	2.2E-03	2.2E-03	0.00
PP stau	1029	65	0.150	1.250	0.440	0.052 ± 0.010	0	0.605	4.0E-06	2.0E-03	2.0E-03	0.00
PP stau	1218	65	0.150	1.250	0.440	0.052 ± 0.010	0	0.612	1.0E-06	2.0E-03	2.0E-03	0.00
PP stau	1409	65	0.175	1.250	0.540	0.053 ± 0.011	0	0.569	0.0E+00	2.2E-03	2.2E-03	0.00
PP stau	1599	65	0.150	1.250	0.440	0.052 ± 0.010	0	0.514	0.0E+00	2.4E-03	2.4E-03	0.00
DY $\|Q\| = 1e$	100	65	0.150	1.250	0.200	0.143 ± 0.029	0	0.110	1.2E+00	1.3E-02	1.3E-02	0.00
DY $\|Q\| = 1e$	200	65	0.150	1.250	0.200	0.143 ± 0.029	0	0.309	1.1E-01	4.0E-03	4.0E-03	0.00
DY $\|Q\| = 1e$	400	65	0.150	1.250	0.260	0.058 ± 0.012	0	0.427	7.3E-03	3.0E-03	3.0E-03	0.00
DY $\|Q\| = 1e$	600	65	0.150	1.250	0.260	0.058 ± 0.012	0	0.471	1.2E-03	2.7E-03	2.7E-03	0.00
DY $\|Q\| = 1e$	800	65	0.150	1.250	0.260	0.058 ± 0.012	0	0.494	2.6E-04	2.6E-03	2.6E-03	0.00
DY $\|Q\| = 1e$	1000	65	0.150	1.250	0.260	0.058 ± 0.012	0	0.493	7.6E-05	2.6E-03	2.6E-03	0.00
DY $\|Q\| = 1e$	1400	65	0.150	1.250	0.260	0.058 ± 0.012	0	0.425	9.0E-06	3.0E-03	3.0E-03	0.00
DY $\|Q\| = 1e$	1800	65	0.150	1.250	0.260	0.058 ± 0.012	0	0.320	1.0E-06	4.0E-03	4.0E-03	0.00
DY $\|Q\| = 1e$	2200	65	0.150	1.250	0.260	0.058 ± 0.012	0	0.201	0.0E+00	6.2E-03	6.2E-03	0.00
DY $\|Q\| = 1e$	2600	65	0.150	1.250	0.260	0.058 ± 0.012	0	0.118	0.0E+00	1.1E-02	1.1E-02	0.00
DY $\|Q\| = 2e$	100	65	0.150	1.250	0.200	0.043 ± 0.009	0	0.011	3.8E+00	1.3E-01	1.3E-01	0.00
DY $\|Q\| = 2e$	200	65	0.150	1.250	0.200	0.043 ± 0.009	0	0.212	3.0E-01	6.1E-03	6.1E-03	0.00
DY $\|Q\| = 2e$	400	65	0.150	1.250	0.200	0.043 ± 0.009	0	0.410	2.3E-02	3.3E-03	3.3E-03	0.00
DY $\|Q\| = 2e$	600	65	0.150	1.250	0.200	0.043 ± 0.009	0	0.482	3.5E-03	2.6E-03	2.6E-03	0.00
DY $\|Q\| = 2e$	800	65	0.150	1.250	0.200	0.043 ± 0.009	0	0.489	8.0E-04	2.6E-03	2.6E-03	0.00
DY $\|Q\| = 2e$	1000	65	0.150	1.250	0.200	0.043 ± 0.009	0	0.452	2.4E-04	2.8E-03	2.8E-03	0.00
DY $\|Q\| = 2e$	1400	65	0.150	1.250	0.200	0.043 ± 0.009	0	0.313	2.7E-05	4.0E-03	4.0E-03	0.00
DY $\|Q\| = 2e$	1800	65	0.150	1.250	0.200	0.043 ± 0.009	0	0.184	4.0E-06	6.8E-03	6.8E-03	0.00
DY $\|Q\| = 2e$	2200	65	0.150	1.250	0.200	0.043 ± 0.009	0	0.120	1.0E-06	1.1E-02	1.1E-02	0.00
DY $\|Q\| = 2e$	2600	65	0.150	1.250	0.200	0.043 ± 0.009	0	0.069	0.0E+00	1.8E-02	1.8E-02	0.00

Table B.5: Tracker-only+MVA results using 2016 data with the same final selection as the standard analysis.

Model	Mass (GeV)	pT> (GeV)	I>	TOF>	MVA>	Bckg. Pred	Obs	SigEff	ThXsec (pb)	ExpXsec (pb)	ObsXsec (pb)	Signif
Gluino f=0.1	200	65	0.300	/	0.200	6.440 ± 1.350	7	0.091	3.4E+03	6.3E-03	7.1E-03	0.19
Gluino f=0.1	400	65	0.300	/	0.200	6.440 ± 1.350	7	0.152	9.5E+01	3.6E-03	3.9E-03	0.19
Gluino f=0.1	600	65	0.300	/	0.200	6.440 ± 1.350	7	0.189	9.1E+00	2.8E-03	3.2E-03	0.19
Gluino f=0.1	800	65	0.300	/	0.200	6.440 ± 1.350	7	0.205	1.5E+00	2.7E-03	3.0E-03	0.19
Gluino f=0.1	1000	65	0.300	/	0.260	2.350 ± 0.484	0	0.215	3.2E-01	1.7E-03	9.6E-04	0.00
Gluino f=0.1	1200	65	0.300	/	0.320	1.080 ± 0.222	0	0.203	8.4E-02	1.6E-03	1.1E-03	0.00
Gluino f=0.1	1400	65	0.300	/	0.440	0.303 ± 0.062	0	0.184	2.5E-02	1.3E-03	1.3E-03	0.00
Gluino f=0.1	1600	65	0.300	/	0.580	0.090 ± 0.019	0	0.154	8.0E-03	1.5E-03	1.5E-03	0.00
Gluino f=0.1	1800	65	0.300	/	0.680	0.036 ± 0.007	0	0.128	2.7E-03	1.9E-03	1.9E-03	0.00
Gluino f=0.1	2000	65	0.300	/	0.800	0.011 ± 0.002	0	0.107	9.7E-04	2.2E-03	2.2E-03	0.00
Gluino f=0.1	2200	65	0.300	/	0.840	0.007 ± 0.002	0	0.085	3.6E-04	2.8E-03	2.8E-03	0.00
Gluino f=0.1	2600	65	0.300	/	0.860	0.005 ± 0.001	0	0.053	5.0E-05	4.5E-03	4.5E-03	0.00
GluinoN f=0.1	100	65	0.300	/	0.200	6.440 ± 1.350	7	0.002	8.2E+04	3.7E-01	4.0E-01	0.19
GluinoN f=0.1	1000	65	0.300	/	0.260	2.350 ± 0.484	0	0.183	3.2E-01	2.0E-03	1.3E-03	0.00
GluinoN f=0.1	1200	65	0.300	/	0.300	1.370 ± 0.281	0	0.185	8.4E-02	1.7E-03	1.3E-03	0.00
GluinoN f=0.1	1400	65	0.300	/	0.420	0.365 ± 0.075	0	0.167	2.5E-02	1.4E-03	1.4E-03	0.00
GluinoN f=0.1	1600	65	0.300	/	0.520	0.146 ± 0.030	0	0.145	8.0E-03	1.6E-03	1.6E-03	0.00
GluinoN f=0.1	1800	65	0.300	/	0.680	0.036 ± 0.007	0	0.121	2.7E-03	1.9E-03	1.9E-03	0.00
GluinoN f=0.1	2000	65	0.300	/	0.820	0.009 ± 0.002	0	0.098	9.7E-04	2.4E-03	2.4E-03	0.00
GluinoN f=0.1	2600	65	0.300	/	0.860	0.005 ± 0.001	0	0.053	5.0E-05	4.4E-03	4.4E-03	0.00
Gluino f=0.5	200	65	0.300	/	0.200	6.440 ± 1.350	7	0.046	3.4E+03	1.3E-02	1.4E-02	0.19
Gluino f=0.5	400	65	0.300	/	0.200	6.440 ± 1.350	7	0.085	9.5E+01	7.0E-03	7.3E-03	0.19
Gluino f=0.5	600	65	0.300	/	0.200	6.440 ± 1.350	7	0.109	9.1E+00	5.3E-03	5.6E-03	0.19
Gluino f=0.5	800	65	0.300	/	0.200	6.440 ± 1.350	7	0.120	1.5E+00	4.4E-03	5.1E-03	0.19
Gluino f=0.5	1000	65	0.300	/	0.260	2.350 ± 0.484	0	0.125	3.2E-01	3.0E-03	1.9E-03	0.00
Gluino f=0.5	1200	65	0.300	/	0.340	0.854 ± 0.175	0	0.118	8.4E-02	2.9E-03	2.0E-03	0.00
Gluino f=0.5	1400	65	0.300	/	0.500	0.173 ± 0.035	0	0.106	2.5E-02	2.2E-03	2.2E-03	0.00
Gluino f=0.5	1600	65	0.300	/	0.580	0.090 ± 0.019	0	0.089	8.0E-03	2.7E-03	2.7E-03	0.00
Gluino f=0.5	1800	65	0.300	/	0.720	0.025 ± 0.005	0	0.073	2.7E-03	3.2E-03	3.2E-03	0.00
Gluino f=0.5	2000	65	0.300	/	0.840	0.007 ± 0.002	0	0.059	9.7E-04	4.1E-03	4.1E-03	0.00
Gluino f=0.5	2200	65	0.300	/	0.840	0.007 ± 0.002	0	0.048	3.6E-04	5.0E-03	5.0E-03	0.00
Gluino f=0.5	2600	65	0.300	/	0.860	0.005 ± 0.001	0	0.028	5.0E-05	8.3E-03	8.3E-03	0.00
GluinoN f=0.5	100	65	0.300	/	0.200	6.440 ± 1.350	7	0.001	8.2E+04	5.2E-01	5.3E-01	0.19
GluinoN f=0.5	1000	65	0.300	/	0.260	2.350 ± 0.484	0	0.138	3.2E-01	2.6E-03	1.6E-03	0.00
GluinoN f=0.5	1200	65	0.300	/	0.340	0.854 ± 0.175	0	0.140	8.4E-02	2.3E-03	1.7E-03	0.00
GluinoN f=0.5	1400	65	0.300	/	0.440	0.303 ± 0.062	0	0.127	2.5E-02	1.8E-03	1.8E-03	0.00
GluinoN f=0.5	1600	65	0.300	/	0.560	0.102 ± 0.021	0	0.109	8.0E-03	2.1E-03	2.1E-03	0.00
GluinoN f=0.5	1800	65	0.300	/	0.760	0.018 ± 0.004	0	0.091	2.7E-03	2.6E-03	2.6E-03	0.00
GluinoN f=0.5	2000	65	0.300	/	0.780	0.014 ± 0.003	0	0.072	9.7E-04	3.3E-03	3.3E-03	0.00
GluinoN f=0.5	2600	65	0.300	/	0.860	0.005 ± 0.001	0	0.039	5.0E-05	6.0E-03	6.0E-03	0.00
Stop	100	65	0.300	/	0.200	4.660 ± 0.950	6	0.107	1.4E+03	4.9E-03	5.8E-03	0.55
Stop	200	65	0.300	/	0.200	4.660 ± 0.950	6	0.178	6.1E+01	2.9E-03	3.5E-03	0.55
Stop	400	65	0.300	/	0.200	4.660 ± 0.950	6	0.217	1.8E+00	2.3E-03	2.9E-03	0.55
Stop	600	65	0.300	/	0.220	3.500 ± 0.713	2	0.243	1.7E-01	1.7E-03	1.3E-03	0.00
Stop	800	65	0.300	/	0.360	0.754 ± 0.153	0	0.241	2.8E-02	1.4E-03	9.7E-04	0.00
Stop	1000	65	0.300	/	0.520	0.211 ± 0.043	0	0.237	6.0E-03	9.9E-04	9.9E-04	0.00
Stop	1200	65	0.300	/	0.700	0.061 ± 0.013	0	0.224	1.6E-03	1.1E-03	1.1E-03	0.00
Stop	1400	65	0.300	/	0.840	0.022 ± 0.004	0	0.204	4.5E-04	1.2E-03	1.2E-03	0.00
Stop	1600	65	0.300	/	0.860	0.018 ± 0.004	0	0.178	1.4E-04	1.3E-03	1.3E-03	0.00
Stop	1800	65	0.300	/	0.900	0.012 ± 0.003	0	0.155	4.6E-05	1.5E-03	1.5E-03	0.00
Stop	2000	65	0.300	/	0.940	0.007 ± 0.002	0	0.117	1.6E-05	2.0E-03	2.0E-03	0.00
Stop	2200	65	0.300	/	0.940	0.007 ± 0.002	0	0.091	6.0E-06	2.6E-03	2.6E-03	0.00
StopN	100	65	0.300	/	0.200	4.660 ± 0.950	6	0.011	1.4E+03	4.5E-02	5.9E-02	0.55
StopN	200	65	0.300	/	0.200	4.660 ± 0.950	6	0.046	6.1E+01	1.1E-02	1.4E-02	0.55
StopN	400	65	0.300	/	0.200	4.660 ± 0.950	6	0.116	1.8E+00	4.3E-03	5.1E-03	0.55
StopN	600	65	0.300	/	0.240	2.640 ± 0.538	2	0.163	1.7E-01	2.1E-03	2.2E-03	0.00

Continued on next page

Table B.5 – continued from previous page

Model	Mass (GeV)	pT> (GeV)	I>	TOF>	MVA>	Bckg. Pred	Obs	Seff	ThXsec (pb)	ExpXsec (pb)	ObsXsec (pb)	Signif
StopN	800	65	0.300	/	0.340	0.898 ± 0.183	0	0.189	2.8E-02	1.7E-03	1.2E-03	0.00
StopN	1000	65	0.300	/	0.500	0.244 ± 0.050	0	0.192	6.0E-03	1.2E-03	1.2E-03	0.00
StopN	1200	65	0.300	/	0.700	0.061 ± 0.013	0	0.187	1.6E-03	1.3E-03	1.3E-03	0.00
StopN	1600	65	0.300	/	0.860	0.018 ± 0.004	0	0.146	1.4E-04	1.6E-03	1.6E-03	0.00
StopN	1800	65	0.300	/	0.900	0.012 ± 0.003	0	0.126	4.6E-05	1.9E-03	1.9E-03	0.00
StopN	2000	65	0.300	/	0.940	0.007 ± 0.002	0	0.091	1.6E-05	2.6E-03	2.6E-03	0.00
StopN	2200	65	0.300	/	0.940	0.007 ± 0.002	0	0.075	6.0E-06	3.2E-03	3.2E-03	0.00
GMSB stau	200	65	0.300	/	0.200	45.300 ± 9.280	60	0.266	2.8E-01	6.3E-03	1.1E-02	1.23
GMSB stau	247	65	0.300	/	0.320	9.240 ± 1.910	17	0.349	8.8E-02	1.9E-03	4.0E-03	1.90
GMSB stau	308	65	0.300	/	0.380	5.250 ± 1.100	5	0.421	2.5E-02	1.2E-03	1.2E-03	0.00
GMSB stau	432	65	0.300	/	0.600	1.130 ± 0.229	0	0.538	3.9E-03	6.1E-04	4.4E-04	0.00
GMSB stau	494	65	0.300	/	0.740	0.587 ± 0.119	0	0.576	1.9E-03	3.8E-04	3.8E-04	0.00
GMSB stau	651	65	0.300	/	0.880	0.313 ± 0.064	0	0.639	4.1E-04	3.6E-04	3.6E-04	0.00
GMSB stau	745	65	0.300	/	0.960	0.219 ± 0.045	0	0.660	1.9E-04	3.6E-04	3.6E-04	0.00
GMSB stau	871	65	0.300	/	0.980	0.200 ± 0.041	0	0.665	6.9E-05	3.6E-04	3.6E-04	0.00
GMSB stau	1029	65	0.300	/	0.980	0.200 ± 0.041	0	0.674	2.2E-05	3.4E-04	3.4E-04	0.00
GMSB stau	1218	65	0.300	/	0.980	0.200 ± 0.041	0	0.652	6.0E-06	3.6E-04	3.6E-04	0.00
GMSB stau	1409	65	0.300	/	0.980	0.200 ± 0.041	0	0.609	2.0E-06	3.7E-04	3.7E-04	0.00
GMSB stau	1599	65	0.300	/	0.980	0.200 ± 0.041	0	0.489	1.0E-06	4.9E-04	4.9E-04	0.00
PP stau	156	65	0.300	/	0.340	15.300 ± 3.100	25	0.180	2.0E-02	4.9E-03	1.0E-02	1.76
PP stau	200	65	0.300	/	0.460	6.900 ± 1.390	8	0.210	8.0E-03	2.9E-03	3.4E-03	0.37
PP stau	247	65	0.300	/	0.580	3.720 ± 0.751	3	0.240	3.7E-03	1.9E-03	1.7E-03	0.00
PP stau	308	65	0.300	/	0.760	1.610 ± 0.325	0	0.274	1.5E-03	1.2E-03	8.6E-04	0.00
PP stau	494	65	0.300	/	0.980	0.622 ± 0.126	0	0.367	1.9E-04	6.6E-04	6.5E-04	0.00
PP stau	557	65	0.300	/	0.980	0.622 ± 0.126	0	0.390	1.1E-04	6.7E-04	6.0E-04	0.00
PP stau	651	65	0.300	/	0.980	0.622 ± 0.126	0	0.424	4.9E-05	5.4E-04	5.4E-04	0.00
PP stau	745	65	0.300	/	0.980	0.622 ± 0.126	0	0.465	2.4E-05	6.0E-04	5.0E-04	0.00
PP stau	871	65	0.300	/	0.980	0.622 ± 0.126	0	0.472	1.0E-05	5.1E-04	4.9E-04	0.00
PP stau	1029	65	0.300	/	0.980	0.622 ± 0.126	0	0.483	4.0E-06	4.8E-04	4.8E-04	0.00
PP stau	1218	65	0.300	/	0.980	0.622 ± 0.126	0	0.496	1.0E-06	6.0E-04	4.7E-04	0.00
PP stau	1409	65	0.300	/	0.980	0.622 ± 0.126	0	0.472	0.0E+00	5.9E-04	5.0E-04	0.00
PP stau	1599	65	0.300	/	0.920	0.807 ± 0.163	0	0.422	0.0E+00	8.0E-04	5.6E-04	0.00
DY $\|Q\| = 1e$	100	65	0.300	/	0.200	20.900 ± 4.400	34	0.089	1.2E+00	1.3E-02	2.8E-02	1.86
DY $\|Q\| = 1e$	200	65	0.300	/	0.200	20.900 ± 4.400	34	0.262	1.1E-01	4.2E-03	8.7E-03	1.86
DY $\|Q\| = 1e$	400	65	0.300	/	0.400	1.320 ± 0.270	0	0.377	7.3E-03	8.7E-04	6.7E-04	0.00
DY $\|Q\| = 1e$	600	65	0.300	/	0.700	0.229 ± 0.047	0	0.406	1.2E-03	5.9E-04	5.9E-04	0.00
DY $\|Q\| = 1e$	800	65	0.300	/	0.900	0.086 ± 0.018	0	0.433	2.6E-04	5.8E-04	5.8E-04	0.00
DY $\|Q\| = 1e$	1000	65	0.300	/	0.980	0.055 ± 0.011	0	0.423	7.6E-05	5.8E-04	5.8E-04	0.00
DY $\|Q\| = 1e$	1400	65	0.300	/	0.980	0.055 ± 0.011	0	0.335	9.0E-06	7.4E-04	7.4E-04	0.00
DY $\|Q\| = 1e$	1800	65	0.300	/	0.980	0.055 ± 0.011	0	0.260	1.0E-06	9.3E-04	9.3E-04	0.00
DY $\|Q\| = 1e$	2200	65	0.300	/	0.980	0.055 ± 0.011	0	0.176	0.0E+00	1.4E-03	1.4E-03	0.00
DY $\|Q\| = 1e$	2600	65	0.300	/	0.980	0.055 ± 0.011	0	0.105	0.0E+00	2.3E-03	2.3E-03	0.00
DY $\|Q\| = 2e$	100	65	0.300	/	0.200	4.970 ± 1.020	5	0.248	3.8E+00	2.2E-03	2.2E-03	0.01
DY $\|Q\| = 2e$	200	65	0.300	/	0.200	4.970 ± 1.020	5	0.547	3.0E-01	9.8E-04	9.8E-04	0.01
DY $\|Q\| = 2e$	400	65	0.300	/	0.220	3.560 ± 0.728	3	0.670	2.3E-02	6.7E-04	6.5E-04	0.00
DY $\|Q\| = 2e$	600	65	0.300	/	0.360	0.581 ± 0.118	0	0.645	3.5E-03	3.9E-04	3.7E-04	0.00
DY $\|Q\| = 2e$	800	65	0.300	/	0.480	0.163 ± 0.033	0	0.588	8.0E-04	4.1E-04	4.1E-04	0.00
DY $\|Q\| = 2e$	1000	65	0.300	/	0.700	0.017 ± 0.004	0	0.512	2.4E-04	4.9E-04	4.9E-04	0.00
DY $\|Q\| = 2e$	1400	65	0.300	/	0.780	0.005 ± 0.001	0	0.340	2.7E-05	7.3E-04	7.3E-04	0.00
DY $\|Q\| = 2e$	1800	65	0.300	/	0.780	0.005 ± 0.001	0	0.205	4.0E-06	1.2E-03	1.2E-03	0.00
DY $\|Q\| = 2e$	2200	65	0.300	/	0.780	0.005 ± 0.001	0	0.136	1.0E-06	1.8E-03	1.8E-03	0.00
DY $\|Q\| = 2e$	2600	65	0.300	/	0.780	0.005 ± 0.001	0	0.097	0.0E+00	2.5E-03	2.5E-03	0.00

Table B.6: Tracker+TOF+MVA results using 2016 data with the same final selection as the standard analysis.

Model	Mass (GeV)	$p_T >$ (GeV)	$I_{as} >$	$1/\beta >$	MVA>	Bckg. Pred	Obs	SigEff	ThXsec (pb)	ExpXsec (pb)	ObsXsec (pb)	Signif
Gluino f=0.1	200	65	0.175	1.250	0.200	0.180 ± 0.036	0	0.077	3.4E+03	3.2E-03	3.2E-03	0.00
Gluino f=0.1	400	65	0.175	1.250	0.200	0.180 ± 0.036	0	0.125	9.5E+01	1.9E-03	1.9E-03	0.00
Gluino f=0.1	600	65	0.175	1.250	0.200	0.180 ± 0.036	0	0.156	9.1E+00	1.5E-03	1.5E-03	0.00
Gluino f=0.1	800	65	0.175	1.250	0.200	0.180 ± 0.036	0	0.169	1.5E+00	1.4E-03	1.4E-03	0.00
Gluino f=0.1	1000	65	0.175	1.250	0.200	0.180 ± 0.036	0	0.177	3.2E-01	1.3E-03	1.3E-03	0.00
Gluino f=0.1	1200	65	0.175	1.250	0.300	0.035 ± 0.007	0	0.165	8.4E-02	1.4E-03	1.4E-03	0.00
Gluino f=0.1	1400	65	0.175	1.250	0.320	0.027 ± 0.005	0	0.147	2.5E-02	1.6E-03	1.6E-03	0.00
Gluino f=0.1	1600	65	0.175	1.250	0.380	0.013 ± 0.003	0	0.122	8.0E-03	1.9E-03	1.9E-03	0.00
Gluino f=0.1	1800	65	0.175	1.250	0.440	0.007 ± 0.001	0	0.099	2.7E-03	2.4E-03	2.4E-03	0.00
Gluino f=0.1	2000	65	0.175	1.250	0.460	0.006 ± 0.001	0	0.082	9.7E-04	2.9E-03	2.9E-03	0.00
Gluino f=0.1	2200	65	0.175	1.250	0.460	0.006 ± 0.001	0	0.064	3.6E-04	3.7E-03	3.7E-03	0.00
Gluino f=0.1	2600	65	0.175	1.250	0.460	0.006 ± 0.001	0	0.039	5.0E-05	6.1E-03	6.1E-03	0.00
GluinoN f=0.1	1000	65	0.175	1.250	0.460	0.006 ± 0.001	0	0.000	3.2E-01	6.4E-01	6.4E-01	0.00
GluinoN f=0.1	1200	65	0.175	1.250	0.460	0.006 ± 0.001	0	0.000	8.4E-02	1.0E+00	1.0E+00	0.00
GluinoN f=0.1	1400	65	0.175	1.250	0.460	0.006 ± 0.001	0	0.000	2.5E-02	8.4E-01	8.4E-01	0.00
GluinoN f=0.1	1600	65	0.175	1.250	0.460	0.006 ± 0.001	0	0.000	8.0E-03	1.2E+00	1.2E+00	0.00
GluinoN f=0.1	1800	65	0.175	1.250	0.460	0.006 ± 0.001	0	0.000	2.7E-03	9.5E-01	9.5E-01	0.00
GluinoN f=0.1	2000	65	0.175	1.250	0.460	0.006 ± 0.001	0	0.000	9.7E-04	9.4E-01	9.4E-01	0.00
GluinoN f=0.1	2600	65	0.175	1.250	0.460	0.006 ± 0.001	0	0.000	5.0E-05	1.5E+01	1.5E+01	0.00
Gluino f=0.5	200	65	0.175	1.250	0.200	0.180 ± 0.036	0	0.040	3.4E+03	5.8E-03	5.8E-03	0.00
Gluino f=0.5	400	65	0.175	1.250	0.200	0.180 ± 0.036	0	0.070	9.5E+01	3.3E-03	3.3E-03	0.00
Gluino f=0.5	600	65	0.175	1.250	0.200	0.180 ± 0.036	0	0.088	9.1E+00	2.6E-03	2.6E-03	0.00
Gluino f=0.5	800	65	0.175	1.250	0.200	0.180 ± 0.036	0	0.097	1.5E+00	2.4E-03	2.4E-03	0.00
Gluino f=0.5	1000	65	0.175	1.250	0.260	0.062 ± 0.012	0	0.101	3.2E-01	2.3E-03	2.3E-03	0.00
Gluino f=0.5	1200	65	0.175	1.250	0.300	0.035 ± 0.007	0	0.093	8.4E-02	2.6E-03	2.6E-03	0.00
Gluino f=0.5	1400	65	0.175	1.250	0.360	0.017 ± 0.003	0	0.083	2.5E-02	2.9E-03	2.9E-03	0.00
Gluino f=0.5	1600	65	0.175	1.250	0.460	0.006 ± 0.001	0	0.069	8.0E-03	3.5E-03	3.5E-03	0.00
Gluino f=0.5	1800	65	0.175	1.250	0.460	0.006 ± 0.001	0	0.055	2.7E-03	4.4E-03	4.4E-03	0.00
Gluino f=0.5	2000	65	0.175	1.250	0.460	0.006 ± 0.001	0	0.045	9.7E-04	5.3E-03	5.3E-03	0.00
Gluino f=0.5	2200	65	0.175	1.250	0.460	0.006 ± 0.001	0	0.035	3.6E-04	6.8E-03	6.8E-03	0.00
Gluino f=0.5	2600	65	0.175	1.250	0.460	0.006 ± 0.001	0	0.022	5.0E-05	1.0E-02	1.0E-02	0.00
GluinoN f=0.5	1000	65	0.175	1.250	0.380	0.013 ± 0.003	0	0.000	3.2E-01	1.1E+00	1.1E+00	0.00
GluinoN f=0.5	1200	65	0.175	1.250	0.460	0.006 ± 0.001	0	0.000	8.4E-02	1.4E+00	1.4E+00	0.00
GluinoN f=0.5	1400	65	0.175	1.250	0.460	0.006 ± 0.001	0	0.000	2.5E-02	9.4E-01	9.4E-01	0.00
GluinoN f=0.5	1600	65	0.175	1.250	0.460	0.006 ± 0.001	0	0.000	8.0E-03	1.5E+00	1.5E+00	0.00
GluinoN f=0.5	1800	65	0.175	1.250	0.460	0.006 ± 0.001	0	0.000	2.7E-03	1.3E+00	1.3E+00	0.00
GluinoN f=0.5	2000	65	0.175	1.250	0.460	0.006 ± 0.001	0	0.000	9.7E-04	1.3E+00	1.3E+00	0.00
GluinoN f=0.5	2600	65	0.175	1.250	0.460	0.006 ± 0.001	0	0.000	5.0E-05	2.2E+01	2.2E+01	0.00
Stop	100	65	0.175	1.250	0.200	0.025 ± 0.005	0	0.027	1.4E+03	9.4E-03	9.4E-03	0.00
Stop	200	65	0.175	1.250	0.200	0.025 ± 0.005	0	0.063	6.1E+01	3.8E-03	3.8E-03	0.00
Stop	400	65	0.175	1.250	0.200	0.025 ± 0.005	0	0.141	1.8E+00	1.6E-03	1.6E-03	0.00
Stop	600	65	0.175	1.250	0.200	0.025 ± 0.005	0	0.170	1.7E-01	1.4E-03	1.4E-03	0.00
Stop	800	65	0.175	1.250	0.200	0.025 ± 0.005	0	0.175	2.8E-02	1.3E-03	1.3E-03	0.00
Stop	1000	65	0.175	1.250	0.220	0.021 ± 0.004	0	0.170	6.0E-03	1.4E-03	1.4E-03	0.00
Stop	1200	65	0.175	1.250	0.340	0.009 ± 0.002	0	0.159	1.6E-03	1.5E-03	1.5E-03	0.00
Stop	1400	65	0.175	1.250	0.440	0.005 ± 0.001	0	0.142	4.5E-04	1.7E-03	1.7E-03	0.00
Stop	1600	65	0.175	1.250	0.440	0.005 ± 0.001	0	0.121	1.4E-04	2.0E-03	2.0E-03	0.00
Stop	1800	65	0.175	1.250	0.440	0.005 ± 0.001	0	0.104	4.6E-05	2.2E-03	2.2E-03	0.00
Stop	2000	65	0.175	1.250	0.440	0.005 ± 0.001	0	0.083	1.6E-05	2.9E-03	2.9E-03	0.00
Stop	2200	65	0.175	1.250	0.440	0.005 ± 0.001	0	0.067	6.0E-06	3.5E-03	3.5E-03	0.00
StopN	100	65	0.175	1.250	0.200	0.025 ± 0.005	0	0.000	1.4E+03	2.9E+00	2.9E+00	0.00
StopN	200	65	0.175	1.250	0.200	0.025 ± 0.005	0	0.001	6.1E+01	2.9E-01	2.9E-01	0.00
StopN	400	65	0.175	1.250	0.220	0.021 ± 0.004	0	0.004	1.8E+00	6.4E-02	6.4E-02	0.00
StopN	600	65	0.175	1.250	0.420	0.006 ± 0.001	0	0.005	1.7E-01	4.5E-02	4.5E-02	0.00
StopN	800	65	0.175	1.250	0.340	0.009 ± 0.002	0	0.006	2.8E-02	4.2E-02	4.2E-02	0.00
StopN	1000	65	0.175	1.250	0.420	0.006 ± 0.001	0	0.006	6.0E-03	3.6E-02	3.6E-02	0.00

Continued on next page

Table B.6 – continued from previous page

Model	Mass (GeV)	$p_T >$ (GeV)	$I_{as} >$	$1/\beta >$	MVA>	Bckg. Pred	Obs	SigEff	ThXsec (pb)	ExpXsec (pb)	ObsXsec (pb)	Signif
StopN	1200	65	0.175	1.250	0.440	0.005 ± 0.001	0	0.006	1.6E-03	4.1E-02	4.1E-02	0.00
StopN	1600	65	0.175	1.250	0.440	0.005 ± 0.001	0	0.005	1.4E-04	4.5E-02	4.5E-02	0.00
StopN	1800	65	0.175	1.250	0.440	0.005 ± 0.001	0	0.003	4.6E-05	6.9E-02	6.9E-02	0.00
StopN	2000	65	0.175	1.250	0.440	0.005 ± 0.001	0	0.003	1.6E-05	7.2E-02	7.2E-02	0.00
StopN	2200	65	0.175	1.250	0.440	0.005 ± 0.001	0	0.002	6.0E-06	1.1E-01	1.1E-01	0.00
GMSB stau	200	65	0.175	1.250	0.200	0.622 ± 0.125	0	0.279	2.8E-01	8.2E-04	8.4E-04	0.00
GMSB stau	247	65	0.175	1.250	0.200	0.622 ± 0.125	0	0.363	8.8E-02	6.6E-04	6.3E-04	0.00
GMSB stau	308	65	0.175	1.250	0.220	0.483 ± 0.097	0	0.435	2.5E-02	5.3E-04	5.3E-04	0.00
GMSB stau	432	65	0.175	1.250	0.340	0.127 ± 0.025	0	0.547	3.9E-03	4.4E-04	4.4E-04	0.00
GMSB stau	494	65	0.175	1.250	0.400	0.072 ± 0.014	0	0.584	1.9E-03	4.0E-04	4.0E-04	0.00
GMSB stau	651	65	0.175	1.250	0.520	0.026 ± 0.005	0	0.648	4.1E-04	3.6E-04	3.6E-04	0.00
GMSB stau	745	65	0.175	1.250	0.620	0.012 ± 0.002	0	0.666	1.9E-04	3.6E-04	3.6E-04	0.00
GMSB stau	871	65	0.175	1.250	0.700	0.007 ± 0.001	0	0.671	6.9E-05	3.5E-04	3.5E-04	0.00
GMSB stau	1029	65	0.175	1.250	0.740	0.005 ± 0.001	0	0.679	2.2E-05	3.4E-04	3.4E-04	0.00
GMSB stau	1218	65	0.175	1.250	0.740	0.005 ± 0.001	0	0.657	6.0E-06	3.5E-04	3.5E-04	0.00
GMSB stau	1409	65	0.175	1.250	0.740	0.005 ± 0.001	0	0.612	2.0E-06	3.9E-04	3.9E-04	0.00
GMSB stau	1599	65	0.175	1.250	0.740	0.005 ± 0.001	0	0.495	1.0E-06	4.8E-04	4.8E-04	0.00
PP stau	156	65	0.175	1.250	0.200	0.592 ± 0.119	0	0.210	2.0E-02	1.1E-03	1.2E-03	0.00
PP stau	200	65	0.175	1.250	0.200	0.592 ± 0.119	0	0.236	8.0E-03	1.0E-03	1.0E-03	0.00
PP stau	247	65	0.175	1.250	0.280	0.254 ± 0.051	0	0.262	3.7E-03	9.0E-04	9.0E-04	0.00
PP stau	308	65	0.175	1.250	0.360	0.136 ± 0.027	0	0.298	1.5E-03	7.9E-04	7.9E-04	0.00
PP stau	494	65	0.175	1.250	0.740	0.020 ± 0.004	0	0.394	1.9E-04	6.0E-04	6.0E-04	0.00
PP stau	557	65	0.175	1.250	0.840	0.013 ± 0.003	0	0.424	1.1E-04	5.5E-04	5.5E-04	0.00
PP stau	651	65	0.175	1.250	0.860	0.012 ± 0.002	0	0.458	4.9E-05	5.1E-04	5.1E-04	0.00
PP stau	745	65	0.175	1.250	0.880	0.011 ± 0.002	0	0.487	2.4E-05	4.9E-04	4.9E-04	0.00
PP stau	871	65	0.175	1.250	0.940	0.008 ± 0.002	0	0.496	1.0E-05	4.8E-04	4.8E-04	0.00
PP stau	1029	65	0.175	1.250	0.980	0.007 ± 0.001	0	0.504	4.0E-06	4.8E-04	4.8E-04	0.00
PP stau	1218	65	0.175	1.250	0.980	0.007 ± 0.001	0	0.517	1.0E-06	4.6E-04	4.6E-04	0.00
PP stau	1409	65	0.175	1.250	0.980	0.007 ± 0.001	0	0.495	0.0E+00	4.7E-04	4.7E-04	0.00
PP stau	1599	65	0.175	1.250	0.980	0.007 ± 0.001	0	0.440	0.0E+00	5.3E-04	5.3E-04	0.00
DY $\|Q\| = 1e$	100	65	0.175	1.250	0.200	0.307 ± 0.062	0	0.096	1.2E+00	2.9E-03	2.9E-03	0.00
DY $\|Q\| = 1e$	200	65	0.175	1.250	0.200	0.307 ± 0.062	0	0.283	1.1E-01	9.2E-04	9.2E-04	0.00
DY $\|Q\| = 1e$	400	65	0.175	1.250	0.260	0.108 ± 0.022	0	0.397	7.3E-03	6.1E-04	6.1E-04	0.00
DY $\|Q\| = 1e$	600	65	0.175	1.250	0.360	0.033 ± 0.007	0	0.424	1.2E-03	6.5E-04	6.5E-04	0.00
DY $\|Q\| = 1e$	800	65	0.175	1.250	0.540	0.008 ± 0.002	0	0.446	2.6E-04	5.4E-04	5.4E-04	0.00
DY $\|Q\| = 1e$	1000	65	0.175	1.250	0.620	0.005 ± 0.001	0	0.429	7.6E-05	5.7E-04	5.7E-04	0.00
DY $\|Q\| = 1e$	1400	65	0.175	1.250	0.620	0.005 ± 0.001	0	0.334	9.0E-06	7.3E-04	7.3E-04	0.00
DY $\|Q\| = 1e$	1800	65	0.175	1.250	0.620	0.005 ± 0.001	0	0.260	1.0E-06	9.7E-04	9.7E-04	0.00
DY $\|Q\| = 1e$	2200	65	0.175	1.250	0.620	0.005 ± 0.001	0	0.175	0.0E+00	1.4E-03	1.4E-03	0.00
DY $\|Q\| = 1e$	2600	65	0.175	1.250	0.620	0.005 ± 0.001	0	0.101	0.0E+00	2.4E-03	2.4E-03	0.00
DY $\|Q\| = 2e$	100	65	0.175	1.250	0.200	0.115 ± 0.023	0	0.012	3.8E+00	2.2E-02	2.2E-02	0.00
DY $\|Q\| = 2e$	200	65	0.175	1.250	0.200	0.115 ± 0.023	0	0.204	3.0E-01	1.2E-03	1.2E-03	0.00
DY $\|Q\| = 2e$	400	65	0.175	1.250	0.200	0.115 ± 0.023	0	0.396	2.3E-02	6.1E-04	6.1E-04	0.00
DY $\|Q\| = 2e$	600	65	0.175	1.250	0.200	0.115 ± 0.023	0	0.463	3.5E-03	5.3E-04	5.3E-04	0.00
DY $\|Q\| = 2e$	800	65	0.175	1.250	0.240	0.035 ± 0.007	0	0.465	8.0E-04	5.3E-04	5.3E-04	0.00
DY $\|Q\| = 2e$	1000	65	0.175	1.250	0.280	0.015 ± 0.003	0	0.423	2.4E-04	5.7E-04	5.7E-04	0.00
DY $\|Q\| = 2e$	1400	65	0.175	1.250	0.340	0.005 ± 0.001	0	0.298	2.7E-05	8.2E-04	8.2E-04	0.00
DY $\|Q\| = 2e$	1800	65	0.175	1.250	0.340	0.005 ± 0.001	0	0.175	4.0E-06	1.4E-03	1.4E-03	0.00
DY $\|Q\| = 2e$	2200	65	0.175	1.250	0.340	0.005 ± 0.001	0	0.110	1.0E-06	2.2E-03	2.2E-03	0.00
DY $\|Q\| = 2e$	2600	65	0.175	1.250	0.340	0.005 ± 0.001	0	0.068	0.0E+00	3.5E-03	3.5E-03	0.00

Table B.7: Tracker-only+MVA results using 2016 data with the relaxed final selection.

Model	Mass (GeV)	$p_T >$ (GeV)	$I_{as} >$	$1/\beta >$	MVA>	Bckg. Pred	Obs	SigEff	ThXsec (pb)	ExpXsec (pb)	ObsXsec (pb)	Signif
Gluino f=0.1	200	65	0.250	/	0.200	15.200 ± 3.090	16	0.094	3.4E+03	9.5E-03	1.0E-02	0.16
Gluino f=0.1	400	65	0.250	/	0.200	15.200 ± 3.090	16	0.162	9.5E+01	5.1E-03	5.4E-03	0.16

Continued on next page

Table B.7 – continued from previous page

Model	Mass (GeV)	$p_T >$ (GeV)	$I_{as} >$	$1/\beta >$	MVA>	Bckg. Pred	Obs	SigEff	ThXsec (pb)	ExpXsec (pb)	ObsXsec (pb)	Signif
Gluino f=0.1	600	65	0.250	/	0.200	15.200 ± 3.090	16	0.199	9.1E+00	4.2E-03	4.5E-03	0.16
Gluino f=0.1	800	65	0.250	/	0.200	15.200 ± 3.090	16	0.213	1.5E+00	3.8E-03	4.3E-03	0.16
Gluino f=0.1	1000	65	0.250	/	0.280	4.630 ± 0.933	4	0.222	3.2E-01	2.1E-03	2.0E-03	0.00
Gluino f=0.1	1200	65	0.250	/	0.420	1.010 ± 0.203	0	0.209	8.4E-02	1.7E-03	1.1E-03	0.00
Gluino f=0.1	1400	65	0.250	/	0.500	0.489 ± 0.098	0	0.188	2.5E-02	1.2E-03	1.2E-03	0.00
Gluino f=0.1	1600	65	0.250	/	0.640	0.148 ± 0.030	0	0.158	8.0E-03	1.5E-03	1.5E-03	0.00
Gluino f=0.1	1800	65	0.250	/	0.760	0.053 ± 0.011	0	0.130	2.7E-03	1.8E-03	1.8E-03	0.00
Gluino f=0.1	2000	65	0.250	/	0.760	0.053 ± 0.011	0	0.109	9.7E-04	2.2E-03	2.2E-03	0.00
Gluino f=0.1	2200	65	0.250	/	0.760	0.053 ± 0.011	0	0.087	3.6E-04	2.8E-03	2.8E-03	0.00
Gluino f=0.1	2600	65	0.250	/	0.760	0.053 ± 0.011	0	0.054	5.0E-05	4.4E-03	4.4E-03	0.00
GluinoN f=0.1	100	65	0.250	/	0.200	15.200 ± 3.090	16	0.002	8.2E+04	5.4E-01	5.9E-01	0.16
GluinoN f=0.1	1000	65	0.250	/	0.300	3.610 ± 0.727	2	0.189	3.2E-01	2.1E-03	1.8E-03	0.00
GluinoN f=0.1	1200	65	0.250	/	0.400	1.240 ± 0.249	0	0.189	8.4E-02	1.7E-03	1.3E-03	0.00
GluinoN f=0.1	1400	65	0.250	/	0.520	0.413 ± 0.083	0	0.170	2.5E-02	1.4E-03	1.4E-03	0.00
GluinoN f=0.1	1600	65	0.250	/	0.600	0.207 ± 0.042	0	0.148	8.0E-03	1.6E-03	1.6E-03	0.00
GluinoN f=0.1	1800	65	0.250	/	0.760	0.053 ± 0.011	0	0.123	2.7E-03	2.0E-03	2.0E-03	0.00
GluinoN f=0.1	2000	65	0.250	/	0.760	0.053 ± 0.011	0	0.100	9.7E-04	2.3E-03	2.3E-03	0.00
GluinoN f=0.1	2600	65	0.250	/	0.760	0.053 ± 0.011	0	0.055	5.0E-05	4.3E-03	4.3E-03	0.00
Gluino f=0.5	200	65	0.250	/	0.200	15.200 ± 3.090	16	0.048	3.4E+03	1.9E-02	2.0E-02	0.16
Gluino f=0.5	400	65	0.250	/	0.200	15.200 ± 3.090	16	0.091	9.5E+01	9.1E-03	9.8E-03	0.16
Gluino f=0.5	600	65	0.250	/	0.200	15.200 ± 3.090	16	0.114	9.1E+00	7.2E-03	7.8E-03	0.16
Gluino f=0.5	800	65	0.250	/	0.220	10.800 ± 2.190	12	0.125	1.5E+00	5.7E-03	6.3E-03	0.30
Gluino f=0.5	1000	65	0.250	/	0.340	2.280 ± 0.460	2	0.129	3.2E-01	2.9E-03	2.9E-03	0.00
Gluino f=0.5	1200	65	0.250	/	0.420	1.010 ± 0.203	0	0.121	8.4E-02	2.7E-03	1.8E-03	0.00
Gluino f=0.5	1400	65	0.250	/	0.580	0.259 ± 0.052	0	0.108	2.5E-02	2.1E-03	2.1E-03	0.00
Gluino f=0.5	1600	65	0.250	/	0.680	0.106 ± 0.022	0	0.091	8.0E-03	2.6E-03	2.6E-03	0.00
Gluino f=0.5	1800	65	0.250	/	0.760	0.053 ± 0.011	0	0.074	2.7E-03	3.2E-03	3.2E-03	0.00
Gluino f=0.5	2000	65	0.250	/	0.760	0.053 ± 0.011	0	0.060	9.7E-04	4.0E-03	4.0E-03	0.00
Gluino f=0.5	2200	65	0.250	/	0.760	0.053 ± 0.011	0	0.049	3.6E-04	4.9E-03	4.9E-03	0.00
Gluino f=0.5	2600	65	0.250	/	0.760	0.053 ± 0.011	0	0.030	5.0E-05	7.7E-03	7.7E-03	0.00
GluinoN f=0.5	100	65	0.250	/	0.200	15.200 ± 3.090	16	0.001	8.2E+04	7.4E-01	8.0E-01	0.16
GluinoN f=0.5	1000	65	0.250	/	0.320	2.870 ± 0.578	2	0.143	3.2E-01	2.8E-03	2.4E-03	0.00
GluinoN f=0.5	1200	65	0.250	/	0.440	0.835 ± 0.168	0	0.144	8.4E-02	2.3E-03	1.6E-03	0.00
GluinoN f=0.5	1400	65	0.250	/	0.500	0.489 ± 0.098	0	0.129	2.5E-02	1.8E-03	1.8E-03	0.00
GluinoN f=0.5	1600	65	0.250	/	0.640	0.148 ± 0.030	0	0.111	8.0E-03	2.1E-03	2.1E-03	0.00
GluinoN f=0.5	1800	65	0.250	/	0.760	0.053 ± 0.011	0	0.092	2.7E-03	2.6E-03	2.6E-03	0.00
GluinoN f=0.5	2000	65	0.250	/	0.760	0.053 ± 0.011	0	0.073	9.7E-04	3.2E-03	3.2E-03	0.00
GluinoN f=0.5	2600	65	0.250	/	0.760	0.053 ± 0.011	0	0.041	5.0E-05	5.7E-03	5.7E-03	0.00
Stop	100	65	0.250	/	0.200	12.300 ± 2.470	14	0.107	1.4E+03	6.6E-03	8.5E-03	0.41
Stop	200	65	0.250	/	0.200	12.300 ± 2.470	14	0.183	6.1E+01	4.1E-03	4.9E-03	0.41
Stop	400	65	0.250	/	0.200	12.300 ± 2.470	14	0.223	1.8E+00	3.3E-03	4.0E-03	0.41
Stop	600	65	0.250	/	0.260	5.730 ± 1.150	4	0.249	1.7E-01	2.1E-03	1.7E-03	0.00
Stop	800	65	0.250	/	0.420	1.300 ± 0.262	0	0.248	2.8E-02	1.3E-03	9.4E-04	0.00
Stop	1000	65	0.250	/	0.640	0.281 ± 0.056	0	0.244	6.0E-03	9.6E-04	9.6E-04	0.00
Stop	1200	65	0.250	/	0.800	0.093 ± 0.019	0	0.230	1.6E-03	1.0E-03	1.0E-03	0.00
Stop	1400	65	0.250	/	0.860	0.058 ± 0.012	0	0.209	4.5E-04	1.1E-03	1.1E-03	0.00
Stop	1600	65	0.250	/	0.860	0.058 ± 0.012	0	0.183	1.4E-04	1.3E-03	1.3E-03	0.00
Stop	1800	65	0.250	/	0.860	0.058 ± 0.012	0	0.158	4.6E-05	1.5E-03	1.5E-03	0.00
Stop	2000	65	0.250	/	0.860	0.058 ± 0.012	0	0.129	1.6E-05	1.8E-03	1.8E-03	0.00
Stop	2200	65	0.250	/	0.860	0.058 ± 0.012	0	0.104	6.0E-06	2.3E-03	2.3E-03	0.00
StopN	100	65	0.250	/	0.200	12.300 ± 2.470	14	0.011	1.4E+03	6.9E-02	8.4E-02	0.41
StopN	200	65	0.250	/	0.200	12.300 ± 2.470	14	0.046	6.1E+01	1.5E-02	1.9E-02	0.41
StopN	400	65	0.250	/	0.200	12.300 ± 2.470	14	0.119	1.8E+00	6.1E-03	7.2E-03	0.41
StopN	600	65	0.250	/	0.280	4.560 ± 0.918	4	0.167	1.7E-01	2.9E-03	2.7E-03	0.00
StopN	800	65	0.250	/	0.400	1.520 ± 0.307	0	0.194	2.8E-02	1.6E-03	1.2E-03	0.00
StopN	1000	65	0.250	/	0.640	0.281 ± 0.056	0	0.196	6.0E-03	1.2E-03	1.2E-03	0.00
StopN	1200	65	0.250	/	0.820	0.080 ± 0.016	0	0.190	1.6E-03	1.2E-03	1.2E-03	0.00
StopN	1600	65	0.250	/	0.860	0.058 ± 0.012	0	0.148	1.4E-04	1.6E-03	1.6E-03	0.00
StopN	1800	65	0.250	/	0.860	0.058 ± 0.012	0	0.129	4.6E-05	1.9E-03	1.9E-03	0.00
StopN	2000	65	0.250	/	0.860	0.058 ± 0.012	0	0.105	1.6E-05	2.2E-03	2.2E-03	0.00

Continued on next page

Table B.7 – continued from previous page

Model	Mass (GeV)	$p_T >$ (GeV)	$I_{as} >$	$1/\beta >$	MVA>	Bckg. Pred	Obs	SigEff	ThXsec (pb)	ExpXsec (pb)	ObsXsec (pb)	Signif
StopN	2200	65	0.250	/	0.860	0.058 ± 0.012	0	0.086	6.0E-06	2.7E-03	2.7E-03	0.00
GMSB stau	200	65	0.250	/	0.240	61.700 ± 12.500	81	0.288	2.8E-01	7.1E-03	1.3E-02	1.26
GMSB stau	247	65	0.250	/	0.320	22.000 ± 4.440	32	0.374	8.8E-02	2.9E-03	5.0E-03	1.45
GMSB stau	308	65	0.250	/	0.440	8.040 ± 1.620	8	0.452	2.5E-02	1.3E-03	1.4E-03	0.00
GMSB stau	432	65	0.250	/	0.680	2.290 ± 0.460	0	0.569	3.9E-03	6.7E-04	4.2E-04	0.00
GMSB stau	494	65	0.250	/	0.780	1.470 ± 0.296	0	0.607	1.9E-03	5.2E-04	4.0E-04	0.00
GMSB stau	651	65	0.250	/	0.980	0.586 ± 0.118	0	0.667	4.1E-04	3.5E-04	3.5E-04	0.00
GMSB stau	745	65	0.250	/	0.980	0.586 ± 0.118	0	0.685	1.9E-04	3.3E-04	3.3E-04	0.00
GMSB stau	871	65	0.250	/	0.980	0.586 ± 0.118	0	0.685	6.9E-05	3.7E-04	3.4E-04	0.00
GMSB stau	1029	65	0.250	/	0.980	0.586 ± 0.118	0	0.696	2.2E-05	3.6E-04	3.3E-04	0.00
GMSB stau	1218	65	0.250	/	0.980	0.586 ± 0.118	0	0.673	6.0E-06	3.9E-04	3.4E-04	0.00
GMSB stau	1409	65	0.250	/	0.980	0.586 ± 0.118	0	0.628	2.0E-06	4.2E-04	3.7E-04	0.00
GMSB stau	1599	65	0.250	/	0.980	0.586 ± 0.118	0	0.509	1.0E-06	4.8E-04	4.5E-04	0.00
PP stau	156	65	0.250	/	0.360	36.500 ± 7.340	54	0.202	2.0E-02	7.5E-03	1.6E-02	1.70
PP stau	200	65	0.250	/	0.480	17.700 ± 3.540	17	0.237	8.0E-03	4.1E-03	3.9E-03	0.00
PP stau	247	65	0.250	/	0.620	8.820 ± 1.770	10	0.268	3.7E-03	2.2E-03	3.0E-03	0.34
PP stau	308	65	0.250	/	0.820	3.610 ± 0.724	3	0.306	1.5E-03	1.7E-03	1.5E-03	0.00
PP stau	494	65	0.250	/	0.980	1.770 ± 0.355	0	0.402	1.9E-04	9.0E-04	6.0E-04	0.00
PP stau	557	65	0.250	/	0.980	1.770 ± 0.355	0	0.428	1.1E-04	9.2E-04	5.8E-04	0.00
PP stau	651	65	0.250	/	0.980	1.770 ± 0.355	0	0.458	4.9E-05	7.6E-04	5.2E-04	0.00
PP stau	745	65	0.250	/	0.980	1.770 ± 0.355	0	0.496	2.4E-05	7.5E-04	4.5E-04	0.00
PP stau	871	65	0.250	/	0.980	1.770 ± 0.355	0	0.504	1.0E-05	8.2E-04	4.4E-04	0.00
PP stau	1029	65	0.250	/	0.980	1.770 ± 0.355	0	0.513	4.0E-06	6.8E-04	4.8E-04	0.00
PP stau	1218	65	0.250	/	0.980	1.770 ± 0.355	0	0.522	1.0E-06	7.9E-04	4.6E-04	0.00
PP stau	1409	65	0.250	/	0.980	1.770 ± 0.355	0	0.496	0.0E+00	7.9E-04	5.1E-04	0.00
PP stau	1599	65	0.250	/	0.920	2.320 ± 0.466	2	0.444	0.0E+00	8.5E-04	8.5E-04	0.00
DY $\|Q\| = 1e$	100	65	0.250	/	0.200	44.900 ± 9.160	63	0.089	1.2E+00	2.1E-02	4.0E-02	1.50
DY $\|Q\| = 1e$	200	65	0.250	/	0.200	44.900 ± 9.160	63	0.291	1.1E-01	6.0E-03	1.2E-02	1.50
DY $\|Q\| = 1e$	400	65	0.250	/	0.440	2.870 ± 0.577	2	0.406	7.3E-03	1.2E-03	9.5E-04	0.00
DY $\|Q\| = 1e$	600	65	0.250	/	0.740	0.580 ± 0.117	0	0.433	1.2E-03	6.4E-04	5.7E-04	0.00
DY $\|Q\| = 1e$	800	65	0.250	/	0.960	0.187 ± 0.038	0	0.452	2.6E-04	5.5E-04	5.5E-04	0.00
DY $\|Q\| = 1e$	1000	65	0.250	/	0.980	0.166 ± 0.034	0	0.436	7.6E-05	5.6E-04	5.6E-04	0.00
DY $\|Q\| = 1e$	1400	65	0.250	/	0.980	0.166 ± 0.034	0	0.346	9.0E-06	7.0E-04	7.0E-04	0.00
DY $\|Q\| = 1e$	1800	65	0.250	/	0.980	0.166 ± 0.034	0	0.270	1.0E-06	9.1E-04	9.1E-04	0.00
DY $\|Q\| = 1e$	2200	65	0.250	/	0.980	0.166 ± 0.034	0	0.180	0.0E+00	1.3E-03	1.3E-03	0.00
DY $\|Q\| = 1e$	2600	65	0.250	/	0.980	0.166 ± 0.034	0	0.108	0.0E+00	2.3E-03	2.3E-03	0.00
DY $\|Q\| = 2e$	100	65	0.250	/	0.200	12.600 ± 2.540	13	0.248	3.8E+00	3.4E-03	3.3E-03	0.09
DY $\|Q\| = 2e$	200	65	0.250	/	0.200	12.600 ± 2.540	13	0.547	3.0E-01	1.4E-03	1.5E-03	0.09
DY $\|Q\| = 2e$	400	65	0.250	/	0.260	5.220 ± 1.050	4	0.670	2.3E-02	8.0E-04	6.7E-04	0.00
DY $\|Q\| = 2e$	600	65	0.250	/	0.480	0.429 ± 0.086	0	0.645	3.5E-03	3.8E-04	3.8E-04	0.00
DY $\|Q\| = 2e$	800	65	0.250	/	0.680	0.052 ± 0.011	0	0.588	8.0E-04	4.2E-04	4.2E-04	0.00
DY $\|Q\| = 2e$	1000	65	0.250	/	0.680	0.052 ± 0.011	0	0.512	2.4E-04	4.8E-04	4.8E-04	0.00
DY $\|Q\| = 2e$	1400	65	0.250	/	0.680	0.052 ± 0.011	0	0.340	2.7E-05	7.2E-04	7.2E-04	0.00
DY $\|Q\| = 2e$	1800	65	0.250	/	0.680	0.052 ± 0.011	0	0.205	4.0E-06	1.2E-03	1.2E-03	0.00
DY $\|Q\| = 2e$	2200	65	0.250	/	0.680	0.052 ± 0.011	0	0.136	1.0E-06	1.8E-03	1.8E-03	0.00
DY $\|Q\| = 2e$	2600	65	0.250	/	0.680	0.052 ± 0.011	0	0.097	0.0E+00	2.7E-03	2.7E-03	0.00

Table B.8: Tracker+TOF+MVA results using 2016 data with the relaxed final selection.

Model	Mass (GeV)	$p_T >$ (GeV)	$I_{as} >$	$1/\beta >$	MVA>	Bckg. Pred	Obs	SigEff	ThXsec (pb)	ExpXsec (pb)	ObsXsec (pb)	Signif
Gluino f=0.1	200	65	0.150	1.250	0.200	0.322 ± 0.064	0	0.078	3.4E+03	3.0E-03	3.0E-03	0.00
Gluino f=0.1	400	65	0.150	1.250	0.200	0.322 ± 0.064	0	0.128	9.5E+01	1.8E-03	1.8E-03	0.00
Gluino f=0.1	600	65	0.150	1.250	0.200	0.322 ± 0.064	0	0.157	9.1E+00	1.5E-03	1.5E-03	0.00
Gluino f=0.1	800	65	0.150	1.250	0.200	0.322 ± 0.064	0	0.171	1.5E+00	1.4E-03	1.4E-03	0.00
Gluino f=0.1	1000	65	0.150	1.250	0.220	0.220 ± 0.044	0	0.179	3.2E-01	1.3E-03	1.3E-03	0.00
Gluino f=0.1	1200	65	0.150	1.250	0.300	0.065 ± 0.013	0	0.166	8.4E-02	1.4E-03	1.4E-03	0.00

Continued on next page

Table B.8 – continued from previous page

Model	Mass (GeV)	$p_T >$ (GeV)	$I_{as} >$	$1/\beta >$	MVA>	Bckg. Pred	Obs	SigEff	ThXsec (pb)	ExpXsec (pb)	ObsXsec (pb)	Signif
Gluino f=0.1	1400	65	0.150	1.250	0.300	0.065 ± 0.013	0	0.148	2.5E-02	1.6E-03	1.6E-03	0.00
Gluino f=0.1	1600	65	0.150	1.250	0.300	0.065 ± 0.013	0	0.123	8.0E-03	1.9E-03	1.9E-03	0.00
Gluino f=0.1	1800	65	0.150	1.250	0.300	0.065 ± 0.013	0	0.099	2.7E-03	2.4E-03	2.4E-03	0.00
Gluino f=0.1	2000	65	0.150	1.250	0.300	0.065 ± 0.013	0	0.082	9.7E-04	2.9E-03	2.9E-03	0.00
Gluino f=0.1	2200	65	0.150	1.250	0.300	0.065 ± 0.013	0	0.064	3.6E-04	3.8E-03	3.8E-03	0.00
Gluino f=0.1	2600	65	0.150	1.250	0.300	0.065 ± 0.013	0	0.039	5.0E-05	5.9E-03	5.9E-03	0.00
GluinoN f=0.1	1000	65	0.150	1.250	0.300	0.065 ± 0.013	0	0.000	3.2E-01	6.3E-01	6.3E-01	0.00
GluinoN f=0.1	1200	65	0.150	1.250	0.300	0.065 ± 0.013	0	0.000	8.4E-02	1.0E+00	1.0E+00	0.00
GluinoN f=0.1	1400	65	0.150	1.250	0.300	0.065 ± 0.013	0	0.000	2.5E-02	7.8E-01	7.8E-01	0.00
GluinoN f=0.1	1600	65	0.150	1.250	0.300	0.065 ± 0.013	0	0.000	8.0E-03	1.1E+00	1.1E+00	0.00
GluinoN f=0.1	1800	65	0.150	1.250	0.300	0.065 ± 0.013	0	0.000	2.7E-03	9.6E-01	9.6E-01	0.00
GluinoN f=0.1	2000	65	0.150	1.250	0.300	0.065 ± 0.013	0	0.000	9.7E-04	9.5E-01	9.5E-01	0.00
GluinoN f=0.1	2600	65	0.150	1.250	0.300	0.065 ± 0.013	0	0.000	5.0E-05	1.1E+01	1.1E+01	0.00
Gluino f=0.5	200	65	0.150	1.250	0.200	0.322 ± 0.064	0	0.041	3.4E+03	5.9E-03	5.9E-03	0.00
Gluino f=0.5	400	65	0.150	1.250	0.200	0.322 ± 0.064	0	0.072	9.5E+01	3.3E-03	3.3E-03	0.00
Gluino f=0.5	600	65	0.150	1.250	0.200	0.322 ± 0.064	0	0.089	9.1E+00	2.6E-03	2.6E-03	0.00
Gluino f=0.5	800	65	0.150	1.250	0.200	0.322 ± 0.064	0	0.098	1.5E+00	2.4E-03	2.4E-03	0.00
Gluino f=0.5	1000	65	0.150	1.250	0.260	0.115 ± 0.023	0	0.102	3.2E-01	2.3E-03	2.3E-03	0.00
Gluino f=0.5	1200	65	0.150	1.250	0.300	0.065 ± 0.013	0	0.093	8.4E-02	2.5E-03	2.5E-03	0.00
Gluino f=0.5	1400	65	0.150	1.250	0.300	0.065 ± 0.013	0	0.084	2.5E-02	2.8E-03	2.8E-03	0.00
Gluino f=0.5	1600	65	0.150	1.250	0.300	0.065 ± 0.013	0	0.069	8.0E-03	3.4E-03	3.4E-03	0.00
Gluino f=0.5	1800	65	0.150	1.250	0.300	0.065 ± 0.013	0	0.055	2.7E-03	4.3E-03	4.3E-03	0.00
Gluino f=0.5	2000	65	0.150	1.250	0.300	0.065 ± 0.013	0	0.045	9.7E-04	5.3E-03	5.3E-03	0.00
Gluino f=0.5	2200	65	0.150	1.250	0.300	0.065 ± 0.013	0	0.035	3.6E-04	6.9E-03	6.9E-03	0.00
Gluino f=0.5	2600	65	0.150	1.250	0.300	0.065 ± 0.013	0	0.022	5.0E-05	1.1E-02	1.1E-02	0.00
GluinoN f=0.5	1000	65	0.150	1.250	0.300	0.065 ± 0.013	0	0.000	3.2E-01	1.0E+00	1.0E+00	0.00
GluinoN f=0.5	1200	65	0.150	1.250	0.300	0.065 ± 0.013	0	0.000	8.4E-02	1.5E+00	1.5E+00	0.00
GluinoN f=0.5	1400	65	0.150	1.250	0.300	0.065 ± 0.013	0	0.000	2.5E-02	8.8E-01	8.8E-01	0.00
GluinoN f=0.5	1600	65	0.150	1.250	0.300	0.065 ± 0.013	0	0.000	8.0E-03	1.4E+00	1.4E+00	0.00
GluinoN f=0.5	1800	65	0.150	1.250	0.300	0.065 ± 0.013	0	0.000	2.7E-03	1.4E+00	1.4E+00	0.00
GluinoN f=0.5	2000	65	0.150	1.250	0.300	0.065 ± 0.013	0	0.000	9.7E-04	1.3E+00	1.3E+00	0.00
GluinoN f=0.5	2600	65	0.150	1.250	0.300	0.065 ± 0.013	0	0.000	5.0E-05	1.5E+01	1.5E+01	0.00
Stop	100	65	0.150	1.250	0.200	0.049 ± 0.010	0	0.027	1.4E+03	9.0E-03	9.0E-03	0.00
Stop	200	65	0.150	1.250	0.200	0.049 ± 0.010	0	0.063	6.1E+01	3.9E-03	3.9E-03	0.00
Stop	400	65	0.150	1.250	0.200	0.049 ± 0.010	0	0.143	1.8E+00	1.7E-03	1.7E-03	0.00
Stop	600	65	0.150	1.250	0.200	0.049 ± 0.010	0	0.171	1.7E-01	1.4E-03	1.4E-03	0.00
Stop	800	65	0.150	1.250	0.200	0.049 ± 0.010	0	0.177	2.8E-02	1.3E-03	1.3E-03	0.00
Stop	1000	65	0.150	1.250	0.200	0.049 ± 0.010	0	0.171	6.0E-03	1.4E-03	1.4E-03	0.00
Stop	1200	65	0.150	1.250	0.200	0.049 ± 0.010	0	0.161	1.6E-03	1.5E-03	1.5E-03	0.00
Stop	1400	65	0.150	1.250	0.200	0.049 ± 0.010	0	0.143	4.5E-04	1.7E-03	1.7E-03	0.00
Stop	1600	65	0.150	1.250	0.200	0.049 ± 0.010	0	0.122	1.4E-04	1.9E-03	1.9E-03	0.00
Stop	1800	65	0.150	1.250	0.200	0.049 ± 0.010	0	0.105	4.6E-05	2.2E-03	2.2E-03	0.00
Stop	2000	65	0.150	1.250	0.200	0.049 ± 0.010	0	0.083	1.6E-05	2.9E-03	2.9E-03	0.00
Stop	2200	65	0.150	1.250	0.200	0.049 ± 0.010	0	0.067	6.0E-06	3.6E-03	3.6E-03	0.00
StopN	100	65	0.150	1.250	0.200	0.049 ± 0.010	0	0.000	1.4E+03	3.1E+00	3.1E+00	0.00
StopN	200	65	0.150	1.250	0.200	0.049 ± 0.010	0	0.001	6.1E+01	3.0E-01	3.0E-01	0.00
StopN	400	65	0.150	1.250	0.200	0.049 ± 0.010	0	0.004	1.8E+00	6.1E-02	6.1E-02	0.00
StopN	600	65	0.150	1.250	0.200	0.049 ± 0.010	0	0.005	1.7E-01	4.5E-02	4.5E-02	0.00
StopN	800	65	0.150	1.250	0.200	0.049 ± 0.010	0	0.006	2.8E-02	4.2E-02	4.2E-02	0.00
StopN	1000	65	0.150	1.250	0.200	0.049 ± 0.010	0	0.006	6.0E-03	3.6E-02	3.6E-02	0.00
StopN	1200	65	0.150	1.250	0.200	0.049 ± 0.010	0	0.006	1.6E-03	4.1E-02	4.1E-02	0.00
StopN	1600	65	0.150	1.250	0.200	0.049 ± 0.010	0	0.005	1.4E-04	4.5E-02	4.5E-02	0.00
StopN	1800	65	0.150	1.250	0.200	0.049 ± 0.010	0	0.003	4.6E-05	6.8E-02	6.8E-02	0.00
StopN	2000	65	0.150	1.250	0.200	0.049 ± 0.010	0	0.003	1.6E-05	7.2E-02	7.2E-02	0.00
StopN	2200	65	0.150	1.250	0.200	0.049 ± 0.010	0	0.002	6.0E-06	1.1E-01	1.1E-01	0.00
GMSB stau	200	65	0.150	1.250	0.200	1.160 ± 0.233	0	0.285	2.8E-01	1.1E-03	8.1E-04	0.00
GMSB stau	247	65	0.150	1.250	0.200	1.160 ± 0.233	0	0.369	8.8E-02	9.1E-04	6.5E-04	0.00
GMSB stau	308	65	0.150	1.250	0.220	0.905 ± 0.181	0	0.442	2.5E-02	7.6E-04	5.3E-04	0.00
GMSB stau	432	65	0.150	1.250	0.380	0.164 ± 0.033	0	0.555	3.9E-03	4.3E-04	4.3E-04	0.00
GMSB stau	494	65	0.150	1.250	0.420	0.114 ± 0.023	0	0.594	1.9E-03	4.0E-04	4.0E-04	0.00

Continued on next page

Table B.8 – continued from previous page

Model	Mass (GeV)	$p_T >$ (GeV)	$I_{as} >$	$1/\beta >$	MVA>	Bckg. Pred	Obs	SigEff	ThXsec (pb)	ExpXsec (pb)	ObsXsec (pb)	Signif
GMSB stau	651	65	0.150	1.250	0.500	0.058 ± 0.012	0	0.657	4.1E-04	3.6E-04	3.6E-04	0.00
GMSB stau	745	65	0.150	1.250	0.500	0.058 ± 0.012	0	0.672	1.9E-04	3.5E-04	3.5E-04	0.00
GMSB stau	871	65	0.150	1.250	0.500	0.058 ± 0.012	0	0.677	6.9E-05	3.5E-04	3.5E-04	0.00
GMSB stau	1029	65	0.150	1.250	0.500	0.058 ± 0.012	0	0.684	2.2E-05	3.5E-04	3.5E-04	0.00
GMSB stau	1218	65	0.150	1.250	0.500	0.058 ± 0.012	0	0.661	6.0E-06	3.6E-04	3.6E-04	0.00
GMSB stau	1409	65	0.150	1.250	0.500	0.058 ± 0.012	0	0.616	2.0E-06	3.9E-04	3.9E-04	0.00
GMSB stau	1599	65	0.150	1.250	0.500	0.058 ± 0.012	0	0.500	1.0E-06	4.8E-04	4.8E-04	0.00
PP stau	156	65	0.150	1.250	0.200	1.090 ± 0.219	0	0.217	2.0E-02	1.5E-03	1.1E-03	0.00
PP stau	200	65	0.150	1.250	0.240	0.693 ± 0.139	0	0.242	8.0E-03	1.1E-03	9.5E-04	0.00
PP stau	247	65	0.150	1.250	0.320	0.343 ± 0.069	0	0.270	3.7E-03	9.0E-04	9.0E-04	0.00
PP stau	308	65	0.150	1.250	0.440	0.154 ± 0.031	0	0.305	1.5E-03	7.4E-04	7.4E-04	0.00
PP stau	494	65	0.150	1.250	0.660	0.051 ± 0.010	0	0.403	1.9E-04	5.9E-04	5.9E-04	0.00
PP stau	557	65	0.150	1.250	0.660	0.051 ± 0.010	0	0.433	1.1E-04	5.5E-04	5.5E-04	0.00
PP stau	651	65	0.150	1.250	0.660	0.051 ± 0.010	0	0.466	4.9E-05	5.0E-04	5.0E-04	0.00
PP stau	745	65	0.150	1.250	0.660	0.051 ± 0.010	0	0.494	2.4E-05	4.9E-04	4.9E-04	0.00
PP stau	871	65	0.150	1.250	0.660	0.051 ± 0.010	0	0.502	1.0E-05	4.8E-04	4.8E-04	0.00
PP stau	1029	65	0.150	1.250	0.660	0.051 ± 0.010	0	0.512	4.0E-06	4.7E-04	4.7E-04	0.00
PP stau	1218	65	0.150	1.250	0.660	0.051 ± 0.010	0	0.523	1.0E-06	4.6E-04	4.6E-04	0.00
PP stau	1409	65	0.150	1.250	0.660	0.051 ± 0.010	0	0.500	0.0E+00	4.8E-04	4.8E-04	0.00
PP stau	1599	65	0.150	1.250	0.660	0.051 ± 0.010	0	0.445	0.0E+00	5.4E-04	5.4E-04	0.00
DY $\|Q\| = 1e$	100	65	0.150	1.250	0.200	0.538 ± 0.108	0	0.097	1.2E+00	3.1E-03	2.9E-03	0.00
DY $\|Q\| = 1e$	200	65	0.150	1.250	0.200	0.538 ± 0.108	0	0.288	1.1E-01	8.7E-04	8.6E-04	0.00
DY $\|Q\| = 1e$	400	65	0.150	1.250	0.260	0.197 ± 0.039	0	0.402	7.3E-03	6.0E-04	6.0E-04	0.00
DY $\|Q\| = 1e$	600	65	0.150	1.250	0.360	0.062 ± 0.012	0	0.429	1.2E-03	5.7E-04	5.7E-04	0.00
DY $\|Q\| = 1e$	800	65	0.150	1.250	0.380	0.051 ± 0.010	0	0.451	2.6E-04	5.4E-04	5.4E-04	0.00
DY $\|Q\| = 1e$	1000	65	0.150	1.250	0.380	0.051 ± 0.010	0	0.432	7.6E-05	5.6E-04	5.6E-04	0.00
DY $\|Q\| = 1e$	1400	65	0.150	1.250	0.380	0.051 ± 0.010	0	0.337	9.0E-06	7.2E-04	7.2E-04	0.00
DY $\|Q\| = 1e$	1800	65	0.150	1.250	0.380	0.051 ± 0.010	0	0.263	1.0E-06	9.1E-04	9.1E-04	0.00
DY $\|Q\| = 1e$	2200	65	0.150	1.250	0.380	0.051 ± 0.010	0	0.176	0.0E+00	1.4E-03	1.4E-03	0.00
DY $\|Q\| = 1e$	2600	65	0.150	1.250	0.380	0.051 ± 0.010	0	0.101	0.0E+00	2.4E-03	2.4E-03	0.00
DY $\|Q\| = 2e$	100	65	0.150	1.250	0.200	0.164 ± 0.033	0	0.012	3.8E+00	2.2E-02	2.2E-02	0.00
DY $\|Q\| = 2e$	200	65	0.150	1.250	0.200	0.164 ± 0.033	0	0.204	3.0E-01	1.2E-03	1.2E-03	0.00
DY $\|Q\| = 2e$	400	65	0.150	1.250	0.200	0.164 ± 0.033	0	0.396	2.3E-02	6.2E-04	6.2E-04	0.00
DY $\|Q\| = 2e$	600	65	0.150	1.250	0.200	0.164 ± 0.033	0	0.463	3.5E-03	5.3E-04	5.3E-04	0.00
DY $\|Q\| = 2e$	800	65	0.150	1.250	0.240	0.053 ± 0.011	0	0.465	8.0E-04	5.2E-04	5.2E-04	0.00
DY $\|Q\| = 2e$	1000	65	0.150	1.250	0.240	0.053 ± 0.011	0	0.423	2.4E-04	5.7E-04	5.7E-04	0.00
DY $\|Q\| = 2e$	1400	65	0.150	1.250	0.240	0.053 ± 0.011	0	0.298	2.7E-05	8.1E-04	8.1E-04	0.00
DY $\|Q\| = 2e$	1800	65	0.150	1.250	0.240	0.053 ± 0.011	0	0.175	4.0E-06	1.4E-03	1.4E-03	0.00
DY $\|Q\| = 2e$	2200	65	0.150	1.250	0.240	0.053 ± 0.011	0	0.110	1.0E-06	2.2E-03	2.2E-03	0.00
DY $\|Q\| = 2e$	2600	65	0.150	1.250	0.240	0.053 ± 0.011	0	0.068	0.0E+00	3.6E-03	3.6E-03	0.00

BIBLIOGRAPHY

[1] Massimo Persic, Paolo Salucci, and Fulvio Stel. The universal rotation curve of spiral galaxies: 1. The dark matter connection. *Mon. Not. Roy. Astron. Soc.*, 281:27, 1996.

[2] Adam G. Riess et al. Observational evidence from supernovae for an accelerating universe and a cosmological constant. *Astron. J.*, 116:1009–1038, 1998.

[3] Stephen P. Martin. A supersymmetry primer. 1997. [Adv. Ser. Direct. High Energy Phys.18,1(1998)].

[4] S. Dawson. SUSY and such. *NATO Sci. Ser. B*, 365:33–80, 1997.

[5] Keith A. Ulmer. Supersymmetry: experimental status. In *3rd Large Hadron Collider Physics Conference (LHCP 2015) St. Petersburg, Russia, August 31-September 5, 2015*, 2016.

[6] H. Wells Wulsin. Recent CMS searches for exotic phenomena beyond the Standard Model. In *Proceedings, Meeting of the APS Division of Particles and Fields (DPF 2015): Ann Arbor, Michigan, USA, 4-8 Aug 2015*, 2015.

[7] Lorenzo Basso, Alexander Belyaev, Stefano Moretti, and Claire H. Shepherd-Themistocleous. Phenomenology of the minimal B-L extension of the Standard Model: Z' and neutrinos. *Phys. Rev.*, D80:055030, 2009.

[8] Can Kilic, Takemichi Okui, and Raman Sundrum. Vectorlike confinement at the LHC. *JHEP*, 02:018, 2010.

[9] Tao Han, Zongguo Si, Kathryn M. Zurek, and Matthew J. Strassler. Phenomenology of hidden valleys at hadron colliders. *JHEP*, 07:008, 2008.

[10] V. M. Abazov et al. Search for long-lived charged massive particles with the D0 detector. *Phys. Rev. Lett.*, 102:161802, 2009.

[11] T. Aaltonen et al. Search for long-lived massive charged particles in 1.96 TeV $\bar{p}p$ collisions. *Phys. Rev. Lett.*, 103:021802, 2009.

[12] Georges Aad et al. Search for heavy long-lived charged particles with the ATLAS detector in pp collisions at $\sqrt{s} = 7$ TeV. *Phys. Lett.*, B703:428–446, 2011.

[13] Georges Aad et al. Searches for heavy long-lived charged particles with the ATLAS detector in proton-proton collisions at $\sqrt{s} = 8$ TeV. *JHEP*, 01:068, 2015.

[14] Morad Aaboud et al. Search for metastable heavy charged particles with large ionization energy loss in pp collisions at $\sqrt{s} = 13$ TeV using the ATLAS experiment. *Phys. Rev.*, D93(11):112015, 2016.

[15] Vardan Khachatryan et al. Search for heavy stable charged particles in pp collisions at $\sqrt{s} = 7$ TeV. *JHEP*, 03:024, 2011.

[16] Serguei Chatrchyan et al. Searches for long-lived charged particles in pp collisions at $\sqrt{s}$=7 and 8 TeV. *JHEP*, 07:122, 2013.

[17] Vardan Khachatryan et al. Search for long-lived charged particles in proton-proton collisions at $\sqrt{s} = 13$TeV. *Phys. Rev.*, D94(11):112004, 2016.

[18] CMS Collaboration. Search for heavy stable charged particles with 12.9 fb^{-1} of 2016 data. (CMS-PAS-EXO-16-036), 2016.

[19] MissMJ. [CC BY 3.0 (http://creativecommons.org/licenses/by/3.0) or Public domain], via Wikimedia Commons.

[20] G. F. Giudice and R. Rattazzi. Theories with gauge mediated supersymmetry breaking. *Phys. Rept.*, 322:419–499, 1999.

[21] Michael Dine, Yosef Nir, and Yuri Shirman. Variations on minimal gauge mediated supersymmetry breaking. *Phys. Rev.*, D55:1501–1508, 1997.

[22] Jan Heisig and Jrn Kersten. Production of long-lived staus in the Drell-Yan process. *Phys. Rev.*, D84:115009, 2011.

[23] G. F. Giudice and A. Romanino. Split supersymmetry. *Nucl. Phys.*, B699:65–89, 2004. [Erratum: Nucl. Phys.B706,487(2005)].

[24] Aafke Christine Kraan. Interactions of heavy stable hadronizing particles. *Eur. Phys. J.*, C37:91–104, 2004.

[25] Rasmus Mackeprang and Andrea Rizzi. Interactions of coloured heavy stable particles in matter. *Eur. Phys. J.*, C50:353–362, 2007.

[26] Rasmus Mackeprang and David Milstead. An updated description of heavy-hadron interactions in GEANT-4. *Eur. Phys. J.*, C66:493–501, 2010.

[27] A. Kulesza and L. Motyka. Threshold resummation for squark-antisquark and gluino-pair production at the LHC. *Phys. Rev. Lett.*, 102:111802, 2009.

[28] A. Kulesza and L. Motyka. Soft gluon resummation for the production of gluino-gluino and squark-antisquark pairs at the LHC. *Phys. Rev.*, D80:095004, 2009.

[29] Wim Beenakker, Silja Brensing, Michael Kramer, Anna Kulesza, Eric Laenen, and Irene Niessen. Soft-gluon resummation for squark and gluino hadroproduction. *JHEP*, 12:041, 2009.

[30] Wim Beenakker, Silja Brensing, Michael Kramer, Anna Kulesza, Eric Laenen, and Irene Niessen. Supersymmetric top and bottom squark production at hadron colliders. *JHEP*, 08:098, 2010.

[31] W. Beenakker, R. Hopker, and M. Spira. PROSPINO: A Program for the production of supersymmetric particles in next-to-leading order QCD. 1996.

[32] Pavel M. Nadolsky, Hung-Liang Lai, Qing-Hong Cao, Joey Huston, Jon Pumplin, Daniel Stump, Wu-Ki Tung, and C. P. Yuan. Implications of CTEQ global analysis for collider observables. *Phys. Rev.*, D78:013004, 2008.

[33] Lyndon Evans and Philip Bryant. LHC machine. *JINST*, 3:S08001, 2008.

[34] S. Chatrchyan et al. The CMS experiment at the CERN LHC. *JINST*, 3:S08004, 2008.

[35] David Barney. CMS detector 3D image. http://ippog.web.cern.ch/resources/2011/cms-detector-3d-image.

[36] D. Sprenger, M. Weber, R. Adolphi, R. Brauer, L. Feld, K. Klein, A. Ostaptchuk, S. Schael, and B. Wittmer. Validation of Kalman Filter alignment algorithm with cosmic-ray data using a CMS silicon strip tracker endcap. *JINST*, 5:P06007, 2010.

[37] S Chatrchyan et al. Commissioning and Performance of the CMS Pixel Tracker with Cosmic Ray Muons. *JINST*, 5:T03007, 2010.

[38] S Chatrchyan et al. Commissioning and Performance of the CMS Silicon Strip Tracker with Cosmic Ray Muons. *JINST*, 5:T03008, 2010.

[39] Pierre Billoir. Progressive track recognition with a Kalman like fitting procedure. *Comput. Phys. Commun.*, 57:390–394, 1989.

[40] P. Billoir and S. Qian. Simultaneous pattern recognition and track fitting by the Kalman filtering method. *Nuclear Instruments and Methods in Physics Research Section A: Accelerators, Spectrometers, Detectors and Associated Equipment*, 294(1):219 – 228, 1990.

[41] R. Mankel. A Concurrent track evolution algorithm for pattern recognition in the HERA-B main tracking system. *Nucl. Instrum. Meth.*, A395:169–184, 1997.

[42] R. Fruhwirth. Application of Kalman filtering to track and vertex fitting. *Nucl. Instrum. Meth.*, A262:444–450, 1987.

[43] Serguei Chatrchyan et al. Description and performance of track and primary-vertex reconstruction with the CMS tracker. *JINST*, 9(10):P10009, 2014.

[44] Marco Rovere. CMS tracking POG performance plots 2015. https://twiki.cern.ch/twiki/bin/view/CMSPublic/TrackingPOGPlotsPerformance2015, 2016.

[45] Serguei Chatrchyan et al. Performance of CMS muon reconstruction in pp collision events at $\sqrt{s} = 7$ TeV. *JINST*, 7:P10002, 2012.

[46] Vardean Khachatryan et al. Muon performance in early 2016 collision data. CMS-DP-2016-027, 2016.

[47] Vardan Khachatryan et al. The CMS trigger system. *JINST*, 12(01):P01020, 2017.

[48] C. Patrignani and Particle Data Group. Review of particle physics. *Chinese Physics C*, 40(10):100001, 2016.

[49] A. Giammanco. Particle identification with energy loss in the CMS silicon strip tracker. CERN-CMS-NOTE-2008-005, 2007.

[50] Torbjorn Sjostrand, Stephen Mrenna, and Peter Z. Skands. A Brief Introduction to PYTHIA 8.1. *Comput. Phys. Commun.*, 178:852–867, 2008.

[51] Vardan Khachatryan et al. Event generator tunes obtained from underlying event and multiparton scattering measurements. *Eur. Phys. J.*, C76(3):155, 2016.

[52] Torbjorn Sjostrand, Stephen Mrenna, and Peter Z. Skands. PYTHIA 6.4 Physics and Manual. *JHEP*, 05:026, 2006.

[53] Serguei Chatrchyan et al. Measurement of the Underlying Event Activity at the LHC with $\sqrt{s} = 7$ TeV and Comparison with $\sqrt{s} = 0.9$ TeV. *JHEP*, 09:109, 2011.

[54] B. C. Allanach et al. The Snowmass points and slopes: Benchmarks for SUSY searches. *Eur. Phys. J.*, C25:113–123, 2002.

[55] Frank E. Paige, Serban D. Protopopescu, Howard Baer, and Xerxes Tata. ISAJET 7.69: A Monte Carlo event generator for pp, anti-p p, and e+e- reactions. 2003.

[56] Serguei Chatrchyan et al. Measurement of the inclusive W and Z production cross sections in pp collisions at $\sqrt{s} = 7$ TeV. *JHEP*, 10:132, 2011.

[57] Procedure for the LHC Higgs boson search combination in summer 2011. Technical Report CMS-NOTE-2011-005. ATL-PHYS-PUB-2011-11, CERN, Geneva, 2011.

[58] Thomas Junk. Confidence level computation for combining searches with small statistics. *Nucl. Instrum. Meth.*, A434:435–443, 1999.

[59] Alexander L. Read. Presentation of search results: The CL(s) technique. *J. Phys.*, G28:2693–2704, 2002. [,11(2002)].

[60] Glen Cowan, Kyle Cranmer, Eilam Gross, and Ofer Vitells. Asymptotic formulae for likelihood-based tests of new physics. *Eur. Phys. J.*, C71:1554, 2011. [Erratum: Eur. Phys. J.C73,2501(2013)].

[61] W.T Eadie et al. *Statistical methods in experimental physics.* North Holland, Amsterdam, 1971.

[62] F. James. *Statistical methods in experimental physics.* World Scientific, Singapore, 2006.

[63] A. Hoecker, P. Speckmayer, J. Stelzer, J. Therhaag, E. von Toerne, H. Voss, M. Backes, T. Carli, O. Cohen, A. Christov, D. Dannheim, K. Danielowski, S. Henrot-Versille, M. Jachowski, K. Kraszewski, A. Krasznahorkay, Jr., M. Kruk, Y. Mahalalel, R. Ospanov, X. Prudent, A. Robert, D. Schouten, F. Tegenfeldt, A. Voigt, K. Voss, M. Wolter, and A. Zemla. TMVA - Toolkit for Multivariate Data Analysis. *ArXiv Physics e-prints*, March 2007.

[64] C. G. BROYDEN. The convergence of a class of double-rank minimization algorithms 1. general considerations. *IMA Journal of Applied Mathematics*, 6(1):76, 1970.

[65] R. Fletcher. A new approach to variable metric algorithms. *The Computer Journal*, 13(3):317, 1970.

[66] Donald Goldfarb. A family of variable-metric methods derived by variational means. *Mathematics of Computation*, 24(109):23–26, 1970.

[67] D. F. Shanno. Conditioning of quasi-newton methods for function minimization. *Mathematics of Computation*, 24(111):647–656, 1970.

[68] CMS luminosity measurement for the 2015 data-taking period. Technical Report CMS-PAS-LUM-15-001, CERN, Geneva, 2017.

[69] Serguei Chatrchyan et al. Performance of CMS muon reconstruction in pp collision events at $\sqrt{s} = 7$ TeV. *JINST*, 7:P10002, 2012.

BIOGRAPHICAL SKETCH

My name is Andrew Kenjiro Ackert and I am currently a graduate student at Florida State University. Having been born in California, my parents moved to the Big Island of Hawaii when I was around 3 years old. I remained there until I graduated Kealakehe High School as the valedictorian for the class of 2008. After high school I attended Florida State University to pursue a Bachelors of Science degree in Physics. After 4 years and attaining Summa Cum Laude with honors in Physics, I chose to remain at Florida State to pursue my graduate degree in Experimental High Energy Physics due to the program's high reputation in research and the fantastic faculty that I had become familiar with in my tenure as an undergraduate. I have accepted a position with Johns Hopkins Applied Physics Laboratory to work as a researcher in the aerospace defense division.